HETEROGENIZED NITROGEN CONTAINING METAL COMPLEXES OVER SBA-15 FOR ASYMMETRIC TRANSFER HYDROGENATION REACTION

A THESIS SUBMITTED TO THE

UNIVERSITY OF PUNE

FOR THE DEGREE OF

DOCTOR OF PHILOSOPHY

IN CHEMISTRY

By

SURENDRAN PARAMBADATH

(RESEARCH STUDENT)

Dr. A. P. SINGH

(RESEARCH GUIDE)

INORGANIC & CATALYSIS DIVISION

NATIONAL CHEMICAL LABORATORY

PUNE 411 008, (INDIA)

JULY 2008

CERTIFICATE

This is to certify that the work incorporated in the thesis entitled: "**Heterogenized Nitrogen Containing Metal Complexes over SBA-15 For Asymmetric Transfer Hydrogenation Reaction**", submitted by Mr. Surendran Parambadath, for the Degree of **Doctor of Philosophy**, has been carried out by the candidate under my supervision at Catalysis Division, National Chemical Laboratory, Pune 411 008, India. Such material as has been obtained from other sources has been duly acknowledged in the thesis.

Date: Research Guide

Place: Pune (**Dr. A. P. Singh)**

DECLARATION BY RESEARCH SCHOLAR

I hereby declare that the thesis entitled "**Heterogenized Nitrogen Containing Metal Complexes over SBA-15 For Asymmetric Transfer Hydrogenation Reaction**", submitted for the Degree of ***Doctor of Philosophy*** to the University of Pune, has been carried out by me at Catalysis Division, National Chemical Laboratory, Pune 411 008, India, under the supervision of Dr. A. P. Singh. The work is original and has not been submitted in part or full by me for any other degree or diploma to this or any other University.

Date: **Surendran Parambadath**

Inorganic & Catalysis Division
National Chemical Laboratory
Pune-411008

Dedicated to my beloved..... Parents, Brother, Sisters, Wife, Sister-in-law & Teachers..

ACKNOWLEDGEMENTS….

It is my great pleasure to express my heartfelt gratitude to my research supervisor, Dr. A. P. Singh, for his unending support and invaluable guidance throughout the period of this investigation. I sincerely thank him for the care and affection that I received from him in the entire period.

I am indebted to Dr. Rajeev Kumar, Dr. A. V. Ramaswamy and Dr. S. Sivasankar, former Head of Catalysis Division, for allowing me to use all the available facilities in the division, for the stimulating discussions, valuable suggestions and for the constant encouragement and support.

I am very much grateful to Dr. S. Srinivasan, HOD (in-charge), Catalysis and Inorganic Chemistry Division, NCL, who is very kind and generous towards me and the help I received from him is gratefully acknowledged.

I have to acknowledge the friendly and cooperative attitude of all scientific staff of our Division. I would like to thank Dr. C. S. Gopinath, Dr. C. V. V. Sathyanarayana, Dr. S. B. Halligudi, Dr. K. R. Kamble, Dr. S. Umbarkar, Ms. Violet Samuel, Ms. Agashe, Mrs. Nalini Jacob, Dr. Belhekar, Dr. Awate, Mr. Ratnesh K. Jha for their valuable help and cooperation given to me in completing my research work successfully.

I also thank, Dr. P. A. Joy, Dr. Vijayamohanan, Dr. Rajamohanan, Dr. Ajith Kumar, Dr. C. Ramesh, Dr. Veda Ramaswamy, Dr. A. K. Kinage, Dr. Muthukrishnan, Dr. T. Raja, Dr. Selvaraj, Dr. Manikandan, Dr. A. J. Chandwadkar, Dr. Dongare, Dr. R. A. Shaikh and Dr. Kala raj for their help on various occasions. I would like to acknowledge the help received from Mr. Purushothaman, Mr. Madhu, Mr. Milind and Mr. Katti.

I sincerely thank my labmates for their friendly help and kind cooperation during the period of my work. I also thank all my friends in the division and in NCL for their help and support in one way or other, which made my work much easier. I specially thank all my mallu friends, many of them are abroad now, for their love, support and help. They made my life in NCL much better.

I would like to thank all my teachers in various classes for the love and encouragement that I received from them. I take this occasion to thank all my

classmates till M.Tech course whose cooperative attitude helped me very much. Also I thank all well-wishers and friends whose names are not mentioned here.

I would like to thank Dr. S. Sivaram, Director, NCL and Dr. P. Ratnasamy (former Director, NCL) for allowing me to carryout the research work at NCL and CSIR, New Delhi, India, for the financial support in the form of senior research fellowships.

Words are not enough to express my love and gratitude to my family members. It is their love, blessings and prayers that helped me throughout my life. I am very much indebted to them.

Above all, I thank God for his blessings, for forgiving my mistakes, for leading me in the right path and for being there whenever I needed.

Surendran Parambadath.

IMPORTANCE OF CATALYSIS AND CATALYSIS TECHNOLOGY

How important is catalysis? Without it our modern technological society would not have happened! Almost all chemicals, fuels, polymers, and fibers are manufactured in our times by catalytic processes. Catalysis is fundamental to life! In fact,

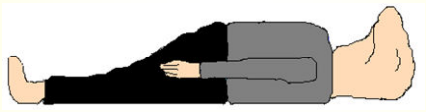

..Without catalysis no form of life could exist!..

"Mother Nature is the best organic chemist on earth and thanks to a wide range of very specific and active enzymes, she can synthesize all kinds of chiral molecules she may need".

TABLE OF CONTENTS

List of Figures

List of Tables

List of Schemes

List of Abbreviations

AES	Atomic Emission Spectroscopy
ADPE	(1S,2R)-(+)-1-amino-1,2-diphenylethanol
AIL	1R,2S-(+)-cis -amino-2-indanol
ATH	Asymmetric Transfer Hydrogenation
BE	Binding Energy
BET	Brunauer-Emmett-Teller
BJH	Barrett-Joyner-Halenda
Bn	Benzene
Bz	Benzyl
BzAIL	NH-benzyl-(1S,2R)-(+)-cis-1-amino-2-indanol
CMC	Critical Micelle Concentration
CMPT	4-(chloromethyl) phenyltrimethoxysilane
CP MAS	Cross Polarization Magic Angle Spinning
CYDN	1,2-diaminocyclohexane
DCM	Dichloromethane
DEPT	Distortionless Enhancement by Polarization Transfer
DPEN	1,2-Diphenylethylenediamine
DRUV-Vis	Diffuse Reflectance Ultraviolet-Visible
ee	Enantiomeric Excess
FSM	Folded Sheet Materials
FTIR	Fourier Transform Infrared
GC	Gas Chromatography
HMM	Hybrid Mesoporous Material
HMS	Hexagonal Mesoporous Silica
HRTEM	High Resolution Transmission Electron Microscopy
ICP-AES	Inductively Coupled Plasma – Atomic Emission Spectrometry
LCT	Liquid Crystal Template
MCM	Mobil's Crystalline Material
NMR	Nuclear Magnetic Resonance

PMO	Periodic Mesoporous Organosilica
Pr	Propyl
PrAIL	NH-propyl-(1S,2R)-(+)-cis-1-amino-2-indanol
PrADPE	NH-propyl-(1S,2R)-(+)-1-amino-1,2-diphenylethanol
SAMS	Self-Assembled Monolayers
SBA	Santa Barbara Amorphous
SDPEN	(*S*,*S*)-DPEN or (*S*,*S*)-1,2-Diphenylethylenediamine
SEM	Scanning Electron Microscopy
SLC	Silicatropic Liquid Crystals
TEM	Transmission Electron Microscopy
TEOS	Tetraethyl orthosilicate
TMS	Tetra Methyl Silane
TOF	Turnover Frequency
TON	Turnover Number
Ts	*p*-Tosyl
TsAIL	NH-(*p*-tosyl)-(1S,2R)-(+)-cis-1-amino-2-indanol
UV-Vis	Ultraviolet-Visible
XPS	X-Ray Photoelectron Spectroscopy
XRD	X-Ray Diffraction

ABSTRACT OF THE THESIS

Chiral alcohols form an important class of intermediates for the pharmaceutical, agrochemical, flavor and fragrance industry. The enantioselective synthesis of chiral secondary alcohols by catalytic reduction of the corresponding ketone is therefore an important transformation in organic synthesis.[1] One of the most attractive methods for this reaction is asymmetric transfer hydrogenation since it can give a high product yield with high enantiomeric excess at relatively mild conditions.

During the past few decades, enantioselective transfer hydrogenation of prochiral carbonyl compounds in homogeneous as well as heterogeneous[2] conditions with transition metal complexes have become more important in the pharmaceutical industry, and consequently in catalytic research as well. Recently, an increased demand has developed for the heterogenization of homogeneous organometallic complex catalysts,[3] the goal of which is to combine the superior activity and selectivity offered by homogeneous catalysts with the ease of separation and recycling of heterogeneous ones. Although, several reports of heterogeneous catalysis by encapsulated materials has been addressed for oxidation, epoxidation and Heck reactions, but attempts to heterogenize some of the industrially relevant homogeneous chiral amino alcohol catalysts for enantioselective as well as chemoselective transfer hydrogenation of carbonyl compounds have been, at best, very limited. Also, a direct comparison of the anchored catalysts with their homogeneous counterparts has not been well investigated with meaningful quantitative data.

Much effort has been devoted to the development of new chiral catalysts and rapid progress has been made in this area.[4] Insight into the mechanism is increasing rapidly and the rational design of catalysts has led to several efficient systems. The utilization

of immobilized catalysts in the asymmetric transfer hydrogenation reaction can provide a significant improvement over the homogeneous process. It enables the long-term use of expensive catalyst and provides a clean and straightforward separation of the product.

The present work primarily focused on the solid-phase synthesis of new asymmetric transfer hydrogenation catalysts as well as the use of these mesoporous silica supported systems in batch reactors is reported. To attain the above goal, we focused initially the design and development of mesoporous SBA-15 molecular sieves using neutral templating route to get high surface area with narrow pore size distributions. Further, the surface modification of SBA-15 was done using various organosilane groups, such as 3-chloropropyltrimethoxysilane, (4-chloromethyl) phenyltriethoxysilane and 2-(4-chloro sulphonylphenyl)ethyltrimethoxysilane by post synthetic route to anchor the desired chiral amino alcohol and further its complexation with metal precursors. We have used (1R,2S)-(+)-*cis*-1-amino-2-indanol and (1S,2R)-(+)-1-amino-1,2-diphenylethanol as chiral auxiliaries and $[RuCl_2(benzene)]_2$ and $[RuCl_2(p\text{-cymene})]_2$ as metal precursors in order to achieve a promising enantioselectivity and catalytic activity by varying the metal source and reaction condition.

The thesis will also focus the preparation of homogeneous chiral metal complexes derived by the modification of (1R,2S)-(+)-*cis*-1-amino-2-indanol and (1S,2R)-(+)-1-amino-1,2-diphenylethanol by various modifiers such as 1-bromopropane, benzylbromide and *p*-toluenesulfonylchloride in order to achieve a better enantioselectivity and catalytic activity by varying the metal source, reaction condition *etc*. The synthesized NH-propyl, NH-benzyl and NH-(*p*-tosyl) derivatives of (1R,2S)-(+)-*cis*-1-amino-2-indanol and NH-propyl derivative of (1S,2R)-(+)-1-

amino-1,2-diphenylethanol was complexed with $[RuCl_2(benzene)]_2$ and $[RuCl_2(p\text{-cymene})]_2$.

Finally the synthesized homogeneous and heterogeneous chiral catalysts were utilized in the asymmetric transfer hydrogenation of simple prochiral ketones under mild reaction conditions. We have used isopropanol as solvent and potassium hydroxide as reaction initiator adopted a temperature of 60^oC. The new catalysts should exhibit high selectivity towards ATH of a class of carbonyl compounds in 2-propanol. The main goal of the thesis is to study the activity difference of two different types of chiral ligands one having fused and other flexible ring system at similar reaction conditions.

The specific problems chosen are:

(i) Synthesis of mesoporous silica material viz. SBA-15

(ii) Synthesis of 3-chloropropyltrimethoxysilane, (4-chloromethyl)phenyltriethoxy silane and 2-(4-chlorosulphonylphenyl)ethyltrimethoxysilane anchored SBA-15 by a post immobilization technique to immobilize the chiral auxiliary.

(iii) Immobilization of (1R,2S)-(+)-*cis*-1-amino-2-indanol and (1S,2R)-(+)-2-amino-1,2-diphenylethanol over organo-functionalized SBA-15 by the refluxing method.

(iv) Synthesis of homogeneous NH-propyl, NH-benzyl and NH-(*p*-tosyl) derivatives of (1R,2S)-(+)-*cis*-1-amino-2-indanol.

(v) Synthesis of homogeneous NH-propyl derivatives of (1S,2R)-(+)-2-amino-1,2-diphenylethanol.

(vi) Synthesis of heterogeneous chiral ruthenium complexes from $[RuCl_2(benzene)]_2$ and $[RuCl_2(p\text{-cymene})]_2$.

(vii) The application of the synthesized homogeneous and heterogeneous complexes

in the asymmetric transfer hydrogenation for the production of chiral secondary alcohols from aromatic ketones under mild reaction conditions.

(viii) Detailed characterization of all these newer homogeneous catalysts and organic-inorganic hybrid materials.

The outline of this thesis is given below:

Chapter 1: Introduction

This chapter presents a brief history of chirality, catalyst and the phenomenon of catalysis. The information about development and applications of various porous materials has been stated. The general introduction about various physicochemical aspects of mesoporous had been mentioned. The different characteristic properties of these materials, synthesis parameters, formation mechanisms, different approaches for surface-functionalization, characterization techniques and the previous reports of various asymmetric hydrogenation catalysts including homogenous and heterogeneous are discussed in brief. The scope and objectives of the present work have been outlined at the end of this chapter.

Chapter 2: Synthesis, Surface modification and characterization of SBA-15

This chapter deals with experimental results on synthesis of SBA-15 molecular sieves and their the functionalization by reactive organic functional groups such as 3-chloropropyltrimethoxysilane, (4-chloromethyl)phenyltriethoxysilane and 2-(4-chloro sulphonylphenyl)ethyltrimethoxysilane. There after immobilization of chiral ligand, (1R,2S)-(+)-*cis*-1-amino-2-indanol followed the preparation of chiral heterogeneous ruthenium complexes by complexing metal precursors such as $[RuCl_2(benzene)]_2$ and

$[RuCl_2(p\text{-cymene})]_2$. The materials were characterized by XRD, ^{29}Si and ^{13}C CP MAS NMR, N_2 sorption technique, FT-IR, UV-Vis, AAS, XPS, TEM and SEM. The main emphasis was given on the local environment of the metal species.

Chapter 3: ATH of Prochiral Ketones Using Heterogeneous Metal Complexes

This chapter describes with the catalytic activity of the synthesized chiral ruthenium complexes in the asymmetric transfer hydrogenation (ATH) of a class of simple aromatic ketones under mild reaction conditions. The transfer hydrogenation has done using various reaction conditions including different substrate, different temperature, various bases, duration of run *etc*.

Chapter 4: ATH using (1*R*,2*S*)-(+)-*cis*-1-amino-2-indanol Based Homogeneous Complexes

This chapter deals with the preparation, characterization and catalytic activity of homogeneous NH-propyl, NH-benzyl and NH-(*p*-tosyl) derivatives of (1R,2S)-(+)-*cis*-1-amino-2-indanol. The materials were characterized by liquid ^1H NMR & ^{13}C NMR, FT-IR and UV-Vis spectroscopy. The main emphasis was given on the local environment of the metal species. The catalytic activity of these synthesized homogeneous chiral ruthenium complexes in the ATH of simple aromatic ketones under mild reaction conditions. The transfer hydrogenation has done under different substrate to catalyst ratio.

Chapter 5: P reparation, characterization and Catalytic activity of Ru-Pr-ADPE and Ru-Pr-ADPE-SBA-15

This chapter describes with the preparation of homogeneous and heterogeneous chiral ruthenium complexes of (1S,2R)-(+)-1-amino-1,2-diphenylethanol by coupling with 1-bromopropane and immobilization over 3-chloropropyltrimethoxysilane functionalized SBA-15 respectively, there after the complexation with two metal precursors such as $[RuCl_2(benzene)]_2$ and $[RuCl_2(p\text{-cymene})]_2$. The materials were characterized by various characterization techniques. The complete characterizations of these samples were carried out by various spectroscopic techniques like XRD, liquid ^{1}H NMR ^{29}Si and ^{13}C CP MAS NMR, N_2 sorption technique, FT-IR, UV-Vis, ICP-AES. The synthesized homogeneous and heterogeneous chiral ruthenium complexes were usefully utilized in the asymmetric transfer hydrogenation of a number of simple aromatic ketones in 2-propanol under mild reaction conditions. The transfer hydrogenation has done using various reaction conditions including different substrate, different temperature, various bases, duration of run etc has conducted in order to get an insight about the kinetics of the reaction.

Chapter 6: Summary and Conclusions

This last chapter elaborately presents the results obtained and the basic findings of the present thesis work.

The arrival at the earlier set scopes and objectives of thesis have been achieved and discussed, like, SBA-15 material has been synthesized and functionalized by various organo-silanes. There after the successful immobilization of chiral ligands, followed the complexation with ruthenium precursors over organo-functionalized SBA-15 have been achieved and discussed. The synthesized catalysts have been characterized by

various instrumental techniques to confirm the existence of mesoporous nature and to confirm the presence of organic functional groups. Then catalytic applications have been performed to prove the promising catalytic nature of the catalysts.

References

1. F. Fache, E. Schulz, M. L. Tommasino, Marc Lemaire. *Chem. Rev.* **2000,** *100,* 2159-2231.
2. Q-H Fan, Y-M Li, A. S. C. Chan. *Chem. Rev.* **2002,** *102,* 3385-3466.
3. R. Noyori, Asymmetric Catalysis in Organic Synthesis, *Wiley-Interscience,* New York, **1994**, 2.
4. (a) S. Hashiguchi, A. Fujii, J. Takehara, T. Ikariya, R. Noyori, *J. Am. Chem. Soc*. **1995**, *117*, 7562. (b) A. Fujii, S. Hashiguchi, N. Uematsu, T. Ikariya, R. Noyori, *J. Am. Chem. Soc*. **1996**, *118*, 2521.

Chapter 1

Introduction & Literature survey

1.1. GENERAL BACKGROUND

1.1.1. Asymmetric Synthesis and Catalysis

There are different ways to define the concept of asymmetric synthesis. We can mention as an example the definition presented by Marckwald in 1904:

"Asymmetric" syntheses are those which produce optically active substances from symmetrically constituted compounds with intermediate use of optically active materials, but with the avoidance of any separations.

In short, we shall say that asymmetric synthesis involves the formation of new stereogenic units in a substrate under the influence of a chiral group which can either exist in the substrate (intramolecular chirality transfer) or be external (intermolecular chirality transfer).

Small amounts of chiral, enantiomerically pure (or enriched) catalysts promote reactions and lead to the formation of large amounts of enantiomerically pure or enriched products is termed as asymmetric catalysis.

1.1.2. Chirality-The magic of nature

Even before the understanding that carbon was tetravalent, the French physicist Biot established that certain organic compounds rotated the plane of polarization of light. However, it was Pasteur who correlated this phenomenon with an asymmetric grouping of atoms within molecules. Kekule´ establishing that carbon has four valences and van't Hoff and Le Bel arranging these valences in a tetrahedral fashion set the stage for one of the most profound features of organic molecules their ability to exist in mirror-image forms.

The world in which we live is chiral. All biological receptors are chiral. Chirality is a very important symmetry property of three dimensional objects. Any object is chiral when it is not superposable on its mirror image. We should remember here that superposable means that one object can be placed on the top of the other so that all parts coincide.

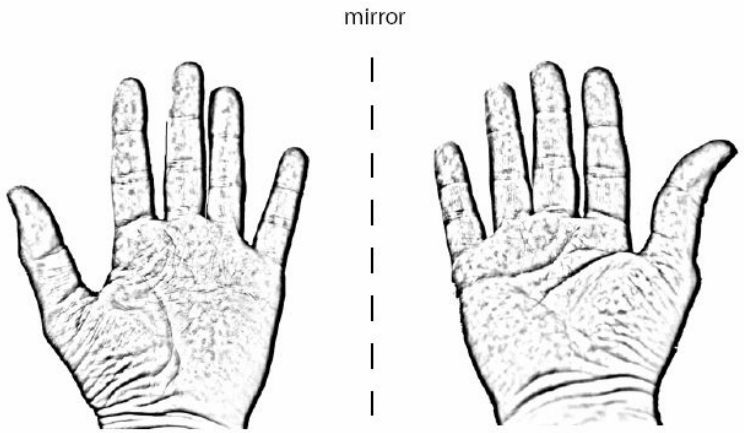

Figure 1.1: Chiral objects: my left and my right hand

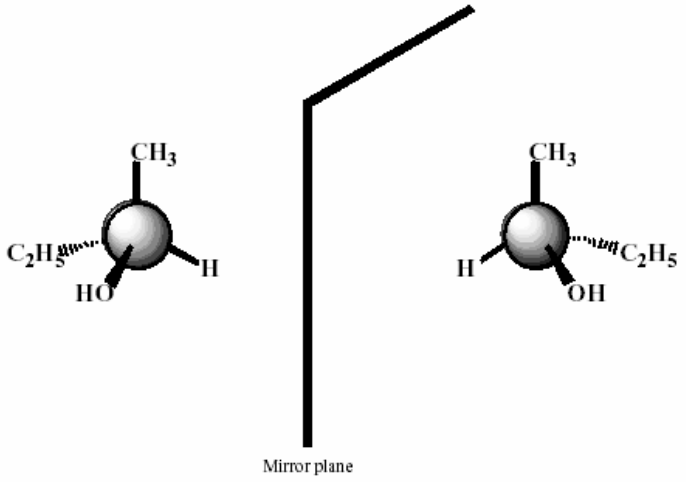

Figure 1.2: The two enantiomers of 2-butanol

Chirality of some familiar objects like our hands (Fig. 1.1) or our feet is very obvious. A left-handed glove would never suit a right hand or vice versa. Have you ever tried to dance with your left foot in a right shoe?

In a chemical context, chirality is applied to the three-dimensional structure of molecules. According to Mislow and Siegel,[1] this carbon atom is the stereogenic centre of the molecule. A chiral molecule and its mirror image are called *enantiomers* and they form an *enantiomeric pair*. Two enantiomers have the same constitutional structure but different three-dimensional structure. Chirality of molecules can be demonstrated with very simple molecules as 2-butanol (Fig. 1.2). The implications of this fundamental feature of organic molecules are immense. Undoubtedly, the richness of the biological world would not exist without this structural feature. Indeed, the very existence of the biological world is likely to have become possible only because of its exquisite use of this phenomenon.

In organic chemistry, chirality is often (but not always) related to the presence of one or several stereogenic centers in the molecule. In most cases this stereogenic centre is a tetrahedral carbon (as in 2-butanol), a phosphorus, sulfur, or in some special cases, a nitrogen atom.

The number of stereoisomers for a compound will depend on the number of stereogenic centers present in its molecule. Thus if *n* is equal to the number of stereogenic centers, there can be 2n stereoisomers. When comparing any two of these stereoisomers either they will be mirror images of each other (in this case they will be *enantiomers*) or they will not (in this case they will be called *diastereoisomers*).

Enantiomers have identical chemical and physical properties in an achiral environment. They have, for instance, the same solubility, melting points and

chromatographic retention times. However, in a chiral environment, there are some properties in which enantiomers differ. We can mention as an example the case of a compound called limonene, which has one enantiomer smelling of oranges and the other of lemons. Here we can clearly see the importance of enantioselective synthesis.

When a biologically active compound such as a drug interacts with chiral receptors, the two enantiomers of the drug will interact differently with possibly different effects. Thus, it is obvious that two enantiomers should be considered as different compounds when screened for pharmacological activity. Today there are a lot of methods to obtain enantiomerically pure compounds, but until recently resolution of racemic mixtures (mixtures containing an equal amount of both enantiomers) was far the most common technique. In this procedure, both enantiomers are allowed to react with an enantiomerically pure compound to form two diastereoisomers, which can be separated by crystallization or chromatography. Subsequently, each diastereoisomer is treated separately to liberate a pure enantiomer. Another method involves using available natural chiral compounds (chiral pool) and derivatizing them. However these methods do not create new stereocenters from achiral substances. Furthermore, despite being very rich, the chiral pool cannot provide all necessary chiral starting materials. For these reasons, asymmetric synthesis provides a powerful alternative for generation of enantiopure compounds.

Diastereoisomers have completely different properties; melting point, boiling point, solubility and so forth. They can be separated by crystallization or by chromatography and often these procedures are used to resolve enantiomeric mixtures. Indeed, by coupling two enantiomers to an enantiomerically pure chiral auxiliary, one obtains two diastereoisomers which can be more easily separated. After

subsequent treatment to recover the chiral auxiliary, the enantiomerically pure compounds can be isolated.

1.1.3. Heterogeneous Asymmetric Catalysis

Catalysis of organic reactions is the key for an efficient synthesis and, thus, represents one of the most economically important technologies.[2] The growing demand for enantiopure compounds in the life sciences has stimulated an increased interest in asymmetric catalysis.[3] Although homogeneous catalysts are often expensive and their separation and recycling troublesome, the field of asymmetric catalysis has been dominated for a long time by homogeneous catalysis because of the excellent selectivities and activities obtained. In more recent years, significant developments in the area of solid-phase chemistry have resulted in enormous progress being made in interdisciplinary research on stereoselective heterogeneous catalysis.[4] The potential advantages of heterogeneous catalysis, such as easy separation, efficient recycling, minimization of metal traces in the product and an improved handling and process control that finally result in overall lower costs are well known. Furthermore, in some cases heterogeneous catalysts are even more selective than their homogeneous counterparts. Ideally, the advantages of homogeneous and heterogeneous catalysis, such as high activity and selectivity on one hand and separation and recycling on the other, should be combined.[5]

However, the different areas of asymmetric heterogeneous catalysis have reached widely different levels of maturity. Whereas the immobilization of homogeneous catalysts on solid supports represents an established field that is on the verge of being applied in industry, the young field of metal–organic catalysts is in a rapidly growing

development phase.

A simplified overview of the advantages and disadvantages of immobilized homogeneous catalysts is given in Table 1.1.

Table 1.1: Evaluation of asymmetric heterogeneous catalysts.

Advantages	Disadvantages
☺ Many homogeneous systems known for immobilization	☻ Additional functionalization of ligands renders their synthesis more costly
☺ A variety of linking techniques exist	☻ Limited access to the active catalysts decreases the reaction rate
☺ Various supports to choose from	☻ Low catalyst loadings
☺ Suited for fast ligand screening	☻ Leaching possible
☺ A few ligands are commercially available	☻ Restriction of degrees of freedom of the catalyst can result in decreased enantioselectivities
☺ Broad spectrum of reactions	
☺ In some cases higher selectivities can be obtained with the heterogeneous than with the homogeneous catalyst	
☺ Rather mature methodology giving predictable results	

Homogeneous asymmetric catalysis[6] has already proven its usefulness in a number of industrial applications, and the chemists involved in the pioneering breakthroughs were recently awarded the Nobel prize.[7] Nevertheless, the efficiency of these processes can be improved even further through the employment of the corresponding

heterogeneous catalysts that are derived from their homogeneous counterparts by immobilization, since the catalyst can be easily separated and recycled, and contamination with metal traces minimized. Immobilization occurs by covalent or noncovalent attachment of the chiral ligand, the metal, or the preassembled complex to the support. The ligand can even be synthesized on the support, thus allowing the efficient synthesis and screening of a library of ligands.[8] The choice of a suitable support plays an important, although not fully understood, role and remains challenging. Numerous problems can occur during the immobilization of a homogeneous catalyst and diminish its performance:

- Undesired interactions between the support and the metal–ligand complex,
- The optimal geometry of the catalyst, crucial for high enantioinduction, is disturbed by the support,
- Unsatisfactory stability of the linkage between the catalyst and support or the catalyst itself which results in leaching,
- Limited accessibility of the active site,
- Undesired isolation of catalyst centers that need to cooperate during the reaction.[9]

1.2. HETEROGENIZATION OF HOMOGENEOUS CATALYSTS

Many homogeneous catalytic systems, though have many attractive properties, *viz*. high selectivity and activity, yet cannot be commercialized because of difficulties associated with the catalyst-product separation from catalyst system, procurement in usual conditions, thermally sensitive and reusability of the catalyst.[10] Hence, the homogeneous reactions that have been commercialized either involve volatile

substrates and products or do not contain thermally sensitive organic ligands. The term heterogenization refers to a process, whereby a homogeneous transition metal complex (including free metal particles, biological molecules, organic species *etc*.) is either immobilized, or anchored, or incorporated or encapsulated in an inert organic (polymer) or inorganic support. These heterogeneous catalysts have a lot of advantages over their homogeneous analogues in:

i. Fixed-bed and continuous flow through operations,
ii. Complete commercial utility on a large scale owing to the economic debits of batch type operations and/or expense of catalyst recovery and recycle,
iii. Maintaining high selectivities and conversions (turn over frequency) of their homogeneous analogues for many reactions, and
iv. Preventing other side reactions e.g. dimerization, alkylation and aggregate formation of the catalyst complex, which normally occurs in solution.

To solve the problems occurring in homogeneous catalyst systems, new processes and catalyst designing are under investigation, which can be broadly divided into two types. In the first case, a catalysts system is designed so that it is solubilized in a solvent that, under some conditions, is immiscible with the reaction products. These reactions involve two phases and are often referred to as Biphasic Systems.[11] The other type involves the metal complex catalyst or metal (in form of nanoparticles) anchored to some kind of soluble or insoluble support, and the separation is carried out by a filtration procedure. This type of process is known as Heterogenizing Homogeneous Catalysts.[12]

Homogeneous catalysts generally provide higher activities, regio- and

stereoselectivities than heterogeneous catalysts; in fact, most chiral catalysts are homogeneous. On the other hand, they are more difficult to separate, recover and reuse than the technically well established heterogeneous catalysts. The properties of these two catalytic systems are different but complementary so it could be very useful to combine their best properties. The heterogenization or immobilization of the homogeneous metal complex in an insoluble support makes it possible for the reacting organometallic complex to keep its high activities and selectivities and also to be recovered and recycled. Consequently, the catalytic complex can be separated from the products and unreacted reagents by an easy filtration, precipitation or phase separation.[13,14] Significant examples of different types of catalyst immobilization, as well as their application in a variety of asymmetric reactions, have recently been reported.[15-25] However, chiral catalysts have also been immobilized in special liquid phases (aqueous, florous, ionic), occluded into membranes, or tethered to dendrimers. In this overview, we have focused on the immobilization of catalytic complexes on solid supports.

The organometallic complex can be immobilized on an organic or inorganic solid support through different anchored or immobilized methods. Amorphous oxides (in particular silica and, to a lesser extent, alumina),[26-27] zeolites,[28-34] pillared clays, LDHs[35] and clay minerals (in particular, smectite laminar minerals) are most routinely used. A wide variety of organic supports, (principally insoluble polymers),[36] take part in the common procedures for immobilizing chiral ligands/catalysts. Although organic supports favor reaction rates that are higher than those of inorganic supports, the random distribution of the ligand units along the polymeric chain and swelling effects may be serious limitations. We have focused on the immobilization of chiral catalysts

on inorganic support (SBA-15), which are generally inert materials based on insoluble porous structures with a highly specific surface area.

The heterogenization via covalently bound ligands onto a solid support is one of the most frequent and versatile ways to heterogenize a chiral transition-metal complex. However, the most important disadvantage is that the ligand has to be functionalized, which means a long and delicate synthetic process and purification. Hydrogenised catalysts are much more complex than their homogeneous counterparts and, therefore, generally, they often provide slight changes in activity and selectivity.

In order to disturb the chiral induction as little as possible, the point of attachment of the tether to the ligand should be as far as possible from the stereogenic centre. The catalyst or ligands can be attached covalently onto the support via one-step or multistep functionalization. The second methodology is the most efficient because it prevents the metal complexes from dimerising and functionalises the ligand through a tether that is usually a linear chain that contains triethoxy- or methoxysilyl groups. The complex modified with the functionalized ligand is then anchored through the alkoxysilyl groups with the external silanols of the support (Scheme 1.1).

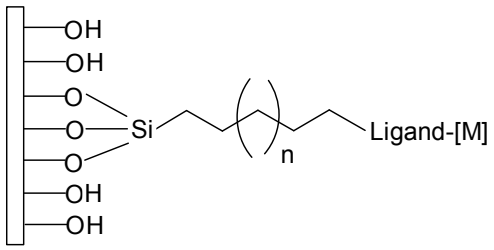

Scheme 1.1: The anchoring of complexes through the alkoxysilyl groups with the external silanols of the support.

1.3. SYNTHESIS AND MECHANISM OF FORMATION OF MESOPOROUS SILICA

Porous solids have extensive commercial applications as adsorbents, catalysts and catalyst supports due to their high surface areas. According to IUPAC definition porous materials may be divided into three types based on their pore dimensions:

Type	Pore Size (Å)
Microporous	< 20
Mesoporous	20-500
Macroporous	> 500

The 'physical chemistry of organized matter' relies on the successful combination of sol–gel chemistry and self-assembly procedures, to uniquely control the texture of materials at the nanometer scale. The growth of soft chemistry derived inorganic or hybrid networks templated by organized surfactant assemblies (structure directing agents) allowed constructing a new kind of materials organized in the mesoscopic scale (2–50 nm): the best example is the ever growing family of mesostructured hybrids and derived mesoporous inorganic materials. Mesoporous silica (with regular pore diameters between 20 and 500 Å) has recently been raised as novel class of materials in heterogeneous catalysis. Silica has no intrinsic catalytic property but it can be used as support and therefore functionalized either by framework substitution or by post-synthesis surface modification.

Mesoporous molecular sieves have attracted considerable attention in recent years since the discovery of the M41S family of mesoporous materials by researchers of the Mobile Oil Corporation. The materials are synthesized by using a silica source and an

organic structure-directing agent *e.g*., cationic surfactants containing long alkyl chain quaternary ammonium compounds containing 10–20 carbons, often followed by the addition of co-surfactants. Originally, this family has been classified into three subgroups: a hexagonal (MCM-41, Mobile Composition of Matter: 2D hexagonal); a cubic (MCM-48), and a lamellar phases (MCM-50). More recently, the so-called SBA-15 (University of California at Santa Barbara; 2D-hexagonal) materials have been prepared by using neutral triblock co-polymers (Pluronic triblock polymer, poly (ethylene oxide)-poly (propylene oxide)-poly (ethylene oxide); $[EO_nPO_mEO_n]$.

1.3.1. Liquid Crystal Templating (LCT) Mechanism

The researchers of Mobil Corporation proposed a 'liquid crystal templating (LCT) mechanism' to explain the formation of M41S type mesoporous materials.[37,38] The mesostructure formation depends on the hydrocarbon chain length of the surfactant tail group,[39] the effect of variation of the surfactant concentration and the additional organic swelling agents. The lowest concentration at which the surfactant molecules aggregate to form spherical isotropic micelles is called critical micelle concentration (CMC_1). Further increase in the surfactant concentration initiates aggregation of spherical into cylindrical or rod-like micelles (CMC_2). There are three main liquid crystalline phases with hexagonal, cubic and lamellar structures. The hexagonal phase is the result of hexagonal packing of cylindrical micelles, the lamellar phase corresponds to the formation of surfactant bilayers and the cubic phase may be regarded as a bicontinous structure.

The Mobil researchers proposed two synthesis mechanisms.[37-38] In the first route, the $C_nH_{2n+1}(CH_3)_3N^+$ surfactant species organize into lyotropic liquid crystal phase,

which can serve as template for the formation of hexagonal MCM-41 structure. First the surfactant micelles aggregate into a hexagonal array of rods, followed by interaction of silicate or aluminate anions present in the reaction mixture with the surfactant cationic head groups. Thereafter condensation of the silicate species occurs, leading to the formation of an inorganic polymeric species. After combusting off the surfactant template by calcination, hexagonally arranged inorganic hollow cylinders are produced (Scheme 1.2).

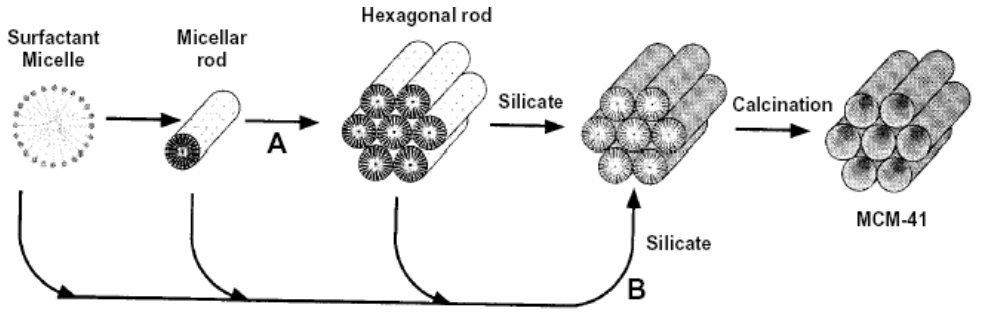

Scheme 1.2: Liquid crystal templating (LCT) mechanism proposed for the formation of MCM-41; (A) liquid crystal phase initiated and (B) silicate anion initiated.

However, the drawback of this synthesis pathway was pointed out by Cheng *et. al,*[42] according to whom the hexagonal liquid-crystal *phase* does not form below 40 % of surfactant concentration. It is known that MCM-41 may be formed at low surfactant concentrations (1 wt %) with respect to water content, and *in situ* ^{15}N NMR spectra indicated that the hexagonal liquid crystalline phase was not present anytime during formation of MCM-41.

In the second route, the hexagonal ordering is initiated by the presence of silicate species in the reaction mixture.[37-38] Chen *et.al* explained that randomly distributed

surfactant micelles with rod-like morphology form initially, and their interaction with silicate oligomers generate randomly oriented surfactant micelles surrounded by two or three silica monolayers.[41] The presence of rod-like micelles in solution was supported by isotropic *in situ* ^{14}N NMR.[43] Further condensation between silicate species on adjacent rods occurs on heating, initiating the long-range hexagonal ordering (Scheme 1.3).

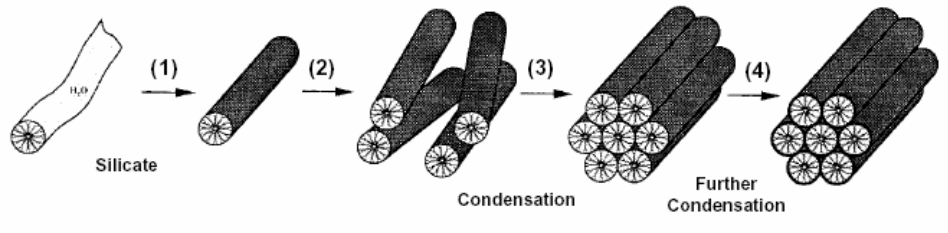

Scheme 1.3: Silicate rod assembly proposed for the formation of MCM-41; (1) and (2) random ordering of rod-like micelles and interaction with silicate species, (3) spontaneous packing of the rods, and (4) remaining condensation of silicate species on further heating.

1.3.2. Charge Density Matching

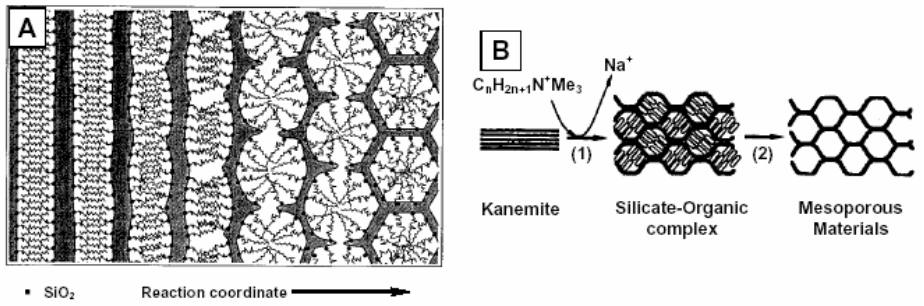

Scheme 1.4: Transformation of surfactant-silicate systems from lamellar to hexagonal mesophases; (A) hexagonal mesophase obtained by charge density matching, and (B) folding of kanemite silicate sheets around intercalated surfactant molecules. [Source:

Refs. 42 and 43]

The 'charge density matching' model proposed by Stucky *et.al.*[42] suggested that condensation occurs between initially formed silicate species by the electrostatic interaction between the anionic silicates and the cationic surfactant head groups. This eventually reduces the charge density and therefore, curvature was introduced into the layers to maintain the charge density balance with the surfactant head groups, which leads to transformation of the lamellar mesostructure into the hexagonal one (Scheme 1.4A). Although this silica-initiated synthesis mechanism has been widely accepted, the presence of an intermediate lamellar species has been disputed.

1.3.3. Folded Sheet Mechanism

The 'folded-sheet mechanism' postulated by Inagaki *et.al.*[43] indicated the presence of intercalated silicate phases in the synthesis medium of the reaction products (Scheme 1.4B). The flexible silicate layers of kanemite fold around the surfactant cations, and cross-linking of the interlayer occurs by condensation of silanol groups on adjacent silicate sheets. On increase of *p*H, the amount of occluded $C_nH_{2n+1}(CH_3)_3N^+$ cations in kanemite increases resulting in expansion of the kanemite interlayers to form another class of regular hexagonal structure called FSM-16.

1.3.4. Silicatropic Liquid Crystals

Firouzi *et.al*. have developed a model based on cooperative organization of inorganic and organic molecular species into 3D structured arrays.[44] According to this model, the physicochemical properties of a particular system were not determined by the organic arrays having long-range preorganized order, but by the dynamic interplay

among ion-pair inorganic and organic species, so that different phases can readily be obtained through small variation of controllable synthesis parameters. The exchange of silicate anions with the surfactant halide counter ions formed the 'silicatropic liquid crystal' (SLC) phase (Scheme 1.5), which exhibited very similar behavior to that of typical lyotropic systems and finally condensed irreversibly into MCM-41.

1.3.5. Generalized Liquid Crystal Templating Mechanism

1.3.5.1. Ionic Route (Electrostatic Interaction)

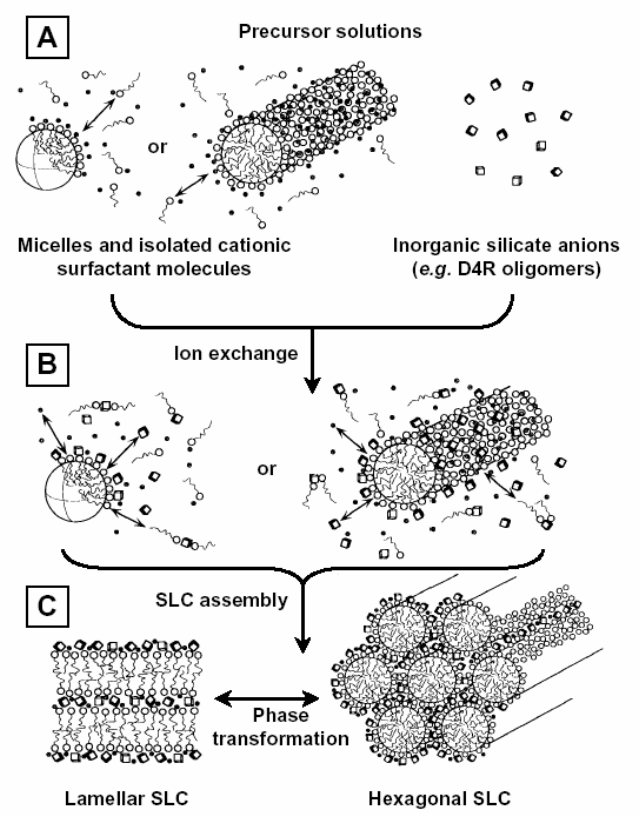

Scheme 1.5: Cooperative organization for the formation of silicatropic liquid crystal phase/silicate-surfactant mesophases; (A) organic and inorganic precursor solutions, (B) preliminary interaction of the two precursor solutions after mixing, and (C) multidentate interaction of the oligomeric silicate units with the surfactant molecules.

[Source: Ref. 44]

Huo *et.al*[45] proposed a generalized mechanism for the formation of mesostructures, which was based on specific types of electrostatic interaction between an inorganic precursor (I) and a surfactant head group (S). In this concept, four different approaches were proposed to synthesize transition metal oxide mesostructures. The first route involves the charge density matching between surfactant cations and inorganic anions (will be referred to as S^+I^- hereafter). The second route deals with the charge-reversed situation, *i.e.*, anionic surfactant and cationic inorganic species (S^-I^+). Both the third and fourth routes are counterion-mediated pathways. The third one demonstrates the assembly of cationic species *via* halide ions (S^-X^+I), while the fourth one depicts the assembly of anionic species *via* alkali metal ions ($S^+X^-I^+$). These synthesis strategies are acceptable for the formation of a wide variety of lamellar, hexagonal or cubic mesophases. However, a general problem negotiated very often is the poor stability of the inorganic framework, which frequently collapses after removal of the surfactant.

1.3.5.2. Neutral Templating Route (Hydrogen Bonding Interaction)

Tanev and Pinnavaia proposed another route to synthesize hexagonal mesoporous silicas (HMS) having thicker pore walls, high thermal stability and smaller crystallite size but, having higher amounts of interparticle mesoporosity and lower degree of long-range ordering of pores than MCM-41 materials.[46] This route is essentially based on hydrogen bonding between neutral primary amines (S_0) and neutral inorganic precursors (I_0), wherein hydrolysis of tetraethyl orthosilicate (TEOS) in an aqueous solution of dodecylamine yields neutral inorganic precursor. Using the same

approach, porous lamellar silicas with vesicular particle morphology have been synthesized with the aid of double headed alkylamines linked by a hydrophobic alkyl chain (α,ω-dialkylamine).

1.3.5.3. Ligand-Assisted Templating Route (Covalent Interaction)

Antonelli and Ying have proposed a ligand-assisted templating mechanism for the synthesis of hexagonally packed mesoporous metal oxide completely stable to surfactant removal.[47] In a typical synthesis, the surfactant was dissolved in the metal alkoxide precursor before addition of water to allow nitrogen–metal covalent bond formation between the surfactant head group and the metal alkoxide precursor. The existence of this covalent interaction was confirmed by ^{15}N NMR spectroscopic studies. In this approach, the structure of the mesophases could be controlled by adjustment of the metal/surfactant ratio, which led to a new class of mesoporous transition metal oxides analogous to M41S family.

1.4. BLOCK COPOLYMERS AS TEMPLATES

Since the pioneering work of the Mobil scientists, a permanent effort is made to develop mesotextured inorganic or hybrid phases, which are potential candidates for a variety of applications, in the fields of catalysis, optics, photonics, sensors, separation, drug delivery, sorption, acoustic or electrical insulation. In the case of mesoporous oxides, the templating relies on supramolecular arrays: micellar systems formed by surfactants or block copolymers (BC) are indeed interesting as supramolecular templates because they are capable to impart larger pores and thicker walls, apart from being industrially available, hazard-free and easy to remove from the mineral framework (by thermal treatment or solvent extraction).

The initial works related to mesostructured oxides described the use of ionic surfactants such as the cationic alkyltrimethylammonium (CTAB, n = 8–18), anionic alkylsulfonates ($C_nSO_3^{2-}$, n = 12–18) or alkyl phosphates as supramolecular templates. These syntheses were performed in extreme (acid or alkaline) *p*H conditions, yielding materials with controlled pore size (15–100 Å). However, two main limitations exist:

(a) Typical wall thickness of 8–13 Å, which is a serious limitation regarding stability for catalysis;

(b) Limited pore size offered by molecular surfactants.

The only way to go beyond 50 Å pore size consisted in employing swelling agents (such as trimethylbenzene), involving complicated synthesis, and irreproducibility (linked to emulsion formation or phase separation). Thus, more versatile supramolecular templates were needed. Amphiphilic BC belongs to an important family of surfactants, widely used in detergency, emulsifying, coating, thickening, *etc*. The self-assembly characteristics of these BC permit to control the superstructure, to vary the typical length scales and to add specific functions. Indeed, the properties of BC can be continuously tuned by adjusting solvent composition; molecular weight or polymer architecture.

Pinnavaia and coworkers were the first to bring the idea of using nonionic surfactants (alkyl amines (C_nNH_2), oligomeric alkyl-poly(ethyleneoxide) ($C_n(PEO)_mOH$), or $(PEO)_m(PPO)_n(PEO)_m$, EO = $–CH_2\text{-}CH_2O–$, and PO = $–CH(CH_3)CH_2O–$ as porogen species, in neutral media. Some advantages of using neutral non-ionic surfactants over the ionic ones were immediately noticed: (a) larger inorganic wall thickness (15–40 Å), enhancing the hydrothermal stability of the mesoporous oxides; (b) easier pore diameter tuning, by varying both the type and the

concentration of the surfactant, (c) easier solvent removal, by solvent extraction; H-bonding (instead of electrostatic) interactions between the template and the inorganic framework should be easier to dissociate. The first mesoporous materials issued MSU-X from the so-called neutral route (S^oI^o) presented low-order wormlike structures. In 1998, the use of neutral surfactant has been extended to ordered mesostructured silicas by Stucky *et.al* The hexagonal SBA-15 silicas are prepared in acidic condition, TEOS being introduced as silica source and a triblock co-polymer [polyethyleneoxide - polypropyleneoxide - polyethyleneoxide (EO_n-PO_m-EO_n) possessing two medium length EO_n hydrophilic blocks surrounding a long and less hydrophilic PO_m block] as surfactant. At low concentration in water, these copolymers from cylindrical aggregates, with the dehydrated PO_m blocks in their cores, surrounded by a corona formed by the hydrated EO_n blocks. At the low *p*H used for synthesis (<2), the EO groups are protonated. Their interaction with positively charged silicate oligomers are mediated by Cl^- anions and the weak $S^+Cl^-I^+$ (S = surfactant; I = inorganic) interactions, is there fore an easy way to induce an increase in the wall thickness of mesoporous silicas and to stabilize them.

1.5. PHYSICOCHEMICAL CHARACTERIZATION

The inorganic–organic hybrid mesostructured materials can be characterized by various techniques, which provide important information about different physicochemical features. The most extensively used techniques can be categorized into the following.

1. Spectroscopic techniques:
    (a) Powder X-ray diffraction (XRD),
    (b) Ultraviolet-visible (UV-Vis) spectroscopy,
    (c) Fourier transform infrared (FTIR) spectroscopy,
    (d) Solid state nuclear magnetic resonance(NMR) spectroscopy,
    (e) X-ray photoelectron spectroscopy (XPS),
    (f) Atomic absorption and emission spectrometry (AAS and AES).
2. Microscopic techniques:
    (a) Scanning electron microscopy (SEM),
    (b) Transmission electron microscopy (TEM).
3. Volumetric techniques:
    (a) Porosity measurements by nitrogen (N_2) adsorption (BET method),
4. Gravimetric techniques:
    (a) Thermogravimetric analyses (TGA),
    (b) Differential thermal analysis (DTA).

1.5.1. X-Ray Diffraction

It is well recognized that X-ray diffraction, based on wide-angle elastic scattering of X-rays, has been the single most important tool to determine the structure of the materials characterized by long-range ordering. The X-ray diffraction patterns are obtained by measurement of the angles at which an X-ray beam is diffracted by the sample. Bragg's equation relates the distance between two *hkl* planes (*d*) and the angle of diffraction (2θ) as:

$$n\lambda = 2d\sin\theta,$$

where λ = wavelength of X-rays, *n* = an integer known as the order of reflection (*h*, *k* and *l* represent Miller indices of the respective planes).[48] From the diffraction patterns, the uniqueness of mesoporous structure,[49] phase purity,[50] degree of crystallinity[50] and unit cell parameters[49] of the semicrystalline hybrid materials can be determined. The identification of phase is based on the comparison of the set of reflections of the sample with that of pure reference phases distributed by International Center for Diffraction Data (ICDD). Unit cell parameter (a_0) of a cubic lattice can be determined by the following equation:

$$a_0 = d_{hkl}\sqrt{(h^2 + k^2 + l^2)}$$

Where, *d* = distance between two consecutive parallel lattice planes having Miller indices *h*, *k* and *l*.

X-ray diffraction broadening analysis has been widely used to characterize supported metal crystallites in the nanoscale. The average size of the nanoparticles can be estimated using the Debye-Scherrer equation:

$$D = k\lambda / \beta\cos\theta,$$

Where, *D* = thickness of the nanocrystal, *k* is a constant, λ = wavelength of X-rays, β = width at half maxima of (111) reflection at Bragg's angle 2θ.[51]

1.5.2. Diffuse Reflectance UV-Vis Spectroscopy

UV-Vis spectroscopy deals with the study of electronic transitions between orbital or bands of atoms, ions or molecules in gaseous, liquid and solid state. In the case of transition metal ions or atoms, any change in their coordination sphere may affect their optical properties and therefore can be characterized by UV-Vis.[52] For solid substances like transition metal containing mesoporous materials, diffuse reflectance

UV-Vis spectroscopy (DRUV-Vis) is applied to determine the ligand field symmetry and oxidation state of the metal inside the solid matrices. Thus DRUV-Vis is a sensitive probe to examine the type of the sites, framework or extra-framework in which that metal ion or cluster exist.[53]

For a vast period of time metallic nanoparticles have fascinated researchers due to their colorful colloidal solutions.[54] Mie explained the origin of this color theoretically by solving Maxwell's equation for the absorption and scattering of electromagnetic radiation by small metallic particles.[55] This absorption of electromagnetic radiation by metallic nanoparticles originates from the coherent oscillation of the valence band electrons induced by an interaction with the electromagnetic field. These resonances are known as surface plasmons, which occur only in the case of nanoparticles and not in the case of bulk metallic particles.[56] Hence, DRUV-Vis can be utilized to study the unique optical properties of the hybrid mesoporous materials containing occluded metallic nanoparticles, exploiting the size and shape dependent surface plasmon resonance.[57]

1.5.3. Fourier Transform Infrared Spectroscopy

Fourier transformed infrared (FTIR) spectroscopy deals with the vibration of chemical bonds in a molecule at various frequencies depending on the elements and types of bonds. After absorbing electromagnetic radiation the frequency of vibration of a bond increases leading to transition between ground state and several excited states. The energy corresponding to these transitions corresponds to the infrared region (4000–400 cm^{-1}) of the electromagnetic spectrum. The term Fourier transform (FT) refers to a recent development in the manner in which the data are collected and

converted from an interference pattern to an infrared absorption spectrum that is like a molecular "fingerprint".[58] In the case of porous silicates, the FTIR spectra in the 400–1300 cm–1 region provides information about the structural details including isomorphous substitution in framework, where as the bands in the 3000–4000 cm^{-1} region allows to determine different Bronsted and Lewis acid sites[59] and silanol groups[60] Acidic and basic properties as well as their strength can also be estimated using carbon dioxide (CO_2), ammonia (NH_3), pyridine, triphenylphosphine (PPh_3) *etc*. as probe molecules and their quantitative estimation by FTIR.[61]

1.5.4. Cross-Polarization Magic Angle Spinning NMR Spectroscopy

Nuclear magnetic resonance (NMR) spectroscopy is one of the most powerful tools to investigate structure and dynamics of a molecular system in liquid phase. Atomic nuclei consisting of odd number of protons and/or neutrons possessing a nuclear spin $I \neq 0$ and consequently a magnetic moment $\mu = \gamma\hbar I$ (γ = gyromagnetic ratio), when placed in a magnetic field of strength B_0, Zeeman interaction results in quantized orientations of the nuclear magnetic moments.[62] The nucleus can adopt $2I + 1$ Eigen states with energies $E(m) = -m\gamma\hbar B_0$, where m = (I, I–1,…., $-I$). Transitions between neighboring energy states ($\Delta m = \pm 1$) can be induced by electromagnetic radiation (energy $E = h\nu$) of frequency,

$$\nu_0 = \gamma B_0/2\pi.$$

The chemical shift interaction arises from secondary local magnetic fields induced by the interaction of the electrons surrounding the nucleus. The induced local field opposes B_0 and hence shields the nucleus under observation. The shielding is spatially anisotropic due to the nonspherical electron distribution around the nucleus.[63]

With the advent of sophisticated solid-state NMR techniques, it has become possible to obtain NMR spectra of solids with spectral resolution comparable to that of liquids[64] Modern high-resolution solid-state NMR spectroscopy allows to elucidate the chemical and structural environment of several atoms (*e.g.* ^{13}C, ^{27}Al, ^{29}Si, ^{31}P, ^{51}V *etc*.) in a solid matrix like that of porous materials.[65] The most popular technique to get high-resolution NMR spectra with narrow line width is the magic angle spinning (MAS), where the solid sample is fast rotated about an axis inclined at a "magic" angle $\theta = 54°44'$ to the direction of B_0. Cross-polarization (CP) technique does not affect the line width of the spectra, but is applied to improve the sensitivity, *i.e.*, the signal to noise ratio (SNR) of the spectra of nuclei with low natural abundance (*e.g.* ^{13}C, ^{29}Si, ^{31}P *etc*.), and to monitor the spatial proximity of nuclei.[66] CP involves indirect excitation of the less abundant nucleus through magnetization transfer from an abundant spin system (*e.g.* 1H).

1.5.5. X-Ray Photoelectron Spectroscopy

X-ray photoelectron spectroscopy (XPS) is widely used for probing the electronic structure of atoms, molecules and condensed matter. When an X-ray photon of energy $h\nu$ is incident on a solid matter, the kinetic energy (E_k) and the binding energy (E_b) of the ejected photoelectrons can be related as follows:

$$E_k = h\nu - E_b.$$

This kinetic energy distribution of the photoelectrons is fabricated by a series of discrete bands, which symbolizes for the electronic structure of the sample.[67] The core level binding energies of all the elements (other than H and He) in all different oxidation states are unique, which provides instant detection of the chemical

composition of the sample after a full range scan.[68] However, to account for the multiplet splitting and satellites accompanying the photoemission peaks, the photoelectron spectra should be interpreted in terms of many-electron states of the final ionized state of the sample, rather than the occupied one-electron states of the neutral species.[69]

1.5.6. Atomic Absorption and Emission Spectrometry

The principle of atomic absorption spectrometry is based on energy absorbed during transitions between electronic energy levels of an atom. When some sort of energy is provided to an atom in ground state by a source such as a flame (temperature ranging from 2100–2800°C), outer-shell electrons are promoted to a higher energy excited state. The radiation absorbed as a result of this transition between electronic levels can be used for quantitative analysis of metals and metalloids present in solid matrices, which have to be dissolved by appropriate solvents before analysis. The basis of quantitative analysis depends on measurement of radiation intensity and the assumption that radiation absorbed is proportional to atomic concentration. Analogy of relative intensity values for reference standards is used to determine elemental concentrations.[70]

Atomic emission spectrometry (AES) is similar to atomic absorption spectrometry (AAS). In both the cases the sample must be atomized in order to obtain usable absorption spectra. However, in contrast to AAS, in AES the sample is heated at a very high temperature (8000–10000°C), where the atoms in the sample are excited to higher energy levels. When the excited atoms are relaxed and fall back to the ground energy level, radiations are emitted. Measurement of the intensities of the emission

forms the basis of quantitative determination.[71]

1.5.7. Scanning Electron Microscopy

Scanning electron microscopy (SEM) is an important tool for morphological characterization of mesoporous molecular sieve materials. A scanning electron microscope can generate an electron beam scanning back and forth over a solid sample. The interaction between the beam and the sample produces different types of signals providing detailed information about the surface structure and morphology of the sample. When an electron from the beam encounters a nucleus in the sample, the resultant Coulombic attraction leads to a deflection in the electron's path, known as Rutherford elastic scattering. A fraction of these electrons will be completely backscattered, reemerging from the incident surface of the sample. Since the scattering angle depends on the atomic number of the nucleus, the primary electrons arriving at a given detector position can be used to produce images containing topological and compositional information.[72]

The high-energy incident electrons can also interact with the loosely bound conduction band electrons in the sample. However, the amount of energy given to these secondary electrons as a result of the interactions is small, and so they have a very limited range in the sample. Hence, only those secondary electrons that are produced within a very short distance from the surface are able to escape from the sample. As a result, high resolution topographical images can be obtained in this detection mode.[73]

1.5.8. Transmission Electron Microscopy

Transmission electron microscopy (TEM) is typically used for high resolution imaging of thin films of a solid sample for microstructural and compositional analysis. The technique involves: (i) irradiation of a very thin sample by a high-energy electron beam, which is diffracted by the lattices of a crystalline or semicrystalline material and propagated along different directions, (ii) imaging and angular distribution analysis of the forward scattered electrons (unlike SEM where backscattered electrons are detected), and (iii) energy analysis of the emitted X-rays.[74] The topographic information obtained by TEM in the vicinity of atomic resolution can be utilized for structural characterization and identification of various phases of mesoporous materials, *viz*., hexagonal, cubic or lamellar.[75] TEM also provides real space image on the atomic distribution in the bulk and surface of a nanocrystal.[76]

1.5.9. Porosity Measurements by N_2 Adsorption

Despite of some theoretical limitations, the Brunauer-Emmett-Teller (BET) method continues to be the most widely used method for the evaluation of surface area, pore volumes and pore size distributions of porous solids from N_2 physisorption isotherm data. The BET equation can be represented as follows:

$$\frac{p}{v(p_o-p)} = \frac{1}{v_m c} + \frac{c-1}{v_m c}\,\frac{p}{p_o}$$

Where, v = volume of N_2 adsorbed by the sample under pressure p, p_0 = saturated vapor pressure at the same temperature, v_m = volume of N_2 adsorbed when the surface is covered with a unimolecular layer, and c = constant for a given adsorbate.[77]

Several computational procedures are available for the derivation of pore size distribution of mesoporous samples from physisorption isotherms. Most popular among them is the Barrett-Joyner-Halenda (BJH) model, which is based on speculative emptying of the pores by a stepwise reduction of p/p_0, and allowance being made for the contraction of the multilayer in those pores already emptied by the condensate.[78,79] The mesopores size distribution is usually expressed as a plot of $\Delta V_p/\Delta r_p$ versus r_p, where V_p = mesopore volume, and r_p = pore radius. It is assumed that the mesopores volume is completely filled at high p/p_0.

1.6. CATALYTIC APPLICATION AND PROSPECTS

The identification of new catalysts for the synthesis of the building blocks for pharmaceutical and agrochemicals continues to attract public interest. In this respect there is a need for catalysts to be designed which are stable, give high yields of the desired products, and can be readily reused. In particular, there is a need for the design of highly selective asymmetric catalysts. Most of this research concerns homogeneous catalysts, but there is also considerable interest in the identification of heterogeneous asymmetric catalysts, since such catalysts readily overcome the problems typically encountered with homogeneous systems, namely product recovery and catalyst separation.[80] To date, three approaches have been taken in the design of heterogeneous enantioselective catalysts: (i) the use of a chiral support for an achiral metal catalyst, (ii) modification of an achiral heterogeneous catalyst using a chiral cofactor, and (iii) the immobilization of a homogeneous catalyst. Among them the most feasible way to circumvent this problem is to "*heterogenize*" the homogeneous catalyst, by means of immobilization, anchoring, or encapsulation on an inorganic

(zeolites or mesoporous materials)[81] or organic (polymeric)[82] solid support. Supported homogeneous catalysts tend to have reduced activities relative to their truly homogeneous analogues. However, this drawback can be offset by the advantages of easy catalyst recovery, reduction of trace metal contamination, maintain the stability of the heterogenized complex and facile methods for parallel screening.

The synthesis of enantiomerically pure chiral compounds has fascinated researchers owing to its immense importance in the fine chemical industry.[83] Among the several strategies developed to produce the desired enantiomer of an optically active compound, asymmetric catalysis offers exclusive and enormous advantages.[84] To date, a number of reports are available in literature, where heterogeneous catalysis by immobilized transition metal complexes on mesoporous silica has been addressed for enantioselective reactions.[85]

1.6.1. Asymmetric Transfer Hydrogenation Reaction (ATH)

Transfer hydrogenation is defined as "*the reduction of multiple bonds with the aid of a hydrogen donor in the presence of a catalyst*".

The process entails hydrogen abstraction from the reagent (hydrogen donor) by means of the catalyst, followed by **(**or in concert with) hydrogen addition to the unsaturated functional group of the substrate (hydrogen acceptor). This can be generalized **as** in eq,

$$\mathbf{DH_2 + A \rightleftharpoons D + AH_2}$$

DH_2 = hydrogen donor; **A** = hydrogen acceptor

By definition, molecular hydrogen is the hydrogen source in catalytic

hydrogenations. In hydrogen-transfer reactions the hydrogen source must be different from dihydrogen. However, the same reductions also occur via catalytic hydrogen transfer reactions where hydrogen is transferred from a donor molecule (DH_2) to the substrate to give reduced substrate and the oxidized donor D. Most of the reagents employed are organic molecules: unsaturated hydrocarbons such as cyclohexene or cyclohexadiene, primary or secondary alcohols like methanol, benzyl alcohol, ammonium formate or propan-2-ol, and formic acid and its salts have been successfully used to this purpose[86]. A primary advantage of this technology is the avoidance of hydrogen gas and pressure equipment. The use of hydrogen donors had some advantages over the use of molecular hydrogen since it avoids the risks and the constraints associated with this reagent as well as the necessity of pressure vessels. Additionally, rate and selectivity of the reaction can be favorably affected by selecting the most appropriate hydrogen donor. Another advantage of this methodology is the requirement for only very low quantities of catalysts; typically less than 1 mol%. Furthermore the ligands employed often are indefinitely stable to the reaction conditions and may be recovered after use. A drawback is the often low catalyst activity and productivity.

The asymmetric reduction of unsaturated compounds provides good opportunities for the simultaneous introduction of new functionalities and new stereogenic elements into the structure of organic compounds. For this reason this process has become one of the most popular tools in asymmetric synthesis and has been exploited in the preparation of a variety of organic products of biological interest featuring diverse functional groups. Among the methodologies presently amenable for this purpose, H-

transfer reduction has gained in recent years a prominent position as to be rated second in order of importance immediately behind asymmetric hydrogenation with molecular hydrogen. The increasing success of this technique follows from its operational simplicity and reduction of the risks associated with the use of an easily inflammable gas of high diffusibility. Two versatile reducing systems have emerged,

1) Isopropanol in the presence of a strong base at 20-40^{o}C is environmentally friendly and easy to handle. A major drawback is reversibility, often leading to incomplete conversions and/or an erosion of *ee* at high conversion. Therefore the reaction is often run dilute, usually 0.1 M in substrate. This limitation can be overcome by distilling the acetone at reduced pressure.

2) Formic acid, usually as an azeotropic 5:2 mixture of HCOOH and NEt_3, in most common solvents, at 20-60^{o}C allows high substrate concentrations, is irreversible and allows high conversions without back-reaction and racemization. Due to evolution of CO_2, the process has to be run in an open system.

Of the plethora of ligands tested, only few are effective and also have a reasonable synthetic scope. Most important are 1,2-amino alcohols, monotosylated diamines and selected phosphino-oxazoline ligands. The choice of the proper metal fragment is crucial and again, only few have proved to be useful. The most active ones are half-sandwich π-complexes, Ru-arene and Rh (and also Ir)-cyclopentadiene complexes. It has been shown that the organometallic fragment stays intact in the catalytic cycle and strongly influences the catalytic properties.

From an industrial stand point the most useful catalysts are those based on

transition metal complexes that are neutral and stable 18-electron catalyst precursor complexes that have the following structural elements:

(a) an η^6/η^5-aryl complexing group;

(b) a metal from Rh, Ir and Ru at the correct oxidation level to give a neutral complex;

(c) a chiral bifunctional ligand modifier with an amine group; and

(d) an anionic leaving group.

To date, a number of reports are available in literature, where heterogeneous catalysis by immobilized transition metal complexes on mesoporous silica has been addressed for enantioselective reactions.[87] But only a few reports are available in the field of asymmetric transfer hydrogenation catalyzed by heterogeneous mesoporous complexes. In this section we will review the catalytic applications and prospects of the "*transition metal complex–mesoporous silica*" composite materials in enantioselective transfer hydrogenation reactions.

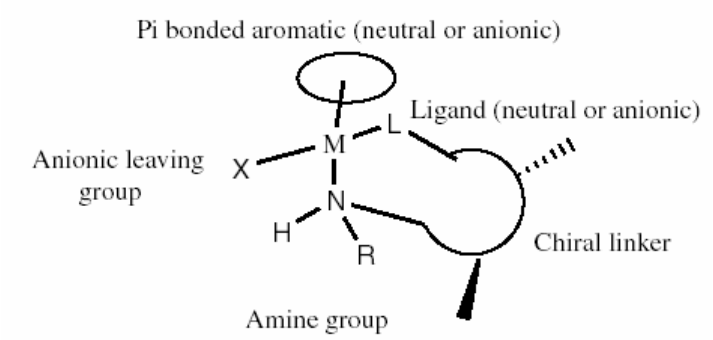

Figure 1.3: General Structure of Asymmetric Transfer hydrogenation catalysts.

1.6.2. Ligands for the enantioselective transfer hydrogenation of ketones

Table 1.2: Ligands used in Asymmetric Transfer Hydrogenation of Acetophenone

1 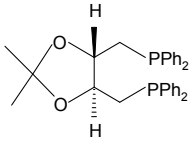

2 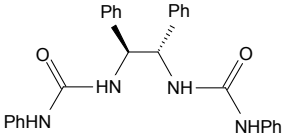

3 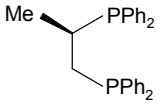

4 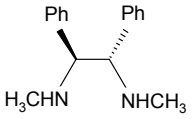

5 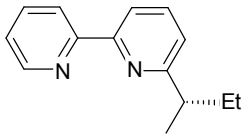

6 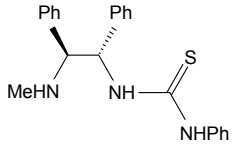

7 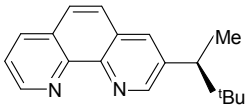

8 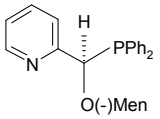

9 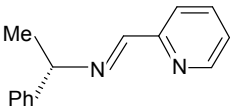

10 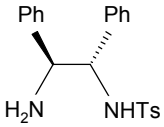

11 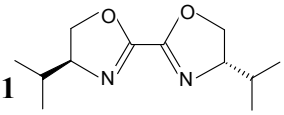

12 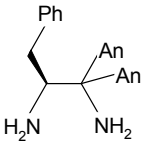

13 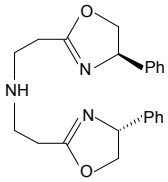

14 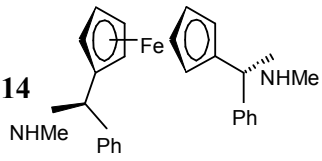

15 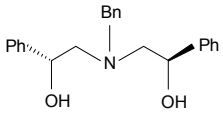

16 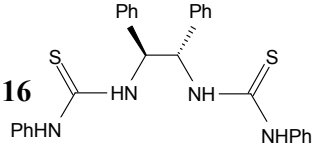

17 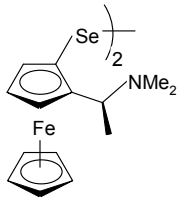

18 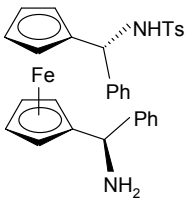

19 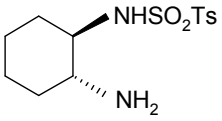

20 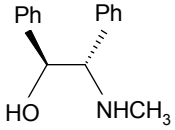

21 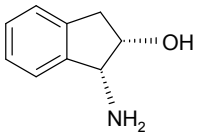

22 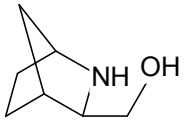

23 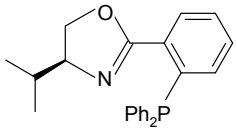

24 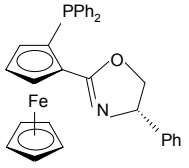

25 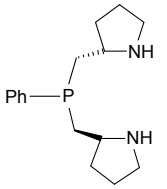

26 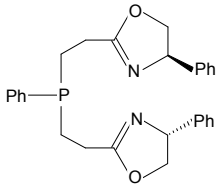

27 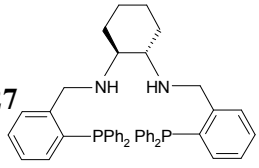

28

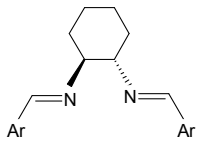

Many ligands have been reported for the enantioselective transfer hydrogenation of ketones, most commonly with rhodium, iridium or ruthenium metals. A brief summary of the most notable ligands, together with a comparison of the relative effectiveness of the prototype acetophenone reduction, is presented below (Table 1.2 & Table. 1.3).

Table 1.3: Important Class of Ligands for ATH of ketones

No:	Class of Ligands
1	Phosphines
2	Pyridine derived chiral ligands containing nitrogen donors
3	Tetrahydrobi(oxazole) ligands
4	Tridentate ligands in Sm(III) complexes
5	Diamine and poly(urea) ligands
6	Diimine ligands
7	Monotosylated diamine ligands
8	β-Amino alcohol ligands
9	Phosphinooxazoline ligands
10	Tridentate P,N-containing ligands
11	Tetradentate diamine/diphosphine ligands

Table 1.4: Asymmetric transfer hydrogenation of acetophenone (hydride source/solvent is isopropanol unless otherwise indicated)

Entry	Ligand	Metal	Time/h	Temp/^{o}C	Yield(%)	ee(%)	Ref.
1	**1**	Ru(II)	111	120	35	4 (S)	88
2	**2**	Rh(I)	168	60	97	43 (R)	89
3	**3**	Rh(I)	3,5	82	60	9 (R)	90
4	**4**	Rh(I)	168	RT	100	67 (R)	91
5	**5**	Rh(I)	-	82	-	7 (R)	92
7	**7**	Rh(I)	4	82	89	63 (S)	93
8	**8**	Ru(II)	1	45	60	60 (R)	94
9	**9**	Ir(I)	-	82	89	37 (S)	95
10	**10**	Ru(II)	15	RT	95	97 (S)	96
11	**10**	Ru(II)	20	RT	99	98 (S)	97
12	**10**	Rh(III)	48	RT	80	90 (S)	98
13	**10**	Ir(III)	48	RT	58	90 (S)	98
14	**11**	Ir(I)	3	80	89	58 (R)	99
15	**12**	Ir(I)	12	RT	74	78 (R)	100
16	**13**	Ru(II)	0.17	82	91	97 (S)	101
17	**14**	Ru(II)	120	-30	95	80 (R)	102
18	**15**	Sm(III)	2	RT	74	96 (R)	103
19	**16**	Ru(II)	9	82	98	87 (S)	104
20	**18**	Ru(II)	24	RT	97	56 (R)	105
21	**18**	Ru(II)	120	RT	42	83 (R)	105
22	**19**	Ru(II)	24	22	97	89 (R)	105
23	**19**	Ru(II)	24	30	99	94 (R)	105
24	**19**	Rh(II)	12	30	85	97 (R)	106
25	**19**	Ir(III)	12	30	36	96 (R)	106
26	**20**	Ru(II)	1	RT	94	92 (S)	107
27	**21**	Ru(II)	1.5	RT	70	91 (S)	108
28	**22**	Ru(II)	5	83	95	95 (S)	109
29	**23**	Ru(II)	0.4	82	74	86 (R)	110
30	**24**	Ru(II)	7	28	80	94 (R)	111
31	**25**	Ru(II)	24	RT	96	20 (R)	112
32	**26**	Ru(II)	0.2	80	72	79 (R)	113
33	**27**	Ru(II)	7	45	93	97 (R)	114
34	**28**	Ru(II)	2-8	82	89	28 (S)	115

1.6.3. Enantioselective Transfer Hydrogenation by Immobilized Transition Metal Complexes

Covalent immobilization of homogeneous catalysts to dendrimers, insoluble

polymers and silica supports, has received considerable attention in recent years. The heterogenization facilitates the separation of the catalyst from reagents and products, simplifies the efficient recovery of the often expensive or toxic catalysts, and potentially allows the adaptation of the immobilized catalysts to continuous flow type processes.

Table 1.5: Literature survey on asymmetric hydrogenation by heterogeneous catalysts

Catalyst[a]	Support	Substrate	Product	ee[b]	Ref
Ru-TsDPEN	polystyrene	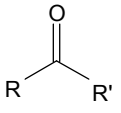	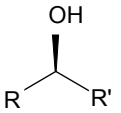	94	117
Ru-TsDPEN	Silica, MCM-41, SBA-15	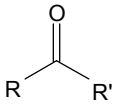	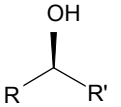	97	118
Rh-COD-(1*S*,2*S*)-DDEN	Polyurea	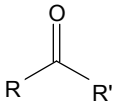	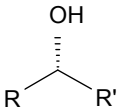	67	119
Rh-PrDACH	Mesoporous Ethane-silica	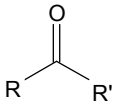	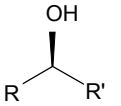	27	120
Ru-TsDPEN	Silica, MCM-41, SBA-15	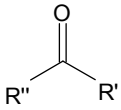	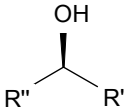	96	121
Ru-NOREPHE	SBA-15	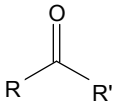	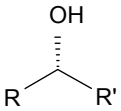	81	122
Ru-TsDPEN	Dendrimers	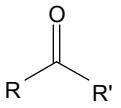	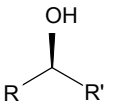	99	123
Ru-Bz-Ephedrine	Silica	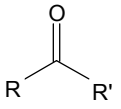	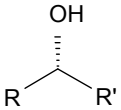	88	124

[a]DPEN = 1,2-diphenylethylenediamine; TsDPEN = [*N*-(*p*-toluenesulfonyl)-1,2-diphenylethylenediamine; COD = 1,5-cyclooctadiene, DDEN = *N*,*N*-dimethyl-1,2-diphenylethanediamine; NOREPHE = Norphederine; PrDACH = Propyl-diaminocyclohexane.
[b]Enantiomeric excess

Unfortunately, the immobilization of chiral catalysts often results in lower activities and enantioselectivities as compared to those observed for their homogeneous counterparts. A wide range of metals and ligand combinations have been demonstrated to effect the ATH reaction. The initial breakthrough in this area came in 1995 with the report from Ohkuma *et.al.*[116] on the use of chiral monotosylated diamine complexes for asymmetric transfer hydrogenation. But when factors like catalyst poisoning and product selectivity come into play, heterogenized homogeneous catalysts become distinctly and significantly beneficial.

1.6.4. Chiral amino alcohols for the enantioselective transfer hydrogenation Reaction

Many ligands have been reported for the enantioselective transfer hydrogenation of ketones, but chiral diamine and amino alcohols are the most common. A brief summary of the most notable homogeneous and heterogeneous chiral amino alcohol metal complexes in asymmetric transfer hydrogenation is presented below,

1.6.4.1. Homogeneous Amino alcohol ligands

The ligand-acceleration effect of simple racemic α-amino alcohols in Ru-catalysed transfer hydrogenation was observed by Noyori.[107] It is noteworthy that of all the ligands which Noyori has tested, α-amino alcohols have proved to afford the highest levels of acceleration to the reduction reactions (some 70-fold over the background rate). Monotosylated diamines gave the second-highest level of rate increase ca. 30-fold over background) whilst all others gave little more than a seven- to eightfold acceleration. The stereochemically rigid amino alcohols also work well in transfer hydrogenation in combination with Ru(II). In the case of (1R,2S)-(+)-cis-1-amino-2-

indanol, deletion of the methylene bridge (i.e. the use of phenylglycinol) results in a dramatic decrease of ee to 23 % thus emphasising the importance of the rigid structure.[108] The introduction of a two-methyl group adjacent to the hydroxy group in **22** (Table 1.3) resulted in a completely unselective reagent. Notably, the use of the ever-popular prolinol gave only an 8 % ee for the transfer hydrogenation of acetophenone.[109] Although α-amino alcohols give excellent results in terms of rate and enantioselectivity, they appear, in common with most other ligands, to be incompatible with the formic acid/triethylamine reduction system.

In addition to chiral diamines, β-amino alcohols are one of the most effective classes of chiral auxiliaries for asymmetric transfer hydrogenations. A variety of β-amino alcohols have been successfully used to generate active catalysts in situ with $[RuCl_2(p\text{-cymene})]_2$, providing moderate to excellent catalytic activity in the ATH reduction of acetophenone. Patti *et.al.* found that (R)-1-N-benzylamino-2-hydroxy-3-ferrocenyl propane provided a 94 % conversion and 70 % ee (R) in 3 h at room temperature. Through optimization of the ligand structure, they were generally able to improve the reaction rate and asymmetric induction by increasing the steric bulk around the amine moiety via N-alkylation. While examining the chiral directive effects of several substituted 2-amino ethanol and norephedrine-based ligands in ATH reactions, van Leeuwen reported that (1R,2S)-N-benzyl-norephedrine provided the highest asymmetric induction. Andersson *et.al.* were successful in developing highly active and selective catalysts from 2-azanorbornyl derivative. Reductions using 2-azanorbornyl derivative were fast, providing 96 % conversion to the alcohol and 96 % ee with a S/C ratio of 5000 in 90 min. Amino alcohol (1R,2S)-*cis*-1-aminoindan-2-ol was developed by Wills *et.al*. and has been evaluated for its effectiveness in the

reduction of various substrates. It should be pointed out that when amino alcohols were used as chiral directors in ATH reactions, the best results were achieved using isopropanol as the hydride source.

1.6.4.2. Heterogeneous Amino alcohol ligands

In the preparation of the immobilized version of the ephedrine derivative ligand[124] **(**with trimethoxysilyl substitution) was prepared as the starting material. Upon refluxing in toluene with a suspension of silica for 18 h, this precursor was immobilized on silica gel. The support could be further modified by reacting the thus formed supported catalyst with dimethyldimethoxysilane. As a result of this modification, the silanol hydroxyl groups on the silica support were protected as alkylsilanes. Alternatively, the immobilized catalyst can be prepared by the introduction of chloromethylphenyl groups on the silica followed by the capping of the silanol groups, and finally the introduction of the chiral amino alcohol moiety. The ruthenium catalyzed asymmetric transfer hydrogenation resulted in 88 % ee at 95 % conversion. Recovery of the catalyst was investigated by performing subsequent batch wise reactions, and the enantioselectivity remained unchanged in most cases.

1.6.5. (1R,2S)-(+)-cis-1-amino-2-indanol and 1S,2R-(+)-1,2-amino-1,2-diphenyl ethanol in enantioselective transfer hydrogenation reaction

The rigid (1R,2S)-(+)-cis-1-amino-2-indanol, 1S,2R-(+)-1,2-amino-1,2-diphenyl ethanol and their derivatives have become useful and effective chiral auxiliaries in several asymmetric synthetic processes because of their availability, ease of recovery, and the high degree of asymmetric induction that results. Very recently, Ghosh and co-workers have brilliantly demonstrated that, not only the C-1 amine, but also the C-

2 hydroxyl moiety of the aminoindanol, can be effectively utilized in several asymmetric synthetic processes because the rigid aminoindanol backbone has a highly defined chiral environment. The homogeneous (1R,2S)-(+)-cis-1-amino-2-indanol has been demonstrated to be an excellent ligand for the Ru(II)-catalyzed transfer hydrogenation of various aromatic ketones with propan-2-ol has conducted by Wills and co-workers[125], they have observed,

Table 1.6: Homogeneous Ru(II)-(1R,2S)-(+)-cis-1-amino-2-indanol catalyzed transfer hydrogenation of acetophenone

Arene	**Time (h)**	**Temp (^{o}C)**	**Yield (%)**	***ee* (%)**
Benzene	1.6	RT	68	69 (S)
Mesitylene	2	RT	73	82 (S)
p-cymene	1.5	RT	70	91 (S)
p-cymene	6.5	0	49	93 (S)
p-cymene	24	-20	47	90 (S)
p-cymene	72	-20	47	84 (S)
p-cymene	18	RT	72	83 (S)
p-cymene[a]	18	RT	77	68 (S)

0.25 mol % $[RuCl_2(\ p\text{-cymene})]_2$, [a]0.5 mol% $[RuCl_2(\ p\text{-cymene})]_2$, 1 mol% ligand.

The wide use of (1R,2S)-(+)-cis-1-amino-2-indanol and N-methylindanol in combination with Ru(II) and isopropanol in a series of ketones for ATH exhibited excellent yield and *ee* at milder reaction conditions.[126] They have used a variety of arenes in the ruthenium precursor in order to find out the effect on the reaction. They

have demonstrated that (1R,2S)-(+)-cis-1-amino-2-indanol is an excellent ligand for the control of asymmetric ruthenium-catalyzed transfer hydrogenation of ketones. The required ligand loading is very low (typically 1 mol %), and yields and enantiomeric excesses are generally excellent.

The overall kinetics of the asymmetric transfer hydrogenation of acetophenone to 1-phenylethanol using a Noyori type homogeneous Ru-catalyst with 1*R*,2*S*)-(+)-*cis*-1-amino-2-indanol was determined in a batch reactor with on-line FT-IR spectroscopy.[128] Analysis of the initial reaction rates using a design of experiments (DOE) strategy indicated that the reaction is an equilibrium reaction. In addition, the initial rate was also affected by the individual reaction products, an indication for product inhibition other than equilibrium effects. The concentration time curves were modeled using various empirical rate laws as well as a rate law based on a postulated mechanism by Noyori. The experimental data were successfully modeled using the latter, thereby supporting its validity. The equilibrium constant of the reaction was found to be about 0.19 at 33°C. The rate law and equilibrium data were applied to model a typical batch reactor setup. The equilibrium conversion of acetophenone is a strong function of the initial acetophenone concentration, with low concentrations leading to high equilibrium conversions.

Noyori reported[128] the use of various chiral 2-amino-1,2-diphenylethanol compounds with up to 92 % ee and greater than 90 % yield with structure. It is noteworthy that it is permitted the reduction of cyclohexylmethyl ketone with 75 % *ee*, a particularly high ee value for that type of substrate.

This ATH of aryl ketones by formate in water with catalysts derived from Ru(II), Rh(III) and Ir(III) complexes of (1*R*,2*S*)-(+)-*cis*-1-amino-2-indanol (AIL) and

(1S,2R)-(+)-2-amino-1,2-diphenylethanol (DPEA), showing that it is feasible in water.[130] Compared with reduction by M-TsDPEN in aqueous formate, the enantioselectivities were lower, however. The performance of the amino alcohol catalysts was significantly influenced by the choice of reduction system. The reaction was sluggish when aqueous HCOOH–NEt_3 of low *p*H was employed; but when performed in water using HCOONa as a hydrogen donor, it gave much better conversions and enantioselectivities. Indeed the reaction rates correlate with the solution *p*H values and there appears to be a *p*H window for optimal rates. Among the three metals, Ir(I) catalysts exhibited a higher activity than either Ru(II) or Rh(III) but furnished a lower enantioselectivity, while the Ru(II) catalysts led to better enantioselectivities. The performance of the amino alcohol ligands may be related to their dissociation from the metal centers in aqueous solution, and could be further improved using other amino alcohols, which are readily available.

Table 1.7: ATH of Ru(II)-(1*R*,2*S*)-(+)-*cis*-1-amino-2-indanol (AIL) and Ru(II)-(1S,2R)-(+)-2-amino-1,2-diphenylethanol (DPEA) in Formic acid/Triethylamine mixture

Catalyst	F/T ratio	Time (h)	Yield (%)	*ee* (%)
Ru-AIL	1.8/1	42	33	45
	1/1.7	40	58	45
Rh-AIL	1.8/1	48	60	14
	1/1.7	150	90	87
Ir-AIL	1.8/1	48	5	3
	1/1.7	48	17	55
Ru-DPEA	1.8/1	72	11	23
	1/1.7	40	33	52
Rh-DPEA	1.8/1	20	3	37
	1/1.7	20	51	56
Ir-DPEA	1.8/1	48	11	23
	1/1.7	1.5	100	55

Homogeneous N-benzyl-(1R,2S)-(-)-2-amino-1,2-diphenylethanol has been synthesized to optimize the bulky substituents on the nitrogen atom by reek *et.al.*[130] It is used in the transfer hydrogenation reaction of acetophenone at room temperature using a 0.1 M substrate solution and $[RuCl_2(p\text{-cymene})]_2$ and metal precursor. It is observed that the catalytic system exhibited a conversion of 25 % within 20 h with an ee of 20 % indicates the unsupporting nature of benzyl group in the ligand.

The silica-immobilized ruthenium complex of NH-3-(trimethoxysilyl) benzyl-(1S,2R)-(+)-2-amino-1,2-diphenylethanol complex showed very poor performance in the asymmetric transfer hydrogenation of acetophenone in batchwise catalytic runs.[131] Under optimized conditions, this process converts a constant flow of acetophenone into phenylethanol in 9 % yield and 58 % ee. It is surprisingly the catalyst exhibited 58 % ee which is far more selective than the homogeneous analogue for which an ee of 20 % had been reported. The high stability of this system is due to immobilization can give rise to improved catalyst selectivity. In this respect, effective site isolation due to the immobilization of the ruthenium catalyst was found to be of great importance.

1.7. SCOPE OF THIS THESIS

This introduction clearly shows the interest in the catalytic asymmetric transfer hydrogenation (ATH) reaction. The effort that various authors have made to develop chiral catalytic systems for this transformation has been rewarded by obtaining excellent catalytic performances. It is also noteworthy that the intense dedication to develop an environmental and economic viability of chemical transformations through the design of catalytic systems that can be recycled.

At this point, we planned to develop in this thesis the following aspects:

1) To explore the extent of heterogenization process in asymmetric catalysis.

The catalytic behavior of heterogeneous complexes moreover depends on the mode of anchoring to the support and the chemical nature of the tethering molecule. With respect to its special orientation, the accessibility of a metal center for reaction system will differ. The redox properties of active metal center also may change with respect to the inductive properties of the anchoring molecule.

2) To utilize different chiral amino alcohols for making immobilized metal complexes.

Chiral amino alcohols are excellent ligands for asymmetric transfer hydrogenation in combination with suitable metals under suitable reaction conditions. The β-amino alcohol-based Ru(II) catalysts give rise to some of the best results for the ATH of ketones in terms of enantioselectivities and catalytic activities in 2-propanol. We have selected amino alcohols having fused and strainless ring system.

3) To understand how high activity and selectivity can be generated throughout the asymmetric transfer hydrogenation process.

To create an overall picture of the various influences on the catalytic asymmetric transfer hydrogenation reaction, we take into account a model reaction where the substrate is acetophenone, the catalytic system is a bidentated ruthenium complex (sandwich catalyst), the source of chirality is the fused or flexible amino alcohol (N, O). The source of active metal center is a dimeric organo-ruthenium chloride. To

facilitate the analysis, we fixed the reaction conditions and enantiomerically reduced the carbonyl compounds to enantiopure alcohols, before initiating the following systematic study:

4) Extension of the accumulated knowledge on, how heterogeneous chiral catalysts can utilize as an echo friendly system under water as solvent.

Asymmetric reaction in aqueous media has been energetically studied because water is a safe, cheap, and environmentally friendly media. Novel catalytic systems that enable the use of water as a solvent in the asymmetric transfer hydrogenation are not well developed. The catalytic reaction occurs at the interface between water and the organic layer because of the insolubility of organic substrates in water. Thus, the catalytic activity and/or enantioselectivity in aqueous solution were usually low compared to those of the homogeneous catalytic system.

5) Design of a chiral catalytic system that can be easily recovered from the products and reused in the catalytic asymmetric transfer hydrogenation reaction, and which responds to the challenge of improving the environmental and economic viability of the asymmetric process.

The heterogenization facilitates the separation of the catalyst from reagents and products, simplifies the efficient recovery of the often expensive or toxic catalysts, and potentially allows the adaptation of the immobilized catalysts to continuous flow type processes.

1.8. AIM OF THIS STUDY

The primary goal of the research described in this thesis is the design and development of new heterogeneous ruthenium complexes for asymmetric transfer hydrogenation of prochiral aromatic carbonyl compounds. The new catalysts should exhibit high selectivity towards ATH of a variety of carbonyl compounds in 2-propanol as solvent and anhydrous potassium hydroxide as base for initiating the reaction. A second objective has been the modification of the chiral catalyst, in order to achieve better enantioselectivity and catalytic activity by varying the metal source, reaction condition *etc*. The research has concentrated on the modification and utilization of homogeneous catalyst which is moderately active towards the asymmetric transfer hydrogenation of prochiral ketones. The heterogeneous chiral complexes have been synthesized, characterized and tested in the asymmetric transfer hydrogenation reaction. Here we have used two different types of chiral ligands having fused or flexible ring system. The catalytic activity and enantioselectivity of the catalysts were screened with various organic substrates under various reaction parameters also studied.

The outline of this thesis is given below:

Chapter 1 presents brief history of catalyst and the phenomenon of catalysis. The information about development and applications of various porous materials has been stated. The general introduction about various physicochemical aspects of mesoporous had been mentioned. The different characteristic properties of these materials, synthesis parameters, formation mechanisms, different approaches for surface-functionalization, characterization techniques and the previous reports of

various asymmetric hydrogenation catalysts including homogenous and heterogeneous are discussed in brief. The scope and objectives of the present work have been outlined at the end of this chapter.

Chapter 2 deals with the functionalization of SBA-15 with 3-chloropropyltrimethoxy silane, (4-chloromethyl)phenyltrimethoxysilane and 2-(4-chlorosulphonylphenyl)ethyl trimethoxysilane and further immobilization of chiral ligand, (1R,2S)-(+)-*cis*-1-amino-2-indanol followed the preparation of chiral heterogeneous ruthenium complexes by using two metal precursors such as $[RuCl_2(benzene)]_2$ and $[RuCl_2(p\text{-cymene})]_2$. The materials were characterized by XRD, ^{29}Si and ^{13}C CP MAS NMR, N_2 sorption technique, FT-IR, UV-Vis, AAS, XPS, TEM and SEM. The main emphasis was given on the local environment of the metal species.

Chapter 3 deals with the catalytic activity of the synthesized homogeneous and heterogeneous chiral ruthenium complexes in the asymmetric transfer hydrogenation of simple aromatic carbonyl compounds (ketones) under mild reaction conditions. The transfer hydrogenation has done using various reaction conditions including different substrate, different temperature, various bases, duration of run *etc*.

Chapter 4 deals with the preparation, characterization and catalytic activity of homogeneous ruthenium (II) complexes of NH-propyl, NH-benzyl and NH-(*p*-tosyl) derivatives of (1R,2S)-(+)-*cis*-1-amino-2-indanol. The materials were characterized by liquid ^1H NMR & ^{13}C NMR, FT-IR and UV-Vis spectroscopy. The main emphasis was given on the local environment of the metal species. The catalytic activity of

these synthesized homogeneous chiral ruthenium complexes in the ATH of simple aromatic carbonyl compounds (ketones) under mild reaction conditions. The transfer hydrogenation has done using various reaction conditions.

Chapter 5 deals with the preparation of homogeneous and heterogeneous chiral ruthenium complexes of (1S,2R)-(+)-1-amino-1,2-diphenylethanol, by first immobilization over 1-bromopropane and 3-chloropropyltriethoxysilane functionalized SBA-15 respectively, there after the complexation with two metal precursors such as $[RuCl_2(benzene)]_2$ and $[RuCl_2(p\text{-cymene})]_2$. The materials were characterized by various characterization techniques. The complete characterizations of these samples were carried out by various spectroscopic techniques like XRD, liquid ^{1}H NMR ^{29}Si and ^{13}C CP MAS NMR, N_2 sorption technique, FT-IR, UV-Vis, ICP-AES. The catalytic activities of synthesized heterogeneous chiral ruthenium complexes were applied in the asymmetric transfer hydrogenation of a number of simple aromatic ketones in 2-propanol under mild reaction conditions. The transfer hydrogenation has done using various reaction conditions including different substrate, different temperature, various bases, duration of run etc has conducted in order to get an insight about the kinetics of the reaction

Chapter 6 summarizes the results obtained and the basic findings of the present study. The scope of the future work is also discussed at the end of this chapter.

1.9. REFERENCES

1. K. Mislow, J. Siegel, *J. Am. Chem. Soc.* **1984**, *106*, 3319.
2. *Asymmetric Catalysis on Industrial Scale* (Eds.: H. U. Blaser, E. Schmidt), Wiley-VCH, Weinheim, **2004**.
3. S. C. Stinson, *Chem. Eng. News.* **2001**, *79* (40), 79.
4. *Principles and Practice of Heterogeneous Catalysis* (Eds.: J. M. Thomas, W. J. Thomas), Wiley-VCH, Weinheim, **1997**.
5. (a) *Chiral Reactions in Heterogeneous Catalysis*, (Eds.: V. Dubois, G. Jannes), Plenum, New York, **1995**; (b) D. C. Sherrington, Catal. Today **2000**, 57, 87; (c) H.-U. Blaser, B. Pugin, M. Studer in *Chiral Catalyst Immobilization and Recycling* (Eds.: D. E. De Vos, I. F. J. Vankelecom, P. A. Jacobs), Wiley-VCH, Weinheim, **2000**, p.1.
6. (a) *Comprehensive Asymmetric Catalysis* (Eds.: E. N. Jacobsen, A. Pfaltz, H. Yamamoto), Springer, Berlin, **1999**; (b) *Catalytic Asymmetric Synthesis*, 2nd ed. (Eds.:I. Ojima), Wiley, New York, **2000**; (c) T. P. Yoon, E. N. Jacobsen, *Science*. **2003**, *299*, 1691.
7. H. U. Blaser, F. Spindler, M. Studer, *Appl. Catal. A.* **2001**, *221*, 119.
8. A. Weissberg, B. Halak, M. Portnoy, *J. Org. Chem.* **2005**, *70*, 4556.
9. B. Pugin, *J. Mol. Catal. A.* **1996**, *107*, 273.
10. Manassen, J. in *Catalysis, Progress in Research*, Eds.: Basolo, F; Burwell Jr., R. E., Plenum Press: New York, **1973**, 177
11. Herrmann, W. A.; Cornils, B. *Angew. Chem. Intl. Ed.* **1997,** *36*, 1048.
12. Cole-Hamilton, D. J. *Science* **2003**, *299*, 1702.
13. R.Selke, K.Häupke, H.W. Krause, *J. Mol. Catal.* **1989**, *56*, 315.

14. S.J.Shuttleworth, S.M.Allin, P.K.Sharma, *Synthesis* **1997**, 1217

15. H.U.Blaser, *Tetrahedron: Asymmetry* ***1991***, *2*, 843.

16. F.Fache, E.Schulz, M.L.Tommasino, M.Lemaire, *Chem. Rev*. ***2000***, *100*, 2159.

17. O.Piccolo, *Chim. Ind* ***1998***, *80*, 1177.

18. (a) D.Pini, A.Mandoli, A.Petri, P.Salvadori, *Chim. Ind* ***1999***, *81*, 189; (b) P.Salvadori, D.Pini, A.Petri, *Synlett* ***1999***, *8*, 1181.

19. B.Pugin, H.Y.Blaser, *In Comprehensive Asymmetric Catalysis*; Eds. E.N.Jacobsen, A.Pfaltz, H.Yamamoto, Springer: Berlin **1999**, *Vol.3*.

20. C.Bolm, A.Gerlach, *Eur. J. Org. Chem.* **1998**, 21.

21. C.U.Pittman, *In Comprehensive Organometallic Chemistry*; Eds. G.Wilkinson, F.G.A.Stone, E.W.Abel, Pergamon: Oxford **1983**, *ch.55*.

22. (a) H.U.Blaser, B.Pugin, *In Chiral Reactions in Heterogeneous Catalysis*; Eds. G.J.Jannes, V.Dubois, Plenum Press: New York **1995**; (b) D.E.De Vos, I.F.J.Vankelecom, P.A.Jacobs, *In Chiral Catalyst Immobilization and Recycling*; Wiley-VCH: Weinheim, **2000**.

23. B.Clapham, T.S.Reger, K.D.Janda, *Tetrahedron* **2001**, *57*, 4637.

24. C.Saluzzo, R.ter Halle, F.Touxhard, F.Fache, E.Schulz, M.Lemaire, *J. Organomet. Chem.* **2000**, *30*, 603.

25. K.Soai, S.Niwa, *Chem. Rev.* **1992**, *92*, 833.

26. T.Wasaki, Y.Aoiuma, *J. Am. Chem. Soc.***1999**, *121*, 4793.

27. C.J.Brinker, G.W.Scherer, *In Sol-gel Science, the Physics and Chemistry of Sol-gel Processing;* Academic Press **1999**.

28. J.M.Thomas, S.Ramdas, G.R.Millward, J.Klinowsky, M.Audier, J.Conzalex-Calbet, C.A.Fyfe, *J. Solid*. *State Chem.*, **1982**, *45*, 368.

29. A.Corma, *Chem. Rev.* **1997**, *97*, 2373.

30. S.Scurrell, *In La Chimica e l'industria* **1979**, *69*, 219.

31. M.Berry, R.K.Champaneria, J.A.S.Howell, *J. Mol. Catal.* **1986**, *37*, 243.

32. M.E.Davis, J.Schnitzer, J.A.Rosin, *J. Mol. Catal.* **1987**, *39*, 243.

33. J.M.Fraile, J.I.García, J.A.Mayoral, *Chem. Commun.* **1996**, 1319.

34. A.Guerte, M.Iglesias, F.Sánchez, *J. Organomet. Chem.* **1999**, *58*, 186.

35. F.Cavani, F.Trifiro, A.Vaccari, *Catal. Today* **1991**, *11*, 173.

36. (a) Y.Yermakow, I.Yu, B.N.Kuznetsow, V.A.Zakharow, *In Studies in surface science and catalysis*; Elveir scientific publishing company: Amsterdam **1981**, *vol.8*; (b) T.J.Pinnavaia, *Science* **1983**, *220*, 365; (c) J.M.Andersen, *Platinium Metals Rev.* **1997**, *41*, 132; (d) P.Gamez, B.Donjic, F.Fache, M.J.Lemaire, *J. Chem. Soc., Chem. Commun.* **1994**, 1417.

37. C. T. Kresge, M. E. Leonowicz, W. J. Roth, J. C. Vartuli, J. S. Beck, *Nature* **1992**, *359*, 710.

38. J. S. Beck, J. C. Vartuli, W. J. Roth, M. E. Leonowicz, C. T. Kresge, K. D. Schmitt, C. T. -W. Chu, D. H. Olson, E. W. Sheppard, S. B. McCullen, J. B. Higgins, J. L. Schlenker, *J. Am. Chem. Soc.* **1992**, *114*, 10834.

39. J. S. Beck, J. C. Vartuli, G. J. Kennedy, C. T. Kresge, W. J. Roth, S. E. Schramm, *Chem. Mater.* **1994**, *6*, 1816.

40. C. F. Cheng, H. He, W. Zhou, J. Klinowski, *Chem. Phys. Lett.* **1995**, *244*, 117.

41. C.Y. Chen, S. L. Burkett, H. -X. Li, M. E. Davis, *Microporous Mater.* **1993**, *2*, 27.

42. (a) A. Monnier, F. Schuth, Q. Huo, D. Kumar, D. I. Margolese, R. S. Maxwell, G. D. Stucky, M. Krishnamurthy, P. Petroff, A. Firouzi, M. Janicke, B. F. Chmelka, *Science*. **1993**, *261*, 1299. (b) G. D. Stucky, A. Monnier, F. Schuth, Q. Huo, D. I. Margolese, D. Kumar, M. Krishnamurthy, P. Petroff, A. Firouzi, M. Janicke, B. F. Chmelka, *Mol. Cryst. Liq. Cryst.* **1994**, *240*, 187.

43. S. Inagaki, Y. Fukushima, K. Kuroda, J. Chem. Soc., Chem. Commun. **1993**, 680.

44. (a) A. Firouzi, D. Kumar, L. M. Bull, T. Besier, P. Sieger, Q. Huo, S. A. Walker, J. A. Zasadzinski, C. Glinka, J. Nicol, D. I. Margolese, G. D. Stucky, B. F. Chmelka, *Science* **1995**, *267*, 1138. (b) A. Firouzi, F. Atef, A. G. Oertli, G. D. Stucky, B. F. Chmelka, *J. Am. Chem. Soc.* **1997**, *119*, 3596.

45. (a) Q. Huo, D. I. Margolese, U. Ciesla, P. Feng, P. Sieger, R. Leon, P. Petroff, F. Schuth, G. D. Stucky, *Nature* **1994**, *368*, 317. (b) Q. Huo, D. I. Margolese, U. Ciesla, D. G. Demuth, P. Feng, T. E. Gier, P. Sieger, A. Firouzi, B. F. Chmelka, F. Schuth, G. D. Stucky, *Chem. Mater.* **1994**, *6*, 1176.

46. (a) P. T. Tanev, T. J. Pinnavaia, *Chem. Mater*. **1996**, *8*, 2068. (b) P. T. Tanev, T. J. Pinnavaia, Science **1996**, *271*, 1267. (c) P. T. Tanev, T. J. Pinnavaia, *Science* **1995**, *267*, 865.

47. D. M. Antonelli, J. Y. Ying, *Angew. Chem. Int. Ed*. **1996**, *35*, 426.

48. W. H. Bragg, W. L. Bragg, *The Crystalline State*, Vol. 1, McMillan, New York, **1949**.

49. S. Biz, M. Occelli, *Catal. Rev.-Sci. Eng.* **1998**, *40*, 329.

50. G. Bergeret, in: *Handbook of Heterogeneous Catalysis*, Vol. 2, Eds: G. Ertl, H. Knozinger, J. Weitkamp, Wiley-VCH, Weinheim, **1997**, pp. 464–475.

51. R. C. Rau, in: *Advances in X-Ray Analysis*, Vol. 5, Ed: W. M. Mueller, Sir Isaac Pitman and Sons Ltd., London, **1962**, pp. 104–116.

52. C. K. Jorgensen, *Absorption Spectra and Chemical Bonding in Complexes*, Pergamon, New York, **1962**.

53. G. Kortum, *Reflectance Spectroscopy*, Springer, Berlin, **1969**.

54. M. Faraday, *Philos. Trans*. **1857**, *147*, 145.

55. G. Mie, *Ann. Physik* **1908**, *25*, 377.

56. G. C. Papavassiliou, *Prog. Solid State Chem*. **1980**, *12*, 185.

57. (a) S. Link, M. A. El-Sayed, *J. Phys. Chem. B* **1999**, *103*, 4212. (b) C. Burda, T. Green, C. Landes, S. Link, R. Little, J. Petroski, M. A. El-Sayed, in: *Characterization of Nanophase Materials*, Ed: Z. L. Wang, Wiley-VCH, Weinheim, **2000**, Chapter 7, pp. 197–241.

58. P. R. Griffiths, J. A. De Haseth, *Fourier Transform Infrared Spectrometry*, John Wiley and Sons Inc., New York,**1986**.

59. C. C. Freyhardt, M. Tsapatsis, R. F. Lobo, K. J. Balkus, M. E. Davis, *Nature,* **1996**, *381*, 295.

60. P. A. Jacobs, W. Y. Martier, *Zeolites*, **1982**, *2*, 226.

61. J. Ryczkowski, *Catal. Today*, **2001**, *68*, 263.

62. F. A. Rushworth, D. P. Tunstall, *Nuclear Magnetic Resonance*, Gordon and Breach Science Publishers Ltd., London, **1973**.

63. W. W. Paudler, *Nuclear Magnetic Resonance*: *General Concepts and Applications*, John Wiley and Sons Inc., New York, **1987**.

64. M. Mehring, *High Resolution NMR Spectroscopy in Solids*, Springer-Verlag, Berlin, **1976**.

65. G. Engelhardt, D. Michel, *High-Resolution Solid-State NMR of Silicates and Zeolites*, John Wiley and Sons Ltd., Chichester, **1987**.

66. G. Engelhardt, in: *Handbook of Heterogeneous Catalysis*, Vol. 2, Eds: G. Ertl, H. Knozinger, J. Weitkamp, Wiley-VCH, Weinheim, **1997**, pp. 525–539.

67. C. S. Fadley, in: *Electron Spectroscopy: Theory, Techniques and Applications*, Vol. 2, Eds: C. R. Brundle, A. D. Baker, Academic Press, New York, **1978**, pp. 1–156.

68. W. N. Delgass, T. R. Hughes, C. S. Fadley, *Catal. Rev*. **1970**, *4*, 179.

69. 70. W. F. Egelhoff Jr., *Surf. Sci. Rep*. **1987**, 6, 253.

70. J. W. Robinson, *Atomic Absorption Spectroscopy*, Marcel Dekker, New York, **1975**.

71. G. L. Moore, *Introduction to Inductively Coupled Plasma Atomic Emission Spectrometry*, Elsevier, Amsterdam, **1988**.

72. G. Lawes, *Scanning Electron Microscopy And X-Ray Microanalysis*, John Wiley and Sons Ltd., Chichester, **1987**.

73. D. E. Newbury, D. C. Joy, P. Echlin, C. E. Fiori, J. I. Goldstein, *Advanced Scanning Electron Microscopy and X-Ray Microanalysis*, Plenum Press, New York, **1986**.

74. J. R. Fryer, *Chemical Applications of Transmission Electron Microscopy*, Academic Press, San Diego, **1979**.

75. (a) J. M. Thomas, O. Terasaki, P. L. Gai, W. Zhou, J. Gonzalez-Calbet, *Acc. Chem. Res*. **2001**, *34*, 583. (b) V. Alfredsson, M. Keung, A. Monnier, G. D. Stucky, K. K.Unger, F. Schuth, *J. Chem. Soc., Chem. Commun*. **1994**, 921.

76. Z. L. Wang, in: *Characterization of Nanophase Materials*, Ed: Z. L. Wang, Wiley-VCH, Weinheim, **2000**, Chapter 3, pp. 37–80.

77. S. Brunauer, P. H. Emmett, E. Teller, *J. Am. Chem. Soc*. **1938**, *60*, 309.

78. E. P. Barrett, L. G. Joyner, P. P. Halenda, *J. Am. Chem. Soc*. **1951**, *73*, 373.

79. C. -Y. Chen, H. -X. Li, M. E. Davis, *Microporous Mater*. **1993**, *2*, 17.

80. J. Manassen, in: *Catalysis, Progress in Research*, Eds: F. Basolo, R. E. Burwell Jr.,Plenum Press, New York, **1973**, p. 177.

81. D. E. De Vos, M. Dams, B. F. Sels, P. A. Jacobs, *Chem. Rev*. **2002**, *102*, 3615.

82. P. Ermert, in: *Solid-Supported Combinatorial and Parallel Synthesis of Small-Molecular-Weight Compound Libraries*, Eds: D. Obrecht, J. M. Villalgordo, Elsevier, Oxford, **1998**, pp. 44–84.

83. A. N. Collins, G. N. Sheldrake, J. Crosby (Eds), *Chirality in Industry: The Commercial Manufacture and Applications of Optically Active Compounds*, Wiley, New York, **1997**

84. I.Ojima (Ed), *Catalytic Asymmetric Synthesis*, *2nd ed*., Wiley, New York, **2000**

85. C. E. Song, S. Lee, *Chem Rev*. **2002**, *102*, 3495.

86. (a) R. A. Johnstone, A. H. Wilby, *Chem. Rev*. **1985**, *85*, 129; (b) S. Gladiali, G. Mestroni, *Transition Metals for Organic Synthesis*, (Eds.: C. Bolm, M. Beller), Wiley- VCH, Weinheim, **1998**, Vol. 2, p. 81; (c) G. Zassinovich, G. Mestroni, S. Gladiali, *Chem. Rev*. **1992**, *92*, 1051.

87. Ohkuma, T., Ooka, H., Hashiguchi, S., Ikariya, T. and Noyori, R. *Practical Enantioselective Hydrogenation of Aromatic Ketones*. *J. Am. Chem. Soc*. **1995**, *117*, 2675–2616.

88. (A) Bianchi, M.; Matteoli, U.; Menchi, G.; Frediani, P.; Pratesi, S.; Piacenti, F.; Botteghi, C. *J. Organomet. Chem*. **1980**, *198*, 73. (b) M. J. Palmer, M. Wills.; *Tetrahedron: Asymmetry* **1999,** *10,* 2045–2061.

89. Gamez, P.; Dunjic, B.; Lemaire, M. *J. Org. Chem*. **1996**, 61, 5196.

90. Spogliarich, R.; Kaspar, J.; Graziani, M.; Morandini, F. *J. Organomet. Chem*. **1986**, *306*, 407.

91. Gamez, P.; Fache, F.; Mangeney, P.; Lemaire, M. *Tetrahedron Lett*. **1993**, *34*, 6897.

92. Botteghi, C.; Chelucci, G.; Chessa, G.; Delogu, G.; Gladiali, S.; Soccolini, F. J. Organomet. Chem. **1986**, *304*, 217.

93. Gladiali, S.; Pinna, L.; Delogu, G.; De Martin, S.; Zassinovich, G.; Mestroni, G. Tetrahedron: Asymmetry. **1990**, *1*, 635.

94. Yang, H.; Alvarz-Gressier, M.; Lugan, N.; Mathieu, R. Organometallics **1997**, *16*, 1401.

95. Zassinovich, G.; Bettella, R.; Mestroni, G.; Bresciani-Pahor, N.; Geremia, S.; Randaccio, L. *J. Organomet. Chem*. **1989**, *370*, 187.

96. Hashiguchi, S.; Fujii, A.; Takehara, J.; Ikariya, T.; Noyori, R. *J. Am. Chem. Soc*. **1995**, *117*, 7562.

97. Fujii, A.; Hashiguchi, S.; Uematsu, N.; Ikariya, T.; Noyori, R. *J. Am. Chem. Soc*. **1996**, *118*, 2521.

98. (a) Mashima, K.; Abe, T.; Tani, K. *Chem. Lett*. **1998**, 1199. (b) Mashima, K.; Abe, T.; Tani, K. *Chem. Lett*. **1998**, 1201.

99. Müller, D.; Umbricht, G.; Weber, B.; Pfaltz, A. Helv. *Chim. Acta.* **1991**, *74*, 232.

100. Inoue, S. I.; Nomura, K.; Hashiguchi, S.; Noyori, R.; Izawa, Y. *Chem. Lett*. **1997**, 957.

101. Jiang, Y.; Jiang, Q.; Zhang, X. *J. Am. Chem. Soc*. **1998**, *120*, 3817.

102. Schwick, L.; Irelan, T.; Puntener, K.; Knochel, P. *Tetrahedron: Asymmetry*. **1998**, *9*, 1143.

103. Evans, D. A.; Nelson, S. G.; Gagné, M. R.; Muci, A. R. *J. Am. Chem. Soc*. **1993**, *115*, 9800.

104. Touchard, F.; Fache, F.; Lemaire, M. *Tetrahedron: Asymmetry***, 1997**, *8*, 3319.

105. Püntener, K.; Schwink, L.; Knochel, P. *Tetrahedron Lett*. **1996**, *37*, 8165.

106. Murata, K.; Ikariya, T.; Noyori, R. *J. Org. Chem*. **1999**, *64*, 2186.

107. Takehara, J.; Hashiguchi, S.; Fujii, A.; Inoue, S.; Ikariya, T.; Noyori, R. *J. Chem. Soc., Chem. Commun*. **1996**, 233.

108. 109. Palmer, M.; Walsgrove, T.; Wills, M. *J. Org. Chem*. **1997**, *62*, 5226.

109. Alonso, D. A.; Guijarro, D.; Pinho, P.; Temme, O.; Andersson, P. G. *J. Org. Chem*. **1998**, *63*, 2749.

110. Langer, T.; Helmchen, G. *Tetrahedron Lett*. **1996**, *37*, 1381.

111. Sammakia, T.; Strangeland, E. L. *J. Org. Chem*. **1997**, *62*, 6104.

112. Jiang, Y.; Jiang, Q.; Zhu, G.; Zhang, X. *Tetrahedron Lett*. **1997**, *38*, 6565.

113. Jiang, Y.; Jiang, Q.; Zhu, G.; Zhang, X. *Tetrahedron Lett*. **1997**, *38*, 215.

114. Gao, J.-X.; Ikariya, T.; Noyori, R. *Organometallics,* **1996**, *15*, 1087.

115. Krasik, P.; Alper, H. *Tetrahedron,* **1994**, *50*, 4347.

116. C. E. Song, S. Lee, *Chem Rev.* **2002**, *102*, 3495.

117. ter Halle, R.; Schulz, E.; Lemaire, M. *Synlett* **1997**, 1257.

118. Pei-Nian Liu, Pei-Ming Gu, Jin-Gen Deng, Yong-Qiang Tu, and Ya-Ping Ma Eur. *J. Org. Chem*. **2005**, 3221–3227

119. Locatelli, F.; Gamez, P.; Lemaire, M. *J. Mol. Catal. A: Chem.* **1998**, *135*, 89.

120. Dongmei Jiang, Qihua Yang, Jie Yang, Lei Zhang, Guiru Zhu, Weiguang Su, and Can Li. *Chem. Mater*. **2005,** *17*, 6154-6160

121. Pei Nian Liu,a Jin Gen Deng,b Yong Qiang Tu and Shao Hu Wang. *Chem. Commun*., **2004**, 2070–2071

122. Jin, M.J.; Sarkar, M. S.; Takale, V.B.; Park, S.E.; *Bull. Korean Chem. Soc*. 26, **2005**, *11*, 1671-1672.

123. Chen, Y. C.; Wu, T. F.; Deng, J. G.; Liu, H.; Jiang, Y. Z.; Choi, M. C. K.; Chan, A. S. C.; *Chem. Commun.* **2001**, 1488.

124. Sandee, A. J.; Petra, D. G. I.; Reek, J. N. H.; Kamer, P. C. J.; van Leeuwen, P. W. N. M. *Chem. Eur. J.* **2001**, *7*, 1202.

125. Matthew J. Palmer, Jennifer A. Kenny, Tim Walsgrove, Aparecida M. Kawamoto and Martin Wills. *J. Chem. Soc., Perkin Trans*. **2002**, *1*, 416–427.

126. M. Palmer, T. Walsgrove and M. Wills, *J. Org. Chem.*, **1997**, *62*, 5226.

127. Ronald V. Wisman, Johannes G. de Vries, Berth-Jan Deelman, and Hero J. Heeres. *Organic Process Research & Development.* **2006**, *10*, 423-429.

128. Takehara, J.; Hashiguchi, S.; Fujii, A.; Inoue, S.; Ikariya, T.; Noyori, R. *J. Chem. Soc., Chem. Commun*. **1996**, 233.

129. Xiaofeng Wu, Xiaohong Li, Matthew McConville, Ourida Saidi, Jianliang Xiao,; *Journal of Molecular Catalysis A: Chemical***. 2006**, *247*, 153–158.

130. Danielle G. I. Petra, Paul C. J. Kamer, Piet W. N. M. van Leeuwen, Kees Goubitz, Arjen M. Van Loon, Johannes G. de Vries, and Hans E. Schoemaker; *Eur. J. Inorg. Chem.* **1999**, 2335-2341

131. D. G. I. Petra, P. C. J. Kamer, P. W. N. M. van Leeuwen, K. Goubitz, A. M. van Loon, J. G. de Vries, H. E. Schoemaker, *Eur. J. Inorg. Chem*. **1999**, *12*, 2335.

Chapter 2

Synthesis, Characterization & Surface Modification of SBA-15

2.1. INTRODUCTION

The synthesis of ordered mesoporous materials in 1992 sparked worldwide interest in the field of heterogeneous catalysis and separation science.[1-3] The excitement began with the discovery of hexagonally ordered mesoporous silicate structures by Mobil Corporation (M41S materials).[4] They possessed extremely high surface areas and easily accessible, uniform pore sizes. Most importantly the pore sizes exceeded those attainable in zeolites and they could be tuned in the nanometer range by choosing an appropriate surfactant templating system, sometimes with co-solvent or swelling agent. However, the poor hydrothermal stability of such materials has restricted their applications. This placed an emphasis on the search for new structures with new framework compositions, which recently resulted in the synthesis of ordered, hydrothermally stable mesoporous silica, SBA-15,[5,6] thus providing an opportunity for the development of a wide range of applications in the fields of adsorption, catalysis, and advanced materials. To extent the applicability of such materials, it is necessary to modify the surface by organic functional groups for anchoring metals and metal complexes. Several routes are described in the literature for modifying interior pore surfaces in mesoporous solids.[7-10] Grafting of functional organosilanes by using surface hydroxyl groups as anchor points has been widely used. The catalytically active groups can be present in the silane, which are attached to the pore walls, or they can be introduced by subsequent post-synthesis reactions. This can simplify the highly precious catalyst recovery by simple filtration or centrifugation of the reaction mixture after use. Mesoporous materials can offer many attractive features for the heterogenization of homogeneous complexes including uniform large pore size, high surface area, insolubility in organic solvents and inert to many chemical substrates.

In post synthesis method organo-functionalization of the internal surfaces of mesoporous silicates can be achieved by covalent grafting of various organic species on the channel walls.[11]

The grafting process has been widely applied to anchor desired organic functional groups *via* condensation with surface silanol groups of the mesoporous silicate. However, it is somewhat difficult to control the concentration and distribution of organic moieties in the silicate surface mainly due to non-uniform presence of silanols groups in different mesoporous samples.[12] Silanol groups are known to be highly accessible on the external surface towards functionalization.[13] Thus grafting on the external surface can be minimized by passivating the external silanol groups before functionalization of those on the internal surface.[14]

In the preceding chapter, the synthesis mechanism of mesoporous materials, various complex immobilization methods and the available reports in the field of heterogeneous asymmetric transfer hydrogenation by (1R,2S)-(+)-*cis*-1-amino-2-indanol and 1S,2R-(+)-1,2-amino-1,2-diphenyl ethanol have been reviewed. This chapter will present the experimental data regarding (i) the synthesis of siliceous mesoporous SBA-15material, (ii) surface modification of this material by different organic functional groups, *viz*., propylchloro (–$(CH_2)_3$-Cl), benzylchloro (-C_6H_5-CH_2-Cl) and 2-(4-chlorosulphonylphenyl)ethyl- (-C_2H_4-C_6H_4-SO_2-Cl) through post grafting route, and (iii) the heterogenization of chiral amino alcohol ligand, (1R,2S)-(+)-*cis*-1-amino-2-indanol. Additionally the successful formation of the products has been confirmed by different physicochemical characterization techniques also described.

2.2. EXPERIMENTAL

2.2.1. Materials

Tetraethylorthosilicate (TEOS), Pluronic 123 (P123, Average Mol.Wt = 5800), 3-chloropropyltrimethoxysilane (CPTMS), (4-chloromethyl)phenyltriethoxysilane (BzTES), (1R,2S)-(+)-*cis*-1-amino-2-indanol (AIL) and dimethoxydimethylsilane (MeO_2Me_2Si) were purchased from Aldrich. 2-(4-chlorosulfonylphenyl) ethyltrimethoxysilane (TsTMS) was obtained from Acros Chemicals. $[RuCl_2(p\text{-cymene})]_2$ was purchase from Aldrich chemicals (USA). $[RuCl_2(benzene)]_2$ was synthesized according to a literature procedure.[15] The dry reagent grade solvents were obtained from Merck (India) and dried before use according to standard methods. HPLC grade 2-propanol was used for reaction.

2.2.2. Synthesis of siliceous SBA-15

Generally, the synthesis of mesoporous SBA-15 was carried out hydrothermally in an autoclave under autogeneous pressure using polymer surfactants like P123, P103 etc. as templates with hydrochloric acid as mineralizer.

Siliceous SBA-15 was synthesized by the literature procedure[17] with slight modification using the following initial molar gel compositions (Scheme 2.1):

0.043 TEOS: 4.4 g P123 M_{avg} = 5800 $[EO_{20}\text{-}PO_{70}\text{-}EO_{20}]$: 8.33 H_2O: 0.24 HCl

Typically 4.4 g of triblock co-polymer was dispersed in 30 g-distilled water and stirred for 1.5 h. To the resultant solution, 120 g of 2M HCl was added under stirring and the stirring was continued for 2 h. Finally 9 g of TEOS was added drop wise and the mixture was maintained at 35^oC for 24 h without stirring. The resulted heterogeneous mixture was submitted to hydrothermal treatment at 100^oC for 48 h under static condition before recovering the solid material. The crystallized product

was filtered, washed with distilled water and dried in air for 12 h and in oven at 70°C for 12 h and then calcined at 450°C for 8 h in air to remove the template completely. The structure was confirmed by XRD and surface area.

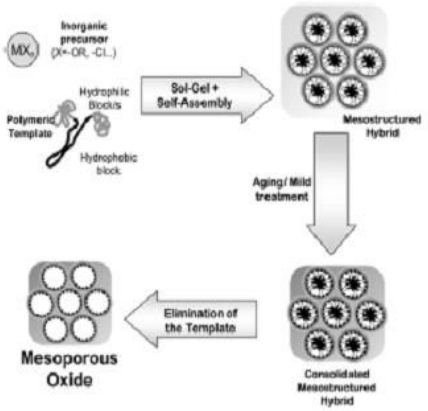

Scheme 2.1: Preparation of SBA-15 by sol-gel method.

2.2.3. Surface Modification of SBA-15 by Post-Synthesis Grafting

All the organosilanes 3-chloropropyltrimethoxysilane (CPTMS), (4-chloromethyl) phenyltriethoxysilane (BzTES) and 2-(4-chlorosulphonylphenyl)ethyltrimethoxy-silane (TsTMS) were grafted over SBA-15 in dry refluxing toluene under inert condition. The passivation of unreacted silanols groups has carried out after the functionalization with excess of dimethoxydimethylsilane in dry toluene under reflux condition.

In a typical procedure,

1 g of SBA-15 was suspended in 50 ml dry toluene and refluxed with a calculated amount of organosilane (CPTMS, BzTES or TsTMS) for 36 h under nitrogen atmosphere. The material was filtered after cooling to ambient temperature, washed with dry toluene and then with dichloromethane. Soxhlet extraction was carried out for 24 h in dichloromethane (DCM) to remove occluded organosilane. The sample was dried in vacuum for 10 h. The materials were designated as follows (Table 2.1).

Table: 2.1: Designation of various organo-functionalized SBA-15 materials*.

Functional Group	Precursor of Functional Group	Support	Functionalization Procedure	Designation
-Propylchloride	CPTMS	SBA-15	Post Grafting	PrCl-SBA-15
-Benzylchloride	BzTES	SBA-15	Post Grafting	BzCl-SBA-15
-Tosylchloride	TsTMS	SBA-15	Post Grafting	TsCl-SBA-15

*All materials were considered before passivation of unreacted silanols groups.
CPTMS: 3-chloropropyltrimethoxysilane,
BzTES: (4-chloromethyl) phenyltriethoxysilane,
TsTMS: 2-(4-chlorosulphonylphenyl)ethyltrimethoxysilane.
PrCl: Propylchloride; BzCl: Benzylchloride & TsCl: Tosylchloride.

The above dried materials were stirred with excess of dimethoxydimethylsilane (MeO_2Me_2Si) in dry toluene for 12 h under reflux condition to passivate the unloaded silanol groups inside and out side the porous material. The filtered sample was washed with dichloromethane (DCM) several times, soxhlet extracted in dichloromethane (DCM) for 24 h and dried under vacuum for 10 h. The resulted materials were designated as follows (Table 2.2).

Table 2.2: Designation of various organically modified SBA-15 materials*.

Material	Capping molecule	Functionalization Procedure	Designation
PrCl-SBA-15	MeO_2Me_2Si	Post Grafting	Pr-SBA-15
BzCl-SBA-15	MeO_2Me_2Si	Post Grafting	Bz-SBA-15
TsCl-SBA-15	MeO_2Me_2Si	Post Grafting	Ts-SBA-15

*All materials were considered after passivation of unreacted silanols groups.
Pr: Propyl; Bz: Benzyl & Ts: Tosyl.

2.2.4. Grafting of (1R,2S)-(+)-*cis*-1-amino-2-indanol inside organo-functionalized SBA-15

A chiral amino alcohol was introduced into the inner surfaces of SBA-15 *via* a nucleophilic substitution mechanism (Scheme 2.2, 2.3 & 2.4). The chiral compound chosen here was (1R,2S)-(+)-*cis*-1-amino-2-indanol (AIL).

1 g of organo-functionalized SBA-15 (Pr-SBA-15/Bz-SBA-15/Ts-SBA-15) was added to a solution containing 126 mg (0.84 mmol) of (1R,2S)-(+)-*cis*-1-amino-2-indanol and 0.25 ml of triethylamine (NEt_3) in 50 ml of dry toluene, refluxed for 36 h under inert conditions, filtered, washed first with toluene and there after with dichloromethane (DCM), and dried under vacuum. The resulted materials were designated as follows (Table 2.3).

Table 2.3: Designation of chiral amino alcohol modified organo-functionalized SBA-15.

Organo-modified material	Chiral amino alcohol	Designation
Pr-SBA-15	(1R,2S)-(+)-*cis*-1-amino-2-indanol	PrAIL-SBA-15
Bz-SBA-15	(1R,2S)-(+)-*cis*-1-amino-2-indanol	BzAIL-SBA-15
Ts-SBA-15	(1R,2S)-(+)-*cis*-1-amino-2-indanol	TsAIL-SBA-15

AIL: (1R,2S)-(+)-*cis*-1-amino-2-indanol.

Pr: Propyl, Bz: Benzyl & Ts: Tosyl.

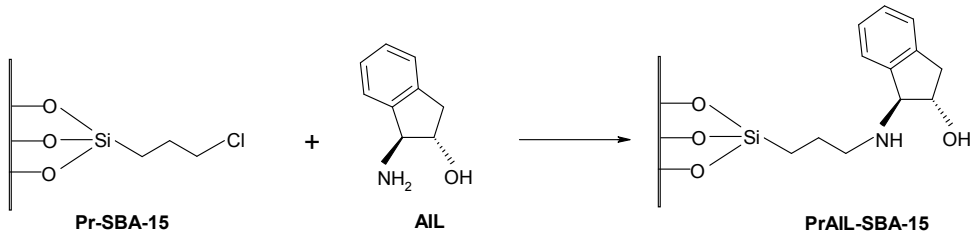

Scheme 2.2: Grafting of (1R,2S)-(+)-*cis*-1-amino-2-indanol over Pr-SBA-15

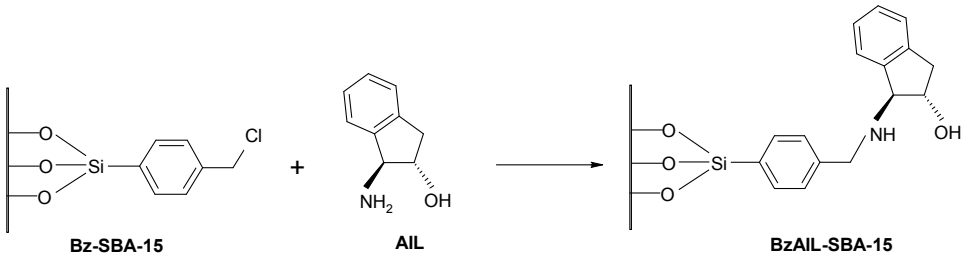

Scheme 2.3: Grafting of (1R,2S)-(+)-*cis*-1-amino-2-indanol over Bz-SBA-15

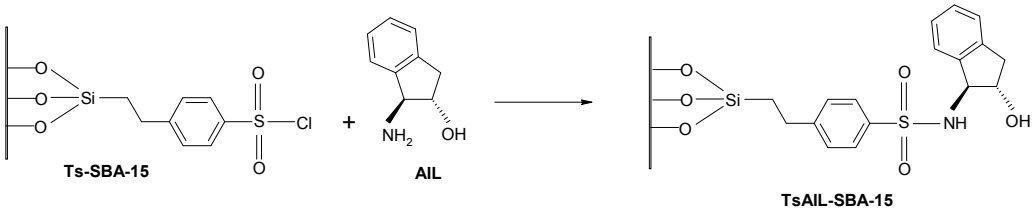

Scheme 2.4: Grafting of (1R,2S)-(+)-*cis*-1-amino-2-indanol over Ts-SBA-15

2.2.5. Preparation of $[RuCl_2(benzene)]_2$ and $[RuCl_2(p\text{-cymene})]_2$

2 g of $RuCl_3.xH_2O$ was dissolved in 100 ml dry ethanol and refluxed with 10 ml 1,3-cyclohexadiene for 4 h under N_2 atmosphere. The brown precipitate was filtered, washed several times with dry methanol and dried in vacuum resulted $[RuCl_2(benzene)]_2$. Yield = 95%, 1.83 g

2 g of $RuCl_3.xH_2O$ was dissolved in 100 ml dry methanol and refluxed with 10 ml α-phellandrene for 4 h under N_2 atmosphere. The precipitate was filtered, washed several times with dry methanol and dried in vacuum resulted $[RuCl_2(p\text{-cymene})]_2$. Yield = 65%,

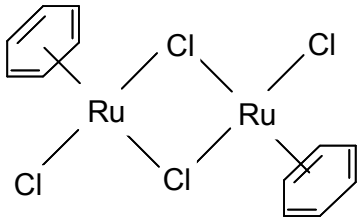

$[RuCl_2(benzene)]_2$

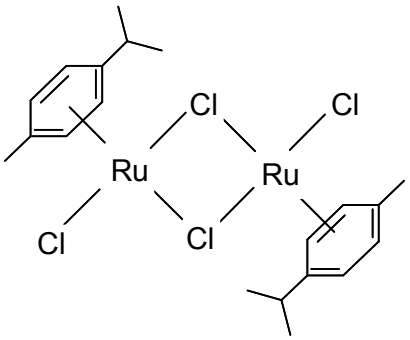

$[RuCl_2(p\text{-cymene})]_2$

2.2.6. Anchoring of $[RuCl_2(benzene)]_2$ and $[RuCl_2(p\text{-cymene})]_2$ complexes over AIL-functionalized SBA-15

The $[RuCl_2(benzene)]_2$ and $[RuCl_2(p\text{-cymene})]_2$ complexes were anchored into the AIL-functionalized SBA-15 materials applying the following method (Scheme 2.5, 2.6 & 2.7).

1 g of AIL-functionalized SBA-15 material (PrAIL-SBA-15/BzAIL-SBA-15/ TsAIL-SBA-15) was treated with 36 mg of $[RuCl_2(benzene)]_2$ or $[RuCl_2(p\text{-cymene})]_2$ and 0.15 ml of NEt_3 in 30 ml of dry 2-propanol and refluxed for 1 h under N_2 atmosphere, filtered, washed with dry 2-propanol, and dried under vacuum. The resulted materials were designated as given below (Table 2.4),

Table 2.4: Designation of Heterogeneous Ru-Complexes.

Chiral Ligand-modified material	Metal Precursor	Designation
PrAIL-SBA-15	$[RuCl_2(benzene)]_2$	Ru-Bn-PrAIL-SBA-15
	$[RuCl_2(p\text{-cymene})]_2$	Ru-Cy-PrAIL-SBA-15
BzAIL-SBA-15	$[RuCl_2(benzene)]_2$	Ru-Bn-BzAIL-SBA-15
	$[RuCl_2(p\text{-cymene})]_2$	Ru-Cy-BzAIL-SBA-15
TsAIL-SBA-15	$[RuCl_2(benzene)]_2$	Ru-Bn-TsAIL-SBA-15
	$[RuCl_2(p\text{-cymene})]_2$	Ru-Cy-TsAIL-SBA-15

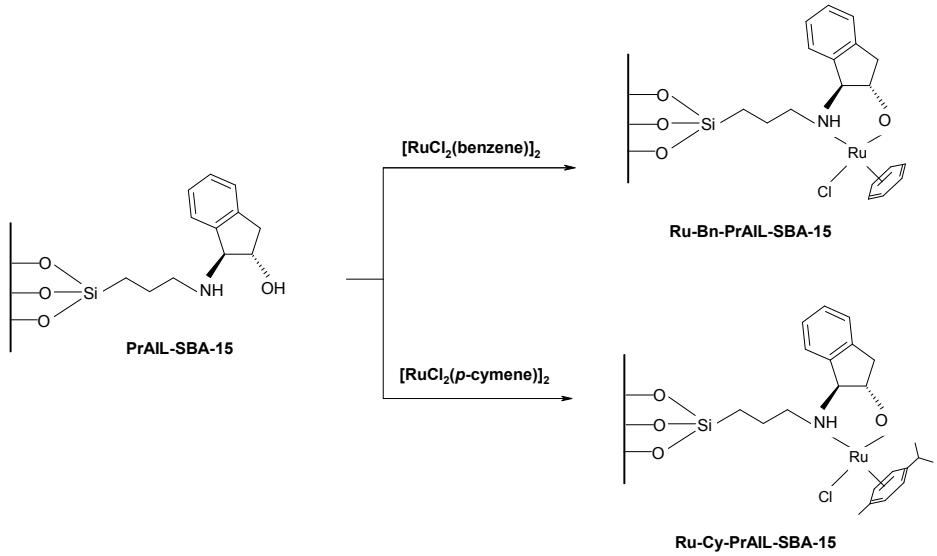

Scheme 2.5: Anchoring of $[RuCl_2(benzene)]_2$ and $[RuCl_2(p\text{-cymene})]_2$ complexes over PrAIL-SBA-15.

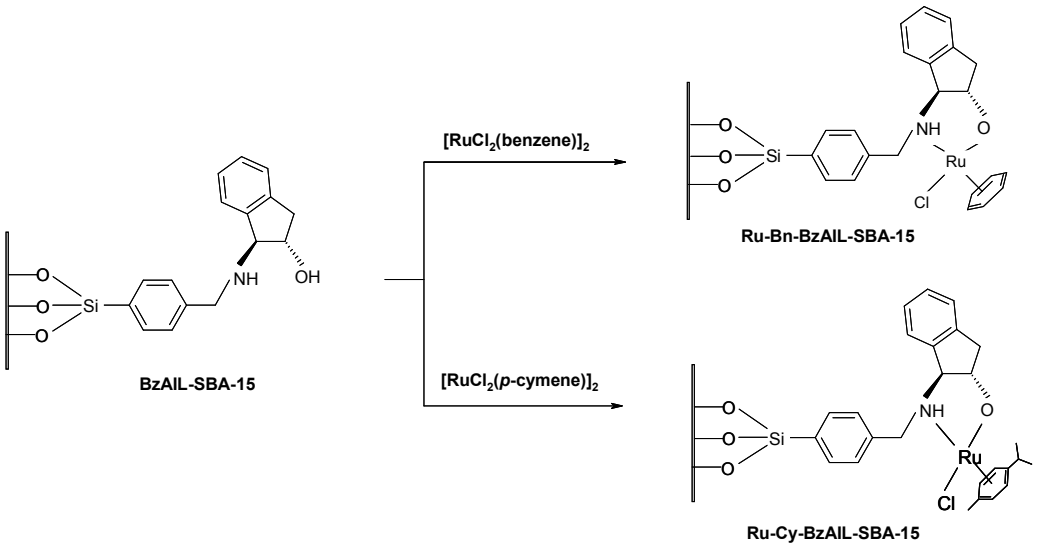

Scheme 2.6: Anchoring of $[RuCl_2(benzene)]_2$ and $[RuCl_2(p\text{-cymene})]_2$ complexes over BzAIL-SBA-15.

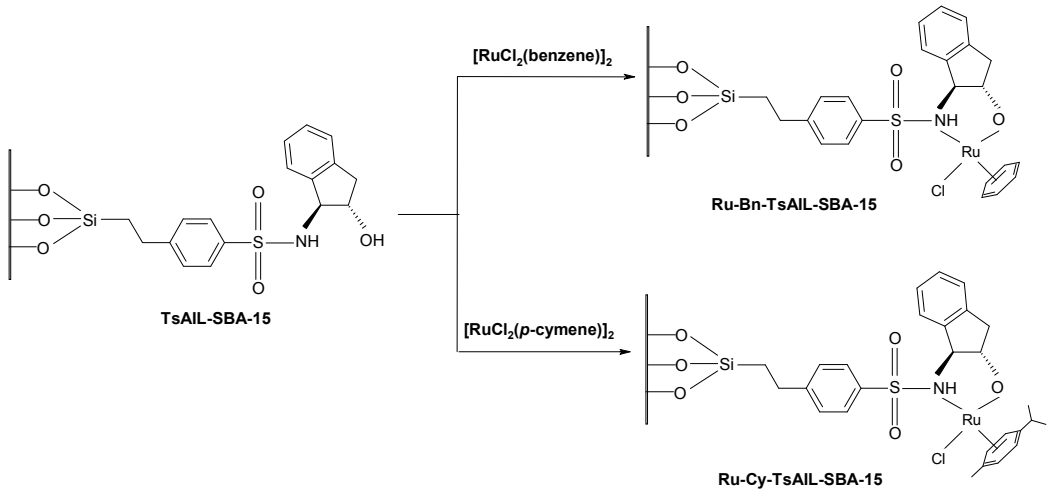

Scheme 2.7: Anchoring of $[RuCl_2(benzene)]_2$ and $[RuCl_2(p\text{-cymene})]_2$ complexes over TsAIL-SBA-15.

2.2.7. Instruments for Characterization

In order to identify the structure, phase purity, degree of crystallinity, unit cell parameters the powder small angle X-ray diffraction analysis was done on a SIEMENS D5005 diffractometer using Cu Kα (λ = 0.154 nm) radiation. The specific surface areas of the samples were determined by the BET method from N_2 adsorption isotherms at 77 K using an Omnisorb CX- 100 Coulter instrument. Before measuring the surface area, the samples were activated at 120^{o}C for 3 h under nitrogen atmosphere. The elemental analysis was done with an EA1108 CHN/S Elemental Analyzer (Carlo Erba Instrument) for establishing the presence and exact fraction of elements in the synthesized materials. Diffuse reflectance UV-Vis spectra of the powder samples were recorded in the range 200-800 nm on Shimadzu UV 2101 PC spectrometer equipped with a diffuse reflectance attachment, using $BaSO_4$ as the reference. The metal loading was found with an inductive couple plasma atomic emission spectroscopy (ICP-AES) on a spectroflame D (Spectro analytic instrument). A Shimadzu FT-IR 8201 PC Diffuse Reflectance Scanning disc technique was used to probe the attached groups and nature of the surface functional groups in the material. 125.757 MHz solid-state ^{29}Si, ^{13}CP MAS NMR studies were carried out on a Bruker DRX-300 NMR spectrometer. The spectrum was recorded under Hartmann-Hahn match condition using a contact time of 1 m/sec and a relaxation delay of 4 sec. The size and morphology of the catalyst was measured with a scanning electron microscope (SEM, JEOL-JSM-520). The TEM observations were made using a JEOL-JEM-1200 EX instrument with 120kV of acceleration voltage to probe the presence of hexagonal mesophase in the extracted material. XPS measurements were performed on a VG Microtech ESCA 3000 instrument using non-monochromatized Mg Kα radiation at pass energy of 50 eV and an electron take off angle of 60^o. The

correction of binding energy (B.E.) was performed by using the C1s peak of carbon at 285 eV as reference.

2.3. CHARACTERIZATION

2.3.1. Powder X-Ray Diffraction

The uniqueness of mesoporous structure, phase purity, degree of orderedness and unit cell parameters of all the siliceous and surface modified mesoporous materials were determined by powder X-ray diffraction (XRD).

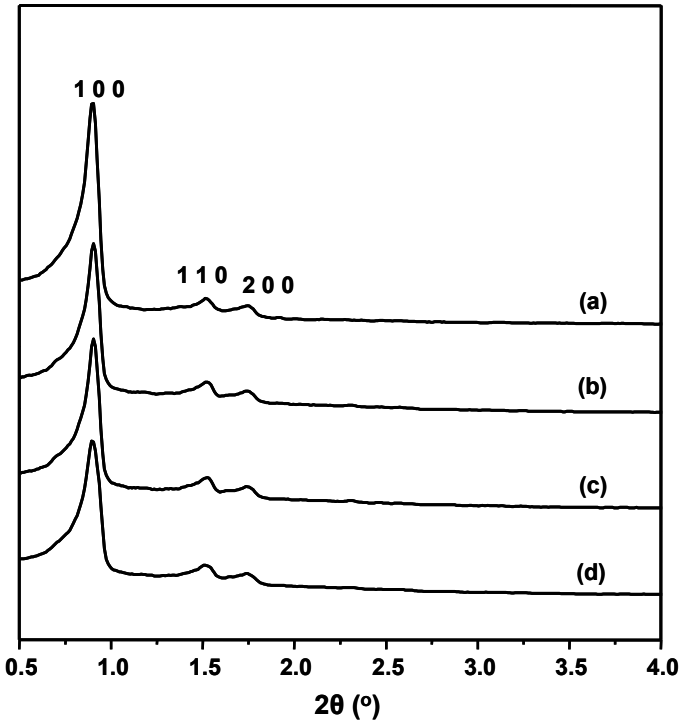

Figure 2.1: Powder XRD patterns recorded from the (a) Calcined SBA-15, (b) Pr-SBA-15, (c) Bz-SBA-15 and (d) Ts-SBA-15 materials.

Figure 2.1 represents the powder XRD patterns recorded from the (a) Calcined SBA-15, (b) Pr-SBA-15, (c) Bz-SBA-15 and (d) Ts-SBA-15 materials. The typical hexagonal phase (*p6mm*) of SBA-15 [main (100) peak with weak (110) and (200) reflections] is clearly visible in all the samples at 2θ = 0.90°, 1.51° and 1.75°, respectively, and a d_{100} spacing value of 105.08 Å. These lattice reflections indicate

high degree of orderedness of the two-dimensional hexagonal mesophases and thus verifying that these samples are typical of hexagonal SBA-15-type materials[15] prepared at *p*H ≤ 2. In all the samples, (110) reflection is more intense than the (200) reflection. It favors more complete condensation of the wall structure due to the higher temperatures preferring at hydrothermal synthesis and further calcination.

As evident from the figure 2.1, the XRD patterns of the samples synthesized after treatment with MeO_2SiMe_2 (Figure. 2.1. (b), (c) and (d)) are almost similar to the parent SBA-15 sample (Figure. 2.1) with small decrease in overall intensity to the 100, 110 and 200 reflections.

It is assumed that the most kinetically accessible Si–OH groups exist on the external walls of the mesoporous silica particles. After treatment with MeO_2SiMe_2, these external silanol groups will be silylated and deactivated for further reaction. Therefore, the purpose of using MeO_2SiMe_2 in the grafting process was to ensure that the anchoring of the desired trialkoxyorganosilane occurs predominantly within the internal walls of SBA-15. If not treated with MeO_2SiMe_2, grafting will occur uncontrollably on the external and internal surfaces of mesoporous silica, which will certainly weaken the orderedness of the materials. Henceforth, the organic-group grafted SBA-15 (Pr-SBA-15, Bz-SBA-15 and Ts-SBA-15) materials mentioned in this chapter will be considered as those synthesized after MeO_2SiMe_2 treatment.

Figure 2.2 shows the powder X-ray diffraction (XRD) patterns recorded from the (a) PrAIL-SBA-15 (b) BzAIL-SBA-15 and TsAIL-SBA-15 materials. From the figure it is clear that after anchoring of the chiral ligand [(1R,2S)-(+)-*cis*-1-amino-2-indanol] an inconsequential decrease in peak intensities to the (100), (110) and (200) reflections were observed without changing the peak positions. This perseverance of

peak positions indicates that, even the presence of a large amount of organic moieties by the partial filling inside the mesopores is less detrimental to the quality of the SBA-15 material. The persistence of the (100), (110) and (200) reflections not only proved the structural stability and existence of long range ordering to the mesophase but also the survival of undisturbed pore wall thickness even after a number of treatments with organic molecules in solvents under radical conditions. All the observations clearly show that the ordered mesoporosity and structural stability of the samples have retained after incorporation of organometallic complexes.

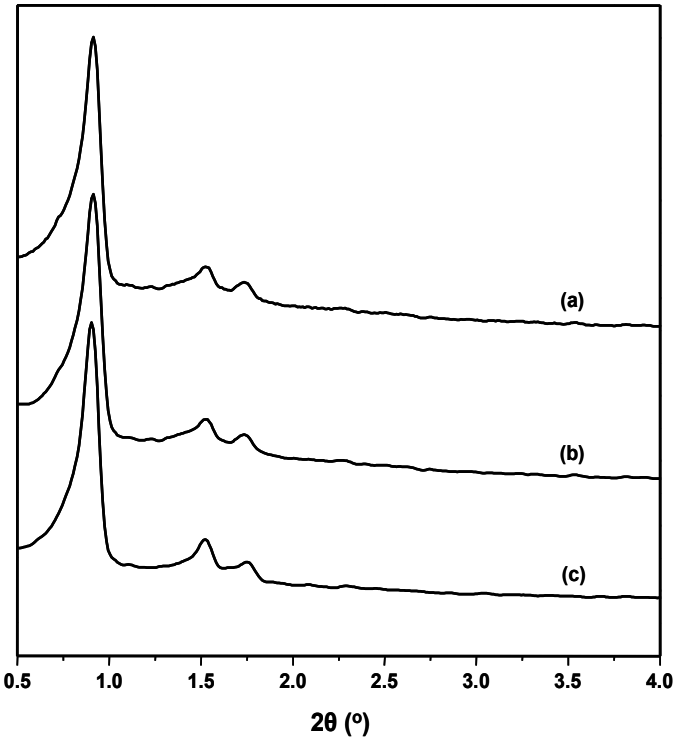

Figure 2.2: Powder XRD patterns recorded from (a) PrAIL-SBA-15 (b) BzAIL-SBA-15 and TsAIL-SBA-15 materials.

Figure 2.3 shows the small angle powder XRD patterns recorded from (a) Ru-Bn-PrAIL-SBA-15, (b) Ru-Cy-PrAIL-SBA-15, (c) Ru-Bn-BzAIL-SBA-15, (d) Ru-Cy-BzAIL-SBA-15, (e) Ru-Bn-TsAIL-SBA-15 and (f) Ru-Cy-TsAIL-SBA-15 materials.

After the loading of metal precursors all the reflections were undisturbed and only the intensity of the peaks slightly decreased. These results indicate the stability of the highly ordered mesoporosity even after incorporation of organic functional groups and Ru-complexes. However, the slight decrease in the peak intensities was observed in the case of the Ru-complex loaded samples, which might be due to partial filling of Ru complexes inside the mesopores. From the above results it is confirmed that the calcined SBA-15 material has a stable pore wall thickness to retain its integrity even after several modification treatments.

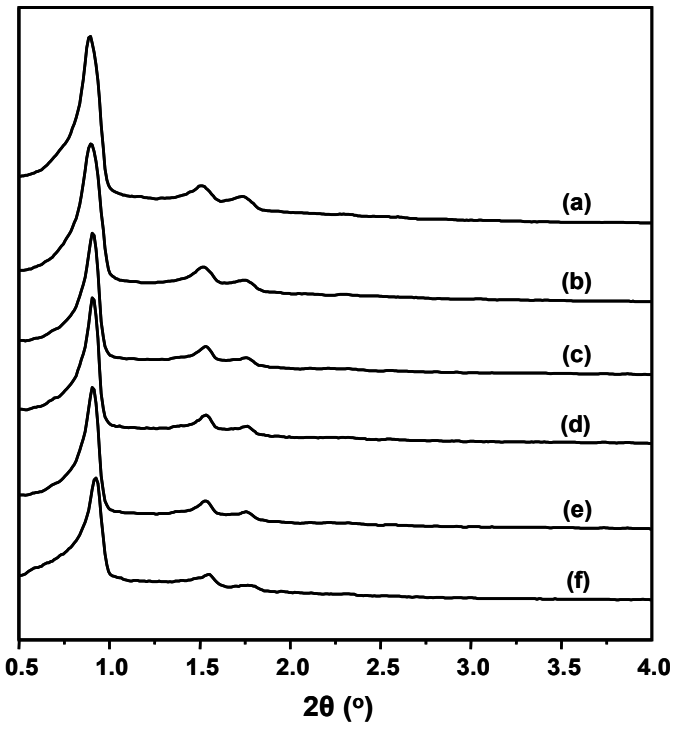

Figure 2.3: Powder XRD patterns recorded from (a) Ru-Bn-PrAIL-SBA-15, (b) Ru-Cy-PrAIL-SBA-15, (c) Ru-Bn-BzAIL-SBA-15, (d) Ru-Cy-BzAIL-SBA-15, (e) Ru-Bn-TsAIL-SBA-15 and (f) Ru-Cy-TsAIL-SBA-15materials.

Table 2.5: Physical characteristics of SBA-15 and organically modified SBA-15 materials.

Material	% Ru (w/w)[a]	d_{hkl} (Å)[b]	a_o (Å)[c]	Pore diameter (Å)	Pore volume (cm^3g^{-1})	Surface area (m^2g^{-1})
SBA-15	-	105.08 (100)	121.47	78	1.16	854
Pr-SBA-15	-	102.63 (100)	118.64	72	0.80	598
Bz-SBA-15	-	102.52(100)	118.52	73	0.80	610
Ts-SBA-15	-	102.71(100)	118.43	72	0.80	600
PrAIL-SBA-15	-	100.25(100)	115.89	66	0.69	477
BzAIL-SBA-15	-	100.32(100)	115.97	71	0.68	501
TsAIL-SBA-15	-	100.54(100)	116.23	66	0.67	485
Ru-Bn-PrAIL-SBA-15	0.51	100.33(100)	115.98	64	0.58	419
Ru-Cy-PrAIL-SBA-15	0.52	100.34(100)	116.00	64	0.59	412
Ru-Bn-BzAIL-SBA-15	0.45	100.41(100)	116.08	70	0.59	459
Ru-Cy-BzAIL-SBA-15	0.46	100.41(100)	116.08	70	0.59	456
Ru-Bn-TsAIL-SBA-15	0.48	100.64(100)	116.34	64	0.58	420
Ru-Cy-TsAIL-SBA-15	0.48	100.61(100)	116.31	64	0.58	420

[a]Analyzed from ICP-AES.

[b]Calculated from XRD patterns ($n\lambda = 2d\sin\theta$, where $n = 1$ and $\lambda = 1.5404$ Å). Values in parentheses are respective principal Miller indices.

[c]$a_o = d_{100} \times 2/\sqrt{3}$.

A comparison of the *d*-spacings and unit cell parameter (a_o) values (calculated from XRD patterns, $a_o = d_{100} \times 2/\sqrt{3}$) of the SBA-15, functionalized SBA-15 and those with anchored Ru-complexes has been presented in Table 2.4. The Ru contents in each material, analyzed by ICP-AES, are also included in the table.

2.3.2. Porosity measurements

Figure 2.4 shows the typical N_2 adsorption-desorption isotherms for (A) Calcined SBA-15, (C) Pr-SBA-15, (E) PrAIL-SBA-15, (G) Ru-Bn-PrAIL-SBA-15 and (I) Ru-Cy-PrAIL-SBA-15 and the corresponding pore size distribution for (B) Calcined SBA-15, (D) Pr-SBA-15, (F) PrAIL-SBA-15, (H) Ru-Bn-PrAIL-SBA-15 and (J) Ru-Cy-PrAIL-SBA-15. All the materials displayed type IV isotherm (definition by IUPAC) with H_1-type hysteresis that is typical of mesoporous materials with cylindrical channels possessing pore diameters between 2 and 50 nm.[15] The calcined SBA-15 sample prepared with $EO_{20}PO_{70}EO_{20}$ (P-123) by reaction at 35°C for 24 hours, heating at 100°C for 48 hours, and subsequent calcination in air at 450°C, yielded an SBA-15 product with a mean pore size of 78 Å, a pore volume of 1.16 cm^3g^{-1}, and a Brunauer-Emmett-Teller (BET) surface area of 854 m^2g^{-1}. Three well distinguished regions of the adsorption isotherm are evident: (i) monolayer-multilayer adsorption, (ii) capillary condensation, and (iii) multilayer adsorption on the outer particle surfaces. A clear type-H1 hysteresis loop is observed, and the capillary condensation occurs at a higher relative pressure ($P/P_o \sim 0.60$), indicating a narrow mesopore size distribution (Figure 2.4 B). The position of the inflection point depends on the diameter of the mesopores, and its sharpness indicates the uniformity of the narrow pore size distribution. The specific surface area, pore volume and pore diameter values of the SBA-15, Pr-SBA-15, PrAIL-SBA-15, Ru-Bn-PrAIL-SBA-15

and Ru-Cy-PrAIL-SBA-15 displayed in Table 2.4. Which were found to be 854 m^2g^{-1}, 78 Å, 1.16 ml/g; 598 m^2g^{-1}, 72 Å, 0.80 ml/g; 477 m^2g^{-1}, 66 Å, 0.69 ml/g; 419 m^2g^{-1}, 64 Å, 0.58 ml/g and 412 m^2g^{-1}, 64 Å, 0.59 ml/g respectively (Table 2.5). The samples showed a remarkable decrease in surface area on progressing the surface modification process and the ligand-modified samples obviously exhibit lower specific surfaces than the parent solids due to the introduction of the organic moieties (ligands and/or Me_2-Si groups), which is also responsible for a reduction of pore volumes and pore diameters. A specific surface area decrease of Pr-SBA-15 and PrAIL-SBA-15 were about 30 % and 44 % after functionalization of calcined SBA-15, which clearly point out the anchoring of a considerable amount of organic molecule inside the pores of calcined silica support. Further a small decrease in specific surface areas for Ru-Bn-PrAIL-SBA-15 (419 m^2g^{-1}) and Ru-Cy-PrAIL-SBA-15 (412 m^2g^{-1}), clearly evident the successful complexation of the immobilized ligand by ruthenium precursors. The surface area values were found to be nearly similar for Ru-Bn-PrAIL-SBA-15 and Ru-Cy-PrAIL-SBA-15 indicates an agreement in metal loading in both the heterogeneous catalysts.

A sharp pore size distribution with a mean value of 78 Å is found for both the adsorption and desorption processes for calcined SBA-15. But for the modified materials (Pr-SBA-15, PrAIL-SBA-15, Ru-Bn-PrAIL-SBA-15 and Ru-Cy-PrAIL-SBA-15), partially narrow and lower pore size distributions were obtained (72-64 Å), which might imply that the chelating ligand and the Me_2Si- groups are more over uniformly distributed through the SBA-15 channel surface in these samples.[16] The occlusion of organic molecules inside the channel of the mesoporous material has been further evidenced from the measurement of pore volume of the synthesized materials. The pore volume is considerably decreasing after functionalization,

immobilization of ligand and further metal complex addition to the calcined SBA-15, indicates the progress of anchoring of the organic moieties inside the channels. But only a small amount of decrease in pore volume compared to the PrAIL-SBA-15 has been observed after the addition of metal precursors, which is further supported by the pore diameter values of these materials that also did not change considerably, while complexation.

The pore volume is considerably decreasing (1.16-0.58/0.59 cm^3g^{-1}) after functionalization, immobilization of ligand and further metal complex addition to the calcined SBA-15, indicating the progress of anchoring of the organic moieties inside the channels. But only a small amount of decrease in pore volume has been observed after the addition of metal precursors to PrAIL-SBA-15. Pore diameter values of these materials, however, did not change considerably even after functionalization and anchoring of the Ru complexes.

The similar type of trend was observed while going from calcined SBA-15 to (Ru-Bn-BzAIL-SBA-15 and Ru-Cy-BzAIL-SBA-15) / (Ru-Bn-TsAIL-SBA-15 and Ru**Cy-TsAIL-SBA-15)**.

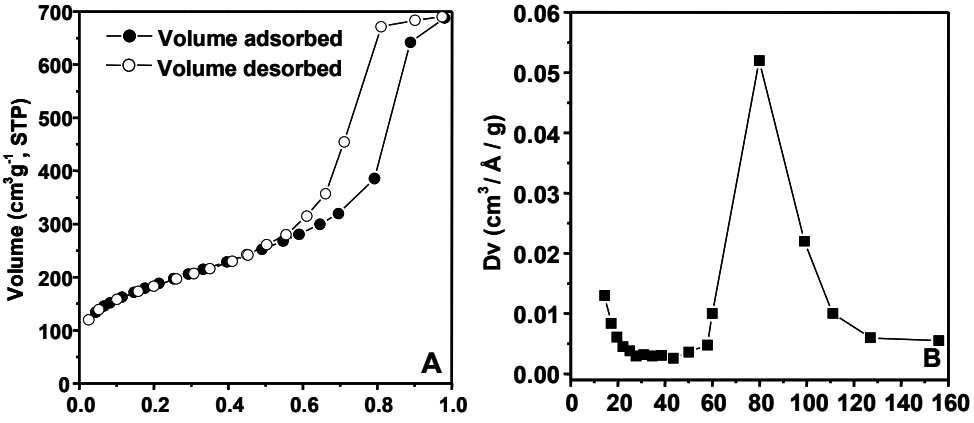

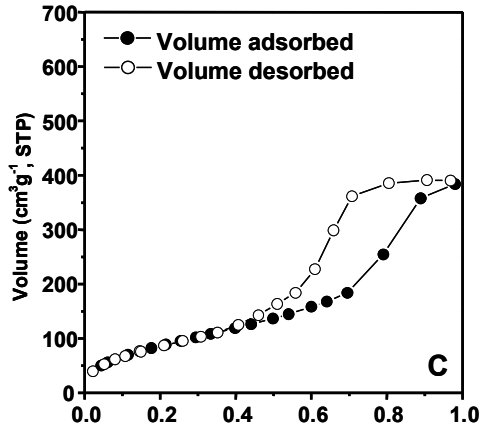
Volume adsorbed
Volume desorbed
Volume (cm3g-1, STP)
C

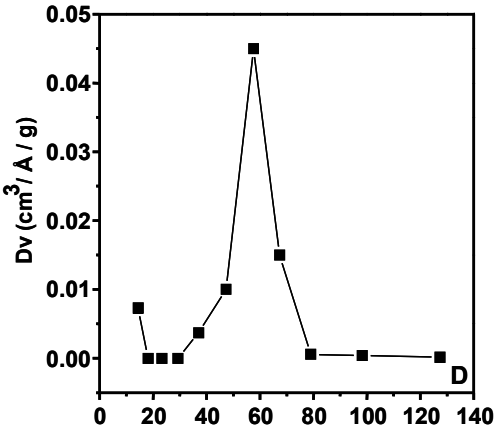
Dv (cm3/ Å / g)
D

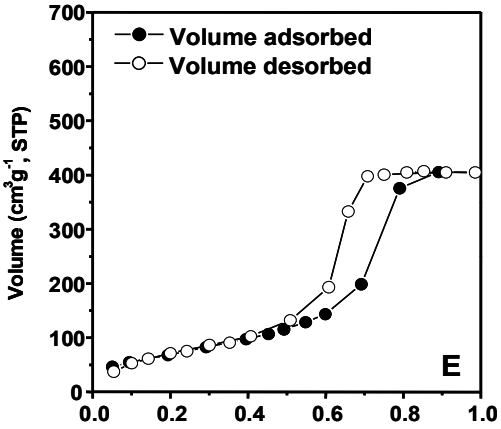
Volume adsorbed
Volume desorbed
Volume (cm3g-1, STP)
E

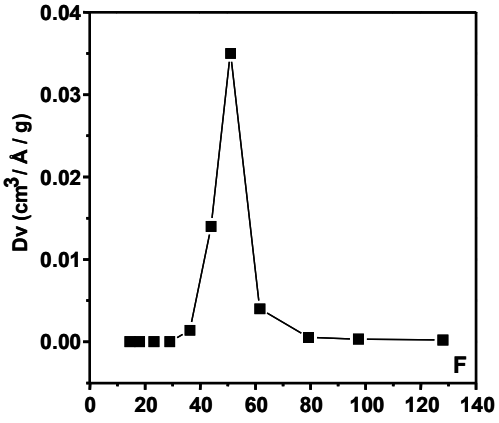
Dv (cm3/ Å / g)
F

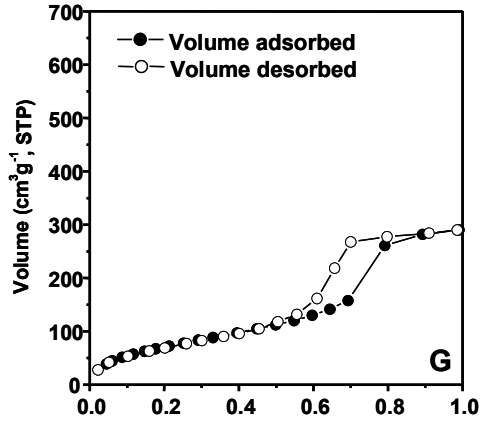
Volume adsorbed
Volume desorbed
Volume (cm3g-1, STP)
G

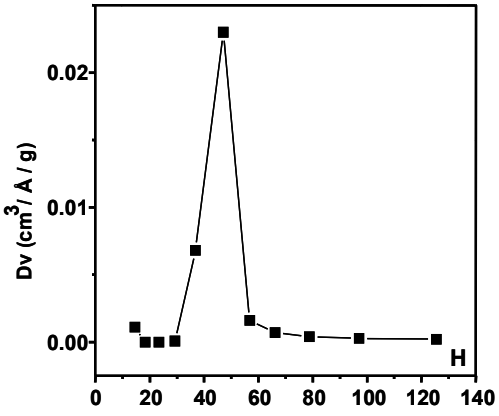
Dv (cm3/ Å / g)
H

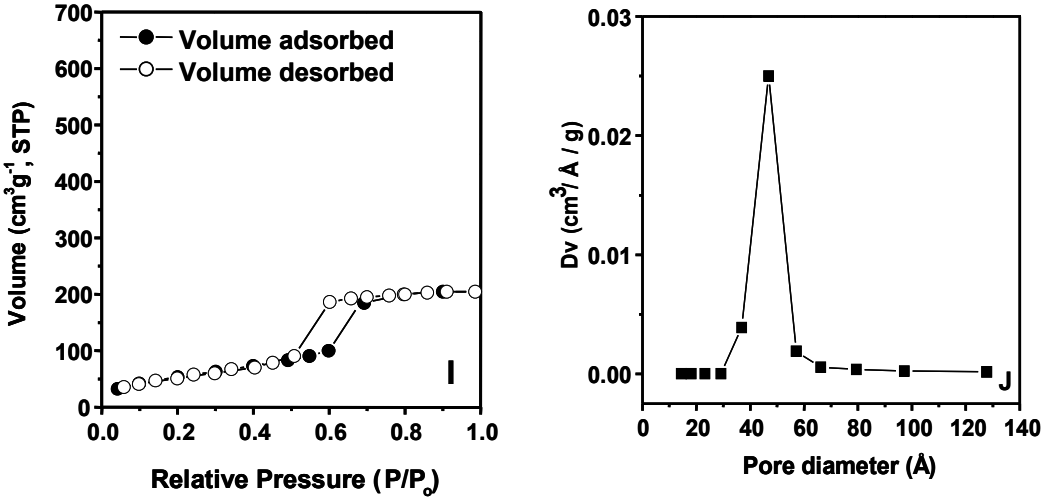

Figure 2.4: N_2 adsorption-desorption isotherms for: (A) SBA-15, (C) Pr-SBA-15, (E) PrAIL-SBA-15, (G) Ru-Bn-PrAIL-SBA-15 and (I) Ru-Cy-PrAIL-SBA-15 samples. Pore size distribution curves for: (B) SBA-15, (D) Pr-SBA-15, (F) PrAIL-SBA-15, (H) Ru-Bn-PrAIL-SBA-15 and (J) Ru-Cy-PrAIL-SBA-15 samples.

The specific surface area, pore volume and pore diameter values [estimated from N_2 sorption isotherms and pore size distribution] of all the siliceous and organo-modified SBA-15 samples are summarized in Table 2.4. The surface area, pore diameter and pore volume values of calcined SBA-15 were found to be 854 m^2g^{-1}, 78 Å, 1.16 ml/g respectively. After grafting of the -PrCl, -BzCl and -TsCl functional groups and further hydroxyl group capping, it was observed that surface areas of the SBA-15 materials were decreased by *ca*. 27–30%, pore volumes were decreased by *ca*. 31%, and pore diameters were decreased by *ca*. 6–8%. Immobilization of chiral ligand [(1R,2S)-(+)-*cis*-1-amino-2-indanol] resulted a further decrease in surface area (*ca*. 40-44%), pore volume (*ca*. 40-42%) and pore diameter (*ca*. 8-15%) values with respect to calcined SBA-15. After complexation with $[RuCl_2(benzene)]_2$ and $[RuCl_2(p\text{-cymene})]_2$, a considerable amount of decrease in surface area (*ca*. 46-52%), pore volume (*ca*. 48-50%) and pore diameter (*ca*. 10-18%) values on comparison with the decrease were observed for the ligand immobilized samples with respect to

calcined SBA-15. All these results strongly indicate that the organic functional groups are located inside the channels.

2.3.3. FTIR Spectra

Figure 2.5 A & B shows the FT-IR spectrum of as-synthesized [curve (a)] and calcined SBA-15 [curve (b)] materials. In both the spectrum a broad band was observed in between 3800 and 3000 cm^{-1}, which correspond to the O–H stretching vibrations. The broadness might be due to the hydrogen bonding with each other or bonding with the surfactant (in the case of as-synthesized material). In calcined SBA-15 [curve (b)] a sharp but small peak has been observed at 3744 cm^{-1} is due to the free –OH groups available after the removal of surfactants, which is not present in the as-synthesized SBA-15 [curve (a)]. Additionally, in calcined SBA-15 a sharp band between 1650 and 1600 cm^{-1} is due to the bending vibrations of surface O–H groups and water molecules occluded in the pores. In addition to the above bands, the as-synthesized SBA-15 shows two weak bands at around 3200–2800 and 1500–1300 cm^{-1} which are due to the C–H stretching and bending vibrations[18] of methylene group in the template material. These bands are absent in the calcined SBA-15, which shows that the template removal is complete and successful. In all the samples a sharp peak at 800 cm^{-1} is observed, which is due to Si-O stretching bond.

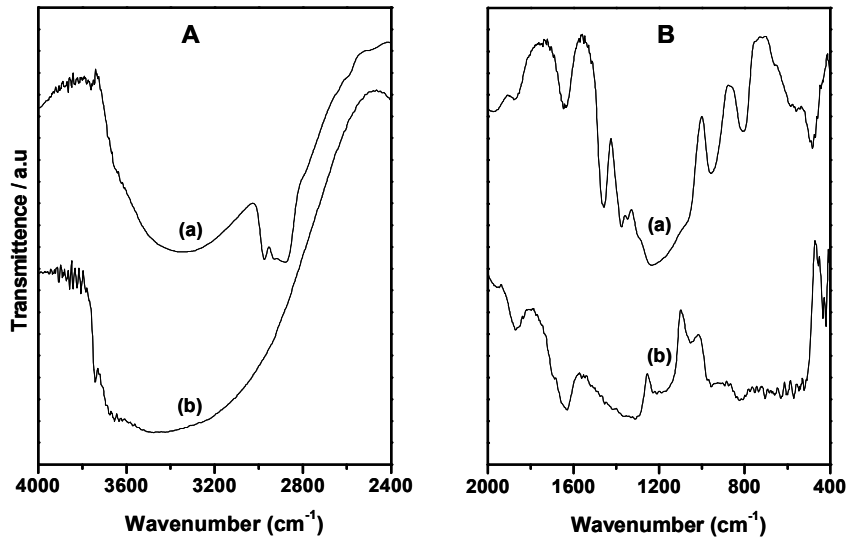

Figure 2.5: (A) & (B) represents the FT-IR spectrum of as-synthesized [curve (a)] and calcined SBA-15 [curve (b)].

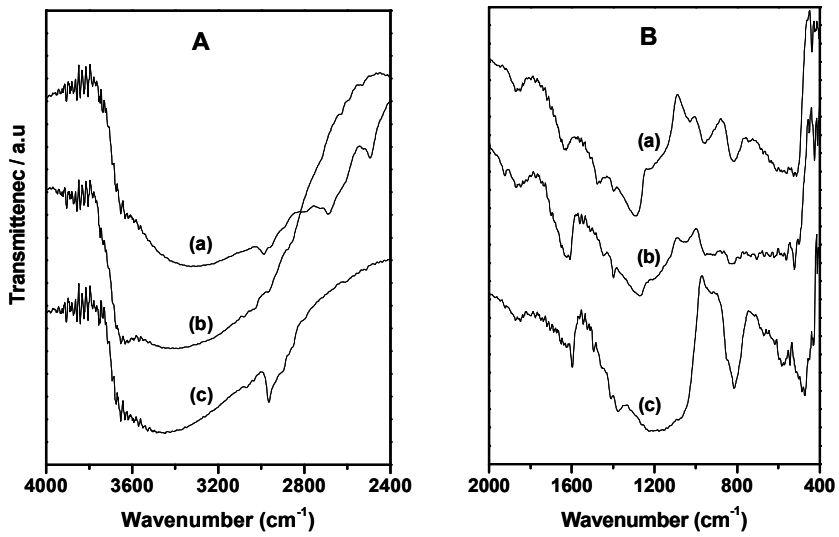

Figure 2.6: (A) & (B) represents the FT-IR spectrum of (a) Pr-SBA-15 (b) Bz-SBA-15 and (c) Ts-SBA-15.

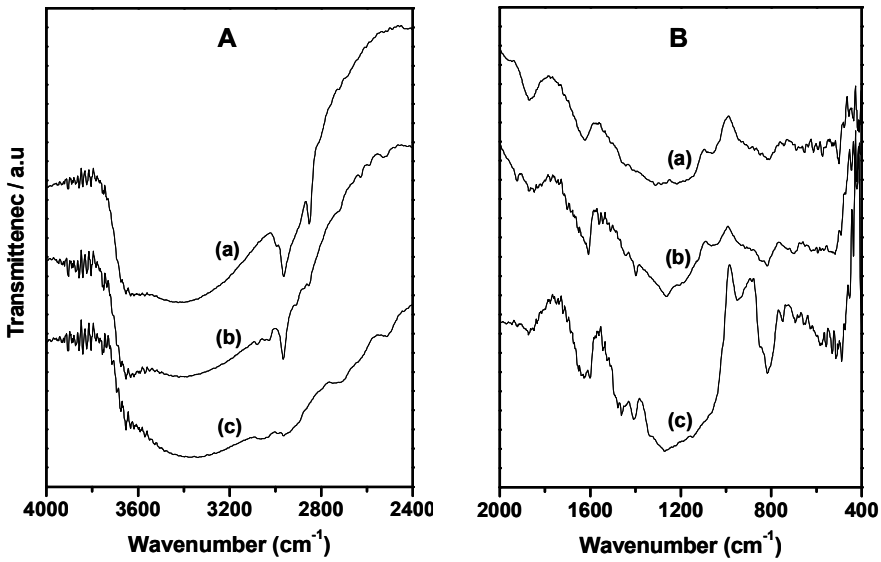

Figure 2.7: (A) & (B) represents the FT-IR spectrum of (a) PrAIL-SBA-15 (b) BzAIL-SBA-15 and (c) TsAIL-SBA-15.

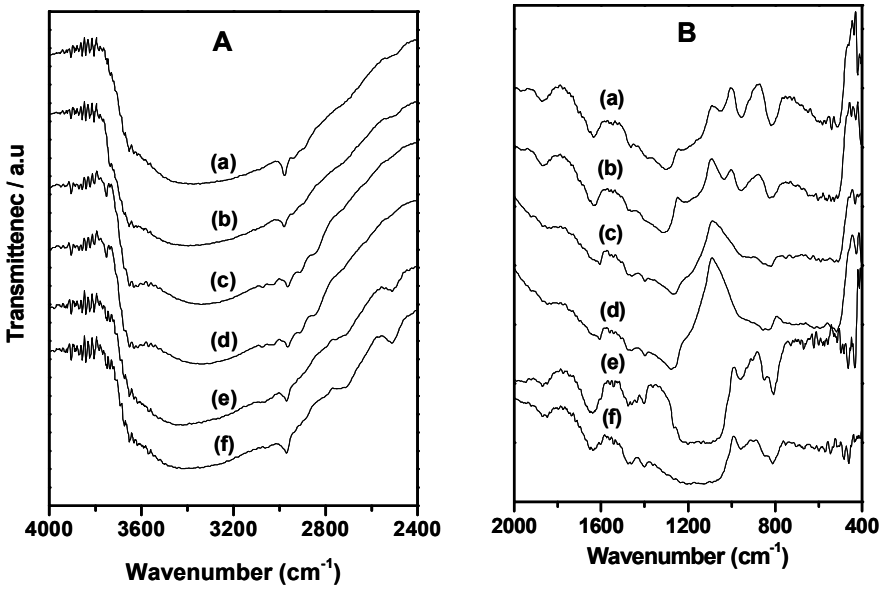

Figure 2.8: (A) & (B) represents the FT-IR spectrum of (a) Ru-Bn-PrAIL-SBA-15 (b) Ru-Cy-PrAIL-SBA-15(c) Ru-Bn-BzAIL-SBA-15 (d) Ru-Cy-BzAIL-SBA-15 (e) Ru-Bn-TsAIL-SBA-15 and (f) Ru-Cy-TsAIL-SBA-15.

In the entire spectrum (Figure 2.3, 2.4 & 2.5) two weak bands at around 3000-2900 cm^{-1} corresponds to asymmetrical and symmetrical stretching vibrations of $–CH_2$ groups of the organic moieties. In addition to these bands a broad peak at around 1400-1250 cm^{-1} is due to the C-H bending vibration of the functionalized moieties. A medium sharp band at around 1650-1600 cm^{-1} is indexed to the surface silanol groups,[18] which is further confirmed from the broad band at around 3800-3000 cm^{-1}.

Figure 2.4 (A) & (B) represents the FTIR spectra of (a) Bz-SBA-15 and (b) BzAIL-SBA-15 (c) Ru-Bn-PrAIL-SBA-15 and (d) Ru-Cy-PrAIL-SBA-15. In addition to the above band, the entire spectra show two weak bands at around 3200–2800 and 1500–1300 cm^{-1} which are due to the C–H stretching and bending vibrations[19] of methylene group of functionalized and ligand molecules. In the ligand immobilized material (BzAIL-SBA-15) we have expected a week band at 3260 cm^{-1} for the –NH stretching vibration, which is unresolved due to the overlapping of O–H stretching vibration (3400 and 3650 cm^{-1}) of surface O–H groups and water molecules occluded in the pores. A small and broad band in all spectrums at 702 cm^{-1} represents the C–H bending vibration of methylene group of benzene.[19]

In the spectrum 2.8 B, a small and broad band at 1298 cm^{-1} and the medium band at 1185 cm^{-1}, are due to S=O stretching mode of incorporated tosyl group in all the samples. The C-S link also gives a medium band between 600 and 700 cm^{-1}. It is also observed that a medium band at 1423 cm^{-1} indicates the C=C stretching in-plane vibration of benzene framework. A band at 707cm^{-1} represents the C–H bending vibration of methylene group of benzene.[20]

2.3.4. Solid State NMR

2.3.4.1. ^{29}Si CP MAS NMR Spectra

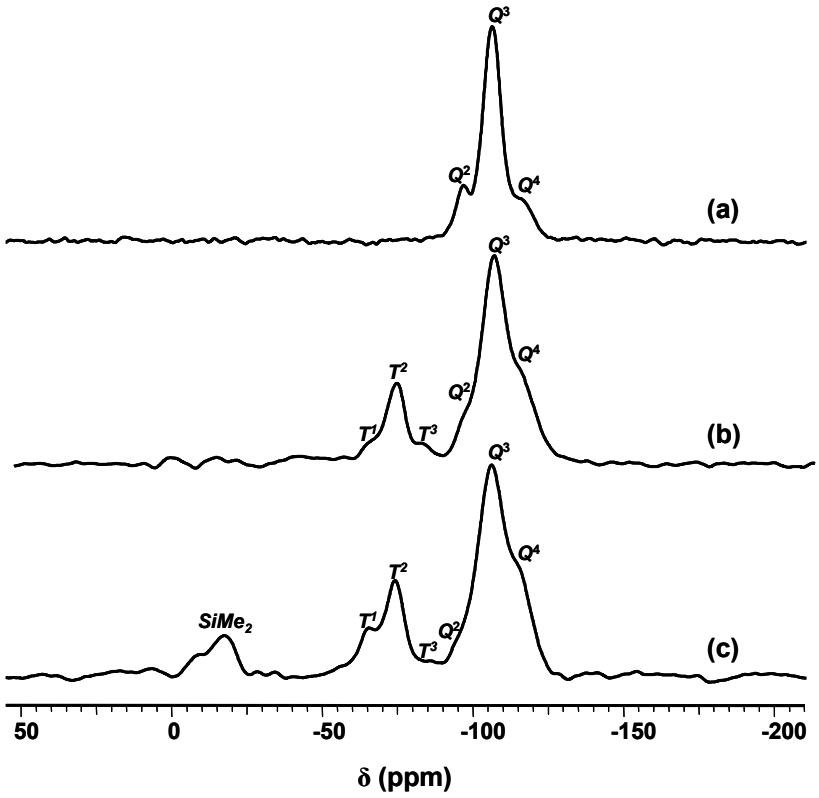

Figure 2.9: ^{29}Si CP MAS NMR spectra of: (a) SBA-15, (b) PrCl-SBA-15 and (c) Pr-SBA-15.

The ^{29}Si CP MAS NMR and ^{13}C CP MAS NMR spectra of the synthesized materials not only disclosed the structural information of the synthesized support material but also removed the ambiguity on the successful functionalization and further immobilization of the ligand over SBA-15. Figure 2.9 represents the ^{29}Si CP MAS NMR spectra of (a) calcined SBA-15, (b) PrCl-SBA-15 and (c) Pr-SBA-15. In the entire spectrum, the strong resonances at $\delta \approx$ -112, -102 and -93 ppm are attributed to Q^4 [SiO_3≡Si-O-Si≡], Q^3 [(SiO_3≡Si-OH] and Q^2 [(SiO_2≡($Si-OH)_2$] species,[21] respectively, present in the silicate framework of SBA-15, PrCl-SBA-15 and Pr-SBA-15. The Q^3 sites are associated with isolated Si-OH groups, and the Q^2 sites

correspond to geminal silandiols. For the modified sample (Figure 2.9b) three additional broad and overlapping signals appear at δ ≈ -78, -70, and -60 ppm, which can be assigned to T^3, T^2, and T^1 organosilica species[22], respectively, with T^2 as the major system. Subsequently, the relative intensity of the Q^2 resonances decreases with a slight increase of Q^4. For figure 2.9c, grafting of the dimethylsilane groups to SBA-15 further decreases the intensity of the Q^2 resonances (almost to the detection limit) and drastically increases the intensity of the Q^4 silicon atoms, while a broad peak at δ ≈ -15 ppm with a shoulder peak at δ ≈ -8 ppm can be assigned to the silicon nuclei of the dimethylsilyl (Me_2Si-) groups.[22] Changes in the relative intensities of the *Q4*, Q^3, and Q^2 signals can be explained by the redistribution of the silicon sites during surface silylation. The relative intensity of Q^4 site is very high when comparing with Q^3 site indicates the formation of a highly condensed stable silica framework. The presence of Q^3 sites indicates the availability of enough surface silanol groups for functionalization. The results presented above suggest that the activity and recyclability of the modified mesoporous material can clearly be improved by decrease of the number of surface Si-OH groups using Me_2MeO_2Si as the silylating agent. As only a small part of the Si-OH groups are consumed during the introduction of the ligand system, the remaining Si-OH groups will provide centers for the adsorption of organic compounds by hydrogen bonding, which will hinder the diffusion to and away from the catalytically active centers in the mesoporous cavities and therefore decrease the overall activity of the catalyst. Our NMR spectroscopic investigations prove that by reacting the surface with Me_2MeO_2Si converts a major part of the Si-OH groups into Si-O-$SiMe_2$ groups and therefore increases the hydrophobicity, which will reduce adsorption effects.[17]

A similar type of trend was observed for the group of materials [SBA-15, BzCl-SBA-15 and Bz-SBA-15] and [SBA-15, TsCl-SBA-15 and Ts-SBA-15].

2.3.4.2. ^{13}C CP MAS NMR spectra

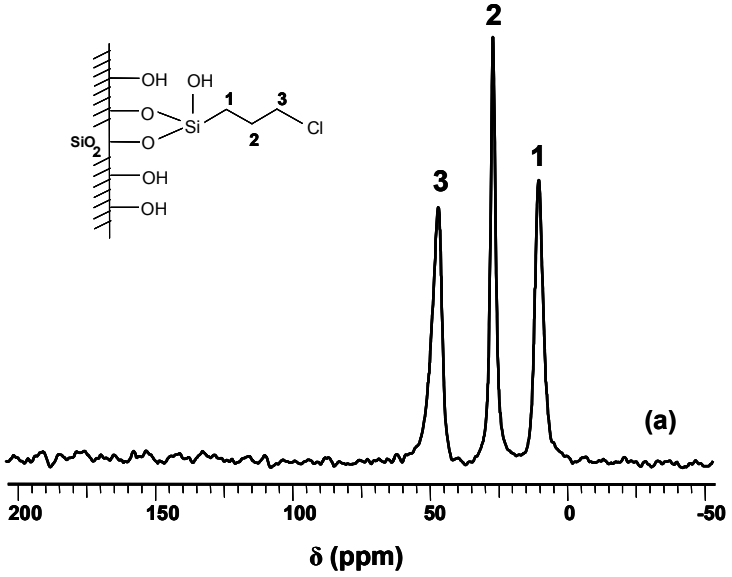

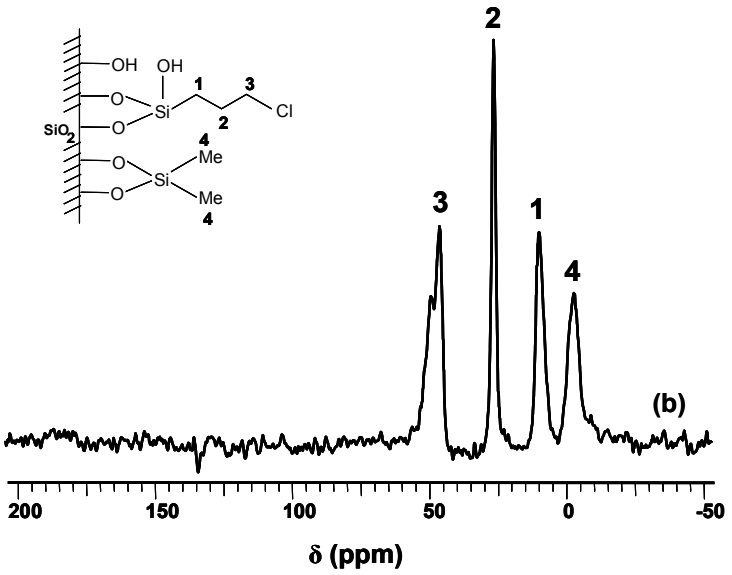

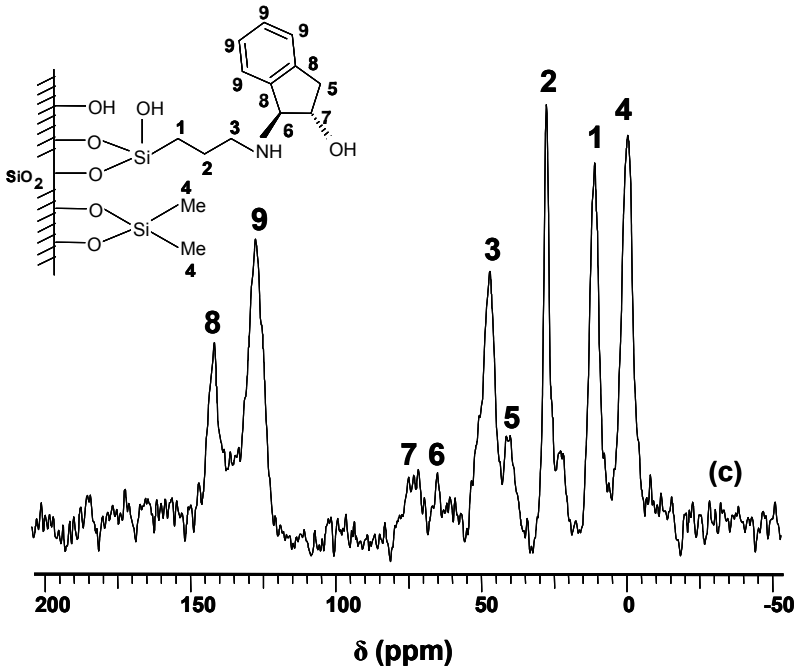

Figure 2.10: ^{13}C CP MAS NMR spectra of (a) PrCl-SBA-15, (b) Pr-SBA-15 and (c) PrAIL-SBA-15.

From ^{13}C CP MAS NMR spectra (Figure 2.10), one could see the signals at chemical shifts characteristics of the organic moieties attached on the surface of (a) PrCl-SBA-15, (b) Pr-SBA-15 and (c) PrAIL-SBA-15. In the spectrum of PrCl-SBA-15, three sharp peaks at chemical shift values δ = 9 ppm, 26 ppm and 46 ppm were observed. These signals were assigned to the carbons **1**, **2** and **3**, respectively in PrCl-SBA-15 [(Figure 2.10a].[23] In PrSBA-15 an additional resonance has observed at δ = -3 ppm along with the three resonances of the propyl carbons, which was attributed to the $–CH_3$ carbon (numbered as **4**) of the protecting molecule [Figure 2.10b]. The simultaneous presence of peaks of carbons in chloropropyl group and methyl group suggest that these two groups were grafted on mesoporous SBA-15. For PrAIL-SBA-15, the ^{13}C CP MAS NMR spectrum clearly shows the persistence of the tethering molecule and the protecting group and few signals at chemical shift values δ = 40, 64,

74, 126 and 141 ppm due to the anchored ligand molecule. In the ligand molecule three types of sp^3 hybridized carbons (numbered as **5**, **6** and **7,** Figure 2.10c and two classes of sp^2 hybridized carbon centers are present (numbered as **8** and **9,** Figure 2.10c). The resonances at δ = 40, 64 and 74 ppm correspond to the carbons **5**, **6** and **7**. The peaks at chemical shift values δ = 126 and 141 ppm are responsible for the phenyl ring[24] in the ligand molecule (numbered as **8** and **9**, Figure 2.10c). The above results clearly evidenced the successful anchoring of tethering, protecting and ligand molecules on mesoporous SBA-15.

Figure 2.11 shows the ^{13}C CP MAS NMR spectra of (a) BzCl-SBA-15 (b) Bz-SBA-15 and (c) BzAIL-SBA-15. In the BzCl-SBA-15 [Figure 2.11(a)] a sharp peak at a chemical shift value of δ = 45 ppm (numbered as **1**) is assigned to the benzyl -CH_2- fragment present in the functional molecule. This -CH_2- is attached with an electronegative chlorine atom, it is observed in the more deshielding area. The existence of the substituted benzene ring of the functional molecule is identified from the remaining signals at δ = 128, 134 and 140 ppm (numbered as **2**, **3** and **4** respectively) in the spectrum.[25] The persistence of the resonance peaks at chemical shift values of δ = 45, 128, 134 and 140 ppm in Bz-SBA-15 and BzAIL-SBA-15 proved the stability of the functional molecule after consecutive treatment with MeO_2SiMe_2 and (1R,2S)-(+)-*cis*-1-amino-2-indanol. Additionally, a sharp peak at δ = 0.7 ppm (numbered as **5)** in Bz-SBA-15 [Figure 2.11(b)] evidenced the presence of –CH_3 group because of the capping of hydroxyl groups by dimethoxydimethylsilane. BzAIL-SBA-15 [Figure 2.11(c)] demonstrates a resonance peak at a chemical shift value 8 ppm (numbered as **6**) corresponds to the cyclic –CH_2- group in the immobilized (1R,2S)-(+)-*cis*-1-amino-2-indanol molecule.[24] A set of peaks in a range of δ = 45-80 ppm indexed as the presence of -N-CH- and -O-CH- carbon atoms.

There is only one set of chemical shift values has been identified for the aromatic carbons of the functional molecule and the ligand molecule, because of the overlapping of resonance peaks for similar carbons atoms.

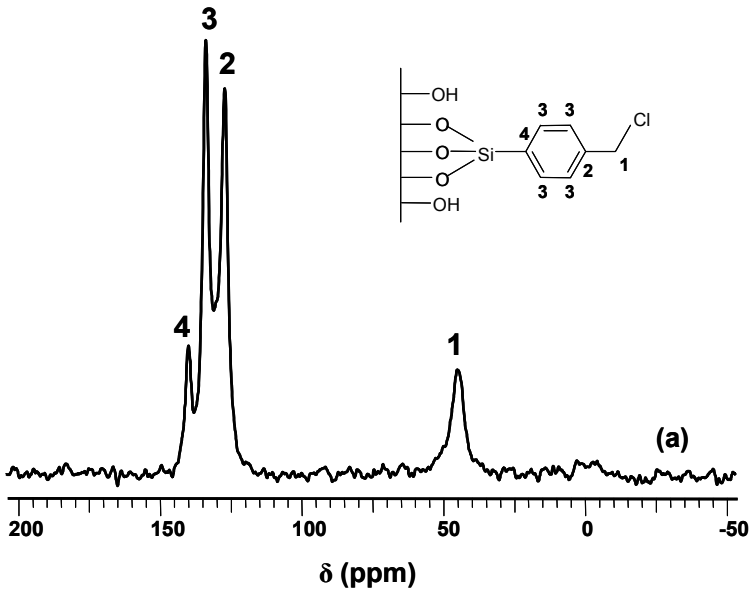

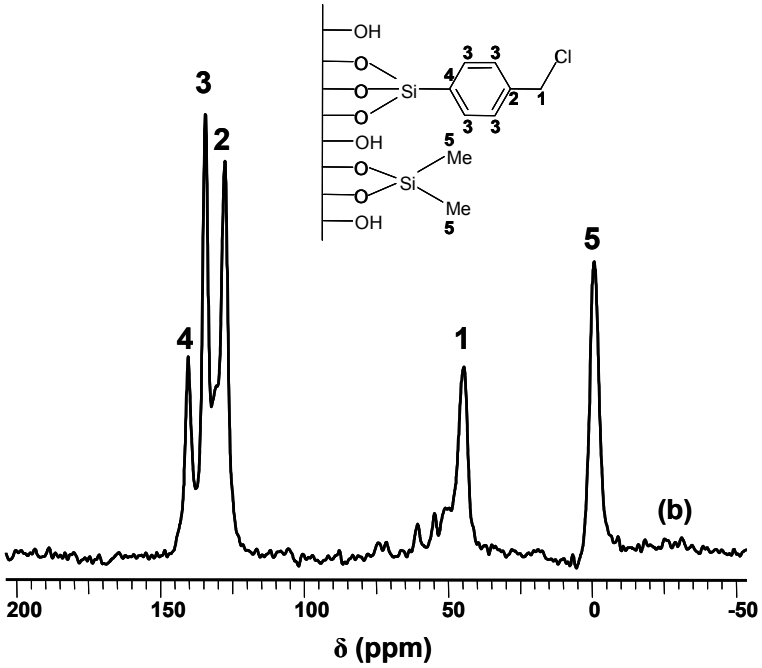

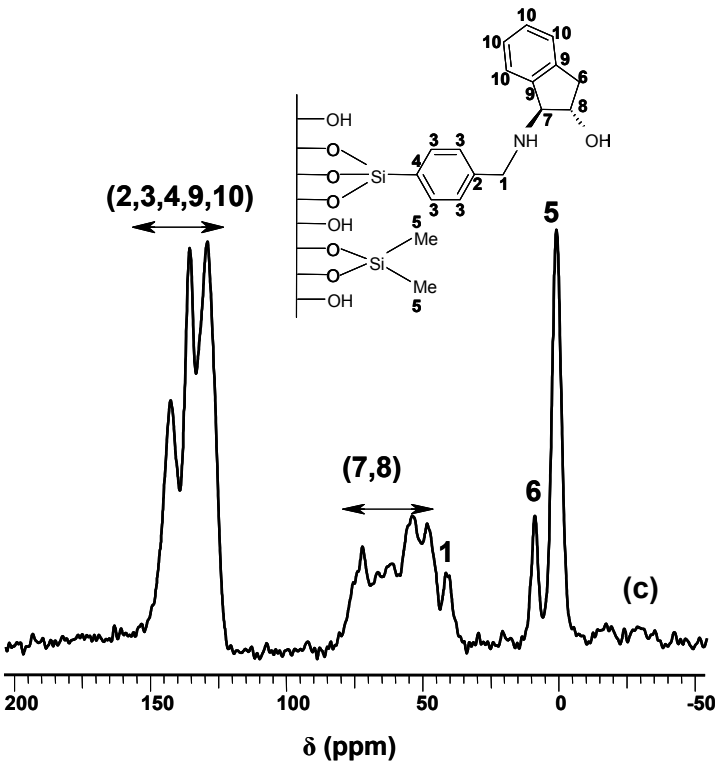

Figure 2.11: ^{13}C CP MAS NMR spectra of (a) BzCl-SBA-15, (b) Bz-SBA-15 and (c) BzAIL-SBA-15.

Figure 2.12 represents the ^{13}C CP MAS NMR spectra of (a) TsCl-SBA-15, (b) Ts-SBA-15 and (c) TsAIL-SBA-15. In the spectrum of TsCl-SBA-15 [Figure 2.12(a)], three prominent sharp peaks at chemical shift values of δ = 13, 28 and 55 ppm (numbered as **1**, **2** and **6**) have been observed in the more shielding area. These signals are due to the presence of -Si-CH_2-, -CH_2-ph- and -OCH_3 respectively.[23a] The existence of the phenyl group is identified from the remaining signals in the spectrum, *ie* δ = 128, 139 and 148 ppm (numbered as **4**, **3** and **5** respectively). For Ts-SBA-15 [Figure 2.12(b)], the ^{13}C CP MAS NMR spectrum clearly shows the existence of an additional peak at δ = 0.5 ppm along with the above mentioned resonance peaks (δ = 13, 28, 55, 128, 139 and 148 ppm), due to the –CH_3 group (numbered as **7**) in the MeO_2SiMe_2 used for capping the free reactive hydroxyl groups in the support.

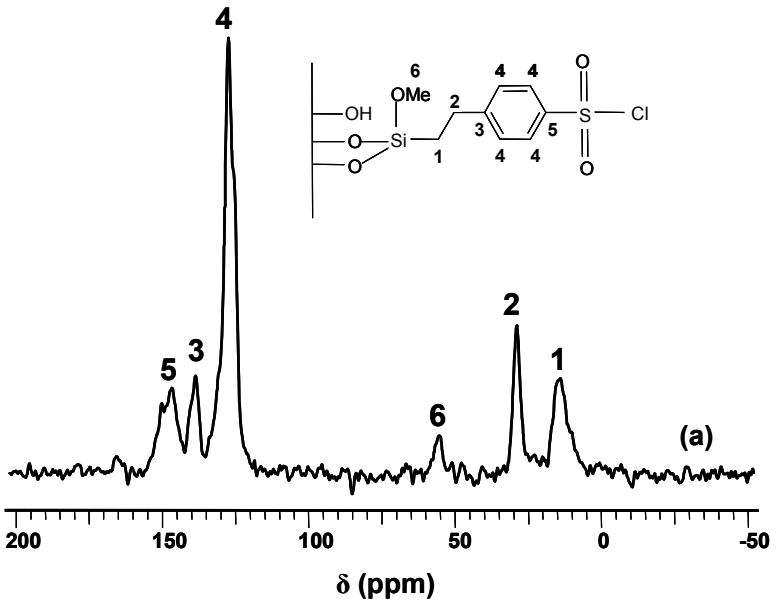
4
6
OMe
4 4
2
OH
O
Si
3
5
S
Cl
O
1
4 4
O
5
3
2
1
6
(a)
200
150
100
50
0
-50
δ (ppm)

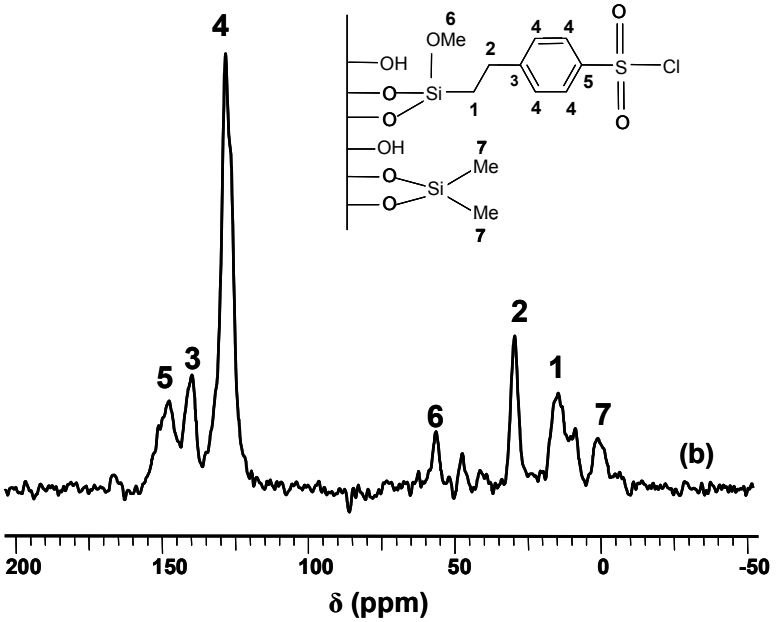
4
6
OMe
4 4
2
OH
O
Si
3
5
S
Cl
O
1
4 4
O
OH
7
Me
O
Si
O
Me
7
5
3
2
1
6
7
(b)
200
150
100
50
0
-50
δ (ppm)

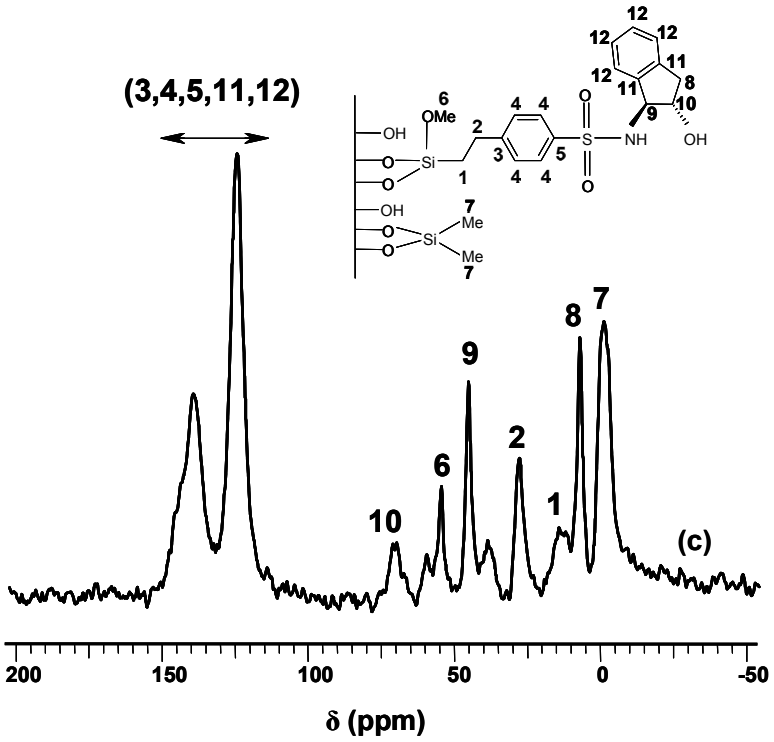

Figure 2.12: ^{13}C CP MAS NMR spectra of (a) TsCl-SBA-15, (b) Ts-SBA-15 and (c) TsAIL-SBA-15.

In the spectrum of TsAIL-SBA-15 [Figure 2.12(c)], immobilized with (1R,2S)-(+)-*cis*-1-amino-2-indanol, peaks at a chemical shift δ = 7, 46 and 72 ppm (numbered as **8**, **9** and **10** respectively) are responsible for cyclic -CH_2-, -N-CH- and -O-CH- respectively in the ligand. The peaks for aromatic carbons in the functional group and the ligand molecule have been observed in the same region of chemical shifts with one broad and one sharp peak in the range of δ = 115-155 ppm. These resonance peaks clearly indicate the immobilization of (1R,2S)-(+)-*cis*-1-amino-2-indanol molecule over Ts-SBA-15 by the removal of a HCl molecule.

2.3.5. UV-Vis studies

Table 2.6: UV-Vis absorbance values of (a) Ru-Bn-PrAIL-SBA-15, (b) Ru-Cy-PrAIL-SBA-15, (c) Ru-Bn-BzAIL-SBA-15, (d) Ru-Cy-BzAIL-SBA-15, (e) Ru-Bn-TsAIL-SBA-15 and (f) Ru-Cy-TsAIL-SBA-15.

Entry	Material	UV-Vis absorbance (nm)
1	Ru-Bn-PrAIL-SBA-15	**422**
2	Ru-Cy-PrAIL-SBA-15	**424**
3	Ru-Bn-BzAIL-SBA-15	**395**
4	Ru-Cy-BzAIL-SBA-15	**400**
5	Ru-Bn-TsAIL-SBA-15	**396**
6	Ru-Cy-TsAIL-SBA-15	**408**

Figure 2.13 illustrates the UV-Vis spectra of (a) Ru-Bn-PrAIL-SBA-15, (b) Ru-Cy-PrAIL-SBA-15, (c) Ru-Bn-BzAIL-SBA-15, (d) Ru-Cy-BzAIL-SBA-15, (e) Ru-Bn-TsAIL-SBA-15 and (f) Ru-Cy-TsAIL-SBA-15 and the values were listed in Table 2.6. A sharp peak at 422 and 424 nm has been observed for Ru-Bn-PrAIL-SBA-15 and Ru-Cy-PrAIL-SBA-15 respectively, metal-to-ligand charge-transfer (MLCT) band; clearly indicate the anchoring of the complex in the surface modified SBA-15[26]. The small difference in absorption peaks (422 nm for Ru-Bn-PrAIL-SBA-15 and 424 nm for Ru-Cy-PrAIL-SBA-15) might be due to the presence of different aromatic rings (benzene for Ru-Bn-PrAIL-SBA-15 and *p*-cymene for Ru-Cy-PrAIL-SBA-15) in the complex materials. For Ru-Bn-BzAIL-SBA-15 and Ru-Cy-BzAIL-SBA-15 a sharp peak at 399 nm in both the materials, metal-to-ligand charge-transfer (MLCT)

band, clearly indicates the anchoring of the complex in the surface modified SBA-15.[25] For Ru-Bn-TsAIL-SBA-15 and Ru-Cy-TsAIL-SBA-15 a sharp peak at 399 nm in both the materials, metal-to-ligand charge- transfer (MLCT) band, clearly indicates the anchoring of the complex in the surface modified SBA-15.

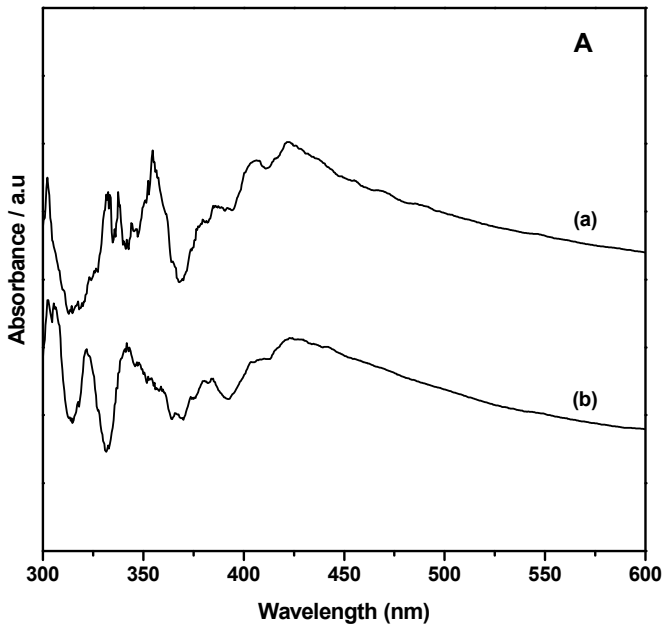

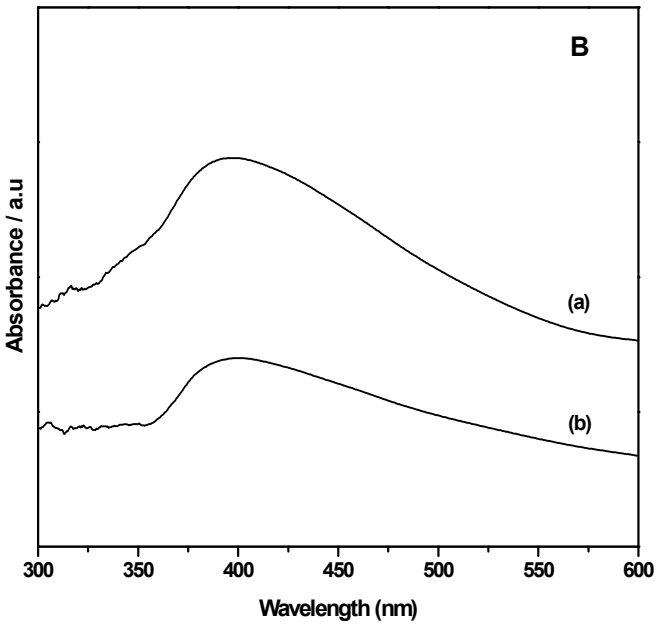

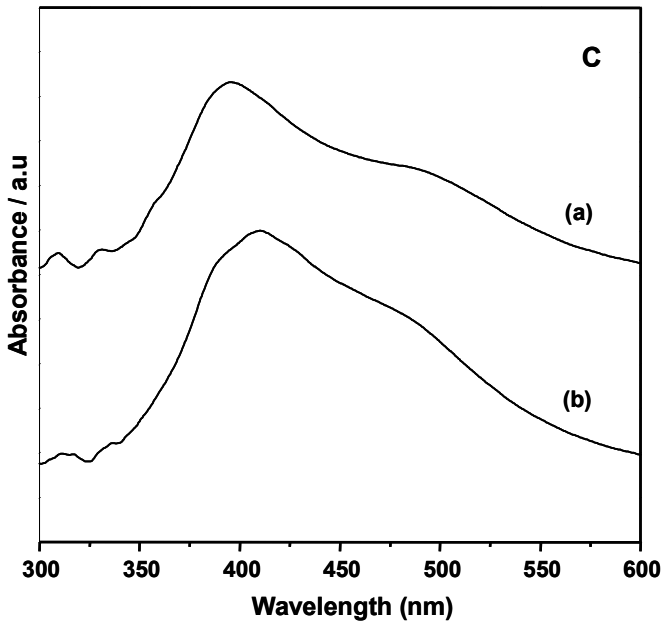

Figure 2.13: UV-Vis spectra of: A [(a) Ru-Bn-PrAIL-SBA-15 and (b) Ru-Cy-PrAIL-SBA-15], B [(a) Ru-Bn-BzAIL-SBA-15 and (b) Ru-Cy-BzAIL-SBA-15], and C [(a) Ru-Bn-TsAIL-SBA-15 and (b) Ru-Cy-TsAIL-SBA-15].

2.3.6. X-Ray Photoelectron Spectra

Usually, the binding energy (BE) of an electron depends strongly not only upon the level from which photoemission occurs but also upon the formal oxidation state of the atoms and the local chemical and physical environments of the resulting compounds.[27] Surface analytical information of the synthesized samples were obtained by x-ray photoelectron spectroscopic analysis and has given additional support for the successful anchoring of the different organic moieties and Ru(II) complexes on to the solid support. Figure 2.14 demonstrates the Si 2p (A), C 1s (B), N 1s (C), O 1s (D), Ru $3p_{3/2}$ (E) and Ru $3d_{5/2}$ (F) core level binding energies (BE) obtained from XPS analysis of PrAIL-SBA-15, Ru-Bn-PrAIL-SBA-15 and Ru-Cy-PrAIL-SBA-15 the synthesized materials. All the samples exhibit BE values of 103.5 eV and 533.0 eV correspond to Si 2p and O 1s core level of the silica material, which

is matching with the literature values very well.[26a] In PrAIL-SBA-15 a BE value of 400.4 eV corresponds to N1s core level, which is not present in Pr-SBA-15 illustrates the successful anchoring of (1R,2S)-(+)-cis-1-amino-2-indanol ligand over Pr-SBA-15. We have used the XPS spectra measured in the range from 279 to 297.5 eV to clarify the oxidation state of the Ru. The peaks that occur in this region are due to the Ru ($3d_{5/2}$ and $3d_{3/2}$) and carbon (C 1s) electron transitions. After complexing with $[RuCl_2(benzene)]_2$ and $[RuCl_2(p\text{-cymene})]_2$, we have expected two additional BE values at *ca*. 280-283 eV and 465 eV corresponding to core level BE's of Ru $3d_{5/2}$ and Ru $3p_{3/2}$ respectively. For both the samples (Ru-Bn-PrAIL-SBA-15 and Ru-Cy-PrAIL-SBA-15), we could have observed a small peak at 280.2 eV for Ru $3d_{3/2}$, which is partially overlapping with the C 1s (285 eV) peak but the Ru $3p_{3/2}$ peak has been observed clearly at 463.9 eV. These binding energies are corresponding to a Ru(II) specieses and it proved not only the structural integrity of the ruthenium precursor but also the unchanged oxidation state of the metal ion even after anchoring with the ligand molecule. The peaks were energy-shifted to the binding energy of C 1s (285 eV) to correct for the charging of the material.

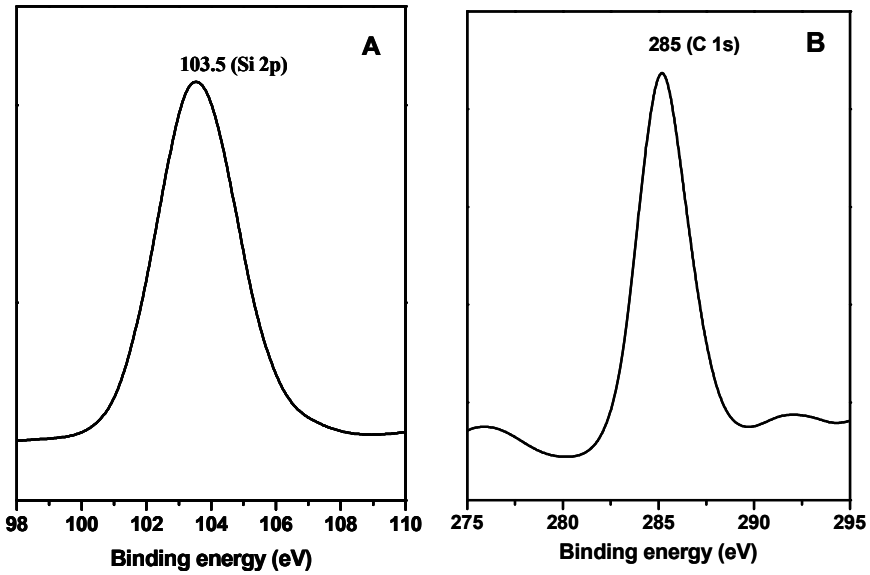

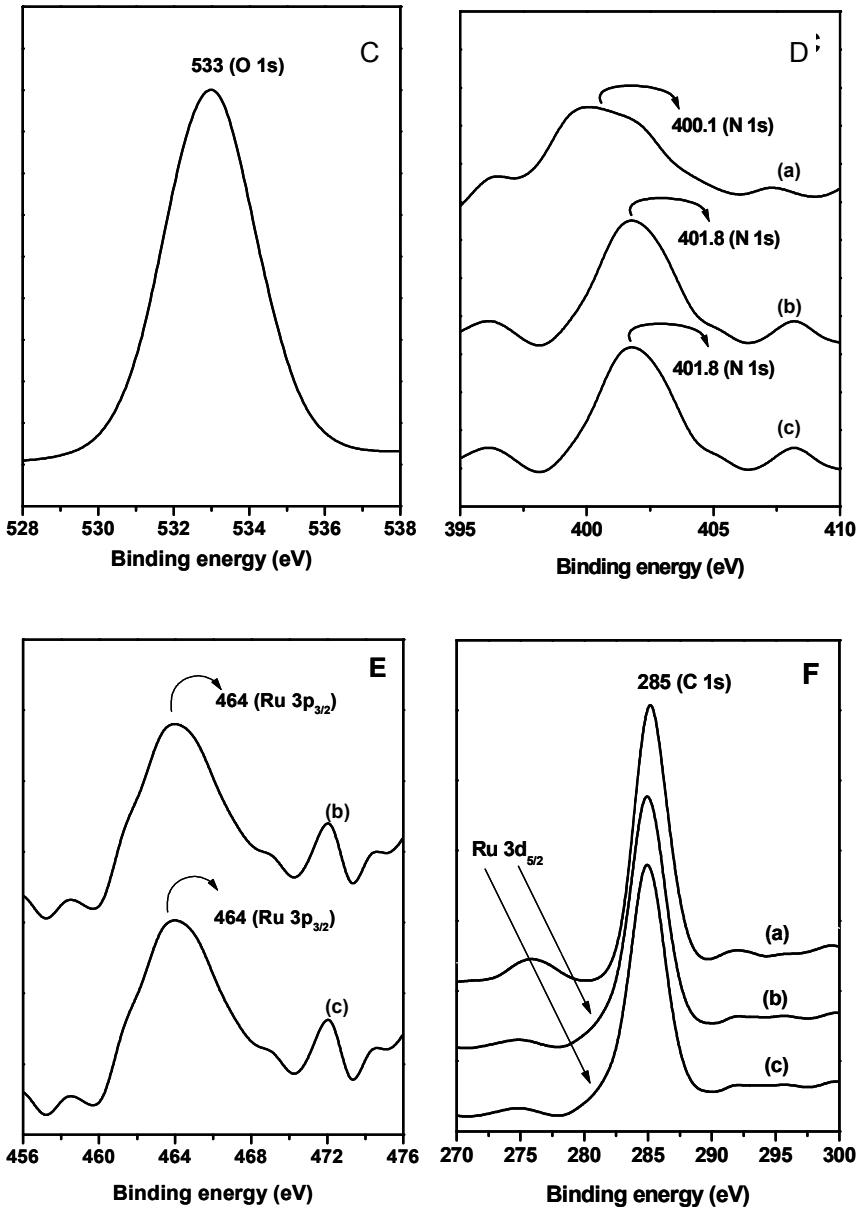

Figure 2.14: XPS spectra of: A (Si 2p), B (C 1s), C (O 1s), D (N 1s), E (Ru $3p_{3/2}$) and F (Ru $3d_{5/2}$). [(a) PrAIL-SBA-15 (b) Ru-Bn-PrAIL-SBA-15 and (c) Ru-Cy-PrAIL-SBA-15].

2.3.7. Transmission Electron Microscopy

It is now apparent that morphology and texture of mesoporous silica are extremely important and it may vary with synthesis parameters.[28] Transmission electron microscopy (TEM) has been used to obtain topographic information about the

mesoporous matrices at near atomic resolution. Figure 2.15 shows the TEM images of calcined SBA-15, along the pore direction (A & B) and perpendicular to the channels (C & D). The image (Figure 2.15 A & B) clearly revealed the formation of a regular hexagonal array of uniform channels having long-range order and the image (Figure 2.15 C & D) exposed the formation of well-defined one-dimensional channels. These results further supported by XRD results presented earlier.

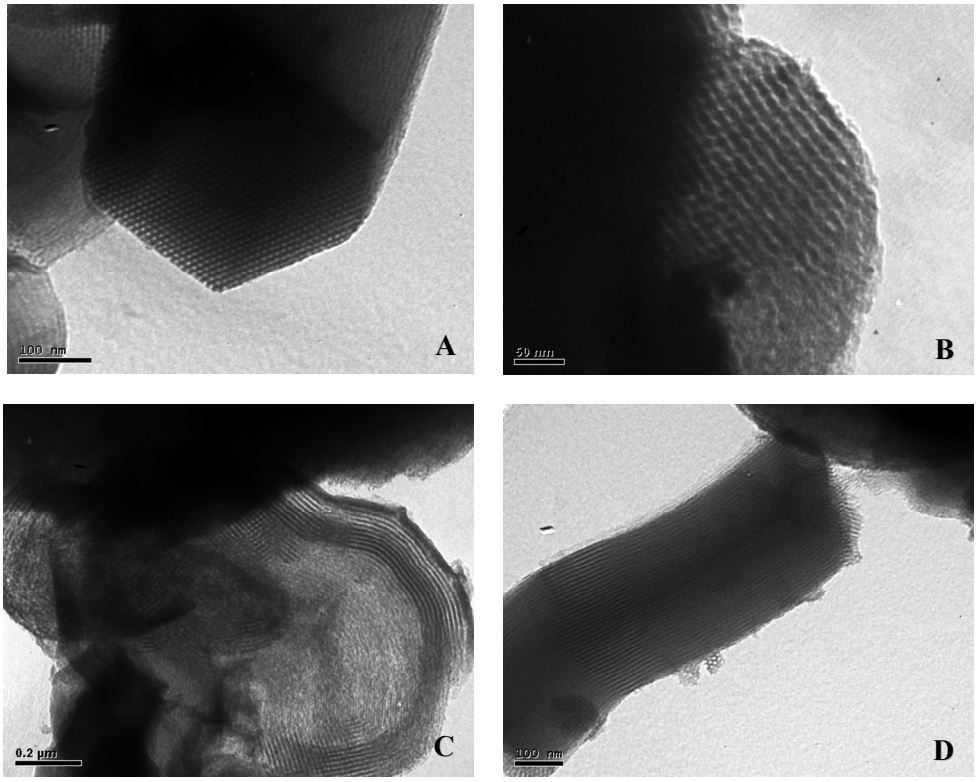

Figure 2.15: Transmission electron micrographs (TEM) of SBA-15: Electron beam was aligned parallel to the main axis of the channel (A & B) and perpendicular to the main axis of the channel (C & D).

2.3.8. Scanning Electron Microscopy

The particle size and morphology of SBA-15 and organo-functionalized SBA-15 samples have been determined by scanning electron microscopy (SEM).[29] Figure 2.16 represents the SEM images of (A) calcined SBA-15, (B) Pr-SBA-15, (C) PrAIL-SBA-

15, (D) Ru-Bn-PrAIL-SBA-15 and (E) Ru-Cy-PrAIL-SBA-15. Calcined SBA-15 shows gyroid like morphology having a particle size *ca.* 2 μm and it reveals a well distributed hexagonal material, which is earlier predicted from XRD patterns.[16a] The particle size is intact even after progressive modifications but a slight change in morphology is observed from gyroid like to disk structure, which is due to the prolonged contact of the material with solvents at drastic synthesis conditions.

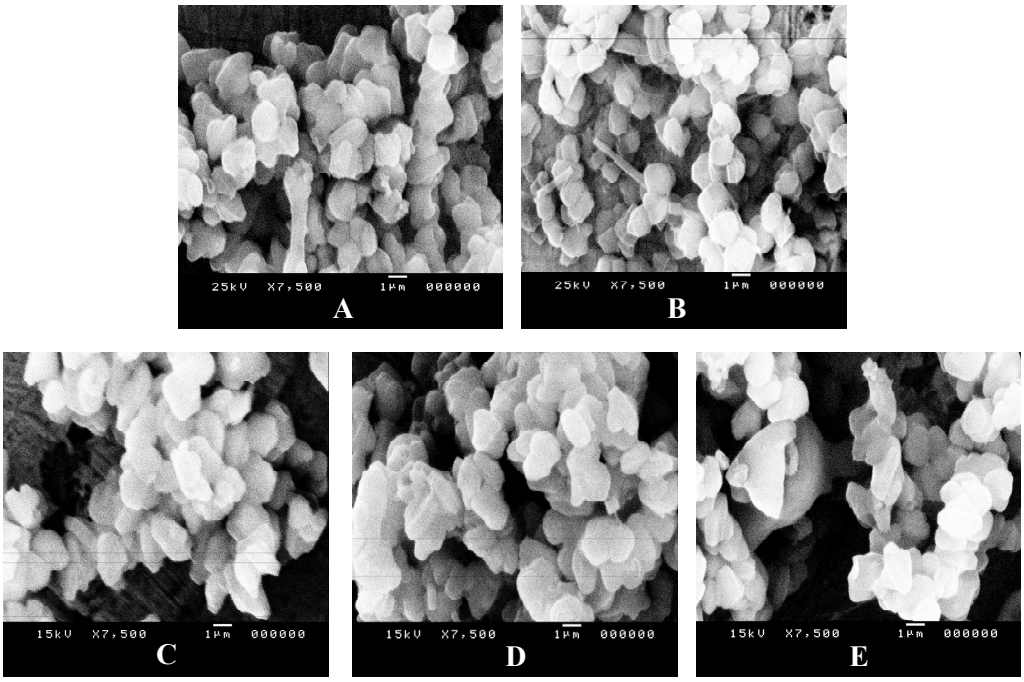

Figure 2.16: Scanning electron micrographs (SEM) of: (A) SBA-15, (B) Pr-SBA-15, (C) PrAIL-SBA-15, (D) Ru-Bn-PrAIL-SBA-15 and (E) Ru-Cy-PrAIL-SBA-15.

2.4. REFERENCES

1. Kresge, C. T.; Leonowicz, M. E.; Roth, W. J.; Vartuli, J. C.; Beck, J. S. *Nature.* **1992**, *359*, 710.
2. Beck, J. S.; Vartuli, J. C.; Roth, W. J.; Leonowicz, M. E.; Kresge, C. T. *J. Am. Chem. Soc*. **1992**, *114*, 10834.
3. Chenite, A.; Page, Y. L. *Chem. Mater*. **1995**, *7*, 1015.
4. A. Stein, B. J. Melde, R. C. Schroden. *Adv. Mater*. **2000**, *12*, 1403.
5. Zhao, D.; Feng, J.; Huo, Q.; Melosh, N.; Fredrickson, G. H.; Chmelka, B. F.; Stucky, G. D. *Science*. **1998**, *279*, 548.
6. Zhao, D.; Huo, Q.; Feng, J.; Chmelka B. F.; Stucky, G. D. *J. Am. Chem. Soc*. **1998**, *120*, 6024.
7. Moller, K.; Bein, T. *Chem. Mater*. **1998**, *10*, 2950.
8. Huo, Q.; Margolese, D. I.; Stucky, G. D. *Chem. Mater*. **1996**, *8*, 1147
9. Burkett, S. L.; Sim, S. D.; Mann, S. *J. Chem. Soc., Chem. Commun*. **1996**, 1367.
10. Babonneau, F.; Leite, L.; Fontlupt. S. *J. Mater. Chem*. 1999, *9*, 175.
11. A. Stein, B. J. Melde, R. C. Schroden. *Adv. Mater*. **2000**, *12*, 1403.
12. A. P. Wight, M. E. Devis. *Chem. Rev*. **2002**, *102*, 3589.
13. M. H. Lim, A. Stein. *Chem. Mater*. **1999**, *11*, 3285.
14. D. S. Shephard, W. Zhou, T. Maschmeyer, J. M. Matters, C. L. Roper, S. Parsons, B. F. G. Johnson, M. J. Duer. *Angew. Chem. Int. Ed*. **1998**, *37*, 2719.
15. Bennett M. A, Smith A. K. *J. Chem. Soc., Dalton Trans*. **1974**, 233-241.

16. (a) Dongyuan Zhao, Jinyu Sun, Quanzhi Li, and Galen D. Stucky. *Chem. Mater*. **2000**, 12, 275-279. (b) Zhao. D, Feng. J, Huo. Q, Melosh. N, Fredrickson G. H. Chmelka B. F.; Stucky, G. D. *Science* (Washington D.C.) **1998**, *279*, 548-552. (c) Zhao, D; Huo, Q.; Feng, J; Chmelka, B. F.; Stucky, G. D. *J. Am. Chem. Soc*. **1998**, *120*, 6024.

17. Mingjun Jia, Andreas Seifert, and Werner R. Thiel., *Chem. Mater*. **2003**, *15*, 2174-2180.

18. (a) M. R. Almeida, C. G. Partano, *J. Appl. Phys*., **1990**, *68,* 4225. (b) E.I. Kamitsos, A.P. Patsis, G. Kordas, *Phys. Rev. B*, **1993**, *48*, 12499. (c) Surendran Parambadath, M. Chidambaram, A. P. Singh, *Catal. Today*. **2004**, *97*, 233.

19. M. Suzuki, S. Ito, T. Kuwahara, *Bull. Chem. Soc. Jpn*. **1983**, *56*, 956–957.

20. M. Chidambaram, D. Curulla-Ferre, A.P. Singh, B.G. Anderson, *J. Catal*. **2003**, *220*, 442–456.

21. (a) Zhao, X. S.; Lu, G. Q. *J. Phys. Chem. B.* **1998**, *102*, 1556-1561. (b) de Juan, F.; Ruiz-Hitzky, E. *Adv. Mater.* **2000,** *12*, 430-432.

22. A.; Pillinger, M.; Pina, A.; Rocha, J.; Romaõ, C. C.; Santos, A. M.; Santos, T. M.; Valente, A. A. *Eur. J. Inorg. Chem.* **2000,** 2263-2270.

23. (a) Hengquan Yang, Gaoyong Zhang, Xinlin Hong, Yinyan Zhu. *Microporous and Mesoporous Materials*. **2004**, *68*, 119–125. (b) Humphrey H.P. Yiu, Paul A. Wright, Nigel P. Botting. *Journal of Molecular Catalysis B: Enzymatic.* **2001**, *15*, 81–92. (c) Sang-Wook Kim, Sung Jin Bae, Taeghwan Hyeon, B. Moon Kim. *Microporous and Mesoporous Materials*. **2001**, *44-45*, 523-529.

24. Dongmei Jiang, Qihua Yang, Hong Wang, Guiru Zhu, Jie Yang, Can Li., *Journal of Catalysis*. **2006**, 239, 65-73.

25. (b) M. Kinugasa, T. Harada, A. Oku, *Tetrahedron Letters*. **1998**, *39*, 4529.

26. (a) Robert J. Staniewicz, Robert F. Sympson, David G. Hendricker Z, *Inorganic Chemistry*. **1977,** *16,* 2166. (b) S. Zakeeruddin, Md. K. Nazeeruddin, R. Humphry-Baker and M. Grätzel, *Inorganica Chimica Acta*. **1999,** *296*, 250.

27. (a) M. A. Wahab, I. Kim and C. S. Ha, *Microporous Mesoporous Mater*. **2004**, 69, 19; (b) J. F. Moulder, W. F. Stickle, P. E. Sobol and K. D. Bornben, *Handbook of X-ray Photoelectron Spectroscopy*, Physical Electronics, USA, October **1995** (c) T. Asefa, M. Kruk, N. Coombs, H. Grondey, M. J. MacLaChlan and G. A. Ozin, *J. Am.Chem. Soc*. **2003,** *125*, 11662.

28. (a) Katsunori Kosuge, Tetsu Sato, Nobuyuki Kikukawa, and Makoto Takemori, *Chem. Mater*. **2004**, *16*, 899-905. (b) D. S. Shephard, W. Zhou, T. Maschmeyer, J. M. Matters, C. L. Roper, S. Parsons, B. F. G. Johnson, M. J. Duer, *Angew. Chem. Int. Ed.* **1998**, *37*, 2719.

29. (a) Katsunori Kosuge, Tetsu Sato, Nobuyuki Kikukawa, and Makoto Takemori, *Chem. Mater*. **2004**, *16*, 899-905.

Chapter 3

ATH of Prochiral Ketones Using Heterogeneous Chiral Metal Complexes

3.1. INTRODUCTION

Chiral alcohols are fundamentally important building blocks in the pharmaceutical and fine chemical industry. There is a constant need to discover and develop new methods capable of supplying such building blocks containing an increasingly diverse range of structural features. The enantioselective synthesis of chiral secondary alcohols by catalytic reduction of the corresponding ketone is becoming an important transformation in organic synthesis.[1] Much effort has been devoted to the development of new chiral catalysts and rapid progress has been made in this area. The best catalysts reported so far are ruthenium(II) complexes with chiral diamine and amino alcohol ligands.[2] Moreover, Noyori's systems based on β-amino alcohols give some of the very best results in terms of enantioselectivity and catalytic activities.[3] Transfer hydrogenation of ketones is a highly efficient method for the synthesis of chiral alcohols, owing to low fractional yields of side products and high product yields in high enantiomeric excess. The reaction conditions are relatively mild and the costs are low as a result of the operational simplicity of this method. Catalytic asymmetric reduction of C=O bonds is a pivotal transformation in organic chemistry to create new stereocenters. Very successful developments in this field have been reported in recent years and a large number of catalytic methods are now available to achieve this goal.[4] Among these, transfer hydrogenation of 2-propanol to prochiral ketones has emerged as a highly efficient technique. In this reversible process (referred to as the Meerwein-Pondorf-Verley reduction) 2-propanol acts simultaneously as a safe inexpensive easy to handle solvent and reductant that is transformed into acetone, which can be readily removed from the reaction mixture. The resulting operational simplicity and high product yields in high enantiomeric

excess for some specific ketones make catalytic transfer hydrogenation a useful complement / alternative to hydrogenation using molecular hydrogen, particularly for small to medium-scale reactions. After a rather long and quite primitive stage, several advances have been accomplished in the last decade for designing efficient hydrogen transfer catalyst systems with some transition metal and lanthanide complexes. Undoubtedly, one of the most significant breakthroughs, reported by Noyori et al., is the use of chlororuthenium(II)arene precursors with chiral monoarylsulfonylated-1,2-diamine or α-amino alcohol ligands.[5] The structurally well-defined [Ru(II)(arene)(TsDPEN)], [TsDPEN-(1R,2R)-N-(*p*-tolylsulfonyl)-1,2-diphenyl ethylene-diamine] systems enable the highly effective reduction of a variety of aryl alkyl and related ketones in above 90% *ee*.

Although a large number of chiral diamine based ruthenium complexes as catalysts have been introduced for catalytic asymmetric transfer hydrogenation reaction to till date in both homogeneous as well as heterogeneous form, only a few reports are available on chiral amino alcohol based ones which have high potential to achieve high enantioselectivities.[6] Moreover, homogeneous catalysts are characterized by high activity and selectivity, which are not generally achieved by the corresponding heterogeneous catalysts.[7] Therefore, during heterogenization of homogeneous catalysts, it was a long held view that any advantages, with regard to work up of the reaction mixture, purity of the product prepared, catalyst recovery and continuous reaction procedure, can only be realized in conjunction with serious disadvantages with regard to activity and selectivity. On this respect, we have tried to expand the utility of a highly strained but active chiral auxiliary such as (1R,2S)-(+)-*cis*-1-amino-2-indanol for asymmetric transfer hydrogenation of carbonyl compounds at milder

conditions. In this chapter we have reported the catalytic activity and enantioselectivity of various tethered (1R,2S)-(+)-*cis*-1-amino-2-indanol as catalysts for asymmetric transfer hydrogenation of simple prochiral ketones in combination with two ruthenium metal precursors such as $[RuCl_2(p\text{-cymene})]_2$ and $[RuCl_2(benzene)]_2$.

3.2. EXPERIMENTAL

3.2.1. Materials

Acetophenone, 4-methylacetophenone, 4-chloroacetophenone, 4-bromo acetophenone, 4-methoxyacetophenone, 2,5-dimethoxyacetophenone, propiophenone were purchased from Aldrich; triethylamine (NEt_3), dried 2-propanol were purchased from Merck, India and were used as received without further purification.

3.2.2. Asymmetric transfer hydrogenation of prochiral ketones

The heterogeneous catalyst (0.0001 mol % Ru content) was taken in a round bottom flask and degassed three times with N_2. Then a stock solution of ketone (0.01 mol %/3 ml 2-propanol) by a syringe followed by KOH solution (0.3 ml, 1 mg/0.1 ml 2-prpanol) was added under inert condition. The reaction mixture was stirred at 60^oC for an appropriate time and there after the catalyst was separated by centrifugation. The reaction mixture was separated and washed with sat. $NaHCO_3$ and then with sat. brine solution and separated using diethyl ether. The solution was saturated by high vacuum and the residue was purified by a short silica gel column eluted by ethyl acetate. Reduced the volume and the catalytic activity and enantiomeric excess (*ee*) were determined by GC analysis.

3.3. ENANTIOSELECTIVE TRANSFER HYDROGENATION OF PROCHIRAL KETONES

3.3.1. Activity of Different Catalysts over Various Substrates

Phenyl alkyl ketones (PhCOAlkyl) are the substrates of choice for the assessment of the synthesized heterogeneous catalysts in transfer hydrogenation reaction. For a given catalytic system, rate and selectivity are sensitive to the steric crowding of the substrates as well as to the electronic properties of the phenyl ring substituents. Later it is proved that along with the substrates the electronic and structural constrains of the active centre of the catalyst itself can control the activity and enantioselectivity.[8] The presence of an electron-withdrawing group on the phenyl ring has generally been found to facilitate the hydrogen transfer reaction and this has been attributed to the hydridic nature of the reducing species involved. As such, owing to the fast hydride transfer, the reactions of –Cl, –Br or -OMe substituted substrates should proceed at higher rate, while reactions with electron-donating substituent ($–CH_3$) should proceed in more controlled manner. In order to elucidate the catalytic activity and enantioselectivity of the synthesized catalysts, the reaction has performed using a procedure similar to the methodology available in literatures for homogeneous chiral amino alcohol complexes.[9]

All the substrates used in this study, its abbreviation, and product information are listed in the Table 3.1. All the heterogeneous catalysts prepared in this study were exploited in the enantioselective transfer hydrogenation of prochiral aromatic ketones, and the results are summarized in Table 3.2-3.4.

Table 3.1: Substrates of choice for Asymmetric Transfer Hydrogenation Reaction

Entry	Substrate	Designation	Product
1	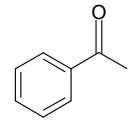 Acetophenone	**ACP**	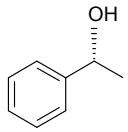 *S*-1-phenylethanol
2	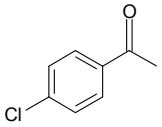 4-chloroacetophenone	**ClACP**	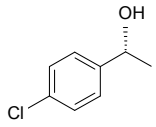 *S*-1-(4-chlorophenyl)ethanol
3	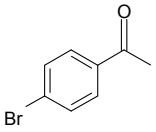 4-bromoacetophenone	**BrACP**	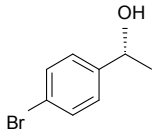 *S*-1-(4-bromophenyl)ethanol
4	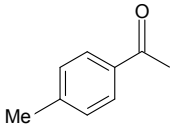 4-methylacetophenone	**MeACP**	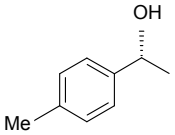 *S*-1-(4-methylphenyl)ethanol
5	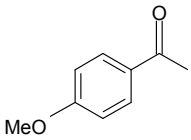 4-methoxyacetophenone	**MeOACP**	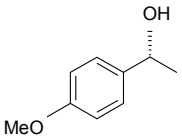 *S*-1-(4-methoxyphenyl)ethanol
6	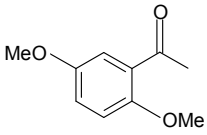 2,5-dimethoxy acetophenone	**DMeOACP**	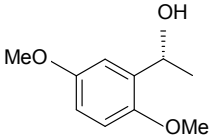 *S*-1-(2,5-dimethoxy phenyl)ethanol
7	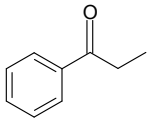 Propiophenone	**PRP**	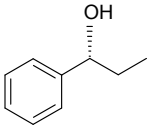 *S*-1-(phenyl)propanol

Table 3.2: ATH of simple prochiral ketones using Ru-Bn-PrAIL-SBA-15 and Ru-Cy-PrAIL-SBA-15

Entry	Substrate	Ru-Bn-PrAIL-SBA-15		Ru-Cy-PrAIL-SBA-15	
		Conversion (%)[a]	*ee* (%)[a]	Conversion (%)[a]	*ee* (%)[a]
1	**ACP**	62	66*	40	88*
2	**ClACP**	83	48	40	85
3	**BrACP**	88	48	53	84
4	**MeACP**	43	60	28	86
5	**MeOACP**	58	60	32	86
6	**DMeOACP**	56	52	26	86
7	**PRP**	77	64	41	84

The reaction was carried out at 60°C for 1 h, using 0.01 mol % of ketone and S/C ratio of 100 in 3 ml solvent. KOH = 3 mg/0.3 ml 2-propanol.

a Determined by GC equipped with a chiral column.
The configuration of alcohol product was *S*.

* Configuration was found by comparing with authentic compound.
All other configurations were found by comparing R_f values with R_f values published in literatures.

Table 3.2 explains the catalytic activities and enantioselectivities of Ru-Bn-PrAIL-SBA-15 and Ru-Cy-PrAIL-SBA-15 under similar reaction conditions. All substrates (ketones 1-7) we have used for screening the performance of catalysts reduced very well with moderate to high enantioselectivity. As a comparison, acetophenone

reduced to 62% with 66% *ee* and 40% with 88% *ee* by using Ru-Bn-PrAIL-SBA-15 and Ru-Cy-PrAIL-SBA-15, respectively (entry 1). While introducing an electron withdrawing group (-Cl or –Br) in the para position of the aromatic ring of ketone enhanced the activity with a slight decrease in *ee* (entry 2) with in 1 h. 4-Chloroacetophenone gave, 83% with 48% *ee* and 40% with 85% *ee* for Ru-Bn-PrAIL-SBA-15 and Ru-Cy-PrAIL-SBA-15, respectively. 4-bromoacetophenone gave, 88% with 48% *ee* and 53% with 84% *ee* for Ru-Bn-PrAIL-SBA-15 and Ru-Cy-PrAIL-SBA-15, respectively. But 4-methoxyacetophenone reduced in a controlled manner with in the same time limit even though the aromatic ring carrying an electron withdrawing group (entry 5). The performance of Ru-Bn-PrAIL-SBA-15 over 2,5-dimethoxyacetophenone was found to be 56% yield and 52% *ee* (entry 6). Here the activity is comparative with that of 4-methoxyacetophenone but a slight decease in *ee* is observed. At the same time Ru-Cy-PrAIL-SBA-15 performed with 26% yield and 86% *ee* (entry 6) in the reaction of 2,5-dimethoxy acetophenone keeping identical *ee* with a slight decrease in conversion than 4-methoxyacetophenone. Propiophenone converted excellently with considerable *ee* (entry 7) for both the catalysts and showed excellent performances of catalysts under our reaction conditions (77% yield with 64% *ee* and 41% yield with 84% *ee* for Ru-Bn-PrAIL-SBA-15 and Ru-Cy-PrAIL-SBA-15, respectively). The reaction product, alcohol, obtained from all the reactions have *S* configuration, which was found for acetophenone by comparing the R_f factor of *S*-1-phenylethanol with the reaction mixture and for all other products the R_f factor of the reaction mixture was compared with the literature procedure.

Table 3.3: ATH of simple prochiral ketones using Ru-Bn-BzAIL-SBA-15 and Ru-Cy-BzAIL-SBA-15

Entry	Substrate	Ru-Bn-BzAIL-SBA-15		Ru-Cy-BzAIL-SBA-15	
		Conversion (%)[a]	*ee* (%)[a]	Conversion (%)[a]	*ee* (%)[a]
1	**ACP**	56	62*	18	77*
2	**ClACP**	60	50	35	60
3	**BrACP**	60	52	34	62
4	**MeACP**	33	60	19	64
5	**MeOACP**	52	53	21	64
6	**DMeOACP**	43	44	14	51
7	**PRP**	49	54	14	70

The reaction was carried out at 60^{o}C for 1 h, using 0.01 mol % of ketone and S/C ratio of 100 in 3 ml solvent. KOH = 3 mg/0.3 ml 2-propanol.

a Determined by GC equipped with a chiral column.
The configuration of alcohol product was *S*.

* Configuration was found by comparing with authentic compound.
All other configurations were found by comparing R_f values with R_f values published in literatures.

Table 3.3 represents the asymmetric transfer hydrogenation of various derivatives of acetophenone by the second set of heterogeneous catalysts (Ru-Bn-BzAIL-SBA-15 and Ru-Cy-BzAIL-SBA-15) in 2-prpanol. Acetophenone reduced 56% and 18% with in 1 h with *ee* values of 62 % and 77% for Ru-Bn-BzAIL-SBA-15 and Ru-Cy-BzAIL-

SBA-15, respectively (entry 1). For instance 4-chloroacetophenone and 4-bromoacetophenone were reduced in 60%, the highest conversion among the substrates, having *ee* values of 50% and 52% for Ru-Bn-BzAIL-SBA-15 (entry 2 & 3). But for Ru-Cy-BzAIL-SBA-15 catalyst, lower activities (35% & 34%) with enhanced *ee* values (60% & 62%) have been observed (entry 2 & 3). The reduction of 4-methylacetophenone gave 33% conversion with 60% *ee* for Ru-Bn-BzAIL-SBA-15 and 19% conversion with 64% *ee* for Ru-Cy-BzAIL-SBA-15 (entry 4). 4-Methoxyacetophenone reduced to 52% conversion with 53% *ee* for Ru-Bn-BzAIL-SBA-15 and 21% conversion with 64% *ee* for Ru-Cy-BzAIL-SBA-15 (entry 5). 2,5-Dimethoxyacetophenone showed a reasonable conversion (43%) and less *ee* (44%) for Ru-Bn-BzAIL-SBA-15 and 14% conversion and 51% *ee* for Ru-Cy-BzAIL-SBA-15 (entry 6). The low *ee* of 2,5-dimethoxyacetophenone is probably a result of steric hindrance that affects access of the carbonyl carbon to the Ru(II)-H hydride. Propiophenone exhibited a yield of 49% and *ee* of 54% for Ru-Bn-BzAIL-SBA-15 and 14% yield and 70% *ee* for Ru-Cy-BzAIL-SBA-15 (entry 7).

Table 3.4: ATH of simple prochiral ketones using Ru-Bn-TsAIL-SBA-15 and Ru-Cy-TsAIL-SBA-15

Entry	Substrate	Ru-Bn-TsAIL-SBA-15		Ru-Cy-TsAIL-SBA-15	
		Conversion (%)[a]	*ee* (%)[a]	Conversion (%)[a]	*ee* (%)[a]
1	**ACP**	31	71*	15	81*
2	**ClACP**	42	48	19	63
3	**BrACP**	40	50	19	61
4	**MeACP**	28	60	13	67
5	**MeOACP**	20	53	12	66
6	**DMeOACP**	23	48	17	61
7	**PRP**	29	43	11	53

The reaction was carried out at 60°C for 1 h, using 0.01 mol % of ketone and S/C ratio of 100 in 3 ml solvent. KOH = 3 mg/0.3 ml 2-propanol.

a Determined by GC equipped with a chiral column.

The configuration of alcohol product was *S*.

* Configuration was found by comparing with authentic compound.

All other configurations were found by comparing R_f values with R_f values published in literatures.

Table 3.4 demonstrates the activity and enantioselectivity of Ru-Bn-TsAIL-SBA-15 and Ru-Cy-TsAIL-SBA-15 over a series of acetophenone derivatives under identical Ru catalyst–ligand loading. From the table it is clear that the synthesized materials are effective for ATH reaction of aromatic ketones. Here acetophenone

reduced to S-1-phenylethanol in 31% yield and 71% *ee* for Ru-Bn-TsAIL-SBA-15 (entry 1), whilst a decreased activity with good *ee* was observed for Ru-Cy-TsAIL-SBA-15 (entry 1, 15% yield and 81% *ee*). By introducing a strong electron withdrawing groups like –Cl or –Br in the para position of the phenyl ring of the aromatic ketone activity increased drastically as shown for the other catalysts reported in the previous tables [(entry 2, for 4-cloroacetophenone, 42% yield with 48% *ee* and 19% yield with 63% *ee* for Ru-Bn-TsAIL-SBA-15 and Ru-Cy-TsAIL-SBA-15, respectively) and (entry 3, for 4-bromo acetophenone, 40% yield with 50% *ee* and 19% yield with 61% *ee* for Ru-Bn-TsAIL-SBA-15 and Ru-Cy-TsAIL-SBA-15, respectively)]. When an electron donating group like methyl group as the substituent (entry 4), it was observed that only 28% yield and 60% ee for Ru-Bn-TsAIL-SBA-15 and 13% yield and 67% ee were observed. 4-Methoxyacetophnone a difficult substrate to reduce also followed the same trend we have observed in the previous tables (Table 2.2 & 2.3). The activity of Ru-Bn-TsAIL-SBA-15 and Ru-Cy-TsAIL-SBA-15 for the reduction of 4-methoxyacetophnone was observed with 20% yield with 53% *ee* and 12% yield with 66% *ee,* respectively (entry 5). 2,5-Dimethoxyacetophenone (entry 6) exhibited little bit higher conversion with less *ee* for both catalysts when comparing with 4-methoxyacetophenone (23% yield with 48% *ee* and 17% yield with 61% *ee* for Ru-Bn-TsAIL-SBA-15 and Ru-Cy-TsAIL-SBA-15, respectively). Propiophenone was reduced to (*S*)-1-phenylpropanol in 29% yield with 43% *ee* and 11% yield with 53% *ee* for Ru-Bn-TsAIL-SBA-15 and Ru-Cy-TsAIL-SBA-15 respectively.

From the tables, it is evident that all the heterogeneous catalysts prepared in this study performed well in the ATH of a series of prochiral ketones with very high to

medium conversion and enantiomeric excess. The most notable points from reaction results are summarized below,

1 Among the catalysts prepared Ru-Bn-PrAIL-SBA-15 and Ru-Cy-PrAIL-SBA-15 were the best catalysts for ATH reaction of prochiral ketones under our reaction conditions.

2 Acetophenone, which is the least hindered molecule, reduced with satisfactory yield and *ee* for all catalysts.

3 The molecules having a -Cl or –Br group (electron withdrawing) in the para position of the phenyl ring of acetophenone tend to increase the conversion with a reduced enantioselectivity.

4 4-Methoxyacetophenone, a difficult molecule to reduce with satisfactory yield and enantioselectivity due to its high reduction potential, reduced with moderate yield and ee for all the catalysts.

5 2,5-Dimethoxyacetophenone doesn't exhibit any reluctance to reduce even though it was the most sterically hindered molecule used in our study. The results were always better over 4-methoxyacetophenone.

6 Among theses phenyl alkyl ketones, a slight increment in the alkyl chain (methyl to ethyl) improved the yield and enantioselectivity, which evident from the results of propiophenone reduction by all synthesized catalysts.

7 The initial rate of the reaction is fast for all of the catalysts at our reaction condition.

3.3.2. Influence of reaction time over conversion and enantioselectivity

The influence of reaction time over the conversion and enantioselectivity in the asymmetric transfer hydrogenation of acetophenone is presented in Figure 3.1. It was noticed that in the case of the heterogeneous catalysts, the conversion towards transfer hydrogenation of C=O bond increases as the reaction proceeds, but enantioselectivity goes on decreasing slightly after 3 h of the reaction.

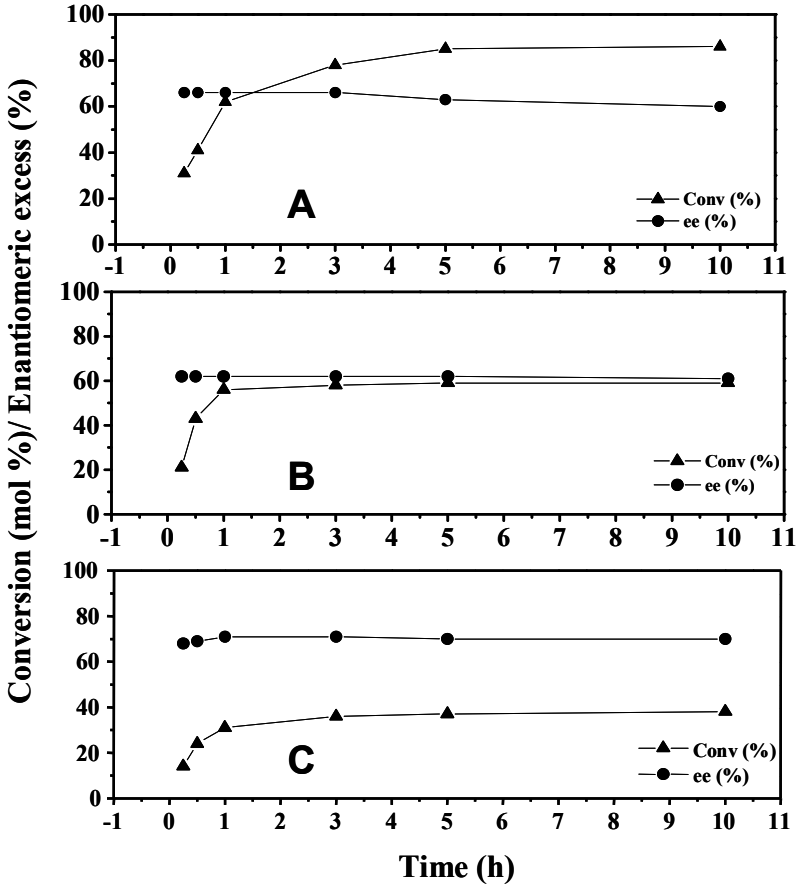

Figure 3.1: Influence of reaction time over conversion and enantioselectivity in the transfer hydrogenation of acetophenone by (A) Ru-Bn-PrAIL-SBA-15 (B) Ru-Bn-BzAIL-SBA-15 and (C) Ru-Bn-TsAIL-SBA-15. Reaction conditions: Acetophenone = 0.01 mol %, S/C = 100, 2-propanol = 3 ml, Temperature = 60 °C and KOH = 0.3 ml (1 mg/0.1 ml 2-propanol).

The reaction reaches maxima at *ca*. 5 h time. The enantiomeric excess values, however, attain a maximum from the very beginning of the reactions and increases in small amounts but after a maximum value (66%), a negligible amount of reduction was observed. This accounts for the high turn over frequency of the catalyst. Because of the reversibility of the reaction, after a particular time interval the reaction attains it maximum conversion. The saturated alcohol produced from the hydrogenation of C=O bond is the kinetically controlled product (KCP), which predominates during the initial stages of the reaction. Moreover the reaction is reversible in nature.

3.3.3. Influence of reaction temperature over conversion and enantioselectivity

Figure 3.2 demonstrates the performance (conversion and enantioselectivity) of various heterogeneous catalysts on the transfer hydrogenation of acetophenone at various reaction temperatures. The results clearly demonstrate that the asymmetric transfer hydrogenation of acetophenone is temperature dependent. As the temperature increases the activity of the catalyst also increases. But the *ee* value decreased as temperature increases as expected. It proved that at lower temperatures (0^oC and 40^oC) the reaction preferring the production of *S* isomer and at higher temperatures (60^oC and 80^oC) a marginal production of *R* isomer is taking place. It is also noticed that the activity of the catalyst is not remarkable while temperature increases from 60^oC to 80^oC.

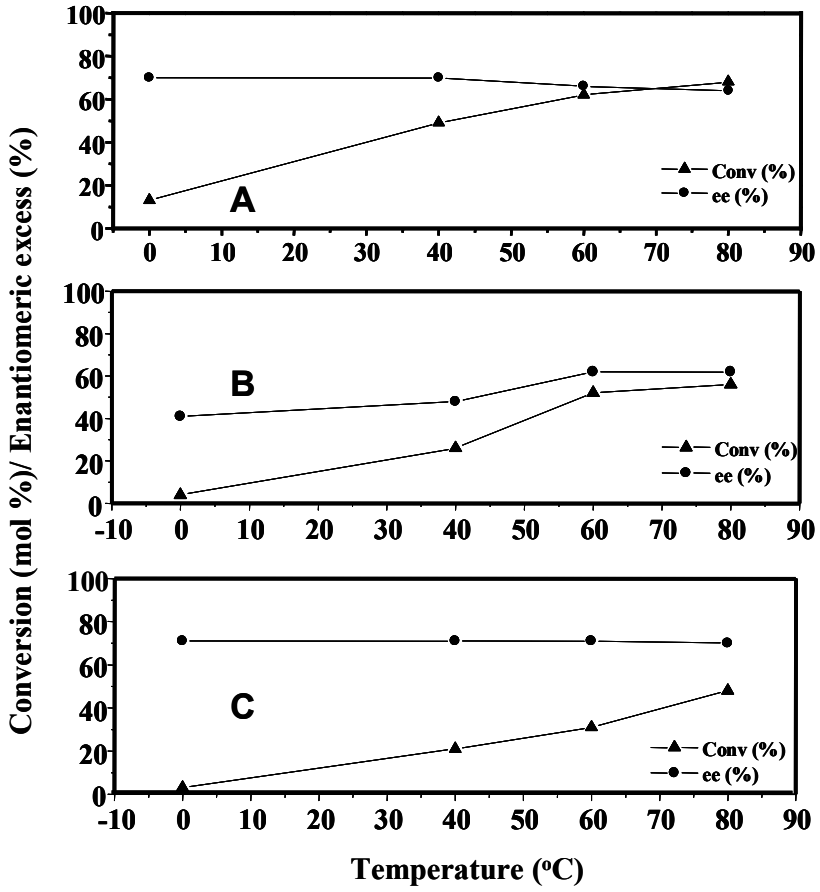

Figure 3.2: Influence of reaction temperature over conversion and enantioselectivity in the transfer hydrogenation of acetophenone by (A) Ru-Bn-PrAIL-SBA-15 (B) Ru-Bn-BzAIL-SBA-15 and (C) Ru-Bn-TsAIL-SBA-15. Reaction conditions: Acetophenone = 0.01 mol %, S/C = 100, Time = 1 h, 2-propanol = 3 ml and KOH = 0.3 ml (1 mg/0.1 ml 2-propanol).

3.3.4. Influence of amount of solvent over conversion and enantioselectivity

The effect of amount of solvent (2-propanol) over the conversion and enantioselectivity in the asymmetric transfer hydrogenation of acetophenone is presented in Figure 3.3.

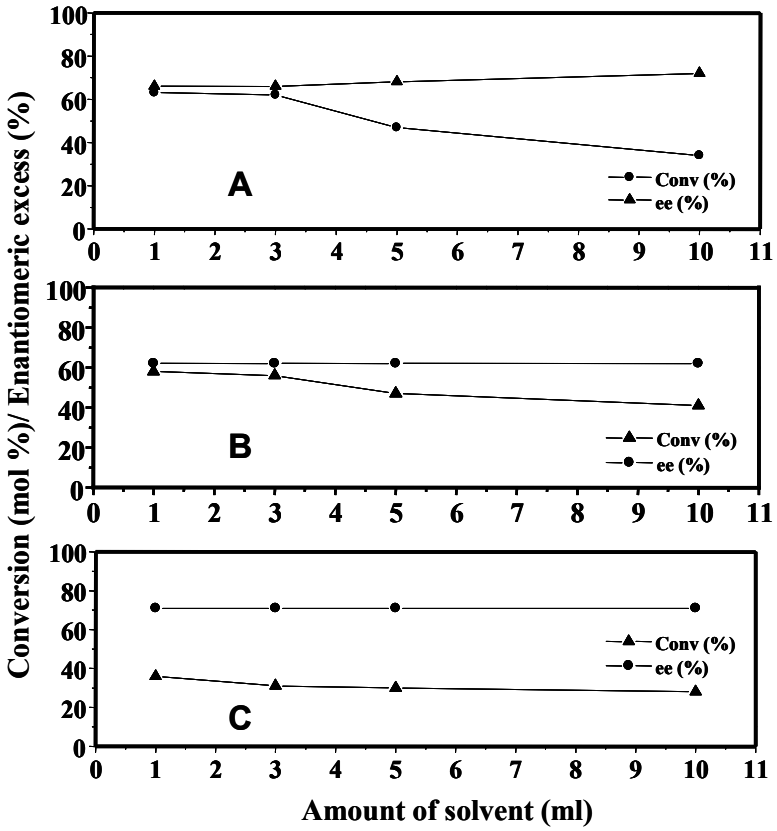

Figure 3.3: Influence of amount of solvent over conversion and enantioselectivity in the transfer hydrogenation of acetophenone by (A) Ru-Bn-PrAIL-SBA-15 (B) Ru-Bn-BzAIL-SBA-15 and (C) Ru-Bn-TsAIL-SBA-15. Reaction conditions: Acetophenone = 0.01 mol %, S/C = 100, Time = 1 h, Temperature = 60 °C and KOH = 0.3 ml (1 mg/0.1 ml 2-propanol).

It is accounted that 2-propanol is acting as a solvent and the proton donor simultaneously. During the course of the reaction it releases a proton and converting itself to acetophenone. Due to the reversibility nature of the process, here is a chance to accept a proton from the reaction products (*S* and *R*-1-phenylethanol) to change back to 2-propanol. So it is necessary to keep an optimum dilution in reaction system to prevent the backward reaction. We have studied the asymmetric reduction of acetophenone keeping 1 ml, 3 ml, 5 ml and 10 ml solvent in the reaction system. The

results illustrate that while increasing the solvent amount from 1 ml to 10 ml the activity goes on decreasing. But the *ee* value increased considerably. So for the reaction 1 ml or 3 ml of solvent is suitable for obtaining a maximum conversion

3.3.5. Influence of amount of base over conversion and enantioselectivity

To initiate the reaction the presence of the base is necessary. We have noticed that the reaction is no more initiating in the absence of a base. So it is obvious that the amount of base has a strong influence in the reaction rate. We have used 0.1, 0.2 ml, 0.3ml and 0.4 ml. base solution from a 0.18 molar solution of KOH in 2-propanol (Figure 3.4). It was manifested that while increasing the amount of base the reaction rate is increasing slightly and the enantioselectivity is intact upto 0.3 ml of base solution. However, when 0.4 ml of base solution is used, the reaction rate is increased drastically and enantioselectivity decreases along with the change in the color of the reaction mixture. The ICP analysis proved the presence of leached metal complexes in the reaction residue after centrifuged out the catalyst. So we have confirmed that the noticed higher activity is due to the leached active metal complexes when using 0.4 ml base solution. The decreased enantioselectivity is due to the progressive reaction rate by the leached metal complex in the solution.

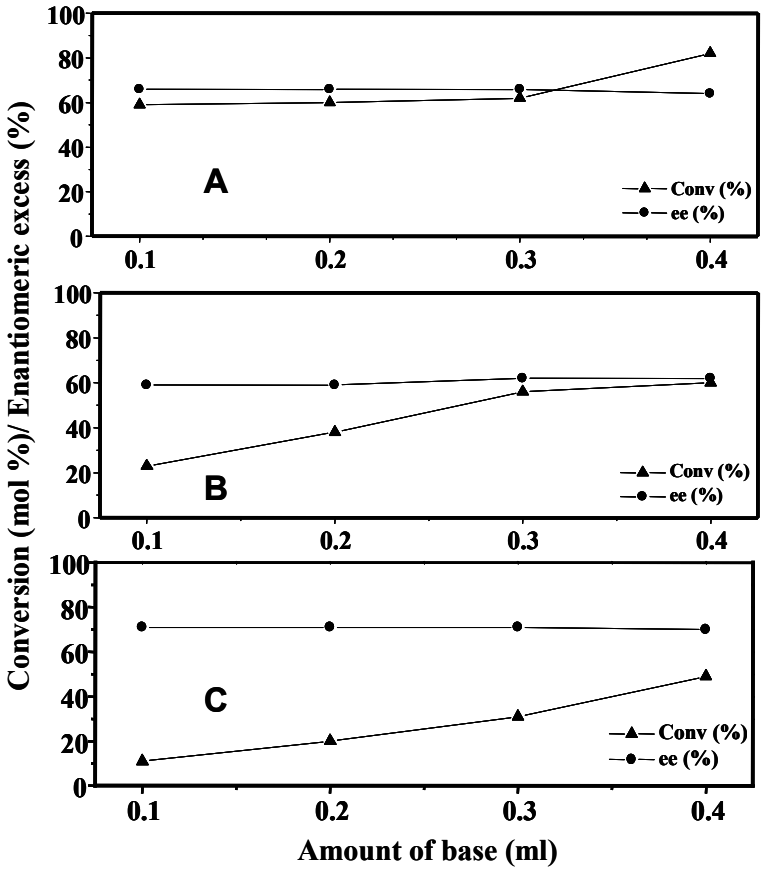

Figure 3.4: Influence of amount of base over conversion and enantioselectivity in the transfer hydrogenation of acetophenone by (A) Ru-Bn-PrAIL-SBA-15 (B) Ru-Bn-BzAIL-SBA-15 and (C) Ru-Bn-TsAIL-SBA-15. Reaction conditions: Acetophenone = 0.01 mol %, S/C = 100, Time = 1 h, Temperature = 60 °C and KOH = 1 mg/0.1 ml 2-propanol.

3.3.6. Recycling study

In order to ensure the stability and activity of recycled catalysts, the recycling study was conducted for a maximum of two runs using acetophenone under the similar reaction conditions used previously for various ketonic substrates. It is effectively worked out by washing the used catalyst with 2-propanol and immediately

used for reaction. To compare the activity of recycled catalyst under different regeneration condition, the recycling study has been conducted by (a) without-stirring in chloroform and (b) with-stirring in chloroform before conducting the reaction.

3.3.6.1. Without-stirring in chloroform

In a typical procedure the used catalyst was washed three times with dry 2-propanol (3x2 ml) and the catalyst was separated by centrifugation. The washed catalyst was transfered to the reaction vessel and immediately added the required amount of acetophenone solution. The reaction was conducted in the presence of KOH (3 mg/0.3 ml 2-propanol) for 1 h at 60^{o}C. The results are summarized in Table 3.5-3.7.

Table 3.5: Recycle studies of the heterogeneous catalysts Ru-Bn-PrAIL-SBA-15 and Ru-Cy-PrAIL-SBA-15 under **"**without-stirring in chloroform" condition for ATH of acetophenone.

	Ru-Bn-PrAIL-SBA-15		**Ru-Cy-PrAIL-SBA-15**	
No. of runs	Conv. (%)	*ee* (%)	Conv. (%)	*ee* (%)
Fresh	62	66	40	88
1	56	66	22	88
2	31	66	12	88

Table 3.6: Recycle studies of the heterogeneous catalysts Ru-Bn-BzAIL-SBA-15 and Ru-Cy-BzAIL-SBA-15 under **"**without-stirring in chloroform" condition for ATH of acetophenone.

	Ru-Bn-BzAIL-SBA-15		**Ru-Cy-BzAIL-SBA-15**	
No. of runs	Conv. (%)	*ee* (%)	Conv. (%)	*ee* (%)
Fresh	56	62	18	77
1	33	66	11	78
2	27	66	8	77

Table 3.7: Recycle studies of the heterogeneous catalysts Ru-Bn-TsAIL-SBA-15 and Ru-Cy-TsAIL-SBA-15 under **"**without-stirring in chloroform" condition for ATH of acetophenone.

	Ru-Bn-TsAIL-SBA-15		**Ru-Cy-TsAIL-SBA-15**	
No. of runs	Conv. (%)	*ee* (%)	Conv. (%)	*ee* (%)
Fresh	31	71	15	81
1	12	70	5	81
2	9	71	2	80

When the recycling studies were conducted "without-stirring in chloroform" condition, it was noted that all the heterogeneous catalysts (Table 3.5-3.7) showed poor catalytic activity with moreover similar enantioselectivity after the first recycling. The catalytic activity drastically decreasing from the first recycling run onwards and after the second recycling run, a substantial amount of metal leaching is

observed from every heterogeneous catalyst this may be due to the continuous treatment of heterogeneous metal complexes with potassium hydroxide. The poor activity may also be due to the inefficiency of taking a hydride ion from the solvent by the active metallic center or it may be due to the lack of Ru-Cl moiety to initiate a fresh reaction in presence of KOH. The ICP-AES analysis of the used catalyst after the second run showed a minor loss of active metal from the catalyst.

3.3.6.2. With-stirring in chloroform

In a typical procedure the used catalyst was washed three times with dry 2-propanol (3x2 ml) and the catalyst was separated by centrifugation. The washed catalyst was stirred in dry chloroform for 30 min under inert atmosphere. The regenerated catalyst was washed again with 2-propanol and recovered by centrifugation. Further the reaction was carried out with the required amount of acetophenone solution and in the presence of KOH (3 mg/0.3 ml 2-propanol) for 1 h at 60^{o}C under inert condition. The results are summarized in Table 3.8-3.10.

Table 3.8: Recycle studies of the heterogeneous catalysts Ru-Bn-PrAIL-SBA-15 and Ru-Cy-PrAIL-SBA-15 under **"**with-stirring in chloroform" condition for ATH of acetophenone.

	Ru-Bn-PrAIL-SBA-15		**Ru-Cy-PrAIL-SBA-15**	
No. of runs	Conv. (%)	*ee* (%)	Conv. (%)	*ee* (%)
Fresh	62	66	40	88
1	58	66	27	87
2	36	66	17	87

Table 3.9: Recycle studies of the heterogeneous catalysts Ru-Bn-BzAIL-SBA-15 and Ru-Cy-BzAIL-SBA-15 under **"**with-stirring in chloroform" condition for ATH of acetophenone.

	Ru-Bn-BzAIL-SBA-15		**Ru-Cy-BzAIL-SBA-15**	
No. of runs	Conv. (%)	*ee* (%)	Conv. (%)	*ee* (%)
Fresh	56	62	18	77
1	39	63	14	78
2	31	61	10	77

Table 3.10: Recycle studies of the heterogeneous catalysts Ru-Bn-TsAIL-SBA-15 and Ru-Cy-TsAIL-SBA-15 under **"**with-stirring in chloroform" condition for ATH of acetophenone.

	Ru-Bn-TsAIL-SBA-15		**Ru-Cy-TsAIL-SBA-15**	
No. of runs	Conv. (%)	*ee* (%)	Conv. (%)	*ee* (%)
Fresh	31	71	15	81
1	15	71	8	81
2	11	71	5	81

When the recycling studies were conducted "with-stirring in chloroform" condition (Table 3.8-3.10), a less amount of activity loss was observed without changing the enantiomeric excess when comparing with the recycling studies conducted "without-stirring in chloroform" condition. This may be assigned that a part of the deactivated catalyst was regenerated to the active pre-catalyst form, Ru-Cl, by capture of HCl while stirring in chloroform at room temperature. The activity loss may be due to the

removal of active metal from the heterogeneous complex by continuous treatment with potassium hydroxide. After the first recycling experiment the activity of the catalyst decreased drastically due to the leaching of active metal complex due to the continues treatment with chloroform. From the above results it is clear that the heterogeneous catalysts can be reused upto two times with a minor loss of catalytic activity.

3.3.7. Conclusion to the activity and enantioselectivity of various heterogeneous catalysts towards various substrates

In conclusion, a series of acetophenone derivatives were used in the asymmetric transfer hydrogenation reaction (Table 3.2-3.4). The reactivity was sometimes not high, but moderate to good enantiomeric excesses were obtained. We have selected 60^{o}C as the reaction temperature; hydrogenation proceeded smoothly at this temperature, which is not low or very high. We have used an excess of base solution in the entire study, which is necessary to initiate the reaction by the formation of a reactive metal hydride. Acetophenone is the least sterically hindered compound among the substrates showed high activity (second to 4-Cl and 4-Br substituted) and enantioselectivity (entry 1 in tables 3.2-3.4). It is observed that in the reaction of the substituted acetophenone, the enantioselectivity was not significantly affected by the type of substituent (electron donating or electron withdrawing at para positions) but the conversion has a marked effect over the type of substituent. Among the electron withdrawing groups attached substrates, 4-chloroacetophenone and 4-bromoacetophenone were reduced in high yield with low enantiomeric excess (entry 2 & 3 in tables 3.2-3.4) than 4-methoxy substituted derivative, showed less activity and enantioselectivity, which may be due to the high reduction potential of the molecule

or the formation of a stable (but labile) complex with reactive metal center by the methoxy oxygen. When comparing the 4-methoxyacetophenone, 2,5-dimethoxyacetophenone reduced slightly higher (but less considerable) yield and less amount of *ee* even though it is more sterically hindered. Normally phenyl alkyl ketones with sterically hindered substituents were reduced to the corresponding alcohols with low enantiomeric excesses but in contrast propiophenone reduced to *S*-1-(phenyl)propanol with higher (in the case of Ru-Bn-PrAIL-SBA-15 and Ru-Cy-PrAIL-SBA-15) or comparative (in the case of Ru-Bn-BzAIL-SBA-15, Ru-Cy-BzAIL-SBA-15, Ru-Bn-TsAIL-SBA-15 and Ru-Cy-TsAIL-SBA-15) conversion and *ee*. It may be due to the less steric hindrance of methyl group over ethyl group and favoring towards reaction. The catalyst is remarkably fast; a conversion of 62% was obtained after 1 h for acetophenone (catalyst Ru-Bn-PrAIL-SBA-15). Monitoring the reaction showed that the reaction rate was fast initially later the rate decreased while progressing the reaction[6b].

A blank reaction, in the absence of amino alcohol ligand, was performed to investigate the effect of the inorganic support on the catalytic reaction. On mixing {$[RuCl_2(\eta^6\text{-benzene})]_2$ / $[RuCl_2(\eta^6\text{-}p\text{-cymene})]_2$} and silica without any ligand, the Ru^{II} precursor adsorbs on the silica, which was concluded from the color change of the silica from white to orange. After thorough washing of the reaction mixture, it showed poor catalytic activity of these Ru species, however, it is negligible {(0.4 % for $[RuCl_2(\eta^6\text{-benzene})]_2$ and 0.1% for $[RuCl_2(\eta^6\text{-}p\text{-cymene})]_2$}. It was concluded from this experiment that immobilization is not effective without tethering molecule linker.[10]

As a comparison with other catalysts, Ru-Bn-PrAIL-SBA-15 and Ru-Cy-PrAIL-SBA-15 are the most active catalysts for the transfer hydrogenation of acetophenone and its derivatives under our reaction conditions. As an example acetophenone reduced 62% with 66% *ee* and 40% and 88% *ee* for Ru-Bn-PrAIL-SBA-15 and Ru-Cy-PrAIL-SBA-15, respectively. But a less activity was obtained for Ru-Bn-BzAIL-SBA-15 and Ru-Cy-BzAIL-SBA-15 (56% yield with 62% *ee* and 18% yield with 77% *ee* respectively) and Ru-Bn-TsAIL-SBA-15 and Ru-Cy-TsAIL-SBA-15 (31% yield with 71% *ee* and 15% yield with 81% *ee* respectively). The less activity may be due to the additional steric hindrance introduced by the benzyl and *p*-tosyl group along with the benzene and *p*-cymene molecules around the active metal center.

It is observed that, the heterogeneous catalyst prepared from $[RuCl_2(benzene)]_2\}$ displayed higher conversion than the catalyst prepared from $[RuCl_2(p\text{-cymene})]_2\}$ for the enantioselective reduction of simple prochiral ketones. But the *ee* results are vice versa and may be due to the favorable special arrangement of sterically hindered *p*-cymene towards enantioselection in the metal complex.[13]

From these results it is clear that both the nature of tethering molecule and the metal precursor have remarkable influence for getting maximum conversion and enantioselection.[11] Among the heterogeneous catalysts, the catalysts prepared by using propyl group as a spacer molecule showed better activity and enantioselectivity for most of the prochiral ketones which may be due to the favorable approach of the substrate molecules to the metal centre because of the less steric hindrance of the propyl group than a benzyl or *p*-tosyl molecule. A small decrease in catalyst activity was found in successive runs. This is probably due to the slow decomposition of catalyst caused by the recycling routine.[14]

3.3.8. Mechanism of heterogeneous asymmetric transfer hydrogenation

The reaction proceeds in a stepwise manner by way of a putative metal hydride, formed by elimination of acetone from 2-propanol, which then undergoes hydride transfer with a coordinated ketone, results the chiral secondary alcohol.

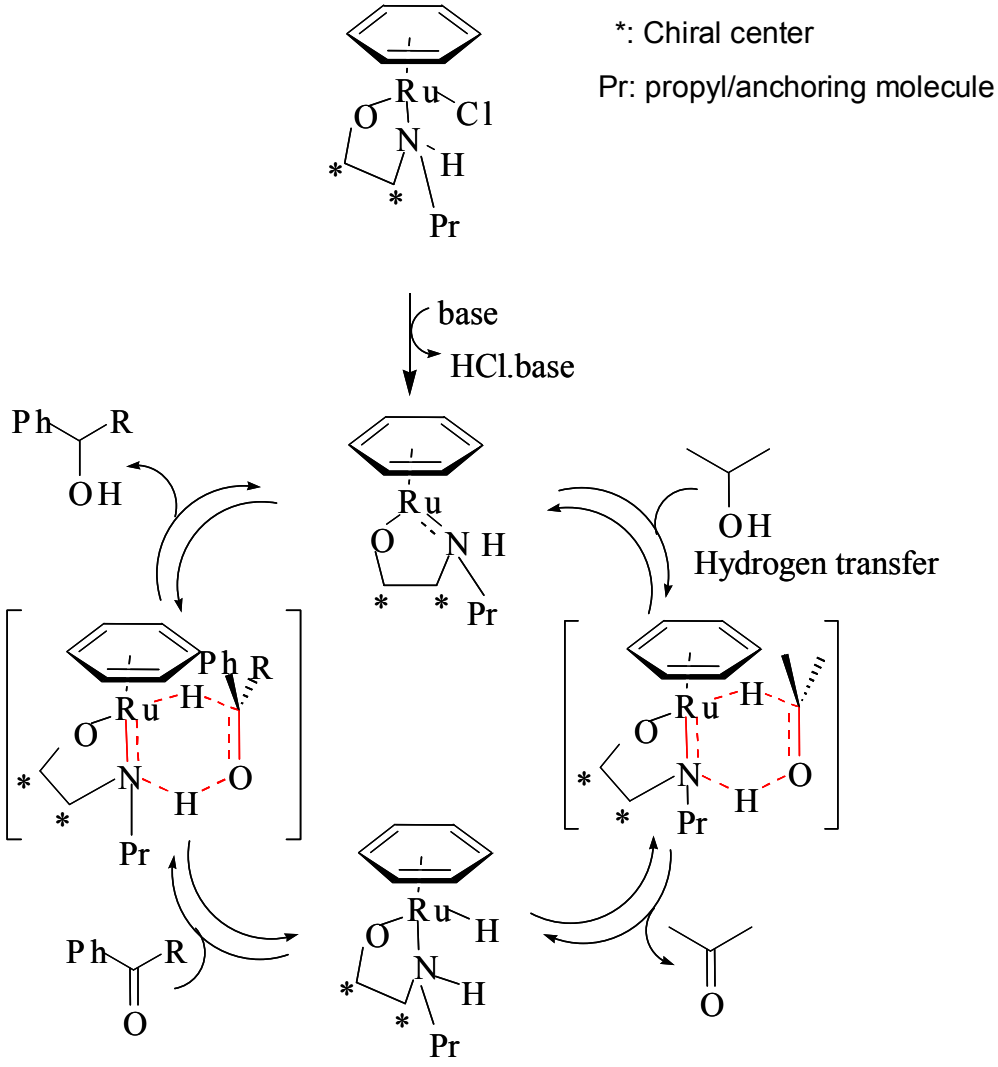

Scheme 3.1: Reaction mechanism of asymmetric transfer hydrogenation of ketone proposed by R. Noyori.[12]

When a chelating ligand having NH_2 and OH groups are mixed with $[RuCl_2(benzene)]_2$ /$[RuCl_2(p\text{-}cymene)]_2$ and base in 2-propanol, a very active catalyst

system will produce. The active form of the catalyst will be RuH-HOCH(R)CH(R)NPr)(η^6-arene) and they are generated from the precursor chloride complexes RuCl-HOCH(R)CH(R)NPr)(η^6-arene) by reaction with a reductant (2-propoxide).

Generation of catalyst,

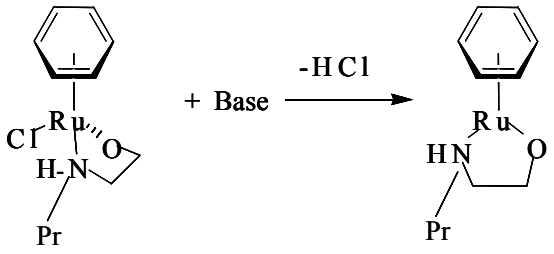

After formation of the catalyst the vacant *d* orbital of Ru will interact with 2-propanol and will abstract a proton leaving acetone to the reaction mixture.

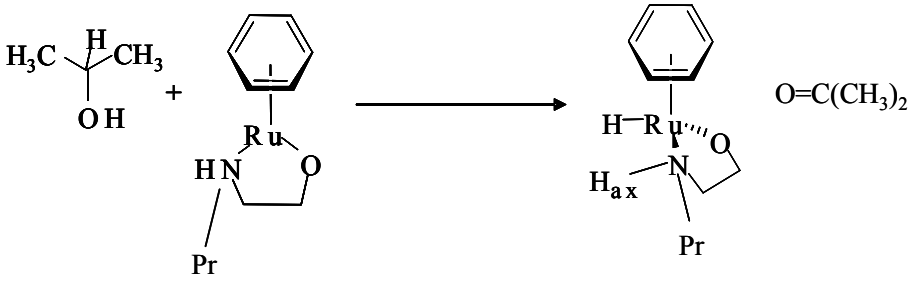

The in-coming substrate is oriented in such a way that it will form a hydrogen bond with the NH hydrogen on the (propylated) amine ligand that is axial with respect to the five-membered Ru–N–C–C–O-ring. The other two points of recognition for chiral induction are proposed to be the hydride (δ^-) to substrate sp^2-carbon (δ^+) contact and a substrate aromatic ring to η^6-ring attractive interaction. Concerted H^-/H^+ transfer produces the alcohol in the (*S*)-configuration and then the hydrido-amine complex is regenerated by reaction with 2-propanol.

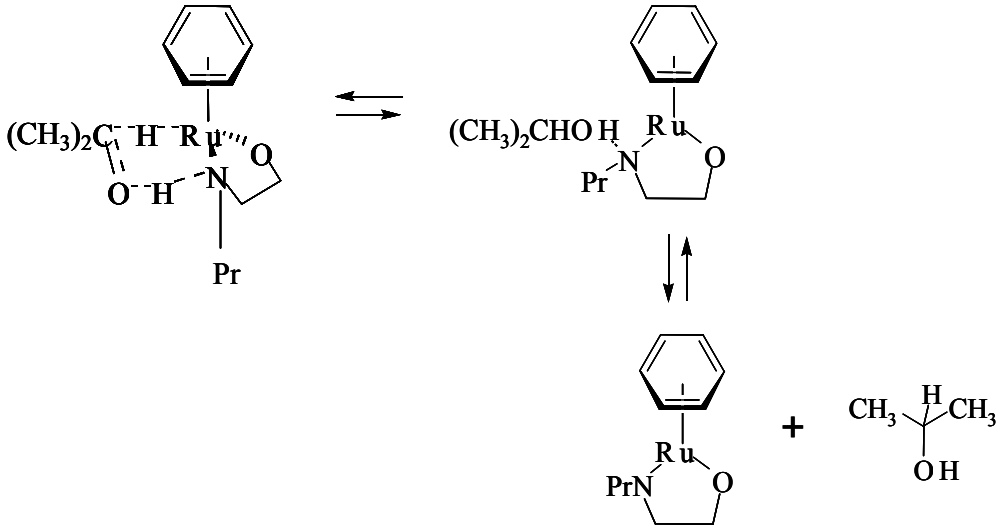

The chloride and hydride complexes have similar Ru(II) d^6, 18 electron, octahedral geometries where the arene ligand is a six-electron donor and occupies three coordination sites. The chiral amino alcohol ligand forms a five-membered ring that is locked into the δ configuration by the tethering molecule and the restricted ring system of the ligand molecule alpha to the nitrogen atom. This locks the configuration of the amino group so that the axial NH is held parallel to the Ru–Cl or Ru–H bond in the respective complexes.

3.4. REFERENCES

1. Q-H Fan, Y-M Li, A. S. C Chan, *Chem. Rev*. **2002**, *102*, 3385-3466.
2. (a) C. Saluzzo, M. Lemaire, *Adv. Synth. Catal.* **2002**, *10*, 344. (b) A. Zanotti-Gerosa, W. Hems, M. Groarke, F. Hancock, *Platinum Metals Rev*, **2005**, *49*, (4), 158–165.
3. R. Noyori, S. Hashiguchi, *Acc. Chem. Res*. **1997,** *30*, 97-102.
4. R. Noyori, T. Ohkuma, *Angew. Chem. Int. Ed*. **2001**, *40*, 40-73.
5. T. Ohkuma, H. Ooka, S. Hashiguchi, T. Ikariya, R. Noyori. *J. Am. Chem. SOC*. **1995**, *117*, 2675-2616.
6. (a) A. J. Sandee, D. G. I. Petra, J. N. H. Reek, P. C. J. Kamer, P. W. N. M. van Leeuwen, *Chem. Eur. J*. **2001**, *7*, No. 6. (b) D. G. I. Petra, P. C. J. Kamer, P. W. N. M. van Leeuwen, K. Goubitz, A. M. van Loon, J. G. de Vries, H. E. Schoemaker, *Eur. J. Inorg. Chem*. **1999**, *12*, 2335.
7. (a) J. Takehara, S. Hashiguchi, A. Fujii, I. Shin-ichi, T. Ikariya, R. Noyori, *Chem. Commun.* **1996**, 233. (b) M. Palmer, T. Walsgrove, M. Wills, *J. Org. Chem*. **1997**, *62*, 5226. (c) D. A. Alonso, D. Guijarro, P. Pinho, O. Temme, P. G. Anderson, *J. Org. Chem*. **1998**, *63*, 2749.
8. S. Gladiali, E. Alberico, *Chem. Soc. Rev*. **2006**, *35*, 226–236.
9. P-N. Liu, P-M. Gu, J-G. Deng, Y.-Q. Tu, Y-P. Ma, *Eur. J. Org. Chem.* **2005**, 3221–3227.
10. (a) P. Gamez, F. Fache, M. Lemaire, *Bull. Soc. Chim. Fr*. **1994**, *131*, 600. (b) D. Brunel, N. Bellocq, P. Sutra, A Cauvel, M. LaspeÂ ras, P. Moreau, F. Di Renzo, A. Galarneau, F. Fajula, *Coord. Chem. Rev*. **1998**, *179*, 1085.
11. K. Everaere, A. Mortreux, M. Bulliard, J. Brussee, A. van der Gen, G.

Nowogrocki, J.-F. Carpentier, *Eur. J. Org. Chem*. **2001**, 275.

12. T. Ikariya, K. Murata, R. Noyori. *Org. Biomol. Chem.*, **2006**, *4*, 393-406.
13. M. J. Palmer, J. A. Kenny, T. Walsgrove, A. M. Kawamoto, M. Wills. *J. Chem. Soc*., *Perkin Trans.*, **2002**, *1,* 416-427.
14. V. Rautenstrauch, X. Hoang-Cong, R. Churlaud, K. Abdur-Rashid, R. H. Morris. *Chem. Eur. J*. **2003**, *9*, 4954-4967.

Chapter 4

ATH Using (1R,2S)-(+)-cis-1-amino-2-indanol Based Homogeneous Complexes

4.1. INTRODUCTION

The results published in literatures in terms of enantioselectivities and catalytic activities proved that homogeneous β-amino alcohol-based Ru(II) catalysts are one of the best catalyst for asymmetric transfer hydrogenation (ATH) of aromatic ketones[1-28] in 2-propanol. Along with Ru(II) complexes, Rh(III) and Ir(III) catalysts also have been reported as efficient catalysts for the ATH of aromatic ketones in 2-propanol as well.[29-31] However, the β-amino alcohol-coordinated Ru(II), Rh(III) and Ir(III) catalysts appear to be incompatible with the azeotropic $HCOOH–NEt_3$ reduction system[6,32] which have proved to be efficient for most diamines and very rare to amino alcohol ligands.[34]

Initially Noyori and co-workers[7] examined the activity and enantioselectivity of a class of amino alcohols having flexible aromatic rings using $Ru_2Cl_4(benzene)_2$ and $Ru_2Cl_4(\eta^6\text{-hexamethylbenzene})_2$ as ruthenium precursors. The chiral Ru complexes were prepared in situ by heating a mixture of $[RuCl_2(\eta^6\text{-arene})]_2$ and β-amino alcohols with a threo or erythro relative configuration and different nitrogen-substitution patterns. A model reaction using acetophenone indicated that various structural parameters including the alkyl substituents on the arene ligands markedly, but not straightforwardly, affect the rate of the reaction and the extent of the enantioselectivity. High enantioselectivity was obtained only when an appropriate arene and chiral amino alcohol auxiliary were combined. Most notably, the presence of a primary or secondary amine end in the amino alcohols is crucial for the catalytic activity; the dimethylamino analogues are totally ineffective. Thus, the combined system consisting of $[RuCl_2(\eta^6\text{-hexamethylbenzene})]_2$ and N-methyl-(1R,2S)-2

amino-1,2-diphenylethanol gave (S)-1-phenylethanol in 92% ee and in 94% yield after 1 h of reaction at 28°C.

Table 4.1: Strained chiral amino alcohols used by Carpentier *et al.*

Entry	Ligand	Catalytic performance			
		Substrate	Time	Conv. (%)	*ee* (%)
1	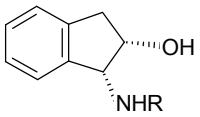 R=H (**1**), CH_2(4-C_6H_4Ph) (**2**)	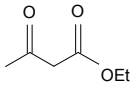	(**1**) 5	99	10
		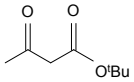	(**2**) 40	99	46
2	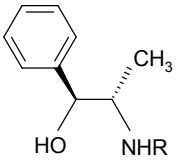 R= Me (**1**), CH_2Ph (**2**)	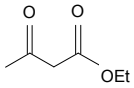	(**1**) 1	99	2
		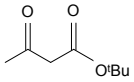	(**2**) 4	99	20
3	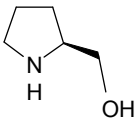	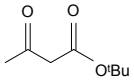	2	40	12
4	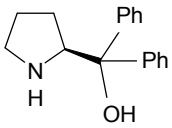	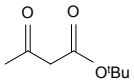	96	5	0
5	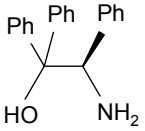	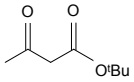	96	3	0
6	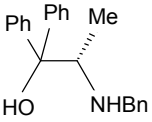	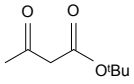	22	3	0

J. F. Carpentier and coworkers[20] exclusively studied the asymmetric transfer hydrogenation of functionalized ketones with (β-amino alcohol)(arene)Ru^{II} catalysts using 2-propanol as the hydrogen source. They have screened various structured

catalysts systematically using a wide variety of $[(\eta^6\text{-arene})RuCl_2]_2$ complexes and β-amino alcohols, some of which were specifically designed for optimized performance. The efficiencies of the catalytic combinations have been evaluated in the reduction of β-oxo esters and ketones bearing heteroatoms at the β-position. It is found that the substituent groups on the β-amino atom have a marked effect on the catalytic performance and enantioselectivity of modified amino alcohols. Along with the modified norephedrine ligands they have screened the performances of some chiral amino alcohols having fused or sterically hindered ring systems with modification over the β-amino atom using aliphatic and aromatic molecules to ensure the solid hand of pendent groups on the catalytic performance (Table 4.1).

Perhaps asymmetric transfer hydrogenation is one of the most useful methods for preparing enantiomerically pure secondary alcohols; there has been huge interest in improving this reaction, especially in respect to finding a cheaper precatalyst. *cis*-1-amino-2-indanol has been employed in such a role in the asymmetric reductions of acetophenone derivatives and a number of *N*-substituted derivatives have been prepared and tested as catalysts claiming quantitative yields and enantiomeric excess greater than 80%. While independent studies have examined the reduction of a range of prochiral ketones with the parent *cis*-1-amino-2-indanol derived catalyst.

Wills and coworkers had intensively studied the use of stereochemically rigid amino alcohols in combination with ruthenium(II) arene complexes, a technique that provides remarkably high catalytic activities when even a very small amount of ligand was employed. In order to maximize asymmetric inductions, they felt that the use of a stereochemically rigid amino alcohol, (1*R*,2*S*)-(+)-*cis*-1-amino-2-indanol, would be beneficial[10]. To ensure the above fact they have compared the activity of (1*R*,2*S*)-(+)-

cis-1-amino-2-indanol against the Ru(II) complexes of (R)-phenylglycinol and N-methyl-(1*R*,2*S*)-(+)-*cis*-1-amino-2-indanol. Patti *et al*. found that (R)-1-N-benzylamino-2-hydroxy-3-ferrocenylpropane provided a 94% conversion and 70% *ee* (R) in 3 h at room temperature. Through optimization of the ligand structure, they were generally able to improve the reaction rate and asymmetric induction by increasing the steric bulk around the amine moiety via N-alkylation.[16] While examining the chiral directive effects of several substituted 2-amino ethanol and norephedrine-based ligands in ATH reactions, van Leeuwen reported that (1R,2S)-N-benzyl-norephedrine provided the highest asymmetric induction.[25] Andersson *et al*. were successful in developing highly active and selective catalysts from 2-azanorbornyl derivative.[11-13] Reductions using this amino alcohol were fast, providing 96% conversion to the alcohol and 96% *ee* with a S/C ratio of 5000 in 90 min. It should be pointed out that when amino alcohols were used as chiral directors in ATH reactions, the best results were achieved using isopropanol as the hydride source. Several research groups have reported on the incompatibility of amino alcohols with formic acid/triethylamine as the hydride source.[6,33]

From the above reports it is proved that rigid *cis*-1-amino-2-indanol and its derivatives are useful and effective chiral auxiliaries in several asymmetric synthetic processes because of their availability, ease of recovery and the high degree of asymmetric induction that results. It is important to note that both enantiomers of *cis*-1-amino-2-indanol [(1R,2S) / (1S,2R)] are readily available from commercial suppliers, are inexpensive and have been extensively used for various types of reactions. The rigid *cis*-1-amino-2-indanol system was used by a Sepracor team (Gao and co-workers) as a chiral auxiliary for the synthesis of the chiral tertiary R-hydroxy

acid functionality found in (*S*)-oxybutynin, a muscarinic receptor antagonist. Very recently, Ghosh and co-workers have brilliantly demonstrated that, not only the C-1 amine, but also the C-2 hydroxyl moiety of the(1R,2S)-(+)-*cis*-1-amino-2-indanol, can be effectively utilized in several asymmetric synthetic processes because the rigid (1R,2S)-(+)-cis-1-amino-2-indanol backbone has a highly defined chiral environment.

In this chapter we focused on the utility of (1R,2S)-(+)-*cis*-1-amino-2-indanol derivatives as chiral auxiliary in combination with Ru(II) arene complexes as catalysts in the homogeneous asymmetric transfer hydrogenation reaction of simple prochiral ketones under milder reaction conditions. We have modified (1R,2S)-(+)-*cis*-1-amino-2-indanol (AIL) using 1-bromopropane, benzyl bromide and *p*-toluene sulfonylchloride to get NH-propyl-(1R,2S)-(+)-*cis*-1-amino-2-indanol (PrAIL), NH-benzyl-(1R,2S)-(+)-*cis*-1-amino-2-indanol (BzAIL) and NH-*p*-toluenesulfonyl-(1R,2S)-(+)-*cis*-1-amino-2-indanol (TsAIL) respectively. The complete characterization of the chiral auxiliaries and the corresponding homogeneous complexes using ^{1}H & ^{13}C NMR, UV-Vis and FT-IR spectra were also included. The synthesized catalysts are successfully utilized in the asymmetric transfer hydrogenation of a series of simple prochiral ketones under mild reaction conditions in 2-propanol.

4.2. EXPERIMENTAL

4.2.1. Materials

(1R,2S)-(+)-*cis*-1-amino-2-indanol, 1-bromopropane, benzyl bromide and *p*-toluene- sulfonylchloride were purchased from Aldrich chemicals, USA. $[RuCl_2(\eta^6$-benzene$)]_2$, $[RuCl_2(\eta^6$-*p*-cymene$]_2$ were prepared according to a published method. All reagent grade solvents were used after purification by standard methods.

4.2.2. Preparation of NH-propyl-(1R,2S)-(+)-*cis*-1-amino-2-indanol

Potassium carbonate (234 mg, 1.7 mmol) was added to (1R,2S)-(+)-*cis*-1-amino-2-indanol (255 mg, 1.7 mmol) in acetonitrile at room temperature. At 0°C, 1-bromopropane (209 mg, 1.7 mmol) was added and the resulting mixture was stirred for 48 h at 70°C. The reaction mixture was filtered and the filtrate evaporated to dryness. The resulted dirty yellow powder was purified by washing with sat. $NaHCO_3$ and then with sat. brine solution after dissolving in dichloromethane. The organic part was separated and further washed with water (4x15 ml) to ensure the complete removal of unreacted (1R,2S)-(+)-*cis*-1-amino-2-indanol. The solution was saturated by high vacuum and the residue was purified by a short silica gel column eluted by ethyl acetate.

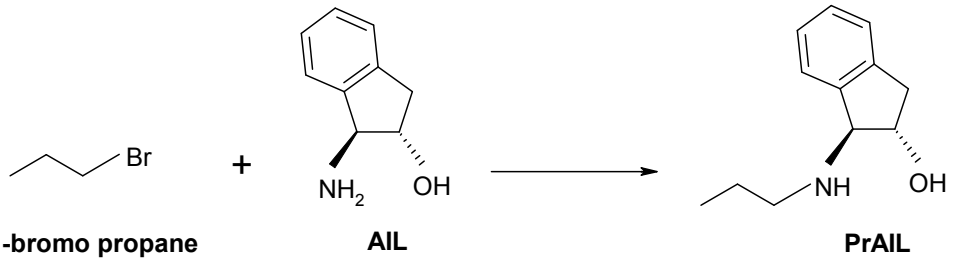

Scheme 4.1: Preparation of PrAIL

4.2.3. Preparation of NH-benzyl-(1R,2S)-(+)-*cis*-1-amino-2-indanol

Potassium carbonate (234 mg, 1.7 mmol) was added to (1R,2S)-(+)-*cis*-1-amino-2-indanol (255 mg, 1.7 mmol) in acetonitrile at room temperature. At 0°C, benzyl bromide (290 mg, 1.7 mmol) was added and the resulting mixture was stirred for 24 h at 70°C. The reaction mixture was filtered and the filtrate evaporated to dryness. The

resulted dirty yellow powder was purified by washing with sat. $NaHCO_3$ and then with sat. brine solution after dissolving in dichloromethane. The organic part was separated and further washed with water (4x15 ml) to ensure the complete removal of unreacted (1R,2S)-(+)-*cis*-1-amino-2-indanol. The solution was saturated by high vacuum and the residue was purified by a short silica gel column eluted by ethyl acetate.

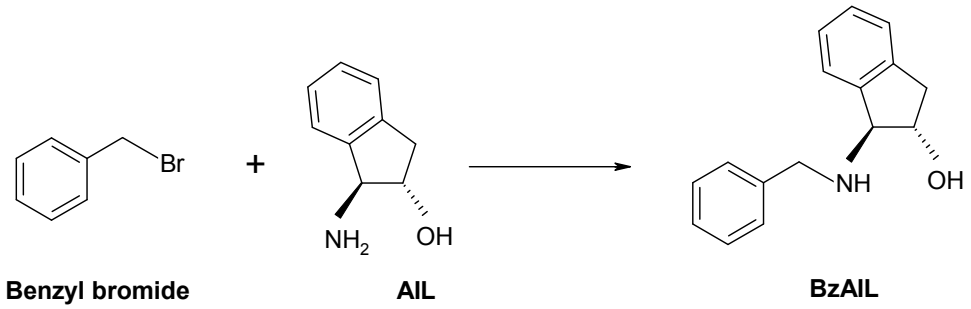

Scheme 4.2: Preparation of BzAIL

4.2.4. Preparation of NH-(*p*-toluenesulfonyl)-(1R,2S)-(+)-*cis*-1-amino-2-indanol

Triethylamine (171 mg, 1.7 mmol) was added to (1R,2S)-(+)-*cis*-1-amino-2-indanol (255 mg, 1.7mmol) in dry dichloromethane at room temperature. At 0^oC, *p*-toluenesulfonylchloride (324 mg, 1.7 mmol) was added slowly and the resulting mixture was stirred for 36 h at 0^oC. The reaction mixture was purified by washing with sat. $NaHCO_3$ and then with sat. brine solution. The organic part was separated and further washed with water (4x15 ml) to ensure the complete removal of unreacted (1R,2S)-(+)-*cis*-1-amino-2-indanol. The solution was saturated by high vacuum and the residue was purified by a short silica gel column eluted by ethyl acetate.

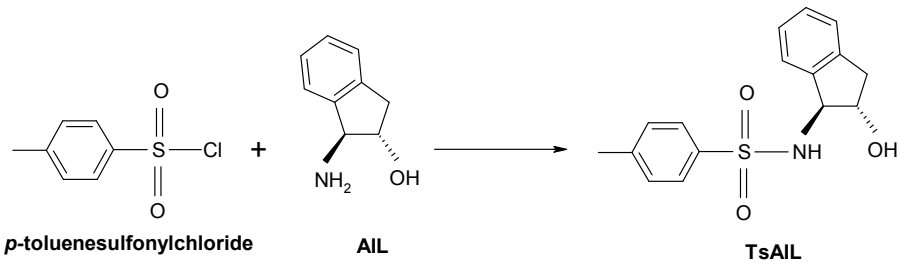

Scheme 4.3: Preparation of TsAIL

4.2.5. Preparation of [{η^6-benzene}{η^2-*N*,*O*-(1R,2S)-(+)-N-propyl-*cis*-1-amino-2-indanol^{-1}}RuCl]/[{η^6-*p*-cymene}{η^2-*N*,*O*-(1R,2S)-(+)-N-propyl-*cis*-1-amino-2-indanol^{-1}}RuCl]

NH-propyl-(1R,2S)-(+)-*cis*-1-amino-2-indanol (38.4 mg, 0.2 mmol), [$RuCl_2(\eta^6$-benzene)]$_2$ / [$RuCl_2(\eta^6$-*p*-cymene]$_2$ (0.1 mmol) and triethylamine (0.056 ml, 0.4 mmol) were taken in 2-propanol (20 ml) and heated at 80 °C for 2 h. The dark red/brown solution was then concentrated to dryness, and the residue was washed with water (10x3 ml) and dried under reduced pressure to afford [{η^6-benzene}{η^2-*N*,*O*-(1R,2S)-(+)-N-propyl-*cis*-1-amino-2-indanol^{-1}}RuCl] *(Ru-Bn-PrAIL)* / [{η^6-*p*-cymene}{η^2-*N*,*O*-(1R,2S)-(+)-N-propyl-*cis*-1-amino-2-indanol^{-1}}RuCl] *(Ru-Cy-PrAIL)* as shining powder.

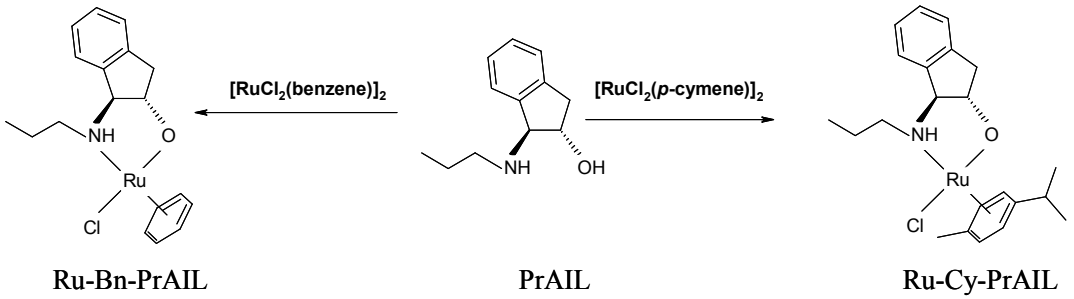

Scheme 4.4: Preparation of Ru-Bn-PrAIL and Ru-Cy-PrAIL

4.2.6. Preparation of [{η^6-benzene}{η^2-*N*,*O*-(1R,2S)-(+)-N-benzyl-*cis*-1-amino-2-indanol^{-1}}RuCl]/[{η^6-*p*-cymene}{η^2-*N*,*O*-(1R,2S)-(+)-N-benzyl-*cis*-1-amino-2-indanol^{-1}}RuCl]

NH-benzyl-(1R,2S)-(+)-*cis*-1-amino-2-indanol (48 mg, 0.2 mmol), [$RuCl_2(\eta^6$-benzene)]$_2$ / [$RuCl_2(\eta^6$-*p*-cymene]$_2$ (0.1 mmol) and triethylamine (0.056 ml, 0.4 mmol) were taken in 2-propanol (20 ml) and heated at 80 °C for 2 h. The dark red/brown solution was then concentrated to dryness, and the residue was washed with water (10x3 ml) and dried under reduced pressure to afford [{η^6-benzene}{η^2-*N*,*O*-(1R,2S)-(+)-N-benzyl-*cis*-1-amino-2-indanol^{-1}}RuCl] *(Ru-Bn-BzAIL)* / [{η^6-*p*-cymene}{η^2-*N*,*O*-(1R,2S)-(+)-N-benzyl-*cis*-1-amino-2-indanol^{-1}}RuCl] *(Ru-Cy-BzAIL)* as shining powder.

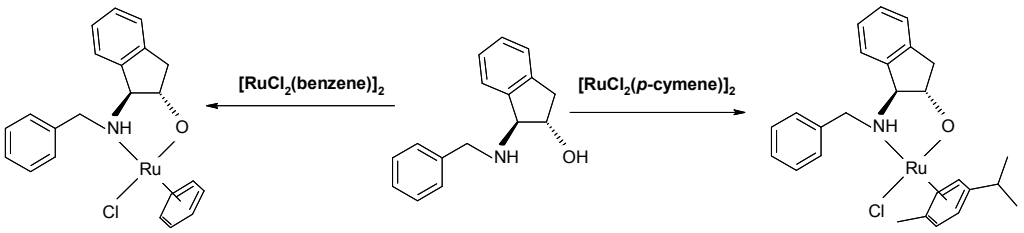

Ru-Bn-BzAIL **BzAIL** **Ru-Cy-BzAIL**

Scheme 4.5: Preparation of Ru-Bn-BzAIL and Ru-Cy-BzAIL

4.2.7. Preparation of [{η^6-benzene}{η^2-*N*,*O*-(1R,2S)-(+)-N-(*p*-toluenesulfonyl)-*cis*-1-amino-2-indanol^{-1}}RuCl] / [{η^6-*p*-cymene}{η^2-*N*,*O*-(1R,2S)-(+)-N-(*p*-toluenesulfonyl)-*cis*-1-amino-2-indanol^{-1}}RuCl]

NH-(*p*-toluenesulfonyl)-(1R,2S)-(+)-*cis*-1-amino-2-indanol (60.8 mg, 0.2 mmol), [$RuCl_2(\eta^6$-benzene)]$_2$ / [$RuCl_2(\eta^6$-*p*-cymene]$_2$ (0.1 mmol) and triethylamine (0.056 ml, 0.4 mmol) were taken in 2-propanol (20 ml) and heated at 80°C for 2 h. The dark red/brown solution was then concentrated to dryness, and the residue was washed

with water (10x3 ml) and dried under reduced pressure to afford [{η^6-benzene}{η^2-*N*,*O*-(1R,2S)-(+)-N-(*p*-toluenesulfonyl)-*cis*-1-amino-2-indanol^{-1}}RuCl] *(Ru-Bn-TsAIL)*/ [{η^6-*p*-cymene}{η^2-*N*,*O*-(1R,2S)-(+)-N-(*p*-toluenesulfonyl)-*cis*-1-amino-2-indanol^{-1}}RuCl] *(Ru-Cy-TsAIL)* as shining powder.

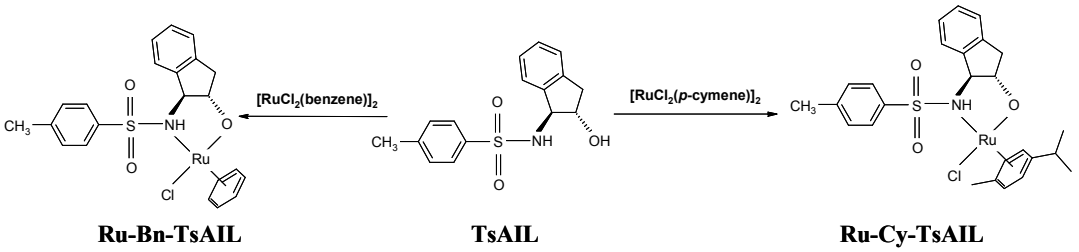

Scheme 4.6: Preparation of Ru-Bn-TsAIL and Ru-Cy-TsAIL

Table 4.2: Designation of various modified (1R,2S)-(+)-*cis*-1-amino-2-indanol.

Functional Group	Precursor of Functional Group	Chiral amino alcohol	Designation
-Propyl	1-bromopropane	(1R,2S)-(+)-*cis*-1-amino-2-indanol	PrAIL
-Benzyl	Benzyl bromide	(1R,2S)-(+)-*cis*-1-amino-2-indanol	BzAIL
-Tosyl	*p*-toluenesulfonylchloride	(1R,2S)-(+)-*cis*-1-amino-2-indanol	TsAIL

Pr: Propyl, Bz: Benzyl & Ts: Tosyl., AIL: (1R,2S)-(+)-*cis*-1-amino-2-indanol.

Table 4.3: Designation of homogeneous Ru-Complexes.

Chiral Ligand-modified material	Metal Precursor	Designation
PrAIL	$[RuCl_2(benzene)]_2$	Ru-Bn-PrAIL
	$[RuCl_2(p\text{-cymene})]_2$	Ru-Cy-PrAIL
BzAIL	$[RuCl_2(benzene)]_2$	Ru-Bn-BzAIL
	$[RuCl_2(p\text{-cymene})]_2$	Ru-Cy-BzAIL
TsAIL	$[RuCl_2(benzene)]_2$	Ru-Bn-TsAIL
	$[RuCl_2(p\text{-cymene})]_2$	Ru-Cy-TsAIL

4.2.8. Asymmetric transfer hydrogenation of simple prochiral ketones using homogeneous catalysts

A stock solution of the homogeneous catalyst was prepared by mixing appropriate amount of ruthenium dimer complex (0.0125 mmol) and the homogeneous ligand (0.05 mmol) in dry 2-propanol (50 ml) was heated at 80^{o}C for 20 minutes under nitrogen. After cooling to room temperature, the solution was transferred *via* cannula to a large sealed Schlenk flask. From the stock solution 0.1 ml of catalyst was transfered to a two necked round bottom flask, followed by ketone (0.01 mol%) in dry degassed 2-propanol (3 ml) and KOH (0.3 ml, 1 mg/0.1 ml 2-prpanol). The reaction was run at 60^{o}C for 1 h. Work up consisted of filtering the dark brown solution through a pad of silica under vacuum (with ethyl acetate washings, 2x50 ml). The combined organic extracts were concentrated *in vacuo* to give the crude product.

4.2.9. Instruments for Characterization

Liquid state ^{1}H and ^{13}C NMR spectra were recorded on a Bruker DRX-300 NMR spectrometer with TMS as internal standard. HRMS data were measured with ESI techniques (Bruker Apex II). . The spectrum was recorded under Hartmann-Hahn match condition using a contact time of 1 m/sec and a relaxation delay of 4 sec. The elemental analyses were done with an EA1108 CHN/S Elemental Analyzer (Carlo Erba Instrument) for establishing the presence and exact fraction of elements in the synthesized materials. A Shimadzu FT-IR 8201 PC Diffuse Reflectance Scanning disc technique was used to probe the attached groups and nature of the surface functional groups in the material. Liquid state UV-Vis spectra of the homogeneous complexes were recorded in the range 200-800 nm on Shimadzu UV 2101 PC spectrometer equipped with a diffuse reflectance attachment, using methanol as solvent. Optical rotation values were measured with a Rudolph IV polarimeter.

4.3. RESULTS AND DISCUSSION

4.3.1. Spectra and Spectral data

Nuclear magnetic resonance spectroscopy is the primary characterization tool to get a clear picture about the structure and functional nature of organic compounds. The evidence for the successful formation of NH-propyl-(1R,2S)-(+)-cis-1-amino-2-indanol, NH-benzyl-(1R,2S)-(+)-cis-1-amino-2-indanol and NH-(*p*-toluenesulfonyl)-(1R,2S)-(+)-cis-1-amino-2-indanol ligands were confirmed primarily from the liquid ^{1}H & ^{13}C nuclear magnetic resonance (NMR) spectral data and further the results obtained from the FT-IR spectral frequencies. To get a clear picture about the results obtained from spectral analysis of modified ligands we have compared the spectral

values of pure compound [(1R,2S)-(+)-cis-1-amino-2-indanol], which was basically used to prepare the modified ligands. To confirm the formation of ruthenium complexes from the above mentioned ligands, the corresponding FT-IR and UV-Vis spectra of complexes were given along with the characterization of the ligands. One can get the clear evidences for the successful formation of modified chiral ligands from (1R,2S)-(+)-cis-1-amino-2-indanol by careful inspection of the spectral data given in the tables (Table. 4.4-4.7). We have utilized the DEPT (distortionless enhancement by polarization transfer) technique to make an exact assignment to the primary, secondary and tertiary carbon atoms. In a DEPT experiment, a sequence of pulses with various delay times are used to create the DEPT spectra where -CH_3 and CH peaks appear as normal and -CH_2- peaks appear inverted. Quaternary C is not usually seen. This way the number of H attached to C can usually be deduced. As a general criterion in a DEPT spectrum, the peak for the carbon atom having an odd hydrogen atom normally shows in the positive phase and the peak for the carbon atom having even hydrogen atoms normally shows in the negative phase or vice versa.

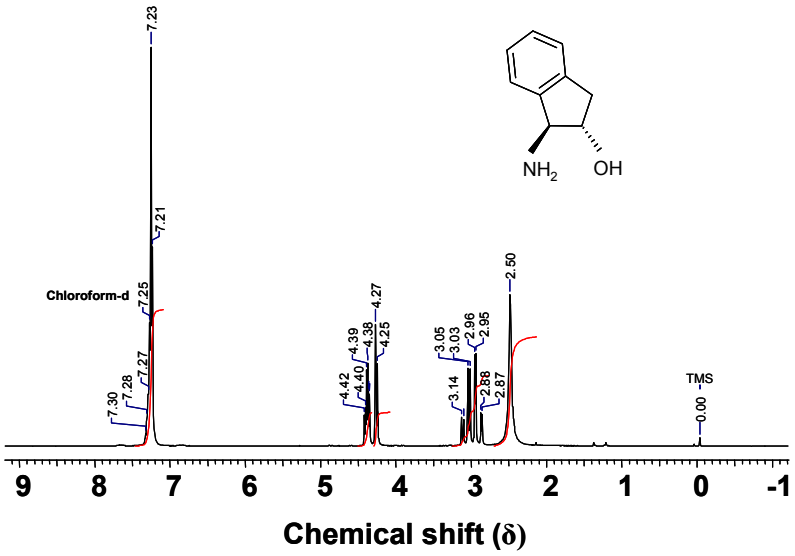

Figure 4.1: ^{1}H NMR spectra of (1R,2S)-(+)-cis-1-amino-2-indanol

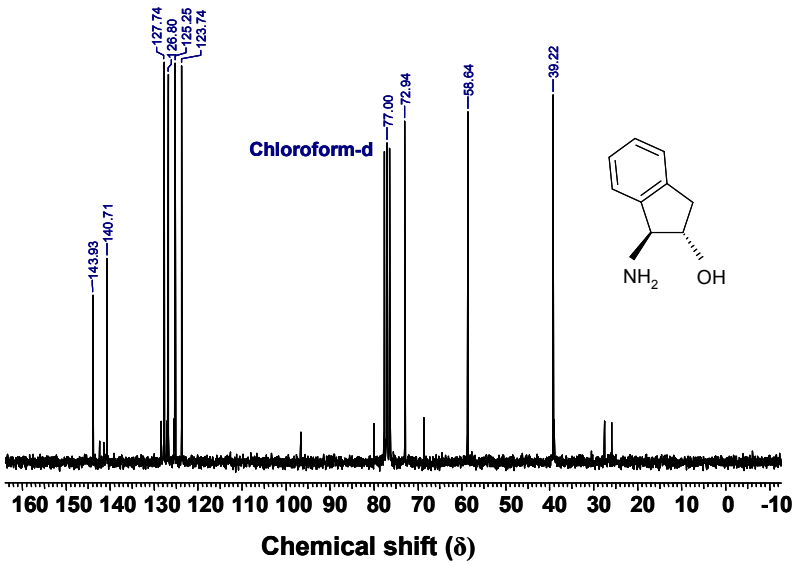

Figure 4.2: ^{13}C NMR spectra of (1R,2S)-(+)-cis-1-amino-2-indanol

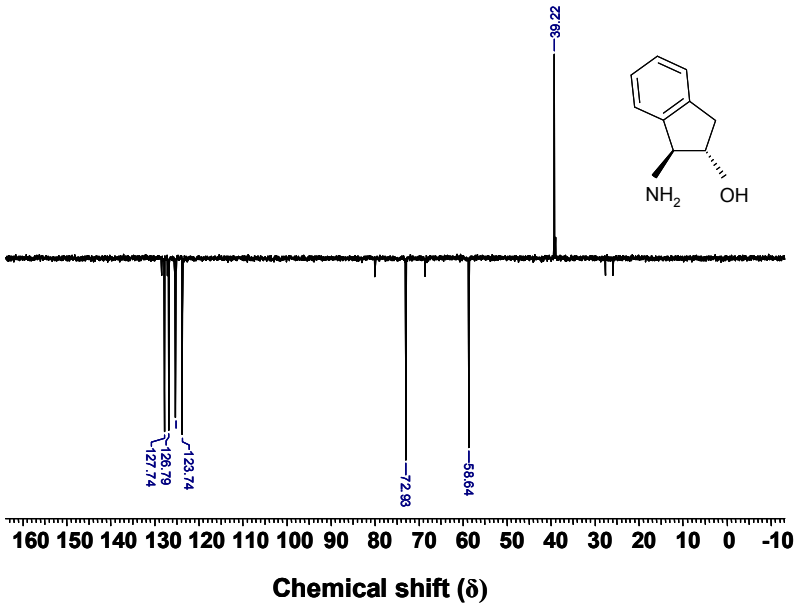

Figure 4.3: ^{13}C NMR (DEPT) spectra (1R,2S)-(+)-cis-1-amino-2-indanol

Spectral result: Figure 4.1 represents the ^{1}H NMR spectra of (1R,2S)-(+)-cis-1-amino-2-indanol. From the figure we can see a singlet peak at a chemical shift value δ = 2.5 ppm due to the presence of N*H* proton, which is indexed to two hydrogen atoms. A multiplet in between δ values 2.87-3.32 ppm indicates the presence of CH_2 protons of the five membered ring and indexed two hydrogen atoms. The proton adjacent to the –NH_2 and –OH groups given a doublet at a chemical shift value δ = 4.28 ppm (indexed to 1 proton) and a multiplet at a chemical shift value in between δ = 4.38-4.42 ppm (indexed to 1 proton), respectively. The aromatic protons given a multiplet in between δ = 7.21-7.30 ppm represents for four protons. It is observed that the C*H* proton adjacent to –OH group show higher chemical shift value (more deshielding area) than the proton adjacent to –NH_2 group due to the higher electronegetivity of the oxygen atom than nitrogen atom which makes the proton more electron deficient. Figure 4.2 and 4.3 represent the ^{13}C NMR and ^{13}C NMR (DEPT) spectra of (1R,2S)-(+)-cis-1-amino-2-indanol, respectively. The δ value of 39.22 ppm (shielding area) corresponds to *C*H_2- carbon of the five membered ring *ie*. *C*H_2CHOH. The carbon atoms directly attached to -NH_2 and –OH groups showed a δ value of 58.64 and 72.94 ppm, respectively. The delta values ranging from 39.22 ppm to 72.94 ppm the carbon atoms appear from shielding to more deshielding area due to the electronegetivity difference of C, N and O atoms directly attached to the corresponding carbon atoms. The aromatic carbon atoms (C_{arom}) given four peaks at δ values 123.74, 125.25, 126.80 and 127.74 ppm along with two quaternary carbon (C_q) atoms of the aromatic ring having the δ values 140.71 and 143.93 ppm in the deshielding area. The ^{13}C NMR (DEPT) spectrum clearly identified the presence of –

CH_2 and –CH carbons separately and the analysis never identified a carbon atom without hydrogen atom.

Table 4.4: Spectral data of (1R,2S)-(+)-cis-1-amino-2-indanol

Source	Aldrich Chemicals
Appearance	Pale brown solid
Molecular weight	150
FT-IR (DRS)	AIL: 2920, 2871 (CH_{strech}) and 1500–1300 (CH_{bend}), 3346 and 3292 (NH_{strech}), 3400-3650 (OH_{strech}), 1580-1620 (benzene), 1605 (C-O_{strech}), 1423 (C=$C_{in\text{-}pane\ strech}$) cm^{-1}.
^{1}H NMR ($CDCl_3$)	AIL, δ = 2.5 (s, 2 H, N*H*), 2.87-3.12 (m, 2 H, CH_2CHOH), 4.28 (d, 1 H, C*H*NH), 4.38-4.42 (m, 1 H, C*H*OH), 7.21-7.30 (m, 4 H, H_{arom}) ppm.
^{13}C NMR ($CDCl_3$)	AIL, δ = 39.22 (*C*H_2CHOH), 58.64 (*C*HNH_2), 72.94 (*C*HOH), 123.74, 125.25, 126.80, 127.74 ($C_{aromatic}$), 140.71, 143.93 (2 C_q).
^{13}C NMR ($CDCl_3$)-(DEPT)	AIL, δ = 39.22 (*C*H_2CHOH), 58.64 (*C*H-NH_2), 72.93 (*C*H-OH), 123.74, 125.25, 126.80, 127.74 ($C_{aromatic}$) ppm.
Elemental analysis	AIL, Calculated: C: 75.00, H: 8.85, N: 7.29, O: 8.33.

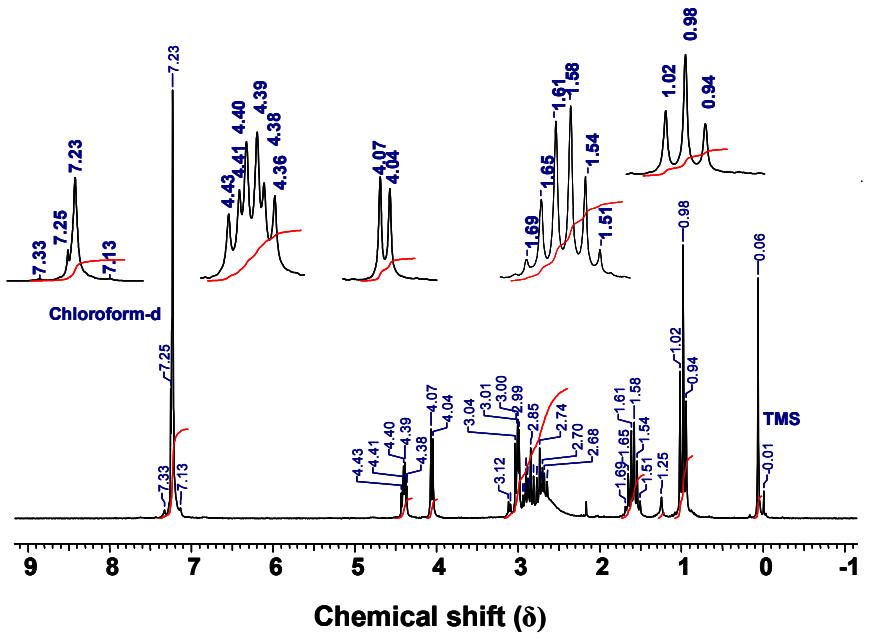

Figure 4.4: ^{1}H NMR spectra of NH-propyl-(1R,2S)-(+)-cis-1-amino-2-indanol

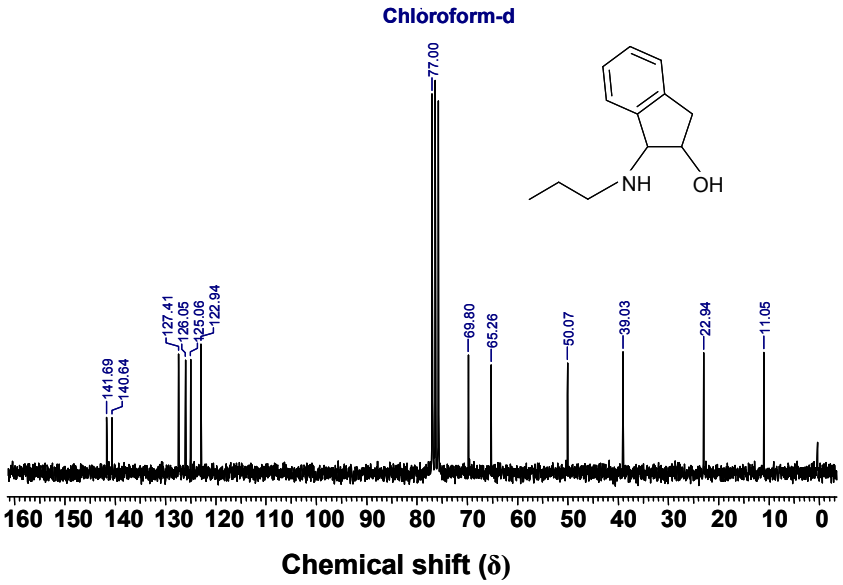

Figure 4.5: ^{13}C NMR spectra of NH-propyl-(1R,2S)-(+)-cis-1-amino-2-indanol

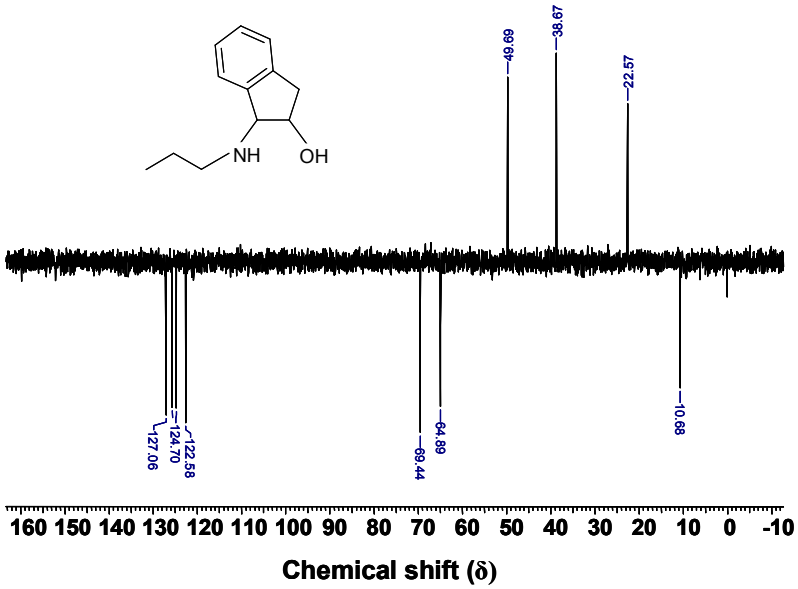

Figure 4.6: ^{13}C-DEPT- NMR-spectra of NH-propyl-(1R,2S)-(+)-cis-1-amino-2-indanol

Spectral result: Figure 4.4 represents the ^{1}H NMR spectra of NH-propyl-(1R,2S)-(+)-cis-1-amino-2-indanol. Here it is observed that a triplet (δ = 0.98 ppm, indexed to three hydrogen atoms), a multiplet (δ = 1.51-1.69 ppm, indexed to two hydrogen atoms) and two doublet of doublet (δ = 2.74-2.68 ppm and δ = 3.00 ppm, indexed to one hydrogen atom each) correspond to C*H*$_3$, CH$_3$C*H*$_2$- and C*H*$_2$NH, respectively of the propyl chain in the ligand. The protons of the basic 1-amino-2-indanol molecule of the ligand showed at chemical shift values of δ = 3.01-3.12 (multiplet, C*H*$_2$CHOH, indexed to two hydrogen atoms), δ = 4.07 ppm (doublet, C*H*NH, indexed to one hydrogen atom), δ = 4.43-4.36 ppm (doublet, C*H*OH, indexed to one hydrogen atom) and δ = 7.13-7.33 ppm (multiplet, H_{arom}, indexed to four hydrogen atoms) are discussed earlier for pure (1R,2S)-(+)-cis-1-amino-2-indanol. Figure 4.5 and 4.6 represent the ^{13}C NMR and ^{13}C NMR (DEPT) spectra of NH-propyl-(1R,2S)-(+)-cis-1-amino-2-indanol, respectively, which clearly identified the various carbon environments present in the ligand. For the propyl carbon atoms it clearly showed three peaks at chemical shift values δ = 11.65 ppm (*C*H$_3$), 22.94 ppm (-*C*H$_2$-CH$_3$) and 65.26 ppm (*C*H$_2$NH). For the 1-amino-2-indanol backbone we have observed δ = 39.03 ppm (*C*H$_2$CHOH), 50.07 ppm (*C*HNH), 69.80 ppm (*C*HOH) and a group of peaks at δ values 122.94, 125.06, 126.05, 127.41 ppm for four aromatic carbon atoms along with two peaks (140.64 and 141.69 ppm) in the more deshielding area for two quaternary carbon atoms. ^{13}C NMR (DEPT) analysis clearly identified the positions of –CH$_2$ carbon atoms from –CH$_3$ and –CH carbon atoms.

Table 4.5: Spectral data of NH-propyl-(1R,2S)-(+)-cis-1-amino-2-indanol

Appearance	Pale brown crystals
Yield	88 %.
Molecular Weight	192
FT-IR (DRS)	PrAIL: 3024-2858 (CH_{strech}), 1500–1300 (CH_{bend}), 3302 (NH_{strech}), 3400-3650 (OH_{strech}), 1580-1620 (benzene), 1612 (C-O_{strech}), 1441 (C=$C_{in\text{-}pane\ strech}$) cm^{-1}. Ru-Bn-PrAIL: 3024-2858, 3400-3650 cm^{-1} Ru-Cy-PrAIL: 3024-2858, 3400-3650 cm^{-1}
^1H NMR ($CDCl_3$)	PrAIL, δ = 0.98 (t, 3 H, C*H*$_3$), 1.51-1.69 (m, 2 H, CH_3CH_2-), 2.74-2.68 (dd, 1 H, C*H*HNH), 3.00 (dd, 1 H, CH*H*NH), 3.01-3.12 (m, 2 H, C*H*$_2$CHOH), 4.07 (d, 1 H, C*H*NH), 4.43-4.36 (m, 1 H, C*H*OH), 7.13-7.33 (m, 4 H, H_{arom}) ppm
^{13}C NMR ($CDCl_3$)	PrAIL, δ = 11.65 (*C*H$_3$), 22.94 (-*C*H$_2$-CH$_3$), 39.03 (*C*H$_2$CHOH), 50.07 (*C*HNH), 65.26 (*C*H$_2$NH), 69.80 (*C*HOH), 122.94, 125.06, 126.05, 127.41 (4 C, *C*H$_{aromatic}$), 140.64, 141.69 (2 C*q*) ppm.
^{13}C NMR ($CDCl_3$)-(DEPT)	PrAIL, 10.68 (*C*H$_3$), 22.57 (-*C*H$_2$-CH$_3$), 38.67 (*C*H$_2$CHOH), 49.69 (*C*HNH), 64.89 (*C*H$_2$NH), 69.44 (*C*HOH), 122.85, 124.70, 125.79, 127.06 (*C*H$_{aromatic}$) ppm.
Elemental analysis	PrAIL, Calculated: C: 75.00, H: 8.85, N: 7.29, O: 8.33. Found: C: 75.22, H: 8.78, N: 7.28, O: 8.15.

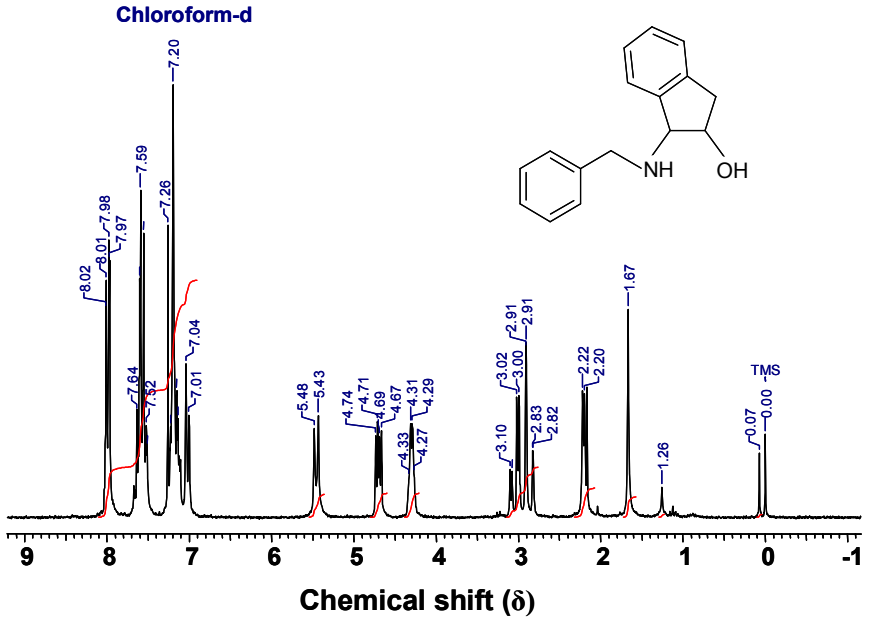

Figure 4.7: ^{1}H NMR spectra of NH-benzyl-(1R,2S)-(+)-cis-1-amino-2-indanol

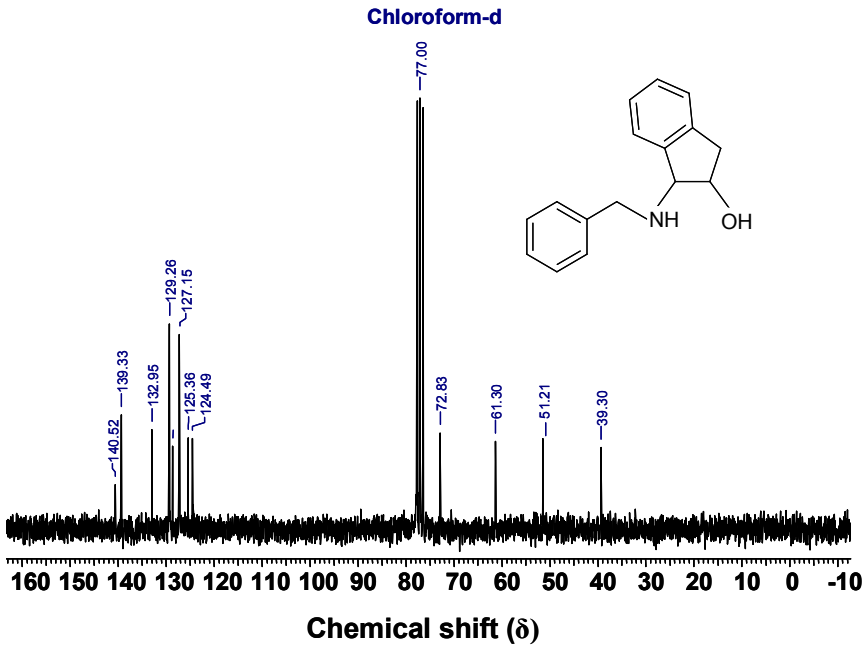

Figure 4.8: ^{13}C NMR spectra of NH-benzyl-(1R,2S)-(+)-cis-1-amino-2-indanol

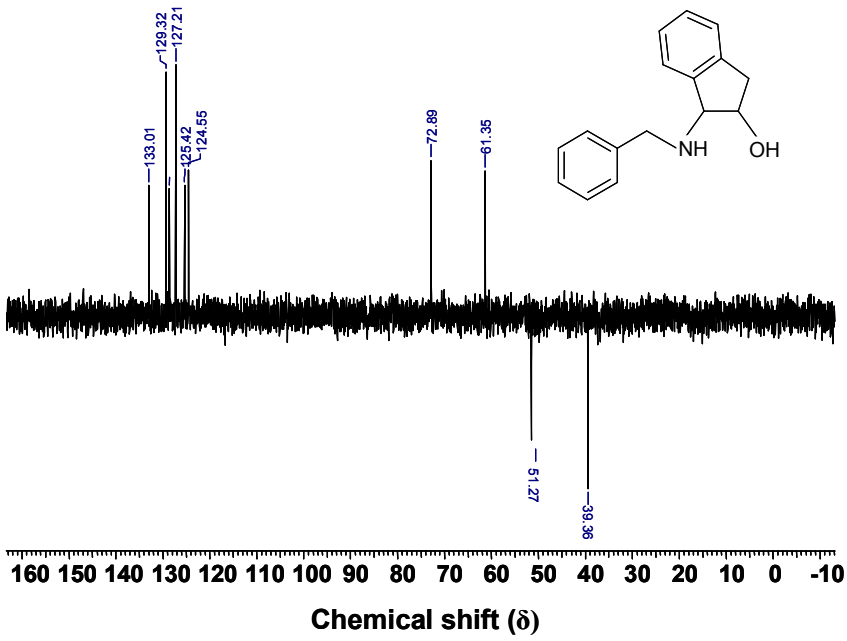

Figure 4.9: ^{13}C-DEPT- NMR-spectra of NH-benzyl-(1R,2S)-(+)-cis-1-amino-2-indanol

Spectral result: Figure 4.7 represents the ^{1}H NMR spectra of NH-benzyl-(1R,2S)-(+)-cis-1-amino-2-indanol. It is clear from the spectrum that two doublets of doublets at chemical shift values in between 2.25-3.10 ppm (indexed to two protons) represent the presence of –CH_2 protons in the five membered ring. The benzyl –CH_2 protons can observe as two doublets in between δ = 4.29-4.31 ppm, which was indexed to two protons. The –C*H* proton of the five membered ring, which is directly attached to the –NH group has been observed as a doublet of doublet at δ = 4.69 ppm as discussed earlier and indexed to one proton. A multiplet in the more deshielding area *i.e.* δ = 5.43 ppm corresponding to the C*H* proton directly attached to the –OH group of the ligand. It is observed clearly a multiplet at δ = 7.15-7.55 ppm corresponding to the aromatic protons, which was indexed to nine protons. Figure 4.8 and 4.9 represent the

^{13}C NMR and ^{13}C NMR (DEPT) spectra of NH-benzyl-(1R,2S)-(+)-cis-1-amino-2-indanol, respectively, which clearly identified the various carbon environments in the ligand. Further δ = 39.30 ppm represents the presence of -*C*H_2 carbon atom in the five membered ring. The benzyl –*C*H_2 carbon showed a peak at δ = 51.21 ppm. The two *C*H carbon atoms of the five membered ring, which are directly attached to NH and OH groups have been observed at δ = 61.30 and 72.83 ppm, respectively. In the Figure 4.8 we can see seven peaks together at chemical shift values of δ = 124.49, 125.36, 127.15, 127.30, 128.85, 129.26, 132.95 ppm corresponding to the aromatic carbon atoms of the benzyl and indanol backbone along with two peaks at δ = 139.33 and 140.52 ppm for two quaternary carbon atoms present in the ligand. ^{13}C NMR (DEPT) spectral analysis distinguished the positions of –CH_2 carbon atoms from –CH carbon atoms. All –CH_2 carbon peaks are arranged below the base line (δ = 39.36 and 51.27 ppm) and the –CH carbon peaks are arranged above the base line [61.35 (*C*HNH), 72.89 (*C*HOH), 124.55, 125.42, 127.21, 127.30, 128.62, 129.32, 133.01 (*C*$H_{aromatic}$)] of the spectrum (Figure 4.9).

Table 4.6: Spectral data of NH-benzyl-(1R,2S)-(+)-cis-1-amino-2-indanol

Appearance	Light yellow solid
Yield	82 %.
Molecular Weight	240
FT-IR (DRS)	BzAIL: 2989-2837 (CH_{strech}), 1500–1300 (CH_{bend}), 3321, 3296 (NH_{strech})cm^{-1}, 3400-3650 (OH_{strech}), 1580-1620 (benzene), 1608 (C-O_{strech}), 1455 (C=$C_{in\text{-}pane\ strech}$) cm^{-1}. Ru-Bn-BzAIL: 3070-2885, 1608, 1455 cm^{-1}. Ru-Cy-BzAIL: 3070-2885, 1608, 1455 cm^{-1}.
^{1}H NMR ($CDCl_3$)	BzAIL, δ = 2.25 (dd, 1 H, C*H*HCHOH), 2.82-3.10 (dd, 1 H, CH*H*CHOH), 4.29 (d, 1 H, C*H*HNH), 4.31 (d, 1 H, CH*H*NH), 4.69 (dd, 1 H, C*H*NH), 5.43 (m, 1 H, C*H*OH), 7.15-7.55 (m, 9 H, H_{arom})
^{13}C NMR ($CDCl_3$)	BzAIL, δ = 39.30 (*C*H_2CHOH), 51.21 (Ph*C*H_2NH), 61.30 (*C*HNH), 72.83 (*C*HOH), 124.49, 125.36, 127.15, 127.30, 128.85, 129.26, 132.95 (9 C, *C*$H_{aromatic}$), 139.33, 140.52 (2 C_q).
^{13}C NMR ($CDCl_3$)-(DEPT)	BzAIL, δ = 39.36 (*C*H_2CHOH), 51.27 (Ph*C*H_2NH), 61.35 (*C*HNH), 72.89 (*C*HOH), 124.55, 125.42, 127.21, 127.30, 128.62, 129.32, 133.01 (*C*$H_{aromatic}$).
Elemental analysis	BzAIL, Calculated: C: 80.00, H: 7.08, N: 7.29, O: 6.66. Found: C: 80.95, H: 7.05, N: 7.14, O: 6.54.

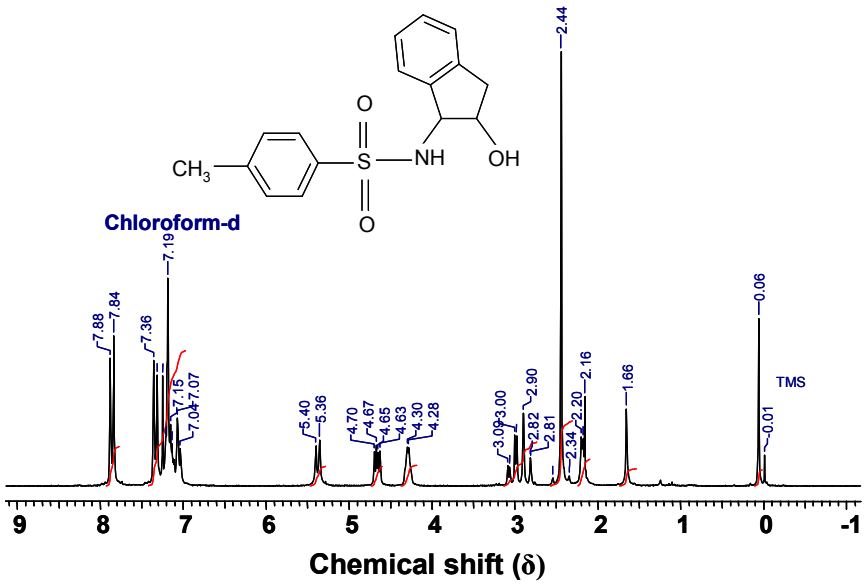

Figure 4.10: ^{1}H NMR spectra of NH-(*p*-toluenesulfonyl)-(1R,2S)-(+)-cis-1-amino-2-indanol

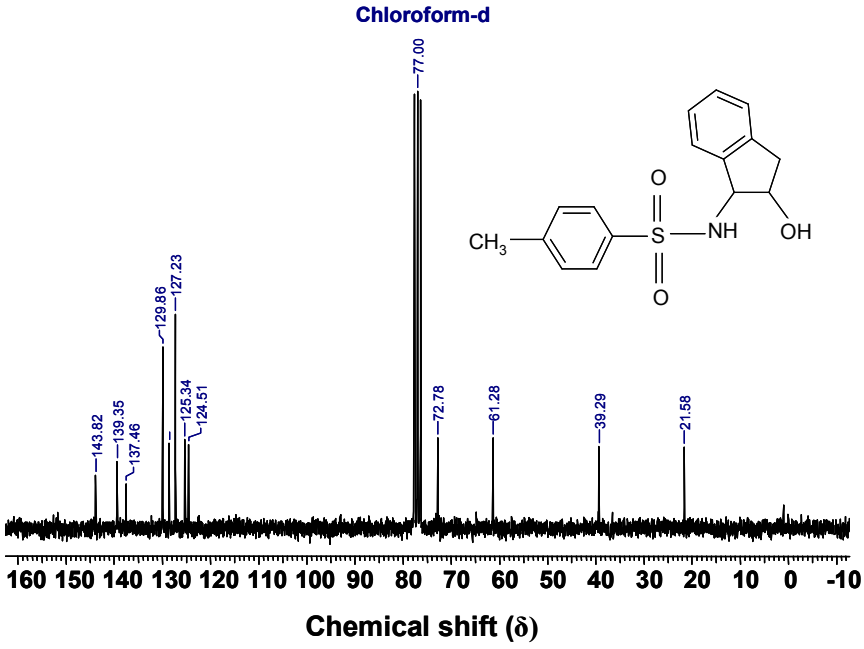

Figure 4.11: ^{13}C NMR spectra of NH-(*p*-toluenesulfonyl)-(1R,2S)-(+)-cis-1-amino-2-indanol

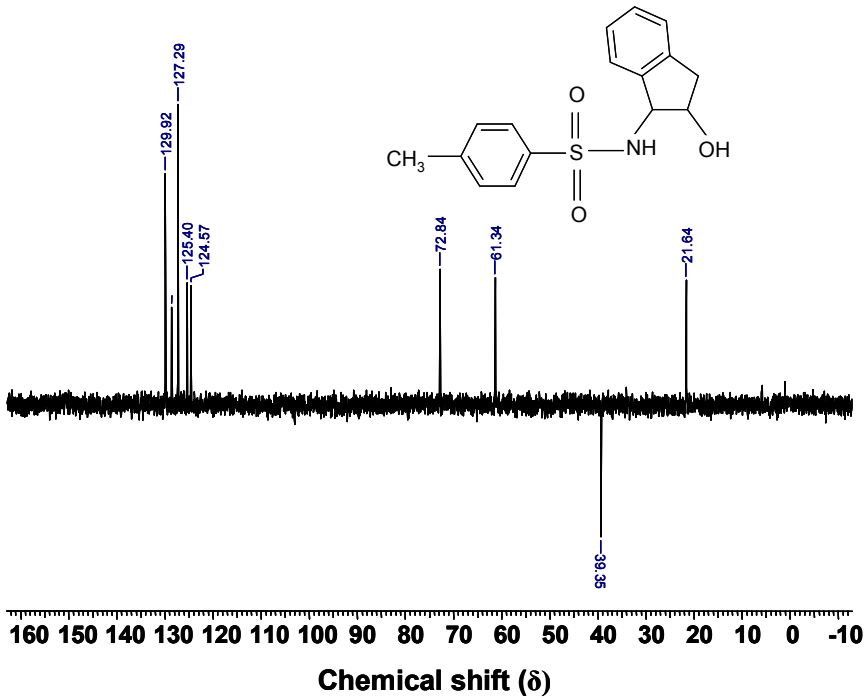

Figure 4.12: ^{13}C-DEPT- NMR-spectra of NH-(*p*-toluenesulfonyl)-(1R,2S)-(+)-cis-1-amino-2-indanol

Spectral result: Figure 4.10 represents the ^{1}H NMR spectra of NH-(*p*-toluenesulfonyl)-(1R,2S)-(+)-cis-1-amino-2-indanol. A singlet peak at δ value 2.44 ppm represents the C*H*$_3$ protons, the most shielded in the ligand, of the methyl group attached to the *p*-tosyl segment of the ligand and indexed to three protons. The chemical shift for C*H*N proton was observed as one doublet and one doublet of doublet at δ values 4.30 and 4.67 ppm, which was indexed to one proton. The chemical shift corresponding to the C*H*O proton was observed at δ value 5.40 ppm as a doublet and was indexed to one proton. The –C*H*$_2$ protons exhibited a doublet of doublet at δ value in between 2.81-3.10 ppm and corresponding to two protons. The N*H* proton and the aromatic protons of the *p*-tosyl ring collectively given a multiplet in between δ values 7.04-7.36 ppm corresponding to five protons clearly observed in

the spectrum evident the successful formation of the ligand. It was also observed a doublet at δ value 7.84 ppm for aromatic protons of the indanol molecule, which was indexed to four protons. Figure 4.11 and 4.12 represent the ^{13}C NMR and ^{13}C NMR (DEPT) spectra of NH-(*p*-tosyl)-(1R,2S)-(+)-cis-1-amino-2-indanol, respectively, which clearly identified the various carbon environments present in the ligand. The ^{13}C NMR peak for methyl carbon atom of the *p*-tosyl moiety appears at a δ value of 21.58 ppm, which was the more shielded sp^3 hybridized carbon atom in the ligand. A chemical shift at 39.29 ppm appears for CH_2 carbon atom of the five membered ring. The chemical shift for the carbon atom directly attached to the nitrogen atom and oxygen atom appear at a δ value of 61.28 ppm and 72.78 ppm, respectively. There are two sets of aromatic carbon atoms present in the ligand, first from *p*-tosyl group and second from indanol molecule. A group of peaks at chemical shift values 124.51, 125.34, 127.23, 128.51 and 129.86 ppm represents the aromatic carbon atoms, which indicates the five different environments of the aromatic carbon atoms present in the ligand. Also the quaternary carbon atoms exhibited four ^{13}C NMR peaks (137.46, 139.35, 139.40 and 143.82 ppm) represent the presence of four quaternary carbon atoms in the ligand. ^{13}C NMR (DEPT) spectra of NH-(*p*-tosyl)-(1R,2S)-(+)-cis-1-amino-2-indanol confirms the above results in which all the representative ^{13}C NMR peaks are present except the peaks for quaternary carbon atoms.

Table 4.7: Spectra data of NH-(*p*-toluenesulfonyl)-(1R,2S)-(+)-cis-1-amino-2-indanol

Appearance	Off-white solid
Yield	96 %.
Molecular Weight	304
FT-IR (DRS)	TsAIL: 3075-2855 (CH_{strech}), 1500–1300 (CH_{bend}), 3295, 3270 (NH_{strech}), 3400-3650 (OH_{strech}), 1580-1620 (benzene), 1598 (C-O_{strech}), 1457 (C=$C_{in\text{-}pane\ strech}$), 1292, 1169 (S-$O_{strech}$), 700-600 (C=$S_{strech}$) cm^{-1}. Ru-Bn-TsAIL: 2982-2868, 1500–1300, 3400-3650, 1292 & 1169, 700-600 cm^{-1}. Ru-Cy-TsAIL: 2982-2868, 1500–1300, 3400-3650, 1292 & 1169, 700-600 cm^{-1}.
^{1}H NMR ($CDCl_3$)	TsAIL, δ = 2.44 (s, 3 H, C*H*$_3$ in *p*-Ts), 2.81-3.10 (dd, 2 H, C*HH*CHOH), 4.3 (d, C*H*N), 4.67 (dd, 1 H, C*H*NH), 5.40 (d, 1 H, C*H*OH), 7.04-7.36 (m, 5 H, N*H*CHC$_6$*H*$_4$-), 7.84 (d, 4 H, *p*-CH_3-C$_6$*H*$_4$-)
^{13}C NMR ($CDCl_3$)	TsAIL, δ = 21.58 (*C*H$_3$ in *p*-Ts), 39.29 (*C*H$_2$CHOH), 61.28 (*C*NH-*p*-Ts), 72.78 (*C*HOH), 124.51, 125.34, 127.23, 128.51, 129.86 (8 C, *C*H$_{aromatic}$), 137.46, 139.35, 139.40, 143.82 (4 C$_q$).
^{13}C NMR ($CDCl_3$)-(DEPT)	TsAIL, δ = 21.64 (*C*H$_3$), 39.35 (*C*H$_2$CHOH), 61.34 (*C*HNH), 72.84 (*C*HOH), 124.57, 125.40, 127.29, 128.51, 129.92 (*C*H$_{aromatic}$).
Elemental analysis	TsAIL, Calculated: C: 63.15, H: 5.59, N: 4.60, O: 15.78, S: 10.52. Found: C: 63.21, H: 5.62, N: 4.59, O: 10.49.

4.3.2. FT-IR Spectra

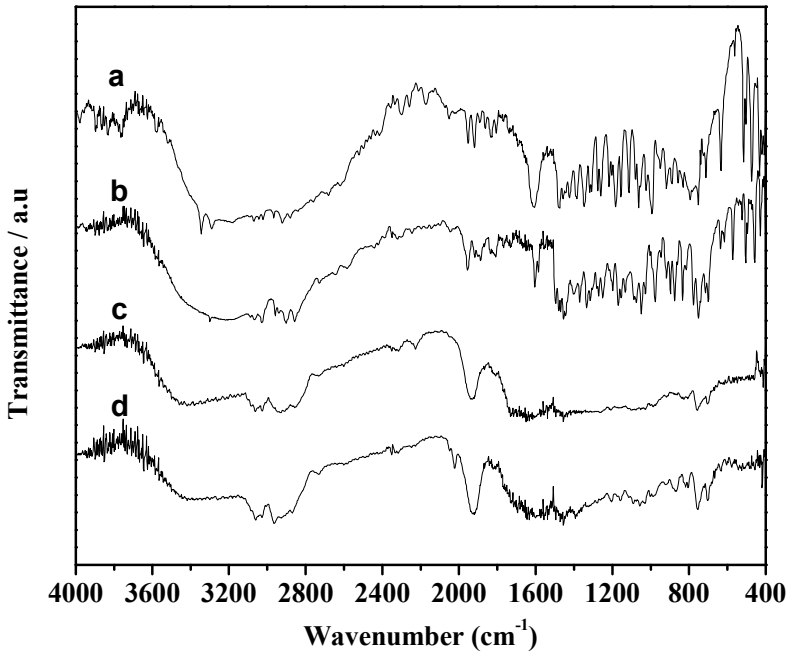

Figure 4.13: FT-IR spectra of (a) AIL (b) PrAIL (c) Ru-Bn-PrAIL and (d) Ru-Cy PrAIL

The principal evidence for construction of homogeneous ligand and complexes are the appearance and loss of IR peaks that correspond to the introduction or transformation of distinct functional groups at each stage in the modification of the basic molecule. Figure 4.13 represents the FT-IR spectra of (a) (1R,2S)-(+)-*cis*-1-amino-2-indanol, AIL (b) NH-propyl-(1R,2S)-(+)-*cis*-1-amino-2-indanol, PrAIL (c) Ru-Bn-PrAIL and (d) Ru-Cy-PrAIL. The FTIR spectra confirm the formation of homogeneous ligand, PrAIL and the chiral ruthenium complexes (Ru-Bn-PrAIL and Ru-Cy-PrAIL) from its metal precursors. In all the spectrum two weak bands at around 3200–2800 cm^{-1} and 1500–1300 cm^{-1}, which are due to the C–H stretching and bending vibrations of methylene group of the cyclic hydrocarbon framework.

Specially, in the spectra of the pure (1R,2S)-(+)-*cis*-1-amino-2-indanol (Figure 4.13, a) , it is observed that two medium bands at 3346 and 3292 cm^{-1} assigns to the stretching vibrations of primary amine ($-NH_2$) group present in the ligand. It is necessary to examine the IR spectra of pure (1R,2S)-(+)-*cis*-1-amino-2-indanol, which will be more comfortable to explain the persistence or disappearance of peaks in the ligand backbone after modification. A broad band between 3400 and 3650 cm^{-1} corresponding to the O–H stretching vibration (hydrogen bonded with the free amino group) and a sharp band between 1650 and 1600 cm^{-1} is due to the bending vibrations of surface O–H groups.[35] The additional sharp band at 3760 cm^{-1} may be due to the stretching vibration of free –OH group (without hydrogen bonding) in the ligand. The peaks in the spectra from 1580 to 1620 cm^{-1} are assigned to the aromatic stretching modes of benzene ring present in the ligand. We can see a sharp peak at 1605 and in between 1200-1000 cm^{-1} corresponding to the C-O stretching vibration of the molecule. The presence of a medium bands at 1423 cm^{-1} indicates the C=C stretching in-plane vibration of benzene framework given further evidence for the presence of aromatic ring.[36]

In the spectra of PrAIL, Ru-Bn-PrAIL and Ru-Cy-PrAIL (Figure 4.13, b, c & d respectively) we can observe the above representative peaks ie, 1444 (C=C) and 1612 (C-O) and 3302 cm^{-1} ($-NH_2$). The marginal shift in the positions of the bands corresponding to C=C, C-O and $-NH_2$ is due to modification to the (1R,2S)-(+)-*cis*-1-amino-2-indanol by primarily due a propyl group and further due to the complexation with ruthenium precursors. The most notable change in the spectra of PrAIL from (1R,2S)-(+)-*cis*-1-amino-2-indanol is the disappearance of one of the representative peak of free $-NH_2$ (3346 cm^{-1}) group, which may be due to the utilization of one of

the –NH proton for anchoring the propyl group. The modification may cause an overall decrease in the density of –NH protons in the final material (PrAIL). By the modification the primary $–NH_2$ group changed to secondary –NH moiety. Another notable change is the marginal increase in intensity of the peaks corresponding to the methylene stretching vibrations at 3200–2800 cm^{-1}, which may be due to the increase in hydrocarbon percentage in the material due to the addition of propyl group.

The most distinguishable changes in the Ru-Bn-PrAIL and Ru-Cy-PrAIL complexes are due to the peak positions of –NH, -CH-, -OH and –C-O vibrational bands. The –NH peak position is totally disappeared due to the negligible percentage of –NH- moiety in the materials after complexation with metal precursors. A further increment in the intensity of –CH- stretching vibrations also observed along with the decrease in intensity of hydrogen bonded –OH groups. It may be due to the utilization of –OH proton for the successful complexation with the metal precursor by one of the Ru-Cl chlorine. The further evidence for the complexation of metal precursor with the ligand was unexplainable due to the overlapping of peaks in the functional group region.

Figure 4.14 demonstrates the FT-IR spectra of (a) AIL (b) BzAIL (c) Ru-Bn-BzAIL and (d) Ru-Cy-BzAIL, respectively. In the entire spectra the strong and broad band between 3650-3400 cm^{-1} corresponding to the stretching mode of hydroxyl groups present in the ligand. Further, it can be seen that the stretching (3989-2837 cm^{-1}) and bending (1500-1300 cm^{-1}) modes of the $–CH_2$ groups of benzyl as well as the ligand framework.[38,39] Along with these bands some characteristic bands such as 3321, 3296 (NH_{strech}), 3400-3650 (OH_{strech}), 1580-1620 (benzene), 1608 and 1200-1000 ($C\text{-}O_{strech}$), 1455 ($C{=}C_{in\text{-}pane\ strech}$) cm^{-1} can also visible in the entire spectra. The

characteristic bands of –NH group is not visible after complexation with ruthenium precursor and this may be due to the decrease in percentage of -NH moiety after introducing a benzene or *p*-cymene molecule. This decrease in intensity was clearly observed while going from AIL to BzAIL also due to utilization of one of the –NH proton for anchoring a benzyl molecule.

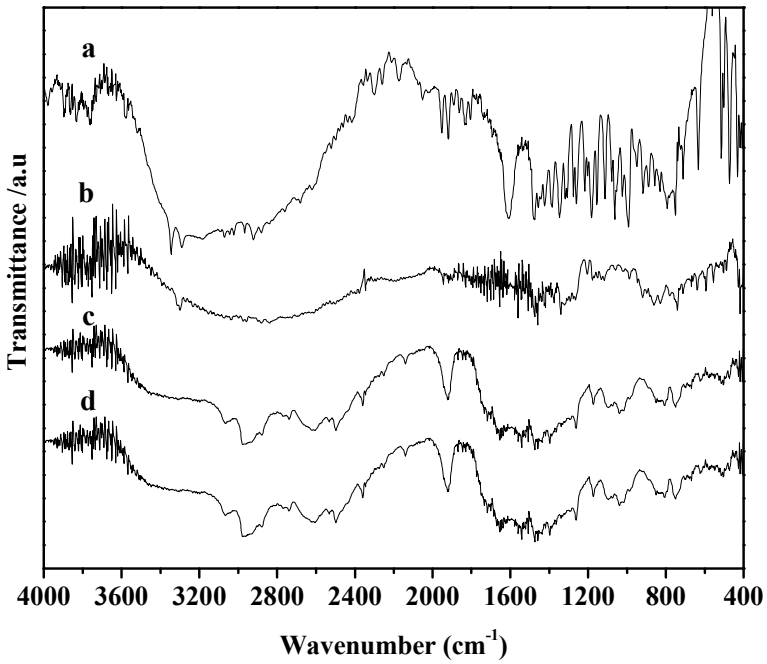

Figure 4.14: FT-IR spectra of (a) AIL (b) BzAIL (c) Ru-Bn-BzAIL and (d) Ru-Cy BzAIL

Figure 4.15 shows the FT-IR spectra (a) AIL (b) TsAIL (c) Ru-Bn-TsAIL and (d) Ru-Cy-TsAIL. The characteristic bands of AIL (Page number X) was discussed earlier and compared with the bands obtained for TsAIL (c) Ru-Bn-TsAIL and (d) Ru-Cy-TsAIL. In the FT-IR spectrum of TsAIL (b), it is clearly observed that the characteristic bands of –NH (3295, 3270 cm^{-1}), and another two broad bands in between 3075-2855 cm^{-1} corresponding to asymmetric and symmetric vibrations, respectively, of the -CH_2 group of the five membered ring in the ligand. A broad band

was observed in between 3400 and 3650 cm^{-1} corresponding to the O–H stretching vibration in all the materials.

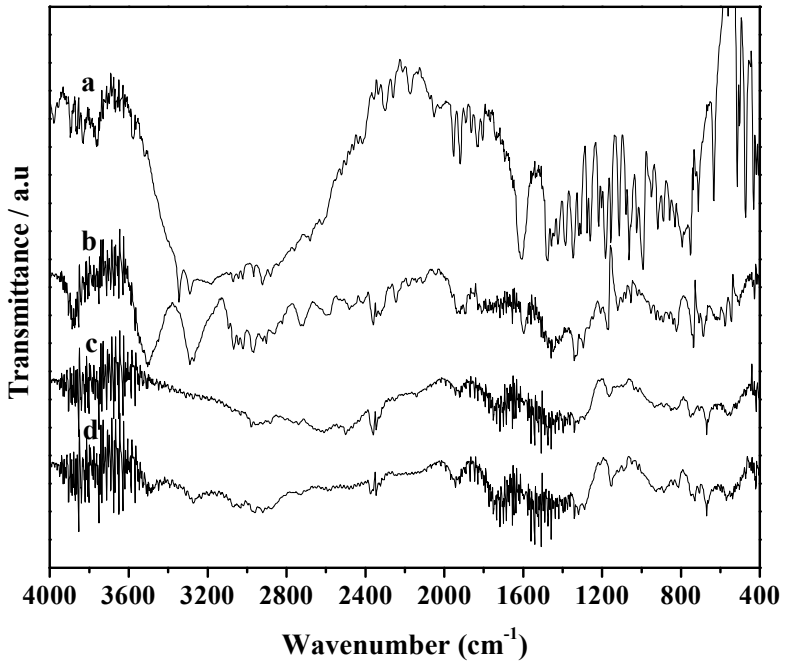

Figure 4.15: FT-IR spectra of (a) AIL (b) TsAIL (c) Ru-Bn-TsAIL and (d) Ru-Cy TsAIL

In addition to the above bands, 1500–1300 cm^{-1} which are due to the C–H stretching and bending vibrations of methylene group of the ligand molecule were also observed. A medium band at 1457 cm^{-1} in the entire spectrum indicates the C=C stretching in-plane vibration of benzene of the *p*-tosyl as well as the indanol framework. In the entire spectrum a band at 707cm^{-1} represents the C–H bending vibration of methylene group of benzene. A small and weak band at around 1598 and 1200-1000 cm^{-1} is the characteristic band of C–O group in the ligand as well as catalyst.

Specially in the FT-IR spectra of TsAIL (c) Ru-Bn-TsAIL and (d) Ru-Cy-TsAIL we have observed a small and intense band at 1292 cm^{-1} and the medium band at 1169

cm^{-1}, are due to S=O stretching mode of the p-tosyl group[37]. The C=S link also gives a medium band between 600 and 700 cm^{-1} and the intensity is decreased after complexation with metal precursors.

4.3.3. UV-Vis Spectra

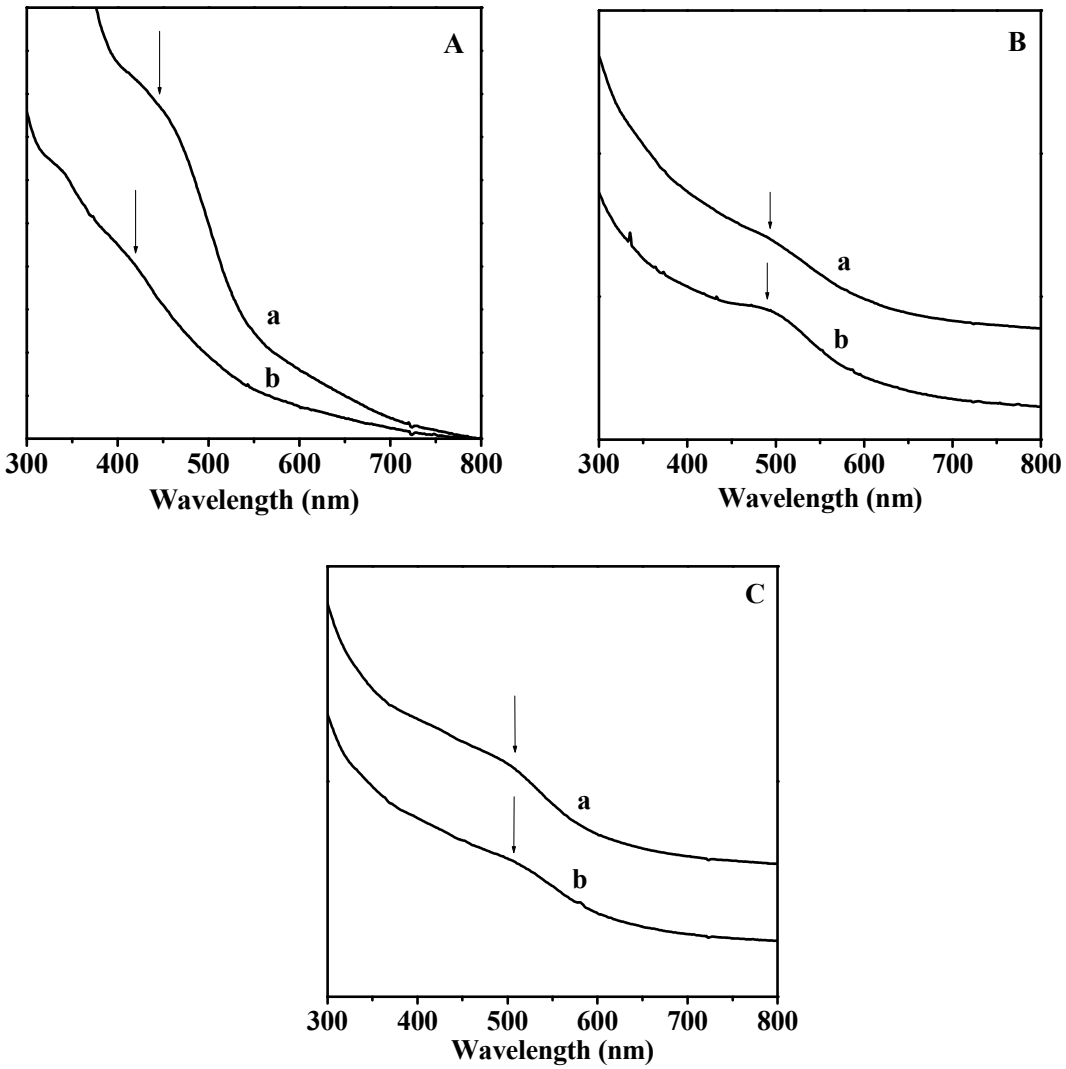

Figure 4.16: UV-Vis spectra of [**A**]: (a) Ru-Bn-PrAIL and (b) Ru-Cy-PrAIL, [**B**] (a) Ru-Bn-BzAIL and (b) Ru-Cy-BzAIL, [**C**]: (a) Ru-Bn-TsAIL and (b) Ru-Cy-TsAIL.

Figure 4.16 illustrates the UV-Vis spectra of [**A**]: (a) Ru-Bn-PrAIL and (b) Ru-Cy-PrAIL, [**B]** (a) Ru-Bn-BzAIL and (b) Ru-Cy-BzAIL, [**C**]: (a) Ru-Bn-TsAIL and (b) Ru-Cy-TsAIL and the values were listed in Table 4.8. All peaks are broad and it is very difficult to tell the exact peak position in order to distinguish the various ligand environments over the metal atom. A broad peak at 445 and 418 nm has been observed for Ru-Bn-PrAIL and Ru-Cy-PrAIL, respectively, metal-to-ligand charge-transfer (MLCT) band; clearly indicate the formation of metal complexes. For Ru-Bn-BzAIL and Ru-Cy-BzAIL a broad peak at 493 nm in both the materials, metal-to-ligand charge- transfer (MLCT) band, clearly indicates the successful formation of the complex. For Ru-Bn-TsAIL and Ru-Cy-TsAIL a broad peak at 508 nm distinguishes the metal-to-ligand charge-transfer (MLCT) band.[40]

Table 4.8: UV-Vis absorbance values of homogeneous complexes

Entry	Material	UV-Vis absorbance (nm)
1	Ru-Bn-PrAIL	445
2	Ru-Cy-PrAIL	418
3	Ru-Bn-BzAIL	493
4	Ru-Cy-BzAIL	493
5	Ru-Bn-TsAIL	508
6	Ru-Cy-TsAIL	508

4.3.4. Asymmetric transfer hydrogenation of simple prochiral ketones using homogeneous catalysts

Table 4.9: ATH using (1R,2S)-(+)-cis-1-amino-2-indanol as ligand (S/C=100)

Entry	Substrate	Ru-Bn-AIL		Ru-Cy-AIL	
		Conversion (%)[a]	*ee* (%)[a]	Conversion (%)[a]	*ee* (%)[a]
1	**ACP**	96	67*	94	90*
2	**ClACP**	99	51	97	80
3	**BrACP**	99	50	96	82
4	**MeACP**	89	71	82	86
5	**MeOACP**	63	69	54	82
6	**DMeOACP**	99	75	97	85
7	**PRP**	95	70	88	82

The reaction was carried out at 60°C for 1 h, using 0.01 mol % of ketone and S/C ratio of 100 in 3 ml solvent. KOH = 3 mg/0.3 ml 2-propanol.

a Determined by GC equipped with a chiral column.
The configuration of alcohol product was *S*.

* Configuration was found by comparing with authentic compound.
All other configurations were found by comparing R_f values with R_f values published in literatures.

The ketones 1-7 were applied to the homogeneous asymmetric transfer hydrogenation in 2-propanol in the presence of KOH using the catalyst Ru-Bn-AIL/Ru-Cy-AIL (Table 4.9). In the investigation of acetophenone (entry 1) the reaction in 2-propanol possesses high reactivity and excellent enantioselectivity (96% yield with 67% *ee* for Ru-Bn-AIL and 94% yield with 90% *ee* over Ru-Cy-AIL) that

was just as good as the results published by Palmer *et al.* This result was not unexpected in view of the known reversibility of transfer hydrogenations using propan-2-ol as the hydrogen source and reinforced the need to avoid an unnecessarily long reaction time. The use of 4-chloroacetophenone and 4-bromoacetophenone (entry 2 & 3) gave only a slight drop in enantioselectivity, whilst affording a more synthetically useful yield of product [4-chloroacetophenone gave, 99% with 51% *ee* and 97% with 80% *ee* over Ru-Bn-PrAIL and Ru-Cy-PrAIL, respectively. 4-Bromoacetophenone gave, 99% with 50% *ee* and 96% with 82% *ee* over Ru-Bn-PrAIL and Ru-Cy-PrAIL, respectively]. Whilst under similar conditions *S*-1-(4-methylphenyl)ethanol was obtained in 89% yield with 71% *ee* over Ru-Bn-PrAIL and 82% yield with 86% *ee* over Ru-Cy-PrAIL from 4-methylacetophenone (entry 4). For 4-methoxyacetophenone (entry 5), the asymmetric reaction gave relatively poor results (63% yield with 69% *ee* for Ru-Bn-PrAIL and 54% yield with 82% *ee* for Ru-Cy-PrAIL), while a much better result (in 99% yield with 75% *ee* for Ru-Bn-PrAIL and 97% yield with 85% *ee* for Ru-Cy-PrAIL) was observed in the transfer hydrogenation reaction of 2,5-dimethoxyacetophenone (entry 6). Propiophenone (entry 7) was reduced to (*S*)-1-phenylpropanol in 95% yield with 70% *ee* and 88% yield with 82% *ee* for Ru-Bn-PrAIL and Ru-Cy-PrAIL, respectively after 1 h at 60^{o}C.

Table 4.10: ATH using NH-propyl-(1R,2S)-(+)-cis-1-amino-2-indanol as ligand (S/C=100)

Entry	Substrate	Ru-Bn-PrAIL		Ru-Cy-PrAIL	
		Conversion (%)[a]	*ee* (%)[a]	Conversion (%)[a]	*ee* (%)[a]
1	**ACP**	88	61*	84	84*
2	**ClACP**	95	59	86	80
3	**BrACP**	95	58	84	80
4	**MeACP**	82	60	75	84
5	**MeOACP**	58	61	44	82
6	**DMeOACP**	78	60	66	82
7	**PRP**	74	52	61	79

The reaction was carried out at 60°C for 1 h, using 0.01 mol % of ketone and S/C ratio of 100 in 3 ml solvent. KOH = 3 mg/0.3 ml 2-propanol.

a Determined by GC equipped with a chiral column.

The configuration of alcohol product was *S*.

* Configuration was found by comparing with authentic compound.

All other configurations were found by comparing R_f values with R_f values published in literatures.

Table 4.10 explains the catalytic activities and enantioselectivities of Ru-Bn-PrAIL and Ru-Cy-PrAIL under similar reaction conditions. All substrates we have used for screening the performance of catalysts reduced very well with high enantioselectivity. As a comparison, acetophenone reduced to 88% with 61% *ee* and 84% with 84% *ee* by using Ru-Bn-PrAIL and Ru-Cy-PrAIL, respectively (entry 1). While introducing an electron withdrawing group (-Cl or -Br) in the para position of the aromatic ring of

ketone enhanced the activity with a slight decrease in *ee* (entry 2) within 1 h [4-chloroacetophenone gave, 95% with 59% *ee* and 86% with 80% *ee* for Ru-Bn-PrAIL and Ru-Cy-PrAIL , respectively. 4-Bromoacetophenone gave, 95% with 58% *ee* and 84% with 80% *ee* for Ru-Bn-PrAIL and Ru-Cy-PrAIL , respectively]. While the results obtained for the aromatic ketone having an electron donating group like -CH_3 (entry 4, 82% yield with 60% *ee* for Ru-Bn-PrAIL and 75% yield with 84% *ee* for Ru-Cy-PrAIL) exactly reverse to that of aromatic ketone having an electron withdrawing group. But it was observed that the performances of Ru-Bn-PrAIL and Ru-Cy-PrAIL over 4-methylacetophenone were comparable with the results obtained for acetophenone even though the yield was less. 4-methylacetophenone reduced to 82% yield with 60% *ee* for Ru-Bn-PrAIL and 75% yield with 84% *ee* for Ru-Cy-PrAIL. But 4-methoxyacetophenone reduced in a controlled manner with in the same time limit even though the aromatic ring carrying an electron withdrawing group (entry 5) as expected with respect to the previous observations. 4-Methoxyacetophenone reduced to 58% yield with 61% *ee* for Ru-Bn-PrAIL and 44% yield with 82% *ee* for Ru-Cy-PrAIL. The performance of Ru-Bn-PrAIL in the case of 2,5-dimethoxyacetophenone was found to give 78% yield and 60% *ee* (entry 6). Here the activity was comparative with that of 4-methoxyacetophenone but a slight decease in *ee* was observed. At the same time Ru-Cy-PrAIL performed with 66% yield and 82% *ee* (entry 6) in the case of 2,5-dimethoxy acetophenone keeping identical *ee* with a slight decrease in conversion than 4-methoxyacetophenone. Propiophenone converted excellently with considerable *ee* (entry 7) for both the catalysts. It showed the excellent performances of the catalysts under our reaction conditions (74% yield with 52% *ee* and 61% with 79% *ee* for Ru-Bn-PrAIL and Ru-Cy-PrAIL,

respectively). The reaction product, alcohol, we obtained from all the reactions having an *S* configuration, which was found for acetophenone by comparing the R_f factor of *S*-1-phenylethanol with the reaction mixture and for all other products the R_f factor of the reaction mixture was compared with the literature procedure.

Table 4.11: ATH using NH-benzyl-(1R,2S)-(+)-cis-1-amino-2-indanol as ligand (S/C=100)

		Ru-Bn-BzAIL		Ru-Cy-BzAIL	
Entry	**Substrate**	Conversion (%)[a]	*ee* (%)[a]	Conversion (%)[a]	*ee* (%)[a]
1	**ACP**	6	60*	2	71*
2	**ClACP**	10	46	6	56
3	**BrACP**	11	44	6	53
4	**MeACP**	5	54	2	59
5	**MeOACP**	4	41	2	49
6	**DMeOACP**	5	40	2	53
7	**PRP**	5	39	2	43

The reaction was carried out at 60°C for 1 h, using 0.01 mol % of ketone and S/C ratio of 100 in 3 ml solvent. KOH = 3 mg/0.3 ml 2-propanol.

a Determined by GC equipped with a chiral column.
The configuration of alcohol product was *S*.

* Configuration was found by comparing with authentic compound.
All other configurations were found by comparing R_f values with R_f values published in literatures.

Table 4.11 represents the asymmetric transfer hydrogenation of various derivatives of acetophenone by the second set of heterogeneous catalysts (Ru-Bn-BzAIL and Ru-

Cy-BzAIL) in 2-prpanol. Acetophenone reduced 6 and 2% with in 1 h with *ee* values of 60 and 71% for Ru-Bn-BzAIL and Ru-Cy-BzAIL, respectively (entry 1). For instance 4-chloroacetophenone and 4-bromoacetophenone were reduced in 46% and 44%, the highest conversion among the substrates, having *ee* values of 46 and 44%, respectively, for Ru-Bn-BzAIL (entry 2 & 3). But for Ru-Cy-BzAIL catalyst, lower activities (6%) with enhanced *ee* values (56 & 53%) have been observed (entry 2 & 3). The reduction of 4-methylacetophenone gave 5% conversion with 54% *ee* for Ru-Bn-BzAIL and 2% conversion with 59% *ee* for Ru-Cy-BzAIL (entry 4). 4-Methoxyacetophenone reduced to 4% conversion with 41% *ee* for Ru-Bn-BzAIL and 2% conversion with 49% *ee* for Ru-Cy-BzAIL (entry 5). 2,5-Dimethoxyacetophenone showed the same level of conversion (5%) and less *ee* (40%) for Ru-Bn-BzAIL and 2% conversion and 53% *ee* for Ru-Cy-BzAIL (entry 6). The low *ee* of 2,5-dimethoxyacetophenone was probably a result of steric hindrance that affects access of the carbonyl carbon to the Ru(II)-H hydride. Propiophenone exhibited a yield of 5% and *ee* of 39% for Ru-Bn-BzAIL and 2% yield and 43% *ee* for Ru-Cy-BzAIL (entry 7).

Table 4.12: ATH using NH-(*p*-toluenesulfonyl)-(1R,2S)-(+)-cis-1-amino-2-indanol as ligand (S/C=100)

Entry	Substrate	Ru-Bn-TsAIL		Ru-Cy-TsAIL	
		Conversion (%)[a]	*ee* (%)[a]	Conversion (%)[a]	*ee* (%)[a]
1	**ACP**	5	69*	2	79*
2	**ClACP**	7	44	5	61
3	**BrACP**	7	46	4	58
4	**MeACP**	4	59	1	63
5	**MeOACP**	4	49	1	63
6	**DMeOACP**	5	45	2	60
7	**PRP**	4	43	2	54

The reaction was carried out at 60°C for 1 h, using 0.01 mol % of ketone and S/C ratio of 25 in 3 ml solvent. KOH = 3 mg/0.3 ml 2-propanol.

a Determined by GC equipped with a chiral column.

The configuration of alcohol product was *S*.

* Configuration was found by comparing with authentic compound.

All other configurations were found by comparing R_f values with R_f values published in literatures.

Table 4.12 demonstrates the activity and enantioselectivity of Ru-Bn-TsAIL and Ru-Cy-TsAIL over a series of acetophenone derivatives under identical Ru catalyst–ligand loading. The activity of Ru-Bn-TsAIL and Ru-Cy-TsAIL over different substrates is unexplainable due to the similar lower conversions at the same reaction conditions but the enantioselectivity varies considerably irrespective of conversion. The conversions of all the substrates for both the catalysts are coming below 10%.

Here acetophenone reduced to S-1-phenylethanol in 5% yield and 59% *ee* for Ru-Bn-TsAIL (entry 1), whilst a decreased activity with good *ee* was observed for Ru-Cy-TsAIL (entry 1, 2% yield and 79% *ee*). By introducing a strong electron withdrawing group like –Cl or –Br in the para position of the phenyl ring of the aromatic ketone activity increased drastically as shown for the other catalysts reported in the previous tables [(entry 2, for 4-cloroacetophenone, 7% yield with 44% *ee* and 5% yield with 61% *ee* for Ru-Bn-TsAIL and Ru-Cy-TsAIL, respectively) and (entry 3, for 4-bromo acetophenone, 7% yield with 46% *ee* and 4% yield with 58% *ee* for Ru-Bn-TsAIL and Ru-Cy-TsAIL , respectively)]. 4-Methoxyacetophnone, a difficult substrate to reduce, also followed the same trend what we have observed in the previous tables (Table 4.8 & 4.9) even though the conversion is very low. The activity of Ru-Bn-TsAIL and Ru-Cy-TsAIL for the reduction of 4-methoxyacetophnone was observed 4% yield with 49% *ee* and 1% yield with 63% *ee*, respectively (entry 5). 2,5-Dimethoxyacetophenone (entry 6) exhibited little bit higher conversion with less *ee* for both catalysts when comparing with 4-methoxyacetophenone (5% yield with 45% *ee* and 2% yield with 60% *ee* for Ru-Bn-TsAIL and Ru-Cy-TsAIL, respectively). Propiophenone was reduced to (*S*)-1-phenylpropanol in 4% yield with 43% ee and 2% yield with 54% *ee* for Ru-Bn-TsAIL and Ru-Cy-TsAIL, respectively.

Table 4.13: ATH using NH-benzyl-(1R,2S)-(+)-cis-1-amino-2-indanol as ligand (S/C=25)

Entry	Substrate	Ru-Bn-BzAIL		Ru-Cy-BzAIL	
		Conversion (%)[a]	*ee* (%)[a]	Conversion (%)[a]	*ee* (%)[a]
1	**ACP**	29	59*	16	68*
2	**ClACP**	45	46	31	55
3	**BrACP**	42	45	30	53
4	**MeACP**	26	54	11	59
5	**MeOACP**	11	40	9	49
6	**DMeOACP**	24	40	18	54
7	**PRP**	24	37	14	41

The reaction was carried out at 60°C for 1 h, using 0.01 mol % of ketone and S/C ratio of 25 in 3 ml solvent. KOH = 3 mg/0.3 ml 2-propanol.

a Determined by GC equipped with a chiral column.
The configuration of alcohol product was *S*.

* Configuration was found by comparing with authentic compound.
All other configurations were found by comparing R_f values with R_f values published in literatures.

Table 4.14: ATH using NH-(p-toluenesulfonyl)-(1R,2S)-(+)-cis-1-amino-2-indanol as ligand(S/C=25)

		Ru-Bn-TsAIL		Ru-Cy-TsAIL	
Entry	**Substrate**	Conversion (%)[a]	*ee* (%)[a]	Conversion (%)[a]	*ee* (%)[a]
1	**ACP**	26	68*	7	79*
2	**ClACP**	32	44	19	60
3	**BrACP**	32	46	18	58
4	**MeACP**	17	58	3	63
5	**MeOACP**	10	49	3	64
6	**DMeOACP**	26	45	10	60
7	**PRP**	19	41	9	51

The reaction was carried out at 60°C for 1 h, using 0.01 mol % of ketone and S/C ratio of 25 in 3 ml solvent. KOH = 3 mg/0.3 ml 2-propanol.

a Determined by GC equipped with a chiral column.

The configuration of alcohol product was *S*.

* Configuration was found by comparing with authentic compound.

All other configurations were found by comparing R_f values with R_f values published in literatures.

Tables 4.13 & 4.14 represent the activity of the chiral complexes prepared from BzAIL and TsAIL in the asymmetric transfer hydrogenation of various acetophenone derivatives at an S/C ratio of 25. From the previous observations (Table 4.10) it is observed that the activity and enantioselectivity of catalysts prepared from PrAIL was

superior over the catalysts prepared from BzAIL and TsAIL in the enantioselective transfer hydrogenation of acetophenone derivatives under our reaction conditions. This may be due to the steric constraint introduced by the various coordinating groups introduced around the active metal centre. At this point of view we are interested to see the activity and enantioselectivity of the catalysts were a function of concentration of the substrate or simply the inactivity of the active metal complex. With this intension we have reduced the concentration of the substrate to one by fourth of the substrate concentration used initially and carried out the reaction at the same conditions applied previously.

The results obtained for Ru-Bn-BzAIL/Ru-Cy-BzAIL (Table 4.13) and Ru-Bn-TsAIL/Ru-Cy-TsAIL (Table 4.14) are displayed above in the asymmetric transfer hydrogenation of substrates 1-7 at S/C ratio of 25. From the tables it was observed that the activity of Ru-Bn-BzAIL/Ru-Cy-BzAIL (Table 4.13) and Ru-Bn-TsAIL/Ru-Cy-TsAIL over various substrates had no marked effect on the relative ratio of substrate concentrations (SC_{100}/SC_{25}, where SC=Substrate Concentration) with corresponding yields of the product (Y_{25}/Y_{100}, where Y=Yield), when considering the corresponding conversions at S/C ratio of 100 or 25. Because of the reciprocal relation between the substrate concentration and yield, we have taken one as an inverse ratio (whether, SC or Y) for comparison. It is interesting that the enantioselectivity not changed for both the catalysts when changing the S/C ratio. From these results it is confirmed that the lower activity of the catalysts are a function of spatial array of ligands over the active metal centre.[41]

4.4. REFERENCES

1. S.E. Clapham, A. Hadzovic, R.H. Morris, *Coord. Chem. Rev*. **2004,** *248*, 2201.
2. K. Everaere, A. Mortreux, J.-F. Carpentier, *Adv. Synth. Catal.* **2003**, *345*, 67.
3. J. Blacker, J. Martin, in: H.-U. Blaser, E. Schmidt (Eds.), Asymmetric Catalysis on Industrial Scale: Challenges, Approaches and Solutions, *Wiley–VCH Verlag, Weinheim*, **2004**.
4. T. Dwars, G. Oehme, *Adv. Synth. Catal.* **2002,** *344*, 239.
5. C. Saluzzo, M. Lemaire, *Adv. Synth. Catal.* **2002,** *344*, 915.
6. M.J. Palmer, M. Wills, *Tetrahedron: Asymmetry*. **1999,** *10*, 2045-2061.
7. R. Noyori, S. Hashiguchi, *Acc. Chem. Res.* **1997,** *30*, 97.
8. G. Zassinovich, G. Mestroni, *Chem. Rev*. **1992,** *92*, 1051.
9. J. Takehara, S. Hashiguchi, A. Fujii, S. Inoue, T. Ikariya, R. Noyori, *Chem. Commun.* **1996,** 233.
10. M. Palmer, T. Walsgrove, M. Wills, *J. Org. Chem.* **1997,** *62*, 5226.
11. (a) D.A. Alonso, D. Guijarro, P. Pinho, O. Temme, P.G. Andersson, *J. Org. Chem.* **1998,** *63*, 2749. (b) Alonso, D. A.; Nordin, S. J. M.; Roth, P.; Tarnai, T.; Andersson, P. G. *J. Org. Chem*. **2000**, *65*, 3116–3122. (c) Alonso, D. A.; Brandt, P.; Nordin, S. J. M.; Andersson, P. G. *J. Am. Chem. Soc.* **1999**, *121*, 9580–9588.
12. S.J.M. Nordin, P. Roth, T. Tarnai, D.A. Alonso, P. Brandt, P.G. Andersson, *Chem. Eur. J*. **2001,** *7*, 1431.
13. P. Brandt, P. Roth, P.G. Andersson, *J. Org. Chem*. **2004,** *69*, 4885.

14. F.K. Cheung, A.M. Hayes, J. Hannedouche, A.S.Y. Yim, M. Wills, *J. Org. Chem.* **2005,** *70*, 3188.

15. V. Rautenstrauch, X. Hoang-Cong, R. Churlaud, K. Abdur-Rashid, R.H. Morris, *Chem. Eur. J.* **2003,** *9*, 4954.

16. A. Patti, S. Pedotti, *Tetrahedron: Asymmetry*. **2003,** *14*, 597.

17. J. Blacker, B. Mellor, US6372931B1 **2002**.

18. M. Pasto, A. Riera, M.A. Pericas, *Eur. J. Org. Chem*. **2002,** 2337.

19. J.W. Faller, A.R. Lavoie, *Organometallics*. **2002,** *21*, 2010.

20. K. Everaere, A. Mortreux, M. Bulliard, J. Brussee, A. van der Gen, G. Nowogrocki, J.-F. Carpentier, *Eur. J. Org. Chem*. **2001**, 275.

21. M. Yamakawa, I. Yamada, R. Noyori, *Angew. Chem. Int. Ed.* **2001,** *40*, 2818.

22. M. Yamakawa, H. Ito, R. Noyori, *J. Am. Chem. Soc*. **2000,** *122*, 1466.

23. D.G.I. Petra, J.N.H. Reek, J.-W. Handgraaf, E.J. Meijer, P. Dierkes, P.C.J. Kamer, J. Brussee, H.E. Schoemaker, P.W.N.M. van Leeuwen, *Chem. Eur. J.* **2000,** *6*, 2818.

24. M. Henning, K. Puntener, M. Scalone, *Tetrahedron: Asymmetry*. **2000,** *11*, 1849.

25. D.G.I. Petra, P.C.J. Kamer, P.W.N.M. van Leeuwen, K. Goubitz, A.M. Van Loon, J.G. de Vries, H.E. Schoemaker, *Eur. J. Inorg. Chem*. **1999,** 2335.

26. Y. Nishibayashi, I. Yakei, S. Uemura, M. Hidai, *Organometallics*. **1999,** *18*, 2291.

27. Y.T. Jiang, Q.Z. Jiang, G.X. Zhu, X.M. Zhang, *Tetrahedron Lett.* **1997,** *38*, 215.

28. T. Langer, G. Helmchen, *Tetrahedron Lett.* **1996,** *37*, 1381.

29. J. Blacker, B. Mellor, WO9842643 **1998**.

30. X.Y. Sun, G. Manos, J. Blacker, J. Martin, S. Gavriilidis, *Org. Process Res. Dev*. **2004,** *8*, 909.

31. D.J. Cross, I. Houson, A.M. Kawamoto, M. Wills, *Tetrahedron Lett.* **2004,** *45*, 843.

32. F.K. Cheung, A.M. Hayes, J. Hannedouche, A.S.Y. Yim, M. Wills, *J. Org. Chem*. **2005,** *70*, 3188.

33. Zassinovich, G.; Mestroni, G.; Gladiali, S. *Chem. Rev.* **1992**, *92*, 1051–1069.

34. X. Wu, X. Li, M. McConville, O. Saidi, J. Xiao, *Journal of Molecular Catalysis A: Chemical.* **2006,** *247*, 153.

35. P.N. Kuznetsov, L.I. Kuznetzova, A.M. Zhyzhaev, G.L. Pashkov, V.V. Boldyrev, *Appl. Catal. A: Gen*. **2002**, *227*, 299-307.

36. M. Suzuki, S. Ito, T. Kuwahara, *Bull. Chem. Soc. Jpn.* **1983**, *56*, 956-957.

37. M. Chidambaram, D. Curulla-Ferre, A.P. Singh, B.G. Anderson, *J. Catal.* **2003**, *220*, 442–456.

38. M.J. Hudson, J.A. Knowles, *J. Mater. Chem.*, **1996**, *6*, 89.

39. J.L. Blin, R. Flamant, B.L. Su, *Int. J. Inorg. Mater.,* **2001**, *3*, 959.

40. (a) S. Murali, C. V. Sastri, B.G. Maiya. *Proc. Indian Acad. Sci.* (*Chem. Sci.*), **2002**, *114*, 4, 403-415. (b) M. Heller,U. S. Schubert. *Macromol. Rapid Commun.* **2002**, *23*, 411-415. (c) Y. Lee, S. Yuan, A. Sanchez, L. Yu. *Chem. Commun*., **2008**, 247-249.

41. D. A. Alonso, B. Brandt, S. J. M. Nordin, P. G. Anderson. *J. Am. Chem. Soc*. **1999**, 121, 9580.

Chapter 5

Preparation, Characterization & Catalytic Activities of Homogeneous & Heterogeneous PrADPE Metal Complexes

5.1. INTRODUCTION

Transition-metal-catalyzed asymmetric hydrogenation is becoming increasingly important for the production of enantiopure pharmaceuticals and agrochemicals. In recent years highly enantioselective catalysts for a broad range of substrates such as olefins, ketones and imines[1-3] have been developed. Most of the catalysts in these categories are homogeneous transition metal complexes. One of the major drawbacks of homogeneous catalysts is the need for separation of the relatively expensive catalysts from the reaction mixture at the end of the process. Heterogenization of the metal complexes provides a way to greatly ease this separation and to improve the recycling of the expensive catalyst.[4] A commonly applied technique is the covalent binding of the complex to a solid support. Immobilization to the surface of silica or a polymer has been more attracted in these attempts because of the comparable activity and enantioselectivity with its homogenous analogous. Among many of the supports, mesoporous silicas offers a better host for chiral ligands due to its uniform large pore size, high surface area, insolubility in organic solvents and inert to many chemical substrates. For silica support simple filtration or centrifugation is enough to separate the highly precious metal catalyst.[5,6] The pore size of these heterogeneous catalysts has been shown a major affect in degree of enantioselectivity of some hydrogenation catalysts. Matrix isolation of chiral catalysts in microporous solids has been limited until recently by the difficulty of obtaining materials with suitable pore characteristics. In this respect the selection of mesoporous materials for the heterogenization of homogeneous chiral catalysts is more reasonable since the tuning of pore diameter is more practical by using appropriate surfactants and synthesis

conditions. A popular method for immobilizing organic groups into the mesoporous materials is the post-synthesis grafting.

The uses of inorganic amorphous and mesoporous silica supports for the preparation of ATH catalysts are still rare. The potential use of silica immobilized chiral diamines for ATH reaction is familiar.[7,8] The silica immobilized chiral amino alcohols for various asymmetric transformations, especially for ATH reaction is still a subject of immense study. The best catalysts reported so far in area are a combination of chiral amino alcohols with ruthenium(II) complexes. The solid-phase synthesis of a series asymmetric transfer hydrogenation catalysts as well as the use of these silica supported systems in batch and flow reactors was reported by Reek and coworkers.[9] Their pioneering work disclosed the unambiguity on the performance of heterogeneous amino alcohols catalysts in asymmetric transfer hydrogenation reaction of aromatic ketones. They have immobilized a number of chiral amino alcohols including (1R,2S)-norephedrine, (1S,2R)-(+)-2-amino-1,2-diphenyl ethanol, (R)-(-)-2-amino-2-phenylethanol, (S)-(+)-2-amino-3-methyl-1-butanol, (R)-(+)-2-amino-3-phenyl-1-propanol and a diamine, (1R,2R)-(+)-1,2-diphenylethylenediamine using *p*-(chloromethyl) phenyltrimethoxysilane as spacer molecule. The heterogeneous NH-benzylated (1S,2R)-(+)-2-amino-1,2-diphenylethanol which shows 58% *ee*, was far more selective than the homogeneous analogous for which an *ee* of 20% had been reported in a batchwise process. The silica immobilized NH-benzylated (R)-(-)-2-amino-2-phenylethanol in combination with ruthenium given 48% yield and 27% *ee* for the first run and 30% yield and 27% *ee* for the second run. A ruthenium mesitylene complex[10] has used in combination with (1R,2S)-(+)-2-amino-1,2-diphenyl-2-(N-methylamino)-ethan-1-ol in the homogeneous ATH reaction of

acetophenone resulted 97% conversion and 56% *ee* with S configuration to the product.

Here we have synthesized an efficient heterogeneous catalytic system for enantioselective transfer hydrogenation of carbonyl compounds, involving anchoring 1S,2R-(+)-1-amino-1,2-diphenylethanol on the inner surfaces of chloropropyl–functionalized SBA-15. Further the active catalysts have been prepared by complexation of the immobilized chiral ligand with metal precursors such as, $[RuCl_2(\eta^6\text{-benzene})]_2$ and $[RuCl_2(\eta^6\text{-}p\text{-cymene})]_2$. In depth characterization of these catalyst systems reveals that the integrity of the mesoporous supports and the Ru(II)-complexes was retained after the immobilization process. Applying these new heterogeneous catalysts, we have obtained fairly good enantioselectivities in the asymmetric transfer hydrogenation (ATH) of C=O bond in aromatic prochiral ketones. Acting as a true heterogeneous catalyst, these show comparable activity and enantioselectivity even after three recycles with negligible amount of leaching of the Ru-complex from the support.

PART A

Preparation, Characterization and Catalytic Activities of Heterogeneous Ru(II)-(1S,2R)-(+)-1-amino-1,2-diphenylethanol Complexes

5.2. EXPERIMENTAL

5.2.1. Materials

Tetraethylorthosilicate (TEOS), Pluronic P123, (1S,2R)-(+)-1-amino-1,2-diphenylethanol (1S,2R-ADPE) and all ketones were purchase from Aldrich chemicals (USA). $[RuCl_2(\eta^6\text{-benzene})]_2$ and $[RuCl_2(\eta^6\text{-}p\text{-cymene})]_2$ were synthesized according to a literature procedure.[11] The reagent grade solvents were obtained from Merck (India) and dried before use according to standard methods. HPLC grade 2-propanol was used for reaction.

Siliceous SBA-15 was synthesized by hydrothermal crystallization, as described in chapter 2.

5.2.2. Modification of SBA-15 using 3-chloropropyltrimethoxysilane

The calcined SBA-15 material (1 g) was first treated with the required amount of 3-chloropropyltrimethoxysilane in 30 ml dry toluene under reflux condition for 36 h. After cooling to ambient temperature, the material was filtered and washed with dichloromethane. Soxhlet extraction was carried out for 24 h in dichloromethane to remove unattached functional molecules. The sample was dried in vacuum for 10 h and was named as (PrCl-SBA-15). The dried material was stirred with excess of dimethoxydimethylsilane (MeO_2Me_2Si) in dry toluene for 24 h under reflux condition to passivate the undisturbed silanol groups inside and out side the porous material.

The filtered sample was washed with dichloromethane several times and dried under vacuum for 10 h. The resulted materials were designated as given in Table 5A.1.

5.2.3. Grafting of (1S,2R)-(+)-1-amino-1,2-diphenylethanol inside organo-functionalized SBA-15

To Pr-SBA-15 (1 g) in 30 ml dry toluene, added a mixture of triethylamine (0.4 ml) and (1S,2R)-(+)-1-amino-1,2-diphenylethanol (0.398 g, 1.83 mmol). The whole mixture was stirred for 24 h under refluxion condition under inert atmosphere. The resulted material was filtered and washed initially with dry toluene and after a 1:1 mixture of dichloromethane and methanol. The material was then stirred in 1:1 dichloromethane/methanol (100 ml) mixture for 2 h at room temperature. Filtered, washed with dichloromethane and dried in vacuum for 10 h. The resulted materials were designated as follows (Table 5A.1).

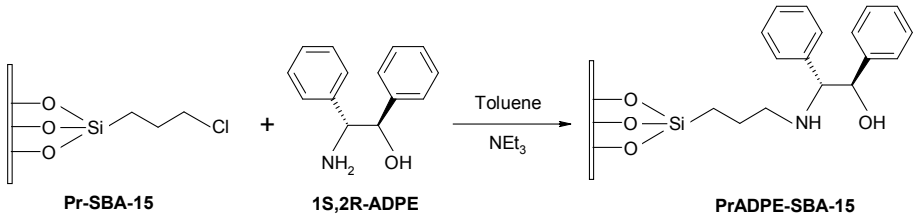

Scheme 5A.1: Grafting of (1S,2R)-(+)-1-amino-1,2-diphenylethanol over Pr-SBA-15

Table: 5A.1: Designation of organo-functionalized SBA-15 materials.

Material	Modifier	Product designation
SBA-15	3-chloropropyltrimethoxysilane	PrCl-SBA-15
PrCl-SBA-15	Dimethyldimethoxysilane	Pr-SBA-15
Pr-SBA-15	(1S,2R)-(+)-1-amino-1,2-diphenylethanol	PrADPE-SBA-15

Pr: Propyl; ADPE: (1S,2R)-(+)-1-amino-1,2-diphenylethanol.

5.2.4. Anchoring of $[Ru^{II}Cl_2(\eta^6\text{-benzene})]_2$ / $[Ru^{II}Cl_2(\eta^6\text{-}p\text{-cymene})]_2$ inside ligand functionalized SBA-15

30 mg of $[Ru^{II}Cl_2(\eta^6\text{-benzene})]_2$ / $[Ru^{II}Cl_2(\eta^6\text{-}p\text{-cymene})]_2$ was taken in 40 ml of dry 2-propanol containing 0.15 ml triethylamine (NEt_3) and refluxed for 1h under inert condition with stirring after the addition of 1 g of PrADPE-SBA-15**.** The final brown solid was filtered off and washed with dry 2-propanol for several times, then dried under vacuum for 12 h at 50^oC. The synthesized materials were named as Ru-Bn-PrADPE-SBA-15, {catalyst prepared from $[Ru^{II}Cl_2(\eta^6\text{-benzene})]_2$} and Ru-Cy-PrADPE-SBA-15, {catalyst prepared from $[Ru^{II}Cl_2(\eta^6\text{-}p\text{-cymene})]_2$}.

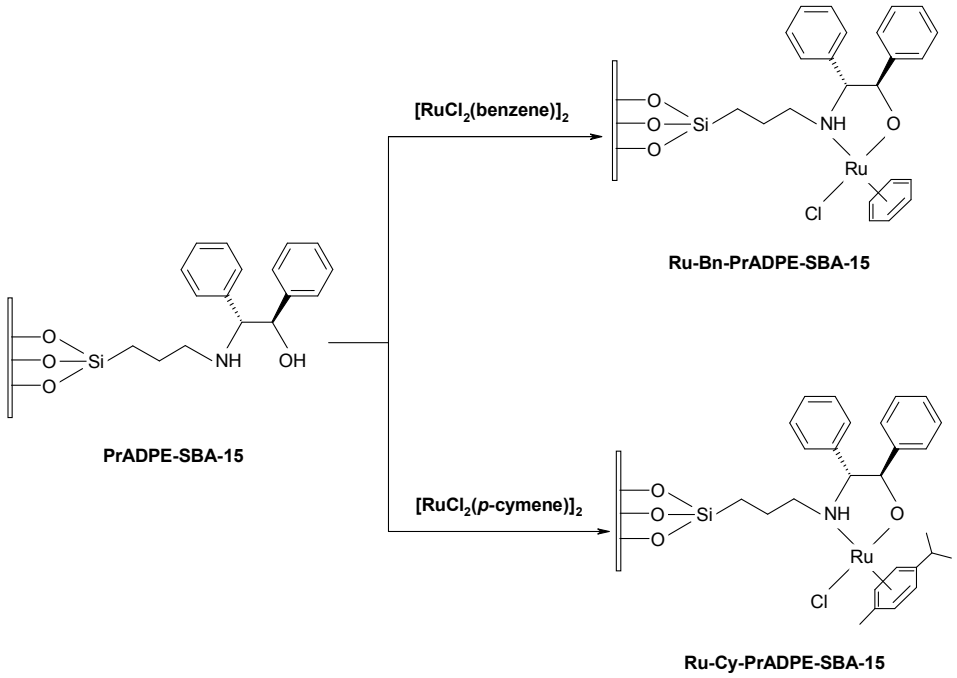

Scheme 5A.2: Anchoring of $[RuCl_2(benzene)]_2$ and $[RuCl_2(p\text{-cymene})]_2$ complexes over PrADPE-SBA-15.

Table: 5A.2: Designation of heterogeneous Ru-Complexes.

Chiral Ligand-modified material	Metal Precursor	Product designation
PrADPE-SBA-15	$[RuCl_2(benzene)]_2$	Ru-Bn-PrADPE-SBA-15
	$[RuCl_2(p\text{-cymene})]_2$	Ru-Cy-PrADPE-SBA-15

Bn: Benzene; Cy: *p*-cymene

5.2.5. Heterogeneous asymmetric transfer hydrogenation of prochiral ketones

0.0001 mol% (Ru content) of the catalyst (Ru-Bn-PrADPE-SBA-15/ Ru-Cy-PrADPE-SBA-15) was taken in a round bottom flask having 3 ml of dry 2-propanol and degassed three times with N_2. The required amount of ketone (0.01 mol %) by a syringe followed by KOH (3 mg) in 2-propanol (0.3 ml) was added under inert condition. The reaction mixture was stirred at 60^oC for an appropriate time and there after quenched by the addition of NH_4Cl (10 ml, sat. aq. solution). After filtration, reaction mixture was washed subsequently with saturated $NaHCO_3$, saturated brine solution and water and the organic layer was separated by using diethyl ether. The residue was purified by a short silica gel column after saturation at high vacuum, eluted by ethyl acetate. The yield and enantiomeric excess (*ee*) were determined by GC analysis.

5.2.6. Instruments for Characterization

Small angle powder XRD patterns were recorded at room temperature on a SIEMENS D5005 diffractometer using Cu Kα (λ = 0.154 nm) radiation. The specific surface areas of the samples were determined by the BET method from N_2 adsorption isotherms at −196^oC using an Omnisorb CX-100 Coulter instrument. Before measuring the surface area, the samples were activated at 120^oC for 3 h under nitrogen atmosphere. The elemental analyses were done with an EA1108 CHN/S Elemental Analyzer (Carlo Erba Instrument) for establishing the presence and exact fraction of elements in the synthesized materials. Diffuse reflectance UV-Vis spectra of the powder samples were recorded in the range 200-800 nm on Shimadzu UV 2101 PC spectrometer equipped with a diffuse reflectance attachment, using $BaSO_4$ as the

reference. The metal loading was found with an inductive couple plasma atomic emission spectroscopy (ICP-AES) on a spectroflame D (Spectro analytic instrument). A Shimadzu FT-IR 8201 PC Diffuse Reflectance Scanning disc technique was used to probe the attached groups and nature of the surface functional groups in the material. 125.757 MHz solid-state ^{29}Si MAS and ^{13}CP MAS NMR studies were carried out on a Bruker DRX-300 NMR spectrometer. The spectrum was recorded under Hartmann-Hahn match condition using a contact time of 1 m/sec and a relaxation delay of 4 sec. Reactions were monitored by TLC using aluminum-backed silica gel 60 (F_{254}) plates, visualized using UV_{254nm} and PMA dip. The catalytic activity and enantiomeric excess (*ee*) were measured on an HP 6890 gas chromatograph equipped with a flame ionization detector and a HP-Chiral 30 m *β*-cyclodextrin capillary column capillary column (30 m × 0.32 mm × 0.25 μm).

5.3. CHARACTERIZATION

5.3.1. Powder X-ray Diffraction

The X-ray diffraction pattern of (a) calcined SBA-15 (b) Pr-SBA-15 (c) PrADPE-SBA-15 (d) Ru-Bn-PrADPE-SBA-15 and (e) Ru-Cy-PrADPE-SBA-15 samples are dominated by the low angle reflections below 5° (2θ) which are shown in Figure 5A.1. It shows a well-resolved pattern with a prominent peak at 0.90°, and two weak peaks at 1.51 and 1.75° 2θ, which match well with the pattern reported for SBA-15[12]. This confirms successful synthesis of SBA-15 silica. The XRD peaks can be indexed to a hexagonal lattice with a *d*(100) spacing of 105 Å, corresponding to a large unit cell parameter a_o= 121 Å ($a_o = 2d(100)/\sqrt{3}$). Some loss in the intensities of the peaks was observed upon modification with 3-CPTMS, (1S,2R)-(+)-1-amino-1,2-

diphenylethanol and further with ruthenium precursors revealing that silylation and partial filling of organic moieties have indeed occurred inside the mesopores, which is less detrimental to the quality of the SBA-15 material. The persistence of the (100), (110) and (200) reflections not only proved the structural stability and existence of long range ordering to the mesophase but also the survival of undisturbed pore wall thickness even after a number of treatments with organic molecules in solvents under radical modification conditions.

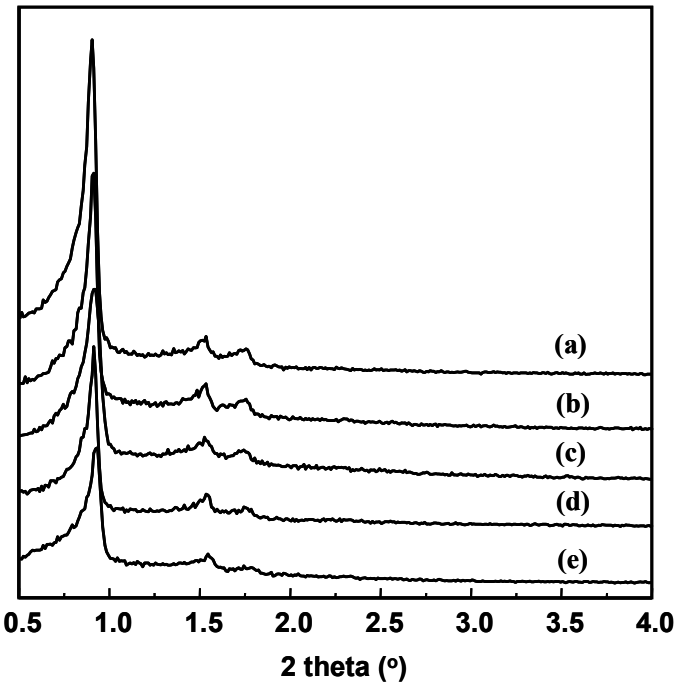

Figure 5A.1: X-ray diffraction pattern of (a) calcined SBA-15 (b) Pr-SBA-15 (c) PrADPE-SBA-15 (d) Ru-Bn-PrADPE-SBA-15 and (e) Ru-Cy-PrADPE-SBA-15

All the observations clearly show that the ordered mesoporosity and structural stability of the samples have retained after incorporation of organometallic complexes.

5.3.2. Specific surface area

The textural properties such as specific surface area and pore size of the support were followed throughout the different modification processes. Nitrogen adsorption data for (a) calcined SBA-15 (b) Pr-SBA-15 (c) PrADPE-SBA-15 (d) (Ru-Bn-PrADPE-SBA-15) and (e) (Ru-Cy-PrADPE-SBA-15) are presented in the Table 5A.1. Calcined SBA-15 material has a Brunauer-Emmett-Teller (BET) surface area of 854 m^2g^{-1}, pore diameter of 78 Å and a pore volume of 1.16 cm^3g^{-1}.

Table 5A.3: Physical characteristics of surface modified SBA-15

Material	% of Ru[a] (w/w)	BET adsorption-desorption measurements[b]		
		Surface area (m^2g^{-1})	Pore diameter (Å)	Pore volume ($cm^3\ g^{-1}$)
SBA-15	----	854	78	1.16
Pr-SBA-15	----	598	72	0.80
PrADPE-SBA-15	----	484	66	0.69
Ru-Bn-PrADPE-SBA-15	0.50	426	64	0.58
Ru-Cy-PrADPE-SBA-15	0.51	421	64	0.59

As reported earlier,[13,14] a tremendous decrease in the specific surface area was observed on modifying SBA-15 with 3-CPTMS, the surface area of SBA-15 decreased from 845 to 598 m^2g^{-1} and the pore diameter reduced from 78 to 72 Å. Upon immobilizing 1S,2R-(+)-1-amino-1,2-diphenylethanol, a further reduction in the

surface area from 598 to 484 m^2g^{-1} and pore diameter from 72 to 66 Å were observed. Further a decreased specific surface areas for Ru-Bn-PrADPE-SBA-15 and Ru-Cy-PrADPE-SBA-15 *ca,* 426 and 421 m^2g^{-1}, respectively, clearly evident the successful complexation of the immobilized ligands by ruthenium precursors. Nearly similar surface area values are obtained for Ru-Bn-PrADPE-SBA-15 and Ru-Cy-PrADPE-SBA-15 indicates an agreement in metal loading in both the heterogeneous catalysts. The reduction in the surface area and pore diameter is due to the lining of the walls of SBA-15 with the organic moieties. Similar trend has also been observed previously.[15,16] The N_2-adsorption measurements and XRD studies confirm the presence of ruthenium complex inside the channels PrADPE-SBA-15.

5.3.3. FT-IR spectra

Figure 5A.2 (A) & (B) represents the FTIR spectra of (a) Pr-SBA-15 and (b) PrADPE-SBA-15 (c) Ru-Bn-PrADPE-SBA-15 and (d) Ru-Cy-PrADPE-SBA-15. In all the samples a sharp peak at 800 cm^{-1} is due to Si-O stretching bond. In addition to the above band, the entire spectra show two weak bands at around 3200–2800 and 1500–1300 cm^{-1} which are due to the C–H stretching and bending vibrations[17,18] of methylene group of functionalized and ligand molecules. In the ligand immobilized material (PrADPE-SBA-15) we have expected a week band at 3260 cm^{-1} for the –NH stretching vibration, which is unresolved due to the overlapping of O–H stretching vibration (3400 and 3650 cm^{-1}) of surface O–H groups and water molecules occluded in the pores. After loading of (1S,2R)-1-amino-1,2-diphenylethanol over Pr-SBA-15, a medium band at 1423 cm^{-1} indicates the

C=C stretching[19] in-plane vibration of benzene framework. A small and weak band at around 1000–1200 cm^{-1} is the characteristic band of C–O group in the amino alcohol. A band at 702cm^{-1} represents the C–H bending vibration of methylene group of benzene.[19]

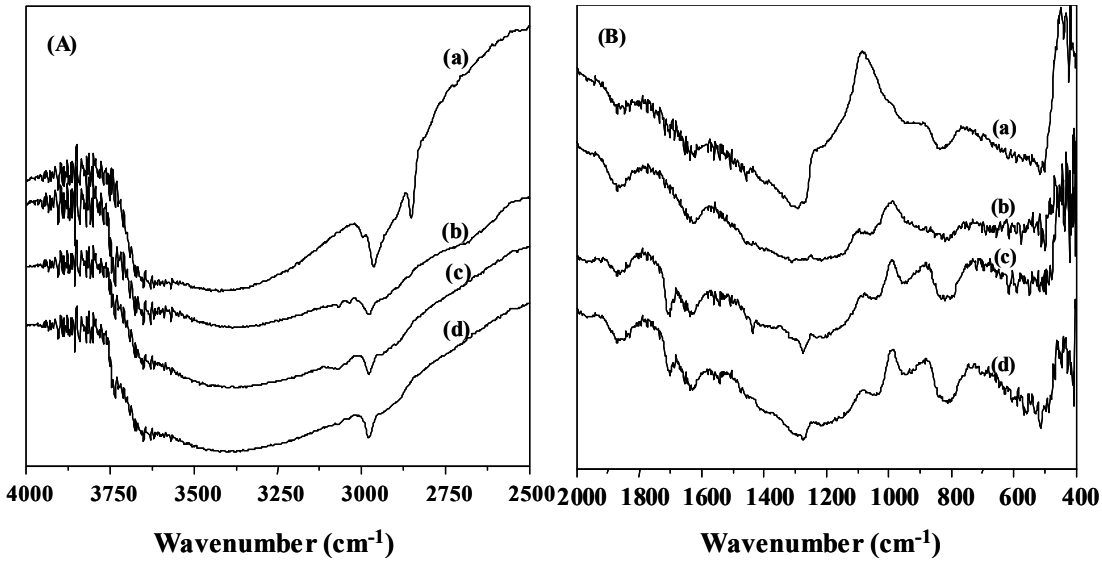

Figure 5A.2: FT-IR spectra of: (a) Pr-SBA-15, (b) PrADPE-SBA-15, (c) Ru-Bn-PrADPE-SBA-15 and (d) Ru-Cy-PrADPE-SBA-15.

5.3.4. ^{13}C CP MAS NMR spectra

Figure 5A.3 represents the ^{1}H-^{13}C coupled CP MAS NMR spectra of (a) PrCl-SBA-15, (b) PrSBA-15 and (c) PrADPE-SBA-15 samples. In all the spectra (Figure 5A.3a), three distinct ^{13}C signals at $\delta \approx 9$, 26 and 46 ppm, which can be assigned to carbon atoms **1**, **2**, and **3**, respectively, of the propyl chain.[20,21] The spectrum of the

silanol groups capped material (PrSBA-15, Figure 3b, silylated with $-SiMe_2$), the free methyl group is evident

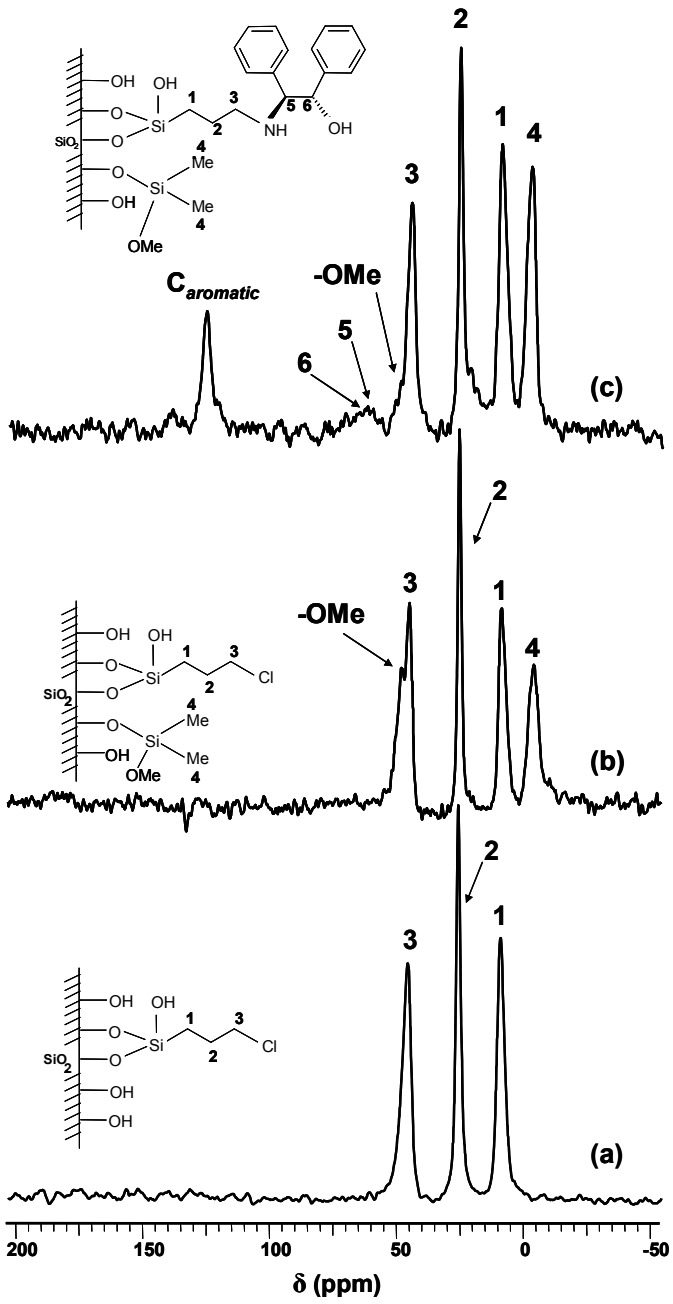

Figure 5A.3: ^{13}C CP MAS NMR spectra of: (a) PrCl-SBA-15 (b) Pr-SBA-15 and (c) PrADPE-SBA-15.

from an additional sharp peak at a chemical shift value of δ ≈ -3 (numbered as **4**) along with the previously mentioned (propyl carbon atoms) resonance peaks. A shoulder peak at a chemical shift value of δ ≈ 49 ppm over the propyl carbon atom, numbered **3**, is due to the free methoxy carbon atom (-OMe) present in the dimethoxydimethylsilane[22] used for capping surface silanol groups. In the spectrum of PrADPE-SBA-15 (Figure 3c) a medium sharp peak peaks at a chemical shift value of δ ≈ 126 ppm having shoulder peak, δ ≈ 130 ppm, in the spectrum (Figure 5A.3c) indicates the presence of phenyl rings, in addition to the broad and overlapping signals at δ ≈ 61 and 63 ppm corresponds to C-NH and C-OH carbon atoms (numbered as **5** and **6**) of the amino alcohol respectively indicate the successful anchoring of (1S,2R)-(+)-1-amino-1,2-diphenylethanol over organo-functionalized SBA-15[17,22].

5.3.5. ^{29}Si CP MAS NMR spectra

^{29}Si CP-MAS NMR spectra provide direct evidence for the incorporation of the covalently linked organic system (Figure 5A.4). The spectrum of the unmodified mesoporous SBA-15 support shows (Figure 5A.4a) three signals at -111, -102, and -93 ppm corresponding to Q^4, Q^3 and Q^2 species of the silica framework [Q^n = $Si(OSi)_n(OH)_{4-n}$, n=2-4].[23,24] The Q^3 sites are associated with isolated Si-OH groups, and the Q^2 sites correspond to geminal silandiols. For the organo-modified and silylated (with $SiMe_2$) samples (Figure 5A.4 b), three broad and overlapping signals appear at -80, -71 and -62 ppm, which can be assigned to T^3, T^2, and T^1 organosilica species [T^m= $RSi(OSi)_m(OEt)_{3-m}$, m=1-3], respectively[25], with T^2 as the major system. In addition to the above peaks, a sharp peak at 19 ppm with a shoulder peak at 10 ppm

can be assigned to the silicon nuclei of the dimethylsilyl (Me_2Si-) groups. The resonance peak at 19 ppm represents to $–SiMe_2$ and the shoulder peak is assigned to $–Si(OH)Me_2$ species present on the surface of the mesoporous material , respectively. In the organo-modified sample the relative intensity of Q^4 species increased considerably while the Q^2 species decreased and fallen down almost to detection limit. This indicates the decrease in the surface silanol groups due to the functionalization and subsequent silylation.[26]

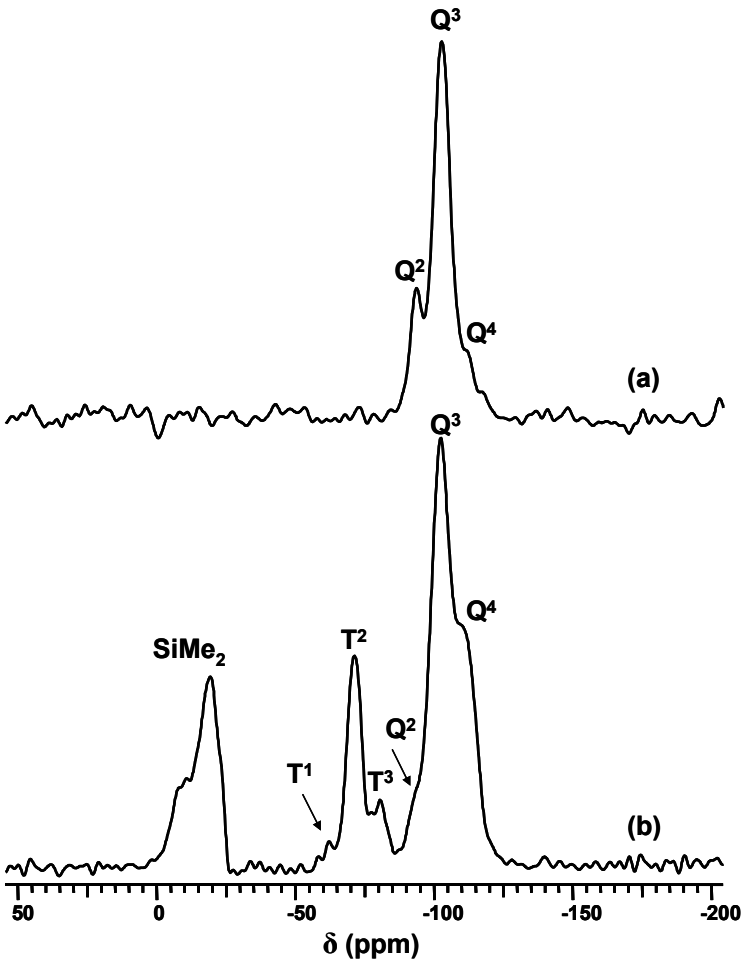

Figure 5A.4: ^{29}Si CP MAS NMR spectra of: (a) SBA-15 and (b) Pr-SBA-15.

5.3.6. UV-Vis spectra

Figure 5A.5 illustrates the UV-Vis spectra of (a) Ru-Bn-PrADPE-SBA-15 and (b) Ru-Cy-PrADPE-SBA-15. A sharp peak at 422 nm in both the materials, metal-to-ligand charge-transfer (MLCT) band, clearly indicates the anchoring of the complex in the surface modified SBA-15.[27] It is reported for many Ru(II) complexes that the redox potential becomes higher as the MLCT transition energy becomes larger.[28,29] Thus, strong absorption bands can be observed in the range of 355–490 nm for many homogeneous and heterogeneous ruthenium(II) metal complexes.

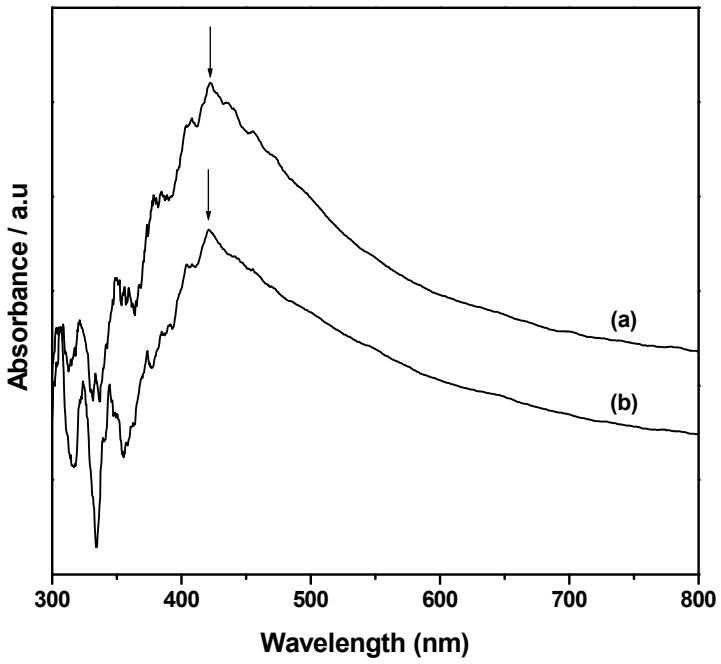

Figure 5A.5: UV-Vis spectra of: (a) Ru-Bn-PrADPE-SBA-15 and (b) Ru-Cy-PrADPE-SBA-15.

5.3.7. Asymmetric Transfer Hydrogenation of Prochiral Ketones

In order to elucidate the catalytic activity and enantioselectivity of the synthesized catalysts, the asymmetric transfer hydrogenation reaction of prochiral ketones has been performed using a procedure similar to the methodology available in literatures for homogeneous chiral amino alcohol complexes.[30] Results are presented in Table 5A.5. All the reactions were carried out under similar reaction conditions in a batch reactor using 2-propanol as solvent as well as proton source. The use of 0.01 mol % prochiral ketone in conjunction with 0.0001 mol % of the ruthenium complex (Ru-Bn-PrADPE-SBA-15/Ru-Cy-PrADPE-SBA-15) and 3 mg of KOH in 2-propanol (0.3 ml) at 60^{o}C temperature resulted in the enantioselective reduction of prochiral ketones to corresponding (R)-alcohol.

5.3.7.1. Effect of various substrates

As can be seen in the Table 5A.5, the heterogeneous catalysts Ru-Bn-PrADPE-SBA-15 and Ru-Cy-PrADPE-SBA-15 exhibited moderate to good catalytic activity and enantioselectivities for various prochiral ketones like acetophenone, 4-chloroacetophenone, 4-bromoacetophenone, 4-methylacetophenone, 4-methoxyacetophenone, propiophenone and 2,5-dimethoxyacetophenone.

Acetophenone reduced 37 and 18% with in 1 h with *ee* values of 30 and 48% for Ru-Bn-PrADPE-SBA-15 and Ru-Cy-PrADPE-SBA-15, respectively (entry 1, Table 5A.5). For instance 4-chloroacetophenone and 4-bromoacetophenone both were reduced in 64%, the highest conversion among the substrates, having *ee* values of 12 and 10% for Ru-Bn-PrADPE-SBA-15(entry 2 & 3, Table 5A.5).

Table 5A.4: Substrates of choice for Asymmetric Transfer Hydrogenation Reaction

Entry	Substrate	Designation	Product
1	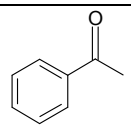 Acetophenone	**ACP**	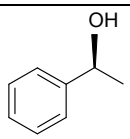 *R*-1-phenylethanol
2	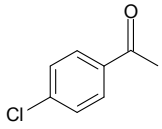 4-chloroacetophenone	**ClACP**	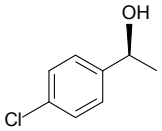 *R*-1-(4-chlorophenyl)ethanol
3	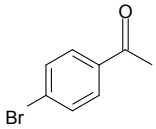 4-bromoacetophenone	**BrACP**	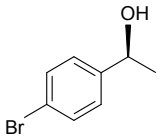 *R*-1-(4-bromophenyl)ethanol
4	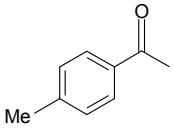 4-methylacetophenone	**MeACP**	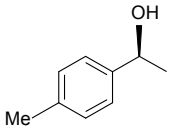 *R*-1-(4-methylphenyl)ethanol
5	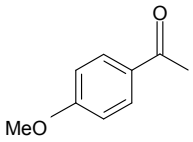 4-methoxyacetophenone	**MeOACP**	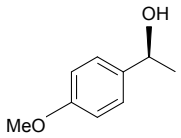 *R*-1-(4-methoxyphenyl)ethanol
6	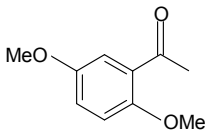 2,5-dimethoxy Acetophenone	**DMeOACP**	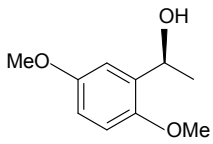 *R*-1-(2,5-dimethoxy phenyl)ethanol
7	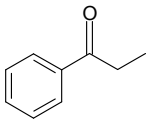 Propiophenone	**PRP**	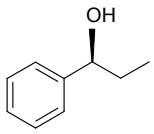 *R*-1-(phenyl)propanol

Table 5A.5: Asymmetric transfer hydrogenation of simple prochiral ketones

Entry	Substrate	Ru-Bn-PrADPE-SBA-15		Ru-Cy-PrADPE-SBA-15	
		Conversion (%)[a]	*ee* (%)[a]	Conversion (%)[a]	*ee* (%)[a]
1	**ACP**	37	30	18	48
2	**ClACP**	64	12	29	38
3	**BrACP**	64	10	30	32
4	**MeACP**	32	20	16	52
5	**MeOACP**	27	18	15	27
6	**DMeOACP**	37	16	20	28
7	**PRP**	64	14	31	26

The reaction was carried out at 60^{o}C for 1 h, using 0.01 mol % of ketone and a S/C ratio of 100 in 3 ml solvent. KOH = 3 mg/0.3 ml 2-propanol.

[a]Determined by GC equipped with a chiral column.

The configuration of alcohol product was R.

But for Ru-Cy-PrADPE-SBA-15 catalyst, lower activities (29 & 30%) with enhanced *ee* values (38 & 32%) have been observed (entry 2 & 3, Table 5A.5). The reduction of 4-methylacetophenone gave 32% conversion with 20% *ee* for Ru-Bn-PrADPE-SBA-15 and 16% conversion with 52% *ee* for Ru-Cy-PrADPE-SBA-15 (entry 4, Table 5A.5). 4-methoxyacetophenone reduced to 27% conversion with 18% *ee* for Ru-Bn-PrADPE-SBA-15 and 15% conversion with 27% *ee* for Ru-Cy-PrADPE-SBA-15 (entry 5, Table 5A.5). 2,5-dimethoxyacetophenone showed a moderated conversion

(37%) and less *ee* (16%) for Ru-Bn-PrADPE-SBA-15 and 20% conversion and 28% ee for Ru-Cy-PrADPE-SBA-15 (entry 7, Table 5A.5). The low *ee* of 2,5-dimethoxyacetophenone is probably a result of steric hindrance that affects access of the carbonyl carbon to the Ru(II)-H hydride. Propiophenone exhibited a yield of 64% and *ee* of 14% for Ru-Bn-PrADPE-SBA-15 and 31% yield and 26% *ee* for Ru-Cy-PrADPE-SBA-15 (entry 6, Table 5A.5). From the results, it is observed that the heterogeneous catalyst (Ru-Bn-PrADPE-SBA-15) prepared from $[RuCl_2(\eta^6\text{-benzene})]_2$ displayed higher conversion than the catalyst (Ru-Cy-PrADPE-SBA-15) prepared from $[RuCl_2(\eta^6\text{-}p\text{-cymene})]_2$ for simple prochiral ketones. But the *ee* results are superior for Ru-Cy-PrADPE-SBA-15 than Ru-Bn-PrADPE-SBA-15 at our reaction conditions and may be due to the favorable special arrangement of sterically hindered *p*-cymene in the metal complex. As a general strategy, the results with the substituted acetophenones suggested that electron-withdrawing groups show higher substrate conversions than electron donating groups. The *ee* results are exactly reverse to conversion strategy.

5.3.7.2. Influence of reaction time over conversion and enantioselectivity

The influence of reaction time over the conversion and enantioselectivity in the transfer hydrogenation of acetophenone is presented in Figure 5A.6. We have conducted the experiment for 15 min (22% cov. and 32% *ee*), 30 min (30% cov. and 30% *ee*), 1 h (37% cov. and 30% *ee*), 2h (40% cov. and 30% *ee*), 5 h (43% cov. and 30% *ee*) and 10 h (44% cov. and 30% *ee*). The results illustrate that the conversion increases with time, as expected, and reaches an optimum value (44%) before 10 h in

the case of the Ru-Bn-PrADPE-SBA-15. The enantiomeric excess values, however, attain a maximum (30%) from the very beginning of the reaction.

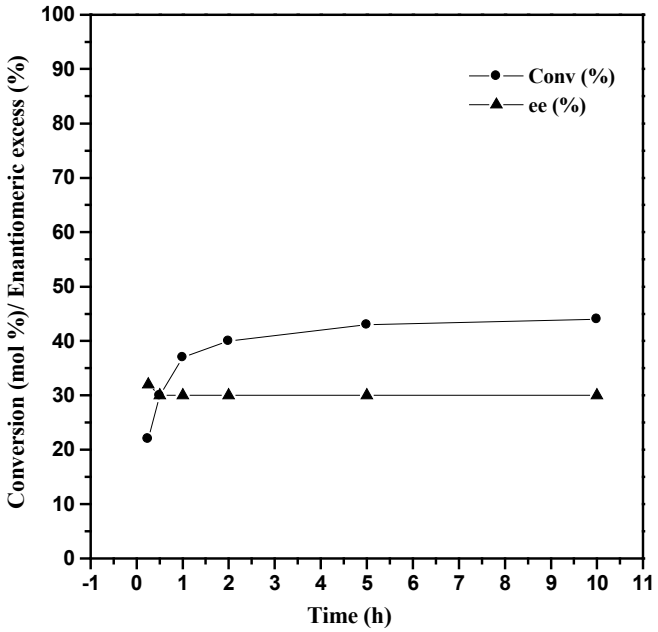

Figure 5A.6: Influence of reaction time on conversion and enantioselectivity in the ATH of acetophenone. The reaction was carried out at 60^{o}C for 1 h, using 0.01 mol % of ketone and a S/C ration of 100 in 3 ml solvent, KOH = 3 mg/0.3 ml 2-propanol. Catalyst used: Ru-Bn-PrADPE-SBA-15.

5.3.7.3. Influence of reaction temperature over conversion and enantioselectivity

Figure 5A.7 demonstrates the performance (conversion and enantioselectivity) of Ru-Bn-PrADPE-SBA-15 under various reaction temperatures in the transfer hydrogenation of acetophenone. We have carried out reaction at 0^{o}C (11% cov. and 31% *ee*), 40^{o}C (20% cov. and 30% *ee*), 60^{o}C (37% cov. and 30% *ee*) and 80^{o}C (48% cov. and 29% *ee*) for our study. The results clearly demonstrate that the asymmetric transfer hydrogenation of acetophenone is temperature dependent. As the temperature

increases the activity of the catalyst also increases. But the *ee* value decreased marginally from 31% to 29% as expected. It proved that at lower temperatures (0°C and 40°C) the reaction preferring the production of *R* isomer and at higher temperatures (60°C and 80°C) a marginal production of *S* isomer is taking place. It is also noticed that the activity of the catalyst is remarkable while going from 60°C (37%) to 80°C (48%).

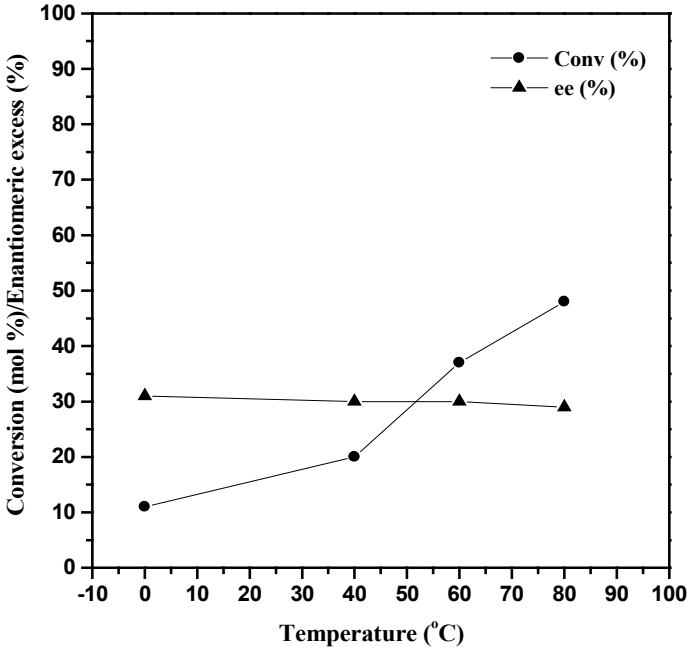

Figure 5A.7: Influence of reaction temperature on conversion and enantioselectivity in the ATH of acetophenone. The reaction was carried for 1 h, using 0.01 mol % of ketone and a S/C ration of 100 in 3 ml solvent, KOH = 3 mg/0.3 ml 2-propanol. Catalyst used: Ru-Bn-PrADPE-SBA-15.

5.3.7.4. Influence of amount of solvent over conversion and enantioselectivity

The effect of amount of solvent (2-propanol) over the conversion and enantioselectivity in the asymmetric transfer hydrogenation of acetophenone is

presented in Figure 5A.8. It is accounted that 2-propanol is acting as a solvent and the proton donor simultaneously. During the course of the reaction it releases a proton and converting itself to acetone. Due to the reversibility nature of the process, here is a chance to accept a proton from the reaction products (*S* and *R*-1-phenylethanol) to change back to 2-propanol. So it is necessary to keep an optimum dilution in reaction system to prevent the

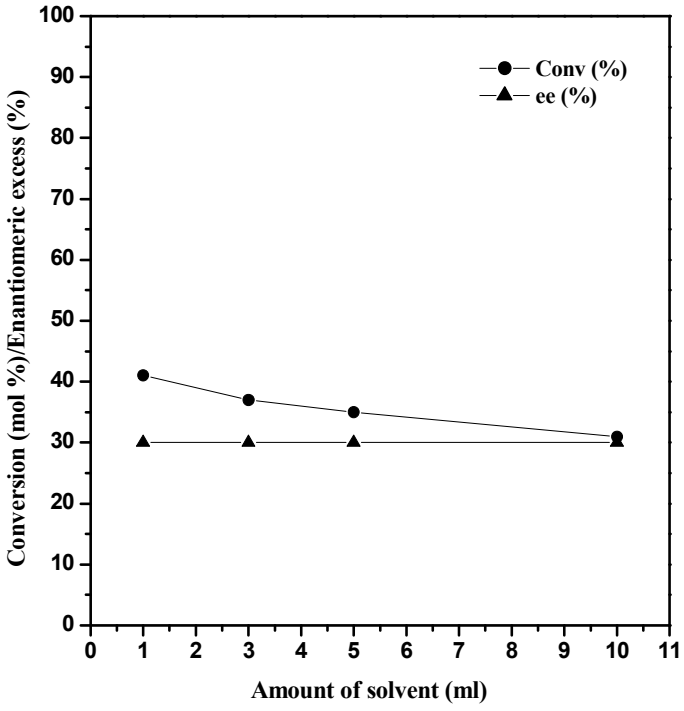

Figure 5A.8: Influence of amount of solvent on conversion and enantioselectivity in the ATH of acetophenone. The reaction was carried out at 60^{o}C for 1 h, using 0.01 mol % of ketone and a S/C ration of 100, KOH = 3 mg/0.3 ml 2-propanol. Catalyst used: Ru-Bn-PrADPE-SBA-15.

backward reaction. We have studied the asymmetric reduction of acetophenone keeping 1 ml (41% cov. and 30% *ee*), 3 ml (37% cov. and 30% *ee*), 5 ml (35% cov. and 30% *ee*) and 10 ml (31% cov. and 30% *ee*) solvent in the reaction system. The

results illustrate that while increasing the solvent amount from 1 ml to 10 ml the activity goes on decreasing from 41% to 31%. But the *ee* values were unchanged even after dilution. It is observed that 1 ml or 3 ml of solvent is suitable for obtaining a maximum conversion. We have selected 3 ml solvent for the ATH of various substrates for considering other factors such as base concentration and reaction temperature.

5.3.7.5. Influence of amount of base over conversion and enantioselectivity

To initiate the reaction the presence of the base is necessary. We have noticed that the reaction is no more initiating in the absence of a base. So it is obvious that the amount of base has a strong influence in the reaction rate. We have used 0.1 ml (16% cov. and 30% *ee*), 0.2 ml (27% cov. and 30% *ee*), 0.3ml (37% cov. and 30% *ee*) and 0.4 ml (47% cov. and 29% *ee*) base solution from a 0.18 molar solution of KOH in 2-propanol for our study and the results are shown in Figure 5A.9. It was manifested that while increasing the amount of base the reaction rate is increasing considerably (from 16% to 47%) and the enantioselectivity (30%) is intact upto 0.3 ml of base solution. While increasing the amount of base to 0.4 ml the reaction rate is drastically increased to (47%) and the enantioselectivity goes down to (29%) along which, the reaction mixture turned colored. The ICP analysis proved the presence of leached metal complexes in the reaction residue after centrifuged out the catalyst. So we have confirmed that the noticed higher activity is due to the leached active metal complexes when using 0.4 ml base solution. The decreased enantioselectivity is due to the progressive reaction rate by the leached metal complex in the solution.

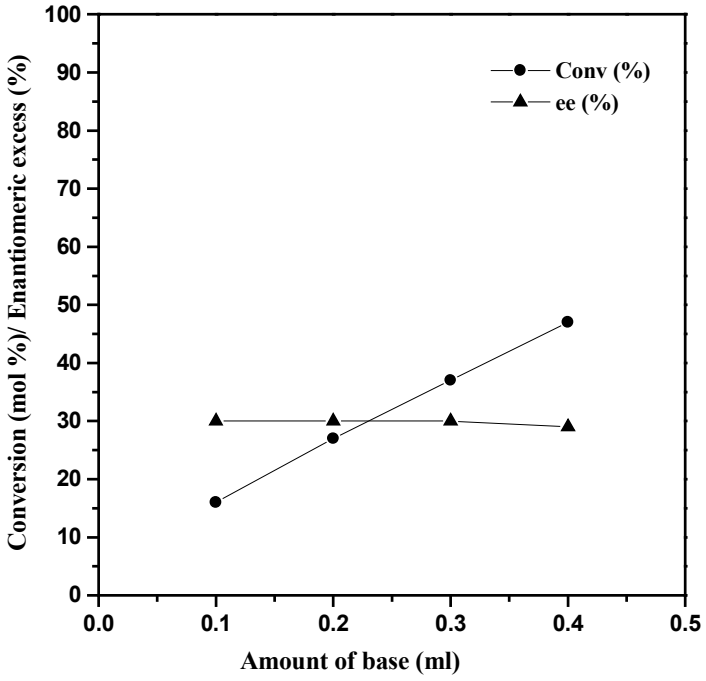

Figure 5A.9: Influence of amount of base on conversion and enantioselectivity in the ATH of acetophenone. The reaction was carried out at 60^{o}C for 1 h, using 0.01 mol % of ketone and a S/C ration of 100 in 3 ml solvent. Catalyst used: Ru-Bn-PrADPE-SBA-15.

5.3.7.6. Recycle studies

The recycling study was done by both regeneration methods (a) without stirring in chloroform and (b) with stirring in chloroform as described previously in chapter 3. The reaction conditions used for recycling study was the exactly same as that of the fresh reaction. The results are summarized in Table 5A.6 and 5A.7. When the recycling was done under without stirring in chloroform condition we have observed an immediate decrease drop of conversion from the first recycling run onwards but the enantioselectivity remains constant. Second recycling run given poor conversions

keeping the enantiomeric excess remains a constant value. It may be due to the inactivity of the previously generated hydride (Ru-H) catalyst towards the hydrogenation process. The ICP-AES analysis of the used catalyst after the first run showed a considerable loss of active metal from the catalyst due to the prolonged contact with the base. But when the recycling was conducted under with stirring in chloroform condition, the activity loss was not decreased for the first recycling after it decreased drastically keeping the enantiomeric excess a constant value. This may be due to the regeneration of active Ru-Cl species was formed by stirring with chloroform. Here we have observed a considerable amount of leaching to the active metal complex from the catalyst by the color change to the reaction mixture. This may be due to the prolonged contact with a more polar solvent like chloroform.

Table 5A.6: Recycle studies of the heterogeneous catalysts for hydrogenation of acetophenone under "without stirring in chloroform" condition for ATH of acetophenone.

	Ru-Bn-PrADPE-SBA-15		**Ru-Cy-PrADPE-SBA-15**	
No. of runs	Conv. (%)	ee (%)	Conv. (%)	ee (%)
Fresh	37	30	10	48
1	16	30	3	47
2	6	31	2	47

Table 5A.7: Recycle studies of the heterogeneous catalysts for hydrogenation of acetophenone under "with stirring in chloroform" condition for ATH of acetophenone.

	Ru-Bn-PrADPE-SBA-15		**Ru-Cy-PrADPE-SBA-15**	
No. of runs	Conv. (%)	ee (%)	Conv. (%)	ee (%)
Fresh	37	30	10	48
1	20	30	5	48
2	8	30	2	48

In conclusion, a class of efficient heterogeneous catalyst systems involving anchoring of various Ru(II)-complexes on the inner surfaces of organo-functionalized SBA-15 molecular sieve, for enantioselective transfer hydrogenation of prochiral ketones were designed. Detailed characterization of these new catalyst systems strongly point towards stable immobilization of the Ru-complexes inside the mesoporous matrices. These newer catalyst systems show moderate activity and enantioselectivity in the aforesaid transfer hydrogenation reaction, and can be recycled effectively and reused several times with minor loss in activity.

PART B

Preparation, Characterization and Catalytic Activities of Homogeneous Ru(II)-(1S,2R)-(+)-1-amino-1,2-diphenylethanol Complexes

5.4. EXPERIMENTAL

5.4.1. Preparation of NH-propyl-(1S,2R)-(+)-1-amino-1,2-diphenylethanol

K_2CO_3 (234 mg, 1.70 mmol) was added to (1S,2R)-(+)-1-amino-1,2-diphenyl ethanol (365 mg, 1.70 mmol) in acetonitrile at room temperature. At 0°C, 1-bromopropane (201 mg, 1.6 mmol) was added and the resulting mixture was stirred for 24 h at 70°C (Scheme 5B.1). The reaction mixture was filtered and evaporated to dryness. The crude solid material was re-dissolved in dichloromethane and was washed subsequently with sat. $NaHCO_3$ (10 ml), sat. brine (10 ml) solution and finally with water (3x10 ml). The organic layer was separated and dried over anhydrous Na_2SO_4. Removal of the solvent resulted NH-propyl-(1S,2R)-(+)-1-amino-1,2-diphenylethanol as a dirty yellow solid. The compound was further purified by column chromatography (silica gel 60, eluent: ethyl acetate).

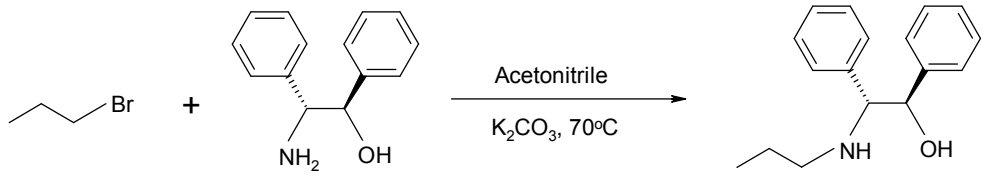

Scheme 5B.1: Preparation of NH-propyl-(1S,2R)-(+)-1-amino-1,2-diphenylethanol **(**PrADPE)

5.4.2. Preparation of Ru(II)-NH-propyl-(1S,2R)-(+)-1-amino-1,2-diphenylethanol

A solution of ruthenium dimer (0.0125 mmol) and (1S,2R)-(+)-1-amino-1,2-diphenylethanol (10.7 mg, 0.05 mmol) in dry 2-propanol (4 ml) was heated at 80^{o}C for 30 minutes under nitrogen (Scheme 5B.2). The solvent was removed after cooling to room temperature.

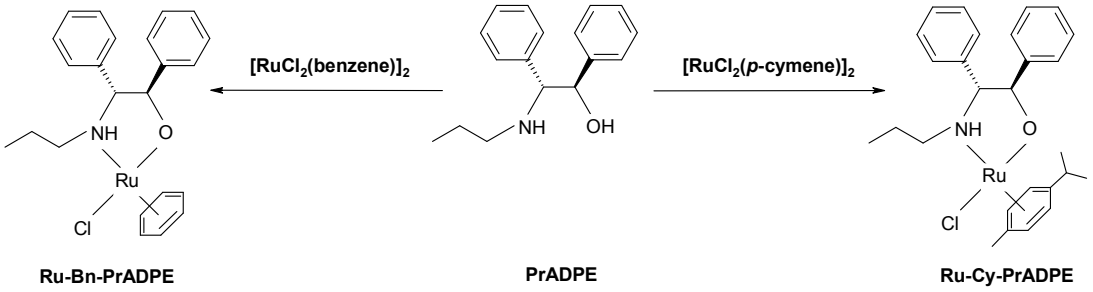

Scheme 5B.2: Preparation of Ru-Bn-PrADPE and Ru-Cy-PrADPE

Table: 5B.1: Designation of homogeneous ligand and Ru-Complexes.

Material	Modifier	Product designation
ADPE	1-bromopropane	PrADPE
PrADPE	$[RuCl_2(benzene)]_2$	Ru-Bn-PrADPE
	$[RuCl_2(p\text{-cymene})]_2$	Ru-Cy-PrADPE

ADPE: (1S,2R)-(+)-1-amino-1,2-diphenylethanol

PrADPE: NH-propyl-(1S,2R)-(+)-1-amino-1,2-diphenylethanol

Bn: Benzene; Cy: *p*-cymene

5.4.3. Homogeneous asymmetric transfer hydrogenation (ATH) of simple prochiral ketones

A stock solution of the homogeneous catalyst was prepared by mixing appropriate amount of ruthenium dimer complex (0.0125 mmol) and the homogeneous ligand (0.05 mmol) in dry 2-propanol (50 ml) was heated at 80^{o}C for 20 minutes under nitrogen. After cooling to room temperature, the solution was transferred *via* cannula to a large sealed Schlenk flask. From the stock solution 0.1 ml of catalyst was transfered to a two necked round bottom flask, followed by ketone (0.01 mol%) in dry degassed 2-propanol (3 ml) and KOH (0.3 ml, 1 mg/0.1 ml 2-prpanol). The reaction was run at 60^{o}C for 1 h. Work up consisted of filtering the dark brown solution through a pad of silica under vacuum (with ethyl acetate washings, 2x50 ml). The combined organic extracts were concentrated *in vacuo* to give the crude product.

5.4.4. Instruments for Characterization

Liquid state ^{1}H and ^{13}C NMR spectra were recorded on a Bruker DRX-300 NMR spectrometer with TMS as internal standard. HRMS data were measured with ESI techniques (Bruker Apex II). . The spectrum was recorded under Hartmann-Hahn match condition using a contact time of 1 m/sec and a relaxation delay of 4 sec. The elemental analyses were done with an EA1108 CHN/S Elemental Analyzer (Carlo Erba Instrument) for establishing the presence and exact fraction of elements in the synthesized materials. A Shimadzu FT-IR 8201 PC Diffuse Reflectance Scanning disc technique was used to probe the attached groups and nature of the surface functional groups in the material. Liquid state UV-Vis spectra of the homogeneous complexes were recorded in the range 200-800 nm on Shimadzu UV 2101 PC spectrometer

equipped with a diffuse reflectance attachment, using methanol as solvent. Optical rotation values were measured with a Rudolph IV polarimeter.

5.5. RESULTS AND DISCUSSION

5.5.1. ^{1}H & ^{13}C NMR Spectra

Figure 5B.1 shows the ^{1}H NMR spectra of (1S,2R)-(+)-1-amino-1,2-diphenylethanol. In which we can see a broad singlet peak at a chemical shift value 1.87 ppm corresponds to the –N*H* protons (indexed to 2 protons). Because of the hydrogen bonding and exchangeable nature of the proton, the peak appears broad. Near to the –NH peak another singlet with reduced intensity is corresponds to the –O*H* proton (indexed to one proton). The concentration of the -OH proton is very less in the ligand due to the higher mobility nature than the –NH protons.

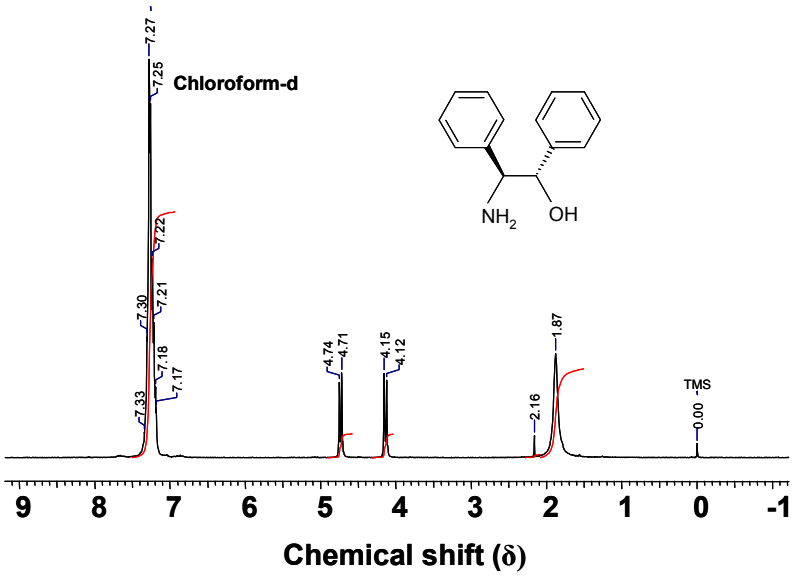

Figure 5B.1: ^{1}H NMR spectra of (1S,2R)-(+)-1-amino-1,2-diphenylethanol

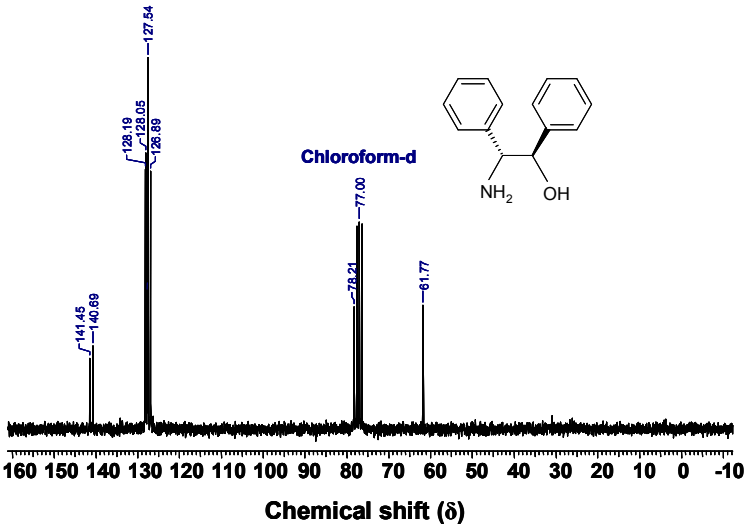

Figure 5B.2: ^{13}C NMR spectra of (1S,2R)-(+)-1-amino-1,2-diphenylethanol

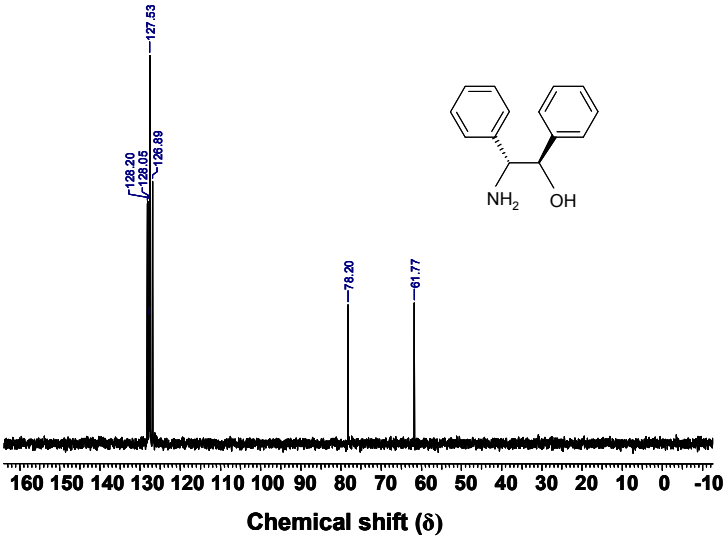

Figure 5B.3: ^{13}C (DEPT) NMR spectra of (1S,2R)-(+)-1-amino-1,2-diphenylethanol

In the spectrum It was observed that two doublets, one at δ = 4.12 ppm (C*H*NH) and the second at δ = 4.71 ppm (C*H*OH), due to the ethyl backbone. Figure 5B.2 and 5B.3 represent the ^{13}C and ^{13}C DEPT NMR spectra of (1S,2R)-(+)-1-amino-1,2-diphenylethanol respectively. In figure 5B.2, we could see four sets of peaks at δ = 61.77, 78.21, 127.54 (five peaks) and 140.69 ppm (two peaks) corresponding to *C*HNH, *C*HOH, $CH_{aromatic}$ and two quaternary carbon atoms respectively. Both the aromatic rings of the ligands are in different chemical environment and five different types of carbon atoms are present. The two quaternary carbon atoms also in different environment and giving separate peaks. In the figure 5B.3, we can see only three sets of peaks at δ = 61.77, 78.21 and 127.54 (five peaks) ppm corresponds to *C*HNH, *C*HOH and $CH_{aromatic}$ carbon atoms. In a DEPT spectrum quaternary carbon atoms will be omitted.

Table 5B.2: (1S,2R)-(+)-1-amino-1,2-diphenylethanol

Source	Aldrich Chemicals
Appearance	White solid
Molecular Weight	213
FT-IR (DRS)	ADPE: 3354, 3194, 3049, 1746, 1663, 1522, 1501, 1200-1000 cm^{-1}.
^1H NMR ($CDCl_3$)	ADPE, δ = 1.87 (broad. s, 1 H, N*H*), 2.16 (s, 1 H, OH), 4.12 (d, 1 H, C*H*NH), 4.71 (d, 1 H, C*H*OH), 7.17-7.33 (m, 10 H, H_{arom}).
^{13}C NMR ($CDCl_3$)	ADPE, δ = 61.77 (CHNH), 78.21 (CHOH), 126.89, 127.54, 127.72, 128.05, 128.19 ($CH_{aromatic}$), 140.69, 141.45 (2 C_q) ppm.
^{13}C NMR ($CDCl_3$)-(DEPT)	ADPE, δ = 61.88 (CHNH), 78.31 (CHOH), 127.00, 127.65, 127.83, 128.16, 128.37 ($CH_{aromatic}$) ppm.
Elemental analysis	Calculated: C: 75.00, H: 8.85, N: 7.29, O: 8.33.

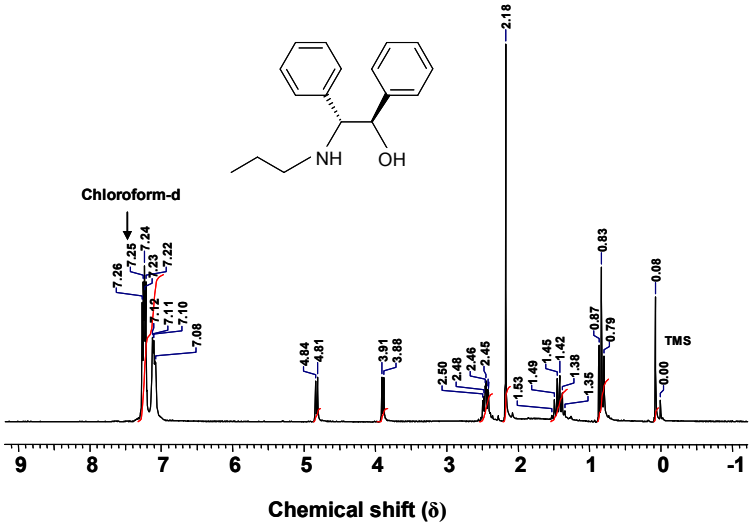

Figure 5B.4: ^{1}H NMR spectra of NH-propyl-(1S,2R)-(+)-1-amino-1,2-diphenylethanol.

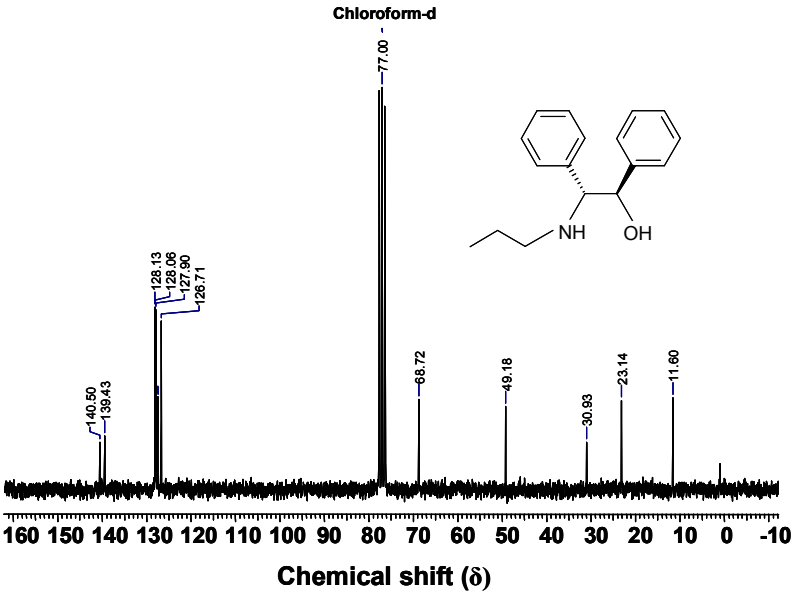

Figure 5B.5: ^{13}C NMR spectra of NH-propyl-(1S,2R)-(+)-1-amino-1,2-diphenylethanol.

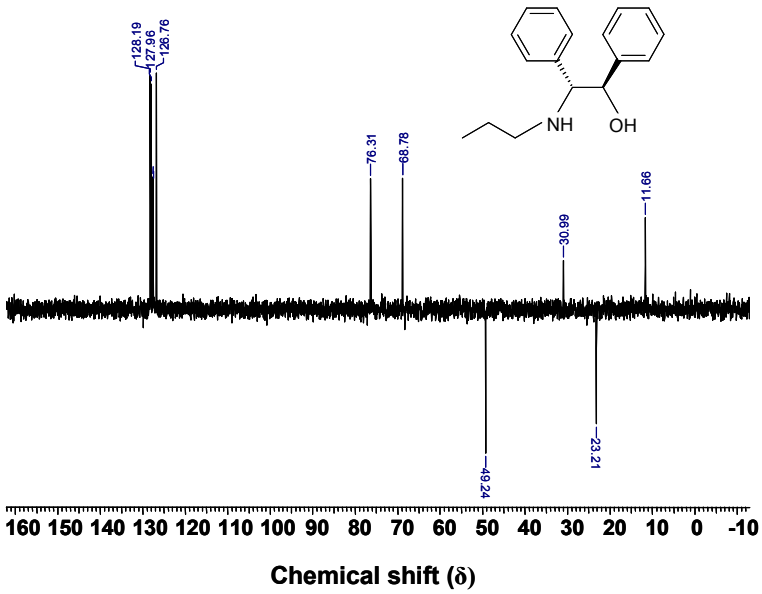

Figure 5B.6: ^{13}C-DEPT NMR-spectra of NH-propyl-(1S,2R)-(+)-1-amino-1,2-diphenylethanol.

Figure 5B.4 represents the ^{1}H NMR spectrum of NH-propyl-(1S,2R)-(+)-1-amino-1,2-diphenylethanol. In the spectrum we could see a triplet at δ = 0.83 ppm in the very low downfield evidenced the C*H*$_3$ protons in the ligand. Near to C*H*$_3$ peaks a branched peak at δ = 1.45 ppm, indexed to two hydrogen atoms which represents the O*H* and N*H* groups. A triplet at δ = 2.18 ppm indicates the presence of C*H*$_2$(CH$_3$)CH$_2$- protons. The multiplet at δ = 2.45 ppm corresponds to the C*H*$_2$ group directly attached to the NH group. Two doublets at δ = 3.84 and 4.76 ppm in the spectrum indicate C*H*NH and C*H*OH respectively. A multiplet at δ = 7.05-7.40 ppm is due to the presence of aromatic ring the ligand and indexed to ten protons. Figure 5B.5 represents the ^{13}C-DEPT NMR-spectra of NH-propyl-(1S,2R)-(+)-1-amino-1,2-diphenylethanol. In the spectrum, the carbon atoms corresponding to the propyl group could see at δ = 11.60 (*C*H$_3$), 23.14 (*C*H$_2$CH$_3$) and 49.18 (*C*H$_2$NH) ppm.

The peak at δ = 68.72 ppm corresponding to *C*HNH carbon atom in the ligand. *C*HOH carbon atom represents a peak at δ = 76.25 ppm. The aromatic carbons given a group of peaks at δ = 126.71, 127.44, 127.49, 127.90, 128.06 and 128.13 ($CH_{aromatic}$), along with two peaks at δ = 139.43 and 140.13 (C_q) ppm. The ^{13}C DEPT NMR spectrum of NH-propyl-(1S,2R)-(+)-1-amino-1,2-diphenylethanol supports the ^{1}H and ^{13}C NMR spectrum results.

Table 5B.3: NH-propyl-(1S,2R)-(+)-1-amino-1,2-diphenylethanol

Appearance	White solid
Yield	Yield: 76 %.
Molecular Weight	255
FT-IR (DRS)	PrADPE: 2830-3040 (CH_{strech}), 1500–1300 (CH_{bend}), 3600-3000 ($-OH_{strech}$), 3319, 3302 ($-NH_{stretch}$), 1580-1620 (benzene), 1607 ($C-O_{strech}$), 1454 ($C=C_{in\text{-}pane\ strech}$) cm^{-1}. Ru-Bn-PrADPE: 2830-3040 (CH_{strech}), 3600-3000 ($-OH_{strech}$), 1580-1620 (benzene), 1644 ($C-O_{strech}$), 1454 ($C=C_{in\text{-}pane\ strech}$) cm^{-1}. Ru-Cy-PrADPE: 2830-3040 (CH_{strech}), 3600-3000 ($-OH_{strech}$), 1580-1620 (benzene), 1644 ($C-O_{strech}$), 1454 ($C=C_{in\text{-}pane\ strech}$) cm^{-1}.
^{1}H NMR ($CDCl_3$)	PrADPE, δ = 0.83 (t, 3 H, C*H*$_3$), 1.45 (br, 2 H, O*H*, N*H*), 2.18 (t, 2 H, C*H*$_2$(CH_3)CH_2-), 2.45 (m, 2 H, C*H*$_2$NH), 3.84 (d, 1 H, C*H*NH), 4.76 (d, 1 H, C*H*OH), 7.05-7.4 (m, 10 H, H_{arom}) ppm.
^{13}C NMR ($CDCl_3$)	PrADPE, δ = 11.60 (*C*H_3), 23.14 (*C*H_2CH_3), 49.18 (*C*H_2NH), 68.72 (*C*HNH), 76.25 (*C*HOH), 126.71, 127.44, 127.49, 127.90, 128.06, 128.13 ($CH_{aromatic}$), 139.43, 140.13 (C_q) ppm.
^{13}C NMR ($CDCl_3$)-(DEPT)	PrADPE, δ = 11.66 (*C*H_3), 23.31 (*C*H_2CH_3), 49.24 (*C*H_2NH), 68.78 (*C*HNH), 76.31 (*C*HOH), 126.76, 127.50, 127.55, 127.96, 128.12, 128.19 ($CH_{aromatic}$) ppm.
Elemental analysis	PrADPE, Calculated: C: 75.00, H: 8.85, N: 7.29, O: 8.33. Found: C: 75.22, H: 8.78, N: 7.28, O: 8.15.

5.5.2. FT-IR spectra

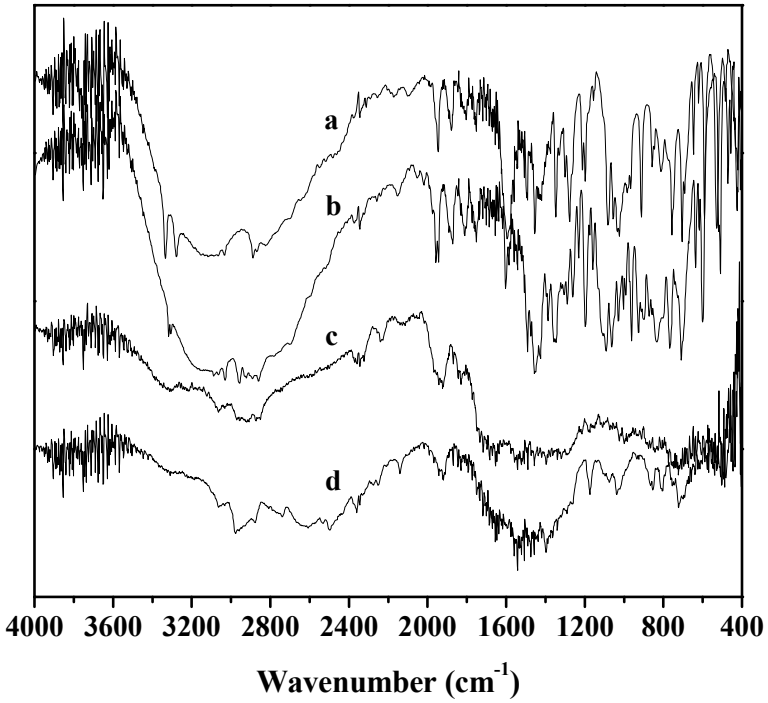

Figure 5B.7: FT-IR spectra of (a) ADPE (b) PrADPE (c) Ru-Bn-PrADPE and (d) Ru-Cy-PrADPE

Figure 5B.7 represents the FT-IR spectra of (a) ADPE (b) PrADPE (c) Ru-Bn PrADPE and (d) Ru-Cy-PrADPE respectively. The FT-IR spectra confirms the formation of homogeneous ligand, NH-propyl-(1S,2R)-(+)-1-amino-1,2-diphenylethanol **(**PrADPE) and the chiral ruthenium complexes, Ru-Bn-PrADPE and Ru-Cy-PrADPE.

The fundamental vibrational modes of pure ADPE, (1S,2R)-(+)-1-amino-1,2-diphenylethanol, have taken as the elementary scale for assigning the successful formation of modified ligand and the ruthenium complexes. From the literatures it was observed that any modification on the organic molecule may cause a appearance/disappearance or shift to fundamental IR bands in the spectrum. For this

purpose we have screened the fundamental vibrational modes of molecular species such as -NH, -C-O, -OH, -CH, and C=C present in (1S,2R)-(+)-1-amino-1,2-diphenylethanol. We have observed two weak band at 3318 and 3305 cm^{-1} assigned to the characteristic bands of $–NH_2$ and another two bands at 2954 and 2857 cm^{-1} corresponding to asymmetric and symmetric vibrations, respectively, of the -CH groups of the ethane part of the molecule. A medium band at 1421 cm^{-1} indicates the C=C stretching in-plane vibration of benzene framework. A band at 704 cm^{-1} represents the C-H bending vibration of methylene group of benzene and a small and strong band at around 1000–1200 and 1655 cm^{-1} are the characteristic band of C-O functional group in the ADPE. A broad band between 3400 and 3650 cm^{-1} corresponds to the stretching vibration and a sharp band between 1650 and 1600 cm^{-1} is due to the bending vibrations of O–H functional group in ADPE.

After modifying with propyl group, PrADPE (Figure 5B.7, b), a broad but more intense peak at around 3200–2800 cm^{-1} and 1500–1300 cm^{-1} are due to the C–H stretching and bending vibrations of methylene group as discussed earlier and a medium band at 1454 cm^{-1} indicates the C=C stretching in-plane vibration of benzene framework were observed. Moreover, the characteristic peaks of –NH group also visible at 3319 and 3302 cm^{-1} even though the percentage of the –NH proton got decreased after modifying with a propyl group. Along with the above peaks we can see the characteristic peaks of –C-O (1607 and 1200-1000 cm^{-1}), -OH (3600-3000 cm^{-1}), C=C (1454 cm^{-1}), have persisted with a marginal shift in the positions of the bands.

The chiral ruthenium complexes of PrADPE (Figure 5B.7, c &d) also showed the above characteristic peaks with some shift in to the peak position, which is clearly evidenced the successful complexation of metal and the result further proved by UV-

Vis studies. The major peaks are, for Ru-Bn-PrADPE: 2830-3040 (CH_{strech}), 3600-3000 ($-OH_{strech}$), 1580-1620 (benzene), 1644 ($C-O_{strech}$), 1454 ($C=C_{in\text{-}pane\ strech}$) cm^{-1}. For Ru-Cy-PrADPE: 2830-3040 (CH_{strech}), 3600-3000 ($-OH_{strech}$), 1580-1620 (benzene), 1644 ($C-O_{strech}$), 1454 ($C=C_{in\text{-}pane\ strech}$) cm^{-1}. Some of the characteristic bands in the functional group region are not visible due to the overlapping of peaks.

5.5.3. UV-Vis spectra

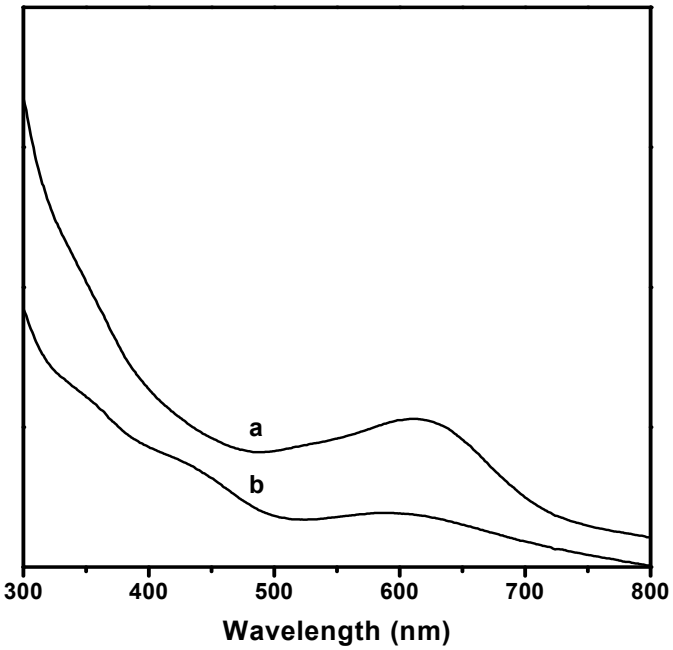

Figure 5B.8: UV-Vis spectra of (a) Ru-Bn-PrADPE and (b) Ru-Cy-PrADPE

Figure 5B.8 represents the UV-Vis spectra of (a) Ru-Bn-PrADPE and (b) Ru-Cy-PrADPE respectively. Here we can see a very broad absorption peak at 435 nm for both the complexes indicate the MLCT of metal to ligand absorption of unsymmetrical Ru(II) complex formed. This indicates the right evidence for the formation of chiral metal complexes. Along with the above mentioned peak it was observed that another peak for both complexes at a high value of UV absorption at

624 nm may due to the weak interaction of metal to ligand.[31] The UV absorption value greatly supported the active metallic centre has a +2 oxidation state and in an octahedral geometry.

5.5.4. Asymmetric transfer hydrogenation of simple prochiral ketones using homogeneous catalysts

Table 5B.4: Asymmetric transfer hydrogenation of simple prochiral ketones

		Ru-Bn-PrADPE		Ru-Cy-PrADPE	
Entry	**Substrate**	Conversion (%)[a]	*ee* (%)[a]	Conversion (%)[a]	*ee* (%)[a]
1	**ACP**	96	28	94	36
2	**ClACP**	98	22	96	31
3	**BrACP**	97	22	94	31
4	**MeACP**	76	27	69	33
5	**MeOACP**	56	24	49	30
6	**DMeOACP**	74	24	62	31
7	**PRP**	69	27	51	32

The reaction was carried out at 60°C for 1 h, using 0.01 mol % of ketone and a S/C ration of 100 in 3 mL solvent. KOH = 0.3 mL (1 mg/0.1 mL 2-propanol).

[a]Determined by GC equipped with a chiral column.

The configuration of alcohol product was *R*.

Ketones from 1-7 were applied to the homogeneous asymmetric transfer hydrogenation in 2-propanol in the presence of KOH using the catalyst Ru-Bn-

PrADPE/Ru-Cy-PrADPE (Table 5B.4). In the investigation of acetophenone (entry 1) we found that the reaction in 2-propanol possesses high reactivity and moderate enantioselectivity (96% yield with 28% *ee* for Ru-Bn-PrADPE and 94% yield with 36% *ee* for Ru-Cy-PrADPE) comparable to the results obtained by Noyori *et al.* This result was not unexpected in view of the known reversibility of transfer hydrogenations using propan-2-ol as the hydrogen source and reinforced the need to avoid an unnecessarily long reaction time. The use of 4-chloroacetophenone and 4-bromoacetiphenonea (entry 2 & 3) gave only a slight drop in enantioselectivity, whilst affording a more synthetically useful yield of product [4-chloroacetophenone gave, 98% with 22% *ee* and 96% with 31% *ee* for Ru-Bn-PrADPE and Ru-Cy-PrADPE, respectively. 4-Bromoacetophenone gave, 97% with 22% *ee* and 94% with 31% *ee* for Ru-Bn-PrADPE and Ru-Cy-PrADPE , respectively]. Whilst under similar conditions *S*-1-(4-methylphenyl)ethanol was obtained in 76% yield with 27% ee for Ru-Bn-PrADPE and 69% yield with 33% ee for Ru-Cy-PrADPE from 4-methylacetophenone (entry 4). For 4-Methoxyacetophenone (entry 5), the asymmetric reaction gave relatively poor results (56% yield with 24% ee for Ru-Bn-PrADPE and 49% yield with 30% ee for Ru-Cy-PrADPE), while a much better result (in 74% yield with 24% ee for Ru-Bn-PrADPE and 62% yield with 31% ee for Ru-Cy-PrADPE) was observed in the transfer hydrogenation reaction of 2,5-dimethoxyacetophenone (entry 6). Propiophenone **(**entry 7) was reduced to (*S*)-1-phenylpropanol in 69% yield with 27% ee and 51% yield with 32% ee for Ru-Bn-PrADPE and Ru-Cy-PrADPE, respectively, after 1 h at 60^{o}C. From the results, it is observed that the homogeneous catalyst (Ru-Bn-PrADPE) prepared from $[RuCl_2(\eta^6\text{-benzene})]_2$ displayed higher conversion than the catalyst (Ru-Cy-PrADPE) prepared from $[RuCl_2(\eta^6\text{-}p\text{-cymene})]_2$ for simple

prochiral ketones. But the *ee* results are superior for Ru-Cy-PrADPE than Ru-Bn-PrADPE at our reaction conditions and may be due to the favorable special arrangement of sterically hindered *p*-cymene in the metal complex. As a general strategy, the results with the substituted acetophenones suggested that electron-withdrawing groups show higher substrate conversions than electron donating groups. The *ee* results are exactly reverse to conversion strategy.

5.6. REFERENCES

1. M. J. Palmer, M. Wills, *Tetrahedron: Asymmetry*. **1999,** *10,* 2045;
2. R. Noyori, S. Hashiguchi, *Acc. Chem. Res*. **1997,** *30,* 97;
3. G. Zassinovich, S. Gladiali, *Chem. Rev*. **1992**, 1051.
4. *Chemical and Engineering News*, August. **1996,** *26,* 25.
5. P. N. Liu, J. G. Deng, Y. Q. Tu, S. H. Wang, *Chem Comm*. **2004,** 2070-2071.
6. P. N. Liu, P. M. Gu, F. Wang, Y. Q. Tu, *Org Letters*. **2004,** *6* (2), 169-172.
7. A. Ghosh, R. Kumar, *Journal of Catalysis*. **2004,** *228,* 386–396.
8. D. J. Bayston, J. L. Fraser, M. R. Ashton, A. D. Baxter, M. E. C. Polywka, E. Moses, *J. Org. Chem*. **1998,** *63,* 3137.
9. A. J. Sandee, D. G. I. Petra, J. N. H. Reek, P. C. J. Kamer, P. W. N. M. van Leeuwen, *Chem. Eur. J*. **2001,** *7* (6) 1202-1208.
10. A. Hayes, G. Clarkson, M. Wills, *Tetrahedron: Asymmetry*. **2004,** *15,* 2079-2084.
11. M. A. Bennett, A. K. Smith, *J. Chem. Soc, Dalton Trans*. **1974,** 233-241.
12. D. Zhao, J. Feng, Q. Huo, N. Melosh, G. H. Fredrickson, B. F. Chmelka, G. D. Stucky, *Science* (Washington D.C.). **1998,** *279,* 548-552.
13. D. Brunel, A. Cauvel, F. Fajula, F. Di Renzo, *Stud. Surf. Sci. Catal*. **1995,** *97,* 173.
14. A. Cauvel, D. Brunel, F. Di Renzo, F. Fajula, in: Proceedings of the 53rd International Meeting on Phys. Chem. 'Organic Coatings,' Am. Inst. Phys. **1996,** *354,* 477.
15. K. Kosuge, T. Sato, N. Kikukawa, M. Takemori, *Chem. Mater*. **2004,** *16,* 899-

905.

16. D. Brunel, N. Bellocq, P. Sutra, A. Cauvel, M. Laspéras, P. Moreau, F. Di Renzo, A. Galarneau, F. Fajula, *Coord. Chem. Rev*. **1998,** *180* (II), 1085.
17. D. Jiang, Q. Yang, H. Wang, G. Zhu, J. Yang, C. Li, *Journal of Catalysis*. **2006,** *239,* 65-73.
18. M. Kinugasa, T. Harada, A. Oku, *Tetrahedron Letters*. **1998,** *39,* 4529.
19. M. Suzuki, S. Ito, T. Kuwahara, *Bull. Chem. Soc. Jpn*. **1983,** *56,* 956-957.
20. H. Yang, G. Zhang, X. Hong, Y. Zhu, *Microporous and Mesoporous Materials*. **2004,** *68,* 119–125.
21. H. H. P. Yiu, P. A. Wright, N. P. Botting, *Journal of Molecular Catalysis B: Enzymatic*. **2001,** *15*, 81-92.
22. D. Jiang, Q. Yang, J. Yang, L. Zhang, G. Zhu, W. Su, C. Li. *Chem. Mater*. **2005,** *17*, 6154-6160.
23. X. S. Zhao, G. Q. Lu, *J. Phys. Chem. B*. **1998,** *102,* 1556-1561.
24. F. de Juan, E. Ruiz-Hitzky, *Adv. Mater*. **2000,** *12,* 430-432.
25. P. Ferreira, I. S. Goncüalves, F. E. Kühn, A. D. Lopes, M. A. Martins, M. Pillinger, A. Pina, J. Rocha, C. C. Romão, A. M. Santos, T. M. Santos, A. A. Valente, *Eur. J. Inorg. Chem*. **2000,** 2263-2270.
26. M. Jia, A. Seifert, W. R Thiel, *Chem. Mater*. **2003,** *15,* 2174-2180.
27. R. J. Staniewicz, R. F. Sympson, D. G. Hendricker Z, *Inorganic Chemistry*, **1977,** *16*, 2166.
28. F. Barigelletti, A. Juris, V. Balzani, P. Belser, A. von Zelewsky, *Inorg. Chem*.

1987, *26,* 4115.

29. K. Mizushima, M. Nakaura, S. Park, H. Nishiyama, H. Monjushiro, K. Harada, M. Haga, *Inorg. Chim. Acta*. **1997,** *261,* 175.

30. J. A. Kenny, M. J. Palmer, A. R. C. Smith, T. Walsgrove, M. Wills, *Synlett*. **1999,** *10,* 1615-1617.

31. S. Campagna. *Inorg. Chem*., **1991**, *30*, 3728-3732.

Chapter 6

Summary & Conclusions

6.1 INTRODUCTION

Due to the cost of the sophisticated chiral ligands, often exceeding that of the noble metal employed, catalyst recovery is of paramount importance for the application of enantioselective metal catalysis to large scale processes. In order to easily recover and recycle asymmetric catalysts, successful approaches involve the immobilization of molecular precursors either onto a support material or into an appropriate phase system so that the catalyst can be quantitatively separated from both product(s) and unreacted reagents by filtration or phase separation. For this purpose, various methodologies and materials have been developed over the last twenty years.

Mesoporous materials are of great interest to the materials community because their pore structures as well as catalytic, adsorbed, conductive and magnetic properties can readily be tailored. A highly ordered large mesoporous silica SBA-15 was synthesized by using amphiphilic triblock copolymers as the structure-directing agents. Our aim was just that of highlighting the great potential and diversity of applications of immobilized amino alcohol complex catalysts in both heterogeneous and homogeneous catalysis. In general, immobilized single-site catalysts have been prepared by covalent anchoring the support material. Silica is the most common inorganic support for the heterogenization of molecular catalysts due to its excellent thermal and chemical stability, ease of handling and diversity of chemical modifications. Silicas have a rigid structure and do not swell in solvents; hence they can be used at both high and low temperature and at high pressure. Just the inflexibility and non-compressibility make silica-tethered catalysts amenable to be employed in many challenging transformations. In order to maintain the stereochemical properties of the parent homogeneous asymmetric catalyst, the ligands

are generally attached to silica by a single, flexible and sufficiently long linker, which also contributes to minimize steric interactions with the support surface.

6.2. SUMMARY

The present thesis gives an account of

1. Synthesis of mesoporous SBA-15 material.
2. Functionalization of SBA-15 with 3-chloropropyltrimethoxysilane, (4-chloro methyl)phenyltrimethoxysilane and 2-(4-chlorosulphonylphenyl)ethyltrimethoxy silane.
3. Immobilization of chiral ligand, (1R,2S)-(+)-*cis*-1-amino-2-indanol/(1S,2R)-(+)-1-amino-1,2-diphenylethanol followed the preparation of chiral heterogeneous ruthenium complexes by using metal precursors such as $[RuCl_2(benzene)]_2$ and $[RuCl_2(p\text{-cymene})]_2$.
4. Preparation of homogeneous NH-propyl, NH-benzyl and NH-(*p*-tosyl) derivatives of (1R,2S)-(+)-*cis*-1-amino-2-indanol and further complexation with $[RuCl_2(benzene)]_2$ and $[RuCl_2(p\text{-cymene})]_2$.
5. Preparation of NH-propyl-(1S,2R)-(+)-1-amino-1,2-diphenylethanol and further complexation with $[RuCl_2(benzene)]_2$ and $[RuCl_2(p\text{-cymene})]_2$.
6. Detailed structural, morphological and chemical characterization of these composite materials using various characterization techniques.
7. Application of these materials as catalysts in heterogeneous/homogeneous enantioselective transfer hydrogenation of prochiral ketones.
8. Detailed kinetic study of asymmetric transfer hydrogenation of acetophenone using various tethered heterogeneous chiral complexes.

9. A major achievement of the present work is the comparative performance study of homogeneous chiral amino alcohol complexes and its corresponding heterogeneous analogous under the similar reaction conditions.

Chapter 1 presents a general introduction about various physicochemical aspects of mesoporous materials with particular emphasis to different synthesis routes and different approaches for their surface modification. Similarly different synthesis routes and different approaches for the synthesis of transition-metal complexes are also included. The various applications of mesoporous materials as support for different catalytically active transition metal complexes and characterization techniques of these composite materials are also discussed in brief. The general concepts of green chemistry in developing catalytic processes are discussed. The scope of the work includes synthesis of Ru-metal complexes and immobilization of these metal complexes in functionalized SBA-15 and their use in catalyzing environmentally benign hydrogenation of various classes of ketones to secondary alcohols using principles of green chemistry, water as preferred reaction medium. Based on the above view, the scope of the work has expanded to the synthesis of Ru-metal complexes using bi-dentate nitrogen containing ligands, their characterization and application for above mentioned transfer hydrogenation reaction.

Chapter 2 provides detailed experimental results on synthesis of SBA-15, functionalization of SBA-15 with 3-chloropropyltrimethoxysilane, (4-chloromethyl) phenyltrimethoxysilane and 2-(4-chlorosulphonylphenyl)ethyltrimethoxysilane and further immobilization of chiral ligand, (1R,2S)-(+)-*cis*-1-amino-2-indanol followed

by the preparation of chiral heterogeneous ruthenium complexes by using two metal precursors such as $[RuCl_2(benzene)]_2$ and $[RuCl_2(p\text{-cymene})]_2$. The complete characterizations of these samples were carried out by various spectroscopic techniques like XRD, ^{29}Si and ^{13}C CP MAS NMR, N_2 sorption technique, FT-IR, UV-Vis, ICP-AES, XPS, TEM and SEM.

Chapter 3 deals with an effective utilization of synthesized Ru-metal complexes and immobilized Ru^{II} complexes on surface modified SBA-15 as novel heterogeneous catalyst system for the asymmetric transfer hydrogenation of simple aromatic carbonyl compounds (ketones) under mild reaction conditions. The transfer hydrogenation has been done using various reaction conditions including different substrate, different temperature, various bases, duration of run *etc*.

Chapter 4 focuses on the preparation, characterization and catalytic activity of homogeneous ruthenium (II) complexes of NH-propyl, NH-benzyl and NH-(*p*-tosyl) derivatives of (1R,2S)-(+)-*cis*-1-amino-2-indanol. The materials were characterized by liquid ^1H NMR & ^{13}C NMR, FT-IR and UV-Vis spectroscopies. The main emphasis was given on the local environment of the metal species. The catalytic activity of these synthesized homogeneous chiral ruthenium complexes in the ATH (Asymmetric Transfer Hydrogenation) of simple aromatic carbonyl compounds (ketones) under mild reaction conditions. The asymmetric transfer hydrogenation has been done under various substrates to catalyst ratio.

Chapter 5 deals with the immobilization of (1S,2R)-(+)-1-amino-1,2-diphenylethanol, followed the preparation of chiral heterogeneous ruthenium complexes by using two metal precursors such as $[RuCl_2(benzene)]_2$ and $[RuCl_2(p\text{-cymene})]_2$ over 3-chloropropyltriethoxysilane functionalized SBA-15. The materials were characterized by various characterization techniques. The complete characterizations of these samples were carried out by various spectroscopic techniques like XRD, ^{29}Si and ^{13}C CP MAS NMR, N_2 sorption technique, FT-IR, UV-Vis, ICP-AES. The catalytic performance of synthesized homogeneous and heterogeneous chiral ruthenium complexes in asymmetric transfer hydrogenation of a number of simple aromatic ketones in 2-propanol under mild reaction conditions has been evaluated. The transfer hydrogenation has been carried out under various reaction conditions including different substrate, different temperature, various bases, duration of run etc in order to get an insight about the kinetics of the reaction. The performance of the synthesized heterogeneous catalysts were compared with the corresponding homogeneous analogous, NH-propyl-(1S,2R)-(+)-1-amino-1,2-diphenylethanol, under the same reaction conditions. The homogeneous catalysts were fully characterized by liquid ^1H & ^{13}C NMR, FT-IR and UV-Vis spectroscopies.

6.3. CONCLUSIONS

6.3.1. Surface Modification and Characterization of Mesoporous Silica

- Highly ordered SBA-15 was synthesized by hydrothermal synthesis method. Powder x-ray diffraction patters of the synthesized SBA-15 exhibited three characteristic 2θ peaks, which strongly suggest the successful preparation of

the support material. The calcined SBA-15 material has a stable pore wall thickness to retain its integrity after several modification treatments. The hexagonal nature of the pores and the long range orderedness of the calcined SBA-15 material were concluded from both the XRD pattern and TEM images. The calcined materials displayed type IV isotherm (definition by IUPAC) with H_1-type hysteresis that is typical of mesoporous materials with cylindrical channels possessing pore diameters between 2 and 50 nm. The pore size distribution measurements proved that the average pore diameter of the synthesized material within the mesoporous range. ^{29}Si CP MAS NMR had given an insight about the availability of sufficient amount of Si-OH groups for further modification.

☼ The calcined SBA-15 was successfully functionalized by 3-chloropropyltri methoxysilane, (4-chloromethyl)phenyltrimethoxysilane and 2-(4-chloro sulphonylphenyl)ethyltrimethoxysilane. The functionalization and further passivation of the silanol groups were ensured by XRD, FT-IR and solid state ^{29}Si & ^{13}C CP MAS NMR spectrum of the modified materials. A negligible decrease in peak intensities to the three distinct XRD reflections was observed by functionalization followed by immobilization of ligand and further complexation with ruthenium precursors. This minor loss indicates that, even the presence of a large amount of organic moieties by the partial filling inside the mesopores is less detrimental to the quality of the SBA-15 material. The occupation of functional moieties inside the pores was further confirmed by the decrease in pore diameter and surface areas of the modified materials. A

regular decrease in intensities to the entire three representative peaks gave an insight about the grafting of organic molecules on the walls of the silica material. The consumption of surface hydroxyl groups were estimated from ^{29}Si CP MAS NMR of the modified materials. A considerable decrease in intensities to the Q^3 sites and a considerable increase in intensities to the Q^4 sites were observed while functionalization and further passivation.

- ☼ The immobilization of chiral ligands over functionalized mesoporous silica material were confirmed by XRD, FT-IR and solid state ^{29}Si & ^{13}C CP MAS NMR spectrum of the chiral ligand modified materials. After ligand loading the persistence of the three XRD reflections with decreased intensities not only proved the structural stability and existence of long-range ordering to the mesophase but also the survival of undisturbed pore wall thickness even after a number of treatments with organic molecules in solvents under radical conditions
- ☼ The successful loading of active half sandwich metal complexes over ligand immobilized materials was confirmed by ICP-AES, UV-Vis and XPS analysis. The UV-Vis spectra of all the heterogeneous and homogeneous catalysts exhibits the characteristic metal to ligand charge transfer absorption band confirms the formation of the metal complexes. The XPS analysis provided the binding energies of representative atoms present in the complexes, which proved the formal oxidation state of the atoms and the local chemical and physical environments of the complexes.

6.3.2. Enantioselective transfer hydrogenation of ketones

Since chiral diamines are notoriously complicated to synthesize in contrast to the large variety and ready availability of chiral amino alcohols, this study has led to intense exploration of [Ru^{II}(arene)(β-aminoalcohol)] systems for rationalizing the enantioselectivity, designing more efficient ligands, improving catalyst activity and broadening the scope of asymmetric hydrogen transfer of functionalized carbonyl compounds in 2-propanol. In this account we summarize our own efforts towards these objectives using (1*R*,2*S*)-(+)-*cis*-1-amino-2-indanol and (1S,2R)-(+)-1-amino-1,2-diphenylethanol. Three essential parameters of these asymmetric hydrogen transfer systems, ie., (i) structure of the β-amino alcohol ligand, (ii) structure of the arene ligand in the ruthenium precursor, and (iii) influence of functional groups of ketones to be reduced, have been studied systematically. The complimentary information (results from homogeneous complexes) thus collected, together with reactivity data of various modified [Ru^{II}(arene)(β-amino alcohol)] complexes, have led to a better understanding of the process with a complete structural effect on the reactivity and enantioselectivity through ATH reaction of functionalized aromatic ketones.

- ☼ Homogeneous Ru(II)-(1R,2S)-(+)-*cis*-1-amino-2-indanol catalysts (Ru-Bn-AIL and Ru-Cy-AIL) show very high reactivity and enantioselectivity at our reaction conditions above 90% conversion and *ee*.
- ☼ Homogeneous Ru(II)-NH-propyl-(1R,2S)-(+)-*cis*-1-amino-2-indanol catalysts (Ru-Bn-PrAIL and Ru-Cy-PrAIL) given a comparative performance in the asymmetric transfer hydrogenation reaction of selected aromatic ketones when

comparing with the activity of pure Ru(II)-(1R,2S)-(+)-*cis*-1-amino-2-indanol catalysts (Ru-Bn-AIL and Ru-Cy-AIL).

- ☼ The order of increase in steric hindrance in between propyl, benzyl and *p*-tosyl as follows,

  Propyl < benzyl < *p*-tosyl

- ☼ Among the homogeneous catalysts, the catalysts prepared from NH-propyl-(1*R*,2*S*)-(+)-*cis*-1-amino-2-indanol exhibited promising activity over the catalysts prepared from NH-benzyl-(1*R*,2*S*)-(+)-*cis*-1-amino-2-indanol and NH-(*p*-tosyl)-(1*R*,2*S*)-(+)-*cis*-1-amino-2-indanol. This may be due to the higher steric hindrance introduced by benzyl and *p*-tosyl groups than a propyl group in the modified ligands which will make the NH protons unavailable to the reaction; especially asymmetric transfer hydrogenation is a bifunctionally controlled reaction.

- ☼ A blank reaction, in the absence of amino alcohol ligand, investigates the effect of adsorbed metal complexes over the inorganic support on the catalytic reaction showed that immobilization is not effective without tethering molecule linker.

- ☼ The activity of heterogeneous Ru-Bn-PrAIL-SBA-15 and Ru-Cy-PrAIL-SBA-15 catalysts were comparative with its homogeneous counterpart (Ru(II)-NH-propyl-(1R,2S)-(+)-*cis*-1-amino-2-indanol, Ru-Bn-PrAIL and Ru-Cy-PrAIL).

- ☼ While monitoring the reduction of acetophenone over Ru-Bn-PrAIL-SBA-15 it was noticed that the reaction rate was fast initially while later the rate decreased as reaction proceeds.

- As a comparison with other catalysts, Ru-Bn-PrAIL-SBA-15 and Ru-Cy-PrAIL-SBA-15 are the most active catalysts for the transfer hydrogenation of acetophenone and its derivatives under our reaction conditions. The less activity of Ru-Bn-BzAIL-SBA-15, Ru-Cy-BzAIL-SBA-15, Ru-Bn-TsAIL-SBA-15 and Ru-Cy-TsAIL-SBA-15 may be due to the additional steric hindrance introduced by the benzyl and *p*-tosyl group along with the benzene and *p*-cymene molecules around the active metal center.
- Homogeneous Ru(II)-NH-propyl-(1S,2R)-(+)-1-amino-1,2-diphenylethanol shows excellent conversion (50-96%) and moderate enantiomeric excess (20-36%) for all the acetophenone derivatives under our reaction conditions.
- The performance of heterogeneous Ru-Bn-PrADPE-SBA-15 and Ru-Cy-PrADPE-SBA-15 were low in terms of conversion and enantioselectivity when comparing with the corresponding homogeneous catalysts (Ru(II)-NH-propyl-(1S,2R)-(+)-1-amino-1,2-diphenylethanol).
- Acetophenone is the least sterically hindered compound among the substrates showed high activity (second to 4-Cl and 4-Br substituted) and enantioselectivity. It is observed that in the reaction of the substituted acetophenone, the enantioselectivity was not significantly affected by the type of substituent (electron donating or electron withdrawing at para positions) but the conversion has a marked effect over the type of substituent. Among the electron withdrawing groups attached substrates, 4-chloroacetophenone and 4-bromoacetophenone were reduced in high yield with low enantiomeric excess than 4-methoxy substituted derivative, showed less activity and

enantioselectivity, which may be due to the high reduction potential of the molecule or the formation of a stable complex with reactive metal center by the methoxy oxygen. When comparing the 4-methoxyacetophenone, 2,5-dimethoxyacetophenone reduced slightly higher yield even though it is more sterically hindered. Propiophenone reduced to *S*-1-(phenyl)propanol with higher or comparable conversion and *ee* when comparing with the reduction of acetophenone under various heterogeneous/homogeneous catalysts.

- ☼ It is observed that, the heterogeneous catalyst prepared from $[RuCl_2(benzene)]_2\}$ displayed higher conversion than the catalyst prepared from $[RuCl_2(p\text{-cymene})]_2\}$ for the enantioselective reduction of simple prochiral ketones. But the *ee* results are vice versa and may be due to the favorable special arrangement of sterically hindered *p*-cymene towards enantioselection in the metal complex.
- ☼ Among the heterogeneous catalysts, the catalysts prepared by using propyl group as a spacer molecule showed better activity and enantioselectivity for most of the prochiral ketones which may be due to the favorable approach of the substrate molecules to the metal centre because of the less steric hindrance of the propyl group than a benzyl or *p*-tosyl molecule. A small decrease in catalyst activity was found in successive runs.
- ☼ The kinetic study using heterogeneous modified Ru(II)-(1*R*,2*S*)-(+)-*cis*-1-amino-2-indanol reveals that the reaction conditions such as temperature, duration of reaction, amount of base and amount of solvent have a strong influence over both conversion and enantiomeric excess.

- ☼ The catalysts recycled to a maximum of two successive runs under two different recycling conditions. All the heterogeneous catalysts show a drastic decrease in activity from the first recycling experiment onwards without changing the enantiomeric excess considerably.
- ☼ As a comparison, the performances of (1*R*,2*S*)-(+)-*cis*-1-amino-2-indanol and (1S,2R)-(+)-1-amino-1,2-diphenylethanol (the two chiral auxiliaries used in this thesis) ligands in combination with $[RuCl_2(benzene)]_2$ and $[RuCl_2(p\text{-cymene})]_2$ over a range of prochiral aromatic ketones, (1*R*,2*S*)-(+)-*cis*-1-amino-2-indanol is more reactive and enantioselective than (1S,2R)-(+)-1-amino-1,2-diphenylethanol even though it has a fused, rigid hydrocarbon backbone.
- ☼ In conclusion the immobilized Ru-amino alcohol complex in SBA-15 as heterogeneous catalyst found to be a promising catalyst in the enantioselective transfer hydrogenation of ketones to secondary alcohols.

Publications/Conferences

LIST OF RESEARCH PUBLICATIONS

1. **"**Synthesis, characterization and catalytic properties of benzyl sulphonic acid functionalized Zr-TMS catalysts".
   Surendran Parambadath, M. Chidambaram, A. P. Singh.
   Catalysis Today. 97 (**2004**) 233.
2. "Designing isolated vanadium sites over mesoporous MCM-41: Characterization and catalytic applications".
   S. Shylesh, **Surendran. Parambadath** and A. P. Singh.
   Bulletin of Catalysis Society of India. *4,* (**2005**), 45**.**
3. "Ru(II)-Chiral (1R,2S)-(+)-*cis*-1-amino-2-indanol immobilized over SBA-15 for asymmetric transfer hydrogenation reaction of prochiral ketones".
   Surendran Parambadath, A. P. Singh.
   Catalysis Today. (Article In Press, Available on 7th July 2008 onwards)
4. **"**Homogeneous and Heterogeneous Ru(II)-NH-propyl-(1R,2S)-(+)-*cis*-1-amino-2-indanol as chiral catalyst for asymmetric transfer hydrogenation reaction of prochiral ketones: A Comparative study **"**.
   Surendran Parambadath, M. Kavitha, K. R. Kamble, A. P. Singh.
   Journal of Catalysis. (Communicated)
5. **"**Mesoporous SBA-15-supported heterogeneous Ru(II) chiral amino alcohol complexes for asymmetric transfer hydrogenation reaction of prochiral ketones**"**.
   Surendran Parambadath, K. R. Kamble, A. P. Singh.
   Journal of Molecular Catalysis A: Chemical. (Communicated).
6. "Asymmetric transfer hydrogenation reaction of prochiral ketones using heterogeneous Ru(II)-NH-(*p*-toluenesulfonyl)-(1R,2S)-(+)-*cis*-1-amino-2-indanol complexes".
   Surendran Parambadath, M. Kavitha, K. R. Kamble, A. P. Singh.
   Journal of Molecular Catalysis A: Chemical. (To be Communicated).
7. "Asymmetric transfer hydrogenation of prochiral ketones using *N*-benzyl and *N*-

(*p*-tosyl) modified Ru(II)-(1R,2S)-(+)-*cis*-1-amino-2-indanol complexes".

Surendran Parambadath, K. R. Kamble, A. P. Singh.

Journal of Molecular Catalysis A: Chemical (To be Communicated).

8. **"**Synthesis, characterization and catalytic activity of chiral Mn (III) salen complex covalently bonded to Mesoporous Alumina".

Surendran Parambadath, Purabi Sarmah, S. Selvakumar, A. P. Singh, Stephane Menage, Olivier Hamelin, Marc Fontecave.

Journal of Molecular Catalysis A: Chemical (To be communicated).

9. "Asymmetric transfer hydrogenation of esters and diketones using homogeneous and heterogeneous Ru(II)-NH-propyl-(1R,2S)-(+)-*cis*-1-amino-2-indanol catalysts".

Surendran Parambadath, K. R. Kamble, A. P. Singh. (Manuscript Under Preparation).

10. "Asymmetric transfer hydrogenation of esters and diketones using homogeneous and heterogeneous Ru(II)-NH-propyl(1S,2R)-(+)-1-amino-1,2-diphenyl ethanol catalysts".

Surendran Parambadath, K. R. Kamble, A. P. Singh. (Manuscript Under Preparation).

CONTRIBUTIONS TO NATIONAL/INTERNATIONAL SYMPOSIA/CONFERENCES

1. Synthesis of silica functionalized sulphonic acid groups for acid catalyzed reactions.
   S. Shylesh, **S. Parambadath**, S. S. Bhoware and A. P. Singh.
   6th National Symposium in Chemistry, Indian Institute of Technology, Kanpur, February **2004** (***Poster Presentation***).
2. Preparation of benzylsulphonic acid functionalized mesoporous Zr-TMS and its application in acylation reaction.
   Surendran Parambadath and A. P. Singh.
   3rd Indo-Pacific (IPCAT-3) catalysis symposium. Thaipai, Thaiwan. December **2004 (*Oral Presentation*).**
3. Benzoylation of toluene with p-toluoyl chloride over triflic acid functionalized mesoporous Zr-TMS catalyst.
   M. Chidambaram, **S. Parambadath**, S. Selva kumar and A.P. Singh.
   17th National symposium on catalysis held at CSMCRI, Bhavnagar, India. January **2005** ***(Oral presentation).***
4. Periodic Mesoporous Silicas vs Periodic Mesoporous Organosilicas.
   S. Shylesh, Prinson P. Samuel, **S. Parambadath** and A. P. Singh.
   National Science Day Celebrations, National Chemical Laboratory, Pune, February **2006** (***Poster Presentation***).
5. Ru(II)-Chiral (1R,2S)-(+)-*cis*-1-amino-2-indanol immobilized over SBA-15 for asymmetric transfer hydrogenation reaction of prochiral ketones.
   Surendran Parambadath and A. P. Singh.
   INDO-US Catalysis for Future Fuels. Indian Institute of Petroleum. April **2007 (*Poster presentation*).**
6. Mesoporous Silica SBA-15-supported (1R,2S)-(+)-*cis*-1-amino-2-indanol as Heterogeneous Chiral Ligand for asymmetric transfer hydrogenation reaction of

prochiral ketones.

Surendran Parambadath and A. P. Singh.

ICAM. Kottayam, Kerala, India. February **2008 (*Oral presentation*).**